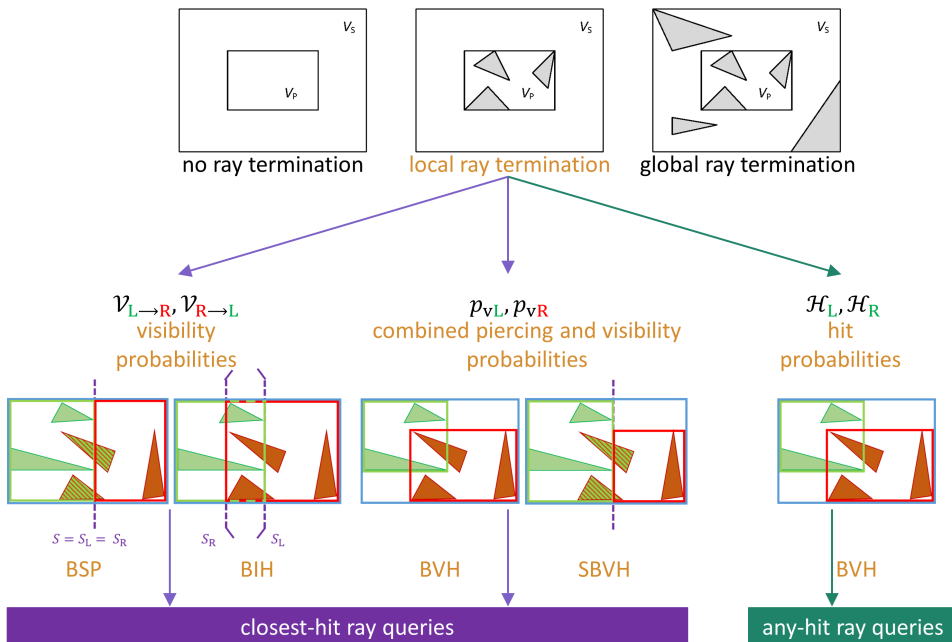


# On the Use of Local Ray Termination for Efficiently Constructing Qualitative BSPs, BIHs and (S)BVHs

Impact on the number of ray intersection tests and ADS node traversal steps

Matthias Moulin, Philip Dutré



## Contents

<b>A. Purpose</b>	<b>5</b>
<b>B. Set-up</b>	<b>5</b>
B.1. Rendering . . . . .	5
B.2. Scenes . . . . .	5
B.3. Partitioning . . . . .	6
B.4. RTSAH build heuristics . . . . .	8
B.5. SRDH build heuristics . . . . .	9
B.6. Voxel traversal order heuristics . . . . .	10
B.7. Tree depth . . . . .	11
B.8. Tree termination . . . . .	11
<b>C. Results</b>	<b>11</b>
C.1. Kd-trees . . . . .	12
C.2. BIHs . . . . .	15
C.3. BVHs . . . . .	16
C.4. SBVHs . . . . .	17
C.5. BVHs dedicated to shadow ray traversal . . . . .	18
C.6. Discussion . . . . .	18

## List of Tables

1.	Our artificial test scenes . . . . .	6
2.	Our realistic test scenes . . . . .	6
3.	Table overview . . . . .	11
4.	Ray tracing statistics summary of ADSs constructed with the RTSAH for our realistic scenes . . . . .	20
5.	Ray tracing statistics summary of BVHs constructed with the SRDH for our realistic scenes . . . . .	20
6.	Ray tracing statistics of kd-trees constructed with the RTSAH for our artificial scenes . . . . .	21
7.	Ray tracing statistics of kd-trees constructed with the RTSAH for our artificial scenes . . . . .	22
8.	Ray tracing statistics of BIHs constructed with the RTSAH for our artificial scenes . . . . .	23
9.	Ray tracing statistics of BIHs constructed with the RTSAH for our artificial scenes . . . . .	24
10.	Ray tracing statistics of BVHs constructed with the RTSAH for our artificial scenes . . . . .	25
11.	Ray tracing statistics of BVHs constructed with the RTSAH for our artificial scenes . . . . .	26
12.	Ray tracing statistics of SBVHs constructed with the RTSAH for our artificial scenes . . . . .	27
13.	Ray tracing statistics of SBVHs constructed with the RTSAH for our artificial scenes . . . . .	28
14.	Tree statistics of kd-trees constructed with the RTSAH for our artificial scenes . . . . .	29
15.	Tree statistics of BIHs constructed with the RTSAH for our artificial scenes . . . . .	30
16.	Tree statistics of BVHs constructed with the RTSAH for our artificial scenes . . . . .	31
17.	Tree statistics of SBVHs constructed with the RTSAH for our artificial scenes . . . . .	32
18.	Ray tracing statistics of kd-trees constructed with the RTSAH for our realistic scenes . . . . .	33
19.	Ray tracing statistics of kd-trees constructed with the RTSAH for our realistic scenes . . . . .	34
20.	Ray tracing statistics of kd-trees constructed with the RTSAH for our realistic scenes . . . . .	35
21.	Ray tracing statistics of BIHs constructed with the RTSAH for our realistic scenes . . . . .	36
22.	Ray tracing statistics of BIHs constructed with the RTSAH for our realistic scenes . . . . .	37
23.	Ray tracing statistics of BIHs constructed with the RTSAH for our realistic scenes . . . . .	38
24.	Ray tracing statistics of BVHs constructed with the RTSAH for our realistic scenes . . . . .	39
25.	Ray tracing statistics of BVHs constructed with the RTSAH for our realistic scenes . . . . .	40
26.	Ray tracing statistics of BVHs constructed with the RTSAH for our realistic scenes . . . . .	41
27.	Ray tracing statistics of SBVHs constructed with the RTSAH for our realistic scenes . . . . .	42
28.	Ray tracing statistics of SBVHs constructed with the RTSAH for our realistic scenes . . . . .	43
29.	Ray tracing statistics of SBVHs constructed with the RTSAH for our realistic scenes . . . . .	44
30.	Tree statistics of kd-trees constructed with the RTSAH for our realistic scenes . . . . .	45
31.	Tree statistics of BIHs constructed with the RTSAH for our realistic scenes . . . . .	46
32.	Tree statistics of BVHs constructed with the RTSAH for our realistic scenes . . . . .	47
33.	Tree statistics of SBVHs constructed with the RTSAH for our realistic scenes . . . . .	48
34.	Ray tracing statistics of BVHs constructed with the SRDH for our artificial scenes . . . . .	49
35.	Tree statistics of BVHs constructed with the SRDH for our artificial scenes . . . . .	50
36.	Ray tracing statistics of BVHs constructed with the SRDH for our realistic scenes . . . . .	51
37.	Tree statistics of BVHs constructed with the SRDH for our realistic scenes . . . . .	52
38.	Time statistics summary of ADSs constructed with the RTSAH and SRDH for our realistic scenes	53
39.	Error distributions of kd-trees constructed with the RTSAH for the Empty Box scene . . . . .	54
40.	Error distributions of kd-trees constructed with the RTSAH for the Empty Box scene . . . . .	55
41.	Error distributions of kd-trees constructed with the RTSAH for the Empty Box scene . . . . .	56
42.	Error distributions of kd-trees constructed with the RTSAH for the Empty Box scene . . . . .	57
43.	Error distributions of kd-trees constructed with the RTSAH for the Empty Box scene . . . . .	58
44.	Error distributions of kd-trees constructed with the RTSAH for the Cornell Box scene . . . . .	59
45.	Error distributions of kd-trees constructed with the RTSAH for the Cornell Box scene . . . . .	60
46.	Error distributions of kd-trees constructed with the RTSAH for the Cornell Box scene . . . . .	61
47.	Error distributions of kd-trees constructed with the RTSAH for the Cornell Box scene . . . . .	62
48.	Error distributions of kd-trees constructed with the RTSAH for the Cornell Box scene . . . . .	63
49.	Error distributions of kd-trees constructed with the RTSAH for the Icosahedron1 scene . . . . .	64
50.	Error distributions of kd-trees constructed with the RTSAH for the Icosahedron1 scene . . . . .	65
51.	Error distributions of kd-trees constructed with the RTSAH for the Icosahedron1 scene . . . . .	66
52.	Error distributions of kd-trees constructed with the RTSAH for the Icosahedron1 scene . . . . .	67
53.	Error distributions of kd-trees constructed with the RTSAH for the Icosahedron1 scene . . . . .	68
54.	Error distributions of kd-trees constructed with the RTSAH for the Icosahedron2 scene . . . . .	69
55.	Error distributions of kd-trees constructed with the RTSAH for the Icosahedron2 scene . . . . .	70
56.	Error distributions of kd-trees constructed with the RTSAH for the Icosahedron2 scene . . . . .	71
57.	Error distributions of kd-trees constructed with the RTSAH for the Icosahedron2 scene . . . . .	72
58.	Error distributions of kd-trees constructed with the RTSAH for the Icosahedron2 scene . . . . .	73



120. Error distributions of BVHs constructed with the RTSAH for the <code>Icosahedron4</code> scene . . . . .	135
121. Error distributions of BVHs constructed with the RTSAH for the <code>Icosahedron4</code> scene . . . . .	136
122. Error distributions of BVHs constructed with the RTSAH for the <code>Icosahedron4</code> scene . . . . .	137

## A. Purpose

In this auxiliary report, we show and discuss the obtained differences in the number of ray intersection tests against geometric primitives and in the number of ADS node traversal steps for ADSs built with the SAH versus our RTSAH and SRDH approximations for a variety of scenes. The ADSs built with our RTSAH approximations aim to accelerate closest-hit ray queries. The ADSs built with our SRDH approximations aim to accelerate any-hit ray queries.

Among our test scenes are some artificially and procedurally generated scenes consisting of a low number of geometric primitives, making an ADS build with a ground truth RTSAH or SRDH computationally feasible for comparison against our approximations. Here, ray sampling is used for evaluating the (plane) visibility probabilities ( $\mathcal{V}_{L \rightarrow R}$  (3.16) and  $\mathcal{V}_{R \rightarrow L}$  (3.17)) involved in the explicit RTSAH cost function (3.4), for evaluating the combined piercing and visibility probabilities ( $p_{vL}$  (3.19) and  $p_{vR}$  (3.20)) involved in the implicit RTSAH cost function (3.18), and for evaluating the (AABB) hit probabilities ( $\mathcal{H}_L$  (3.24) and  $\mathcal{H}_R$  (3.25)) involved in the SRDH cost function (3.23). Furthermore, it is generally not possible to efficiently enumerate a finite set of candidate partitions containing the optimal one for a voxel,  $V_P$ , to partition according to the RTSAH cost metric.<sup>1</sup> To study the characteristics of the cost metric itself, we want to use an excessive number of candidate partitions. For these small scenes, it is computationally feasible to consider  $\mathcal{O}(|G_P|)$  arbitrary candidate splitting planes.

Furthermore, a variety of scenes with difficult but realistic geometric complexity are considered to compare our RTSAH and SRDH approximations against the SAH. Due to the high number of geometric primitives contained in these scenes, it is not computationally feasible to use a ground truth RTSAH or SRDH during the ADS construction, or consider  $\mathcal{O}(|G_P|)$  arbitrary candidate splitting planes for every voxel to partition.

## B. Set-up

This section elaborates more on the set-up of our experiments: the applied rendering techniques (Subsection B.1), the selected test scenes (Subsection B.2), the ADS construction by recursively partitioning a set of geometric primitives (Subsection B.3), the ADS build and voxel traversal order heuristics (Subsections B.4 to B.6), and the remaining ADS constraints (Subsections B.7 to B.8).

### B.1. Rendering

We have implemented our build heuristics and build heuristic framework in `pbrt-v2` [PH10]. Our RTSAH (SRDH) build heuristics are primarily concerned with the number of ray intersection tests to perform against the geometric primitives (e.g., triangles) in the scene as well as the number of ADS node traversal steps for closest-hit (any-hit) ray queries. Here, the ray distribution is assumed to be a parent-exterior isotropic ray distribution (i.e. not targeted to specific viewpoints or light sources). Therefore, we render all our test scenes as ambient occlusion images.<sup>2</sup>

### B.2. Scenes

We have created some artificial test scenes with a low number of geometric primitives (see Table 1). For these scenes, it is computationally feasible to construct ADSs with a ground truth RTSAH or SRDH (see RTSAH E and SRDH E, respectively, below) and use an excessive number of candidate partitions for each voxel to partition to be able to focus only on the cost metric itself and not on the set of candidate partitions, which

<sup>1</sup>For kd-trees constructed with the SAH, the finite set of candidate partitions containing the optimal one according to this cost metric, can be enumerated with a sweeping plane build algorithm in  $\mathcal{O}(|G_P| \log |G_P|)$  time. BVHs and BIHs partition the geometric primitives by spatially grouping their centroids in disjoint sets. The associated candidate partitions can be enumerated with a sweeping plane build algorithm in  $\mathcal{O}(|G_P| \log |G_P|)$  time, but constitute only a finite subset of all possible disjoint groupings of the geometric primitives,  $G_P$ . Enumerating the latter is generally *NP-hard*.

<sup>2</sup>We modified `pbrt-v2`'s `AmbientOcclusionIntegrator` to use cosine weighted (hemi)sphere sampling instead of the incorrect uniform (hemi)sphere sampling.

is outside the scope of this project. **Empty Box** is an empty cube of which one plane is removed. **Cornell Box** and **Icosahedron1** are similar to **Empty Box** but contain two boxes and uniformly stratified icosahedra, respectively. **Icosahedron2** is the same as **Icosahedron1** but without the surrounding box. **Icosahedron3** consists of icosahedra which centroids are exponentially distributed in one dimension and normally distributed in the other two dimensions. **Icosahedron4** contains **Icosahedron3** trapped in some grid of two-sided squares. For these scenes, we only selected one camera viewpoint.

Furthermore, we have chosen some realistic test scenes of difficult but realistic geometric complexity, ranging between 100 k and 1500 k triangles, to illustrate our build heuristics (see Table 2). In each scene, we selected three interesting camera viewpoints.

For each test scene and viewpoint an ambient occlusion image is rendered at a resolution of  $512 \times 512$  pixels using 512 primary (camera) rays per pixel and one shadow (ambient) occlusion ray per primary ray. The length of these ambient occlusion rays is not set to a fixed, finite, maximum distance (i.e. cameras fully enclosed by geometry will result in completely black images).

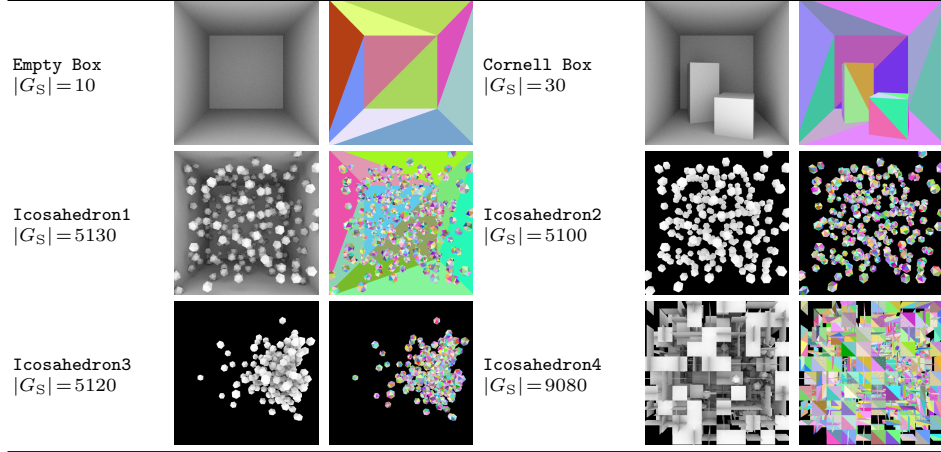


Table 1: Our artificial test scenes with their number of (unique) geometric primitives visualized by ambient occlusion images, and by hashing and rendering the identifiers of the geometric primitives.

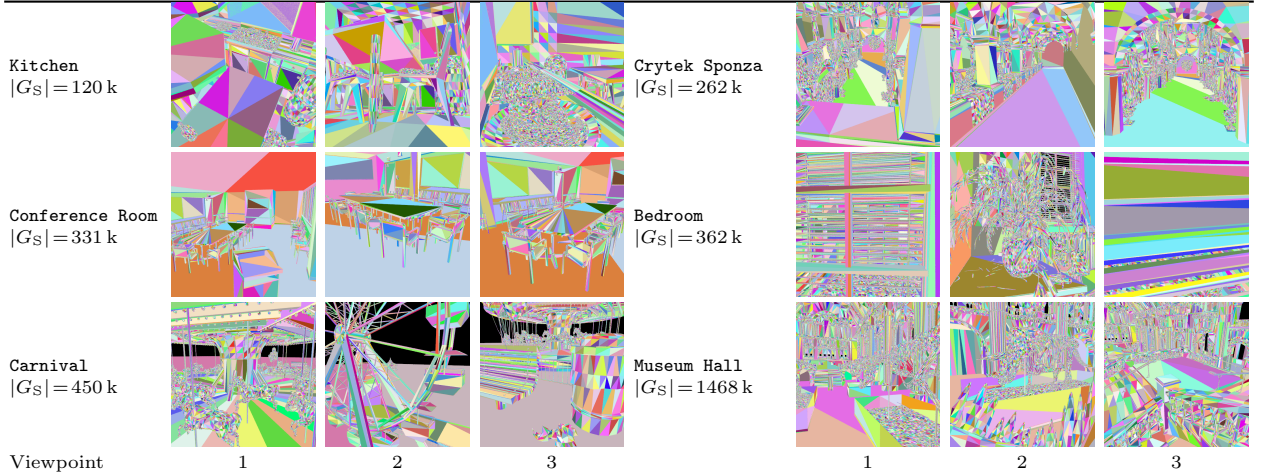


Table 2: Our realistic test scenes with their number of (unique) geometric primitives and chosen viewpoints visualized by hashing and rendering the identifiers of the geometric primitives.

### B.3. Partitioning

In a prerendering phase, a kd-tree, BIH, BVH or SBVH is constructed with one of different build heuristics including the SAH, and our RTSAH and SRDH approximations. For kd-trees constructed with the SAH, only a finite number of candidate splitting planes needs to be considered to find the optimal candidate partition according to this cost metric, namely the six axis-aligned bounding planes of each of the geometric primitives.

Between these splitting planes, the SAH cost function is monotonically increasing or decreasing. The finite set of splitting planes can be enumerated efficiently in a sweeping plane build algorithm with a time complexity of  $\mathcal{O}(|G_s| \log |G_s|)$  [WH06] or  $\mathcal{O}\left(|G_s| (\log |G_s|)^2\right)$  [PH10, PWH16] (depending on the use of sorting operations). For BIHs and BVHs constructed with the SAH, all possible pairs of disjoint groups (containing together all the geometric primitives) need to be considered to find the optimal candidate partition according to this cost metric. The finite set of splitting planes<sup>3</sup> can be enumerated efficiently in a sweeping plane build algorithm with a time complexity of  $\mathcal{O}(|G_s| \log |G_s|)$  [WH06] or  $\mathcal{O}\left(|G_s| (\log |G_s|)^2\right)$ . SBVHs can generally not be built with a sweeping plane approach due to the *chopped binning* [SFD09] (binned extension of *split clipping* [HB02]). Furthermore, a full sweeping plane build algorithm is not applicable to general build heuristics. An alternative is a (parallel) binned algorithm [HKRS02, HMS06, PGpSS06, WH06, SSK07, SFD09] which optionally switches to the full sweeping plane approach or its candidate partitions, based on the number of geometric primitives to partition. Here, the latter differentiates between a full sweeping plane approach and a (adaptive) binned approach considering the candidate partitions of a full sweeping plane approach.

For the RTSAH, we can generally not use a sweeping plane build algorithm since we can generally not enumerate a finite number of candidate splitting planes containing the optimal candidate partition according to this cost metric (e.g., BSPs/kd-trees) and we can generally not increment/decrement the cost in  $\mathcal{O}(1)$  time while sweeping the splitting plane due to the plane visibility probabilities involved in the cost metric (and the tightness of the child voxels). Moulin et al. [MBD15] assume in the kd-tree construction that all geometric primitives overlap none of the candidate splitting planes for the SAH, which removes the need for clipping and enables a sweeping plane build algorithm for their RTSAH APOD|APSA approximations. We can use a similar assumption for approximating  $\mathcal{V}_\perp$  (5.3), but not for approximating  $\mathcal{V}_{\Omega^\perp}$  (5.10). Furthermore, the assumption is very rough in case of large differences in the size of the geometric primitives (e.g., *Carnival* scene). This can be solved by further subdividing large geometric primitives or their AABBs for the ADS construction only [EG07, DK08, GD16]. Instead, we use a binned approach to calculate our RTSAH approximations with clipping as intended. A robust Sutherland-Hodgman [SH74] clipping algorithm is used for clipping planar polygons (i.e. triangles) against axis-aligned planes with finite thickness [Eri04].

Moulin et al. [MBD15] use the sweeping plane SAH build algorithm of `pbrt-v2`, as is, as their reference and use a similar build for their sweeping plane RTSAH APOD|APSA approximations. These build algorithms do not necessarily consider all three primary axes: `pbrt-v2` [PH10] and `pbrt-v3` [PWH16] start with the axis corresponding to the longest spatial extent of the voxel to partition. Another axis is only considered if and only if no valid candidate partition is found along the previous axis. By heuristically pruning splitting axes, ADS construction time can be reduced. We noticed that kd-trees constructed with a full sweeping plane algorithm compared to this heuristical sweeping plane algorithm (which most of the time considers only one axis), result in huge reductions in the number of ray-triangle intersection tests. This holds for both the SAH and RTSAH approximations. Furthermore, after using a full sweeping plane algorithm, we noticed only small positive and negative differences on average between the SAH and RTSAH APSA. Two reasons for originally [MBD15] obtaining large reductions are:

1. The RTSAH APSA [MBD15] selected some radical different splitting planes to change the axis corresponding to the longest spatial extent of the voxels to partition next, compared to the SAH. This explains why the SAH benefits the most of a full sweeping plane algorithm which considers all three primary spatial extents.
2. The RTSAH cost is always smaller than (or exceptionally equal to) the corresponding SAH cost for a given candidate partition by taking local ray termination ( $\mathcal{V}_{L \rightarrow R} \leq 1$  and  $\mathcal{V}_{R \rightarrow L} \leq 1$ ) into account, resulting in a more accurate termination criterium. Havran and Bittner [HB02] try to alleviate this by allowing locally non-optimal split decisions due to the presence of local maxima in the global cost function.

In the remainder, we always consider all three primary axes (as opposed to [PH10, MBD15, PWH16]) but instead use a binned approach since the set of splitting planes sufficient for the SAH is not guaranteed to contain the optimal splitting plane for the RTSAH and since all geometric primitives are not guaranteed to overlap none of the candidate splitting planes (as opposed to [MBD15]).

For the artificial test scenes, we use  $20|G_p|$  equidistant bins for kd-trees and the GK-BVH [PGDS09] contribution of SBVHs, all  $|G_p|+1$  adaptive bins for BIHs, and all  $|G_p|-1$  adaptive bins for BVHs and the BVH contribution of SBVHs for each of the three primary axes at each level of the tree construction, resulting in a

---

<sup>3</sup>Although enumerating all sufficient candidate partitions for BIHs and BVHs is *NP*-hard, enumerating all sufficient candidate splitting planes is not *NP*-hard if one splits based on the centroids of the geometric primitives.

time complexity of  $\mathcal{O}(|G_p|^2)$  for each voxel,  $V_p$ , to partition and a total time complexity of  $\mathcal{O}(|G_s|^2)$  for the ADS construction. For the realistic test scenes, we use a fixed number of 256 equidistant bins<sup>4</sup> ( $\ll |G_s|$ ) for each of the three primary axes at each level of the tree construction, resulting in a time complexity of  $\mathcal{O}(|G_p|)$  for each voxel,  $V_p$ , to partition and a total time complexity of  $\mathcal{O}(|G_s| \log |G_s|)$  for the ADS construction. If  $|G_p| < 256$  for BIHs, BVHs and the BVH contribution of SBVHs, we switch from equidistant bins to all adaptive bins (superset).

## B.4. RTSAH build heuristics

We construct all kd-trees and BIHs using the explicit RTSAH cost function (3.4), and all BVHs and SBVHs using the implicit RTSAH cost function (3.18). We use the following build heuristics:

- SAH (SP): sweeping plane SAH build algorithm for each of the three primary axes at each level of the ADS construction.
- SAH: binned RTSAH approximation that assumes that **no** rays, entering a parent voxel,  $V_p$ , will hit a geometric primitive. The visibility probabilities,  $\mathcal{V}_{L \rightarrow R}$  and  $\mathcal{V}_{R \rightarrow L}$ , between the child voxels,  $V_L$  and  $V_R$ , are approximated as:

$$\mathcal{V}_{L \rightarrow R} \equiv 1 \quad (B.4.1)$$

$$\mathcal{V}_{R \rightarrow L} \equiv 1. \quad (B.4.2)$$

- RTSAH Z: binned RTSAH approximation that assumes that **all** rays, entering a parent voxel,  $V_p$ , will hit a geometric primitive. The visibility probabilities,  $\mathcal{V}_{L \rightarrow R}$  and  $\mathcal{V}_{R \rightarrow L}$ , between the child voxels,  $V_L$  and  $V_R$ , are approximated as:

$$\mathcal{V}_{L \rightarrow R} = \begin{cases} 0, & \text{if } |G_L| \neq 0, \\ 1, & \text{otherwise.} \end{cases} \quad (B.4.3)$$

$$\mathcal{V}_{R \rightarrow L} = \begin{cases} 0, & \text{if } |G_R| \neq 0, \\ 1, & \text{otherwise.} \end{cases} \quad (B.4.4)$$

where  $G_L$  ( $G_R$ ) is the set of geometric primitives contained in the left (right) child voxel of the candidate partition. The visibility probabilities depend on the presence of geometric primitives in the child voxels. This is similar to the evaluation of the visibility probabilities of Ize et al. [IH11] for leaf voxels only.

- RTSAH N: binned RTSAH approximation that assumes that the visibility probabilities,  $\mathcal{V}_{L \rightarrow R}$  and  $\mathcal{V}_{R \rightarrow L}$ , of the child voxels,  $V_L$  and  $V_R$ , are linearly dependent on their number of contained geometric primitives relative to the number of geometric primitives contained in the parent voxel,  $V_p$ :

$$\mathcal{V}_{L \rightarrow R} = 1 - \frac{|G_L|}{|G_p|} \quad (B.4.5)$$

$$\mathcal{V}_{R \rightarrow L} = 1 - \frac{|G_R|}{|G_p|}. \quad (B.4.6)$$

- RTSAH SA: binned RTSAH approximation that assumes that the visibility probabilities,  $\mathcal{V}_{L \rightarrow R}$  and  $\mathcal{V}_{R \rightarrow L}$ , of the child voxels,  $V_L$  and  $V_R$ , are linearly dependent on the sum of the surface areas of their contained geometric primitives relative to the sum of the surface areas of the geometric primitives contained in the parent voxel,  $V_p$ :

$$\mathcal{V}_{L \rightarrow R} = 1 - \frac{\text{SA}_{G_L}}{\text{SA}_{G_p}} \quad (B.4.7)$$

$$\mathcal{V}_{R \rightarrow L} = 1 - \frac{\text{SA}_{G_R}}{\text{SA}_{G_p}}, \quad (B.4.8)$$

where  $\text{SA}_{G_i} := \sum_{j \in \text{clip}(B_i, G_i)} \text{SA}_j$ .

---

<sup>4</sup>The splitting planes strictly lie inside the spatial or centroid extent of a voxel to partition. For BIHs, we use 254 equidistant bins and explicitly consider a candidate partition containing an empty left and a candidate partition containing an empty right child voxel.

- RTSAH E: ground truth RTSAH which uses ray sampling for evaluating the visibility probabilities,  $\mathcal{V}_{L \rightarrow R}$  and  $\mathcal{V}_{R \rightarrow L}$ , involved in the explicit RTSAH cost function (3.4), and the combined piercing and visibility probabilities,  $p_{vL}$  and  $p_{vR}$ , involved in the implicit RTSAH cost function (3.18). Each of these probabilities is sampled with 4096 rays satisfying the associated ray distributions. Due to the ray distribution (i.e. parent-exterior isotropic ray distribution) considered, it is not possible to trace one batch of rays through the scene in an additional preprocess and count the number of these rays passing through each candidate splitting plane as opposed to [BH09,FLF12] (actual ray distribution) and [CCI12] (scene-exterior isotropic ray distribution). Furthermore, the ray sampling can be accelerated via an additional preconstructed ADS for spatial partitioning schemes (e.g., kd-trees), but not for object (e.g., BVH) or hybrid partitioning schemes (e.g., BIH, SBVH). A spatial partitioning scheme ensures that all hit geometric primitives are contained inside the voxel to partition (i.e.  $\in G_P$ ), which is not guaranteed for object or hybrid partitioning schemes. For these reasons, RTSAH E is only computationally feasible for scenes with a very low number of geometric primitives ( $\ll 10k$ , if one uses a single-threaded ADS build [PH10, PWH16]).
- RTSAH ((WC)H)APSA|(WN(WC))HANPSA(2)|EP(2)|(H)APE(2): binned RTSAH approximations as described in the main text.

Here, RTSAH Z|N|SA are only introduced for illustrating the reduction in ADS quality due to artificially low visibility probabilities. The SAH and RTSAH Z are dual: The SAH represents the worst case behaviour whereas the RTSAH Z represents the best case behaviour of the ray tracing cost on average.

We do not consider RTSAH APAD|APOD|OPAD [MBD15] which generally also require ray sampling similar to RTSAH E and thus are of limited use in practice.

## B.5. SRDH build heuristics

We construct BVHs dedicated to the tracing of any-hit (shadow) rays using the SRDH cost function (3.23). We use the following build heuristics:

- SRDH Z: sweeping plane SRDH approximation that assumes that all rays, entering a child voxel, will hit a geometric primitive. The hit probabilities,  $\mathcal{H}_L$  and  $\mathcal{H}_R$ , of the child voxels,  $V_L$  and  $V_R$ , are approximated as:

$$\mathcal{H}_L = \begin{cases} 1, & \text{if } |G_L| \neq 0, \\ 0, & \text{otherwise.} \end{cases} \quad (\text{B.5.1})$$

$$\mathcal{H}_R = \begin{cases} 1, & \text{if } |G_R| \neq 0, \\ 0, & \text{otherwise.} \end{cases} \quad (\text{B.5.2})$$

- SRDH N: sweeping plane SRDH approximation that assumes that the hit probabilities,  $\mathcal{H}_L$  and  $\mathcal{H}_R$ , of the child voxels,  $V_L$  and  $V_R$ , are linearly dependent on their number of contained geometric primitives relative to the number of geometric primitives contained in the parent voxel,  $V_P$ :

$$\mathcal{H}_L = \frac{|G_L|}{|G_P|} \quad (\text{B.5.3})$$

$$\mathcal{H}_R = \frac{|G_R|}{|G_P|}. \quad (\text{B.5.4})$$

- SRDH SA: sweeping plane SRDH approximation that assumes that the hit probabilities,  $\mathcal{H}_L$  and  $\mathcal{H}_R$ , of the child voxels,  $V_L$  and  $V_R$ , are linearly dependent on the sum of the surface areas of their contained geometric primitives relative to the sum of the surface areas of the geometric primitives contained in the parent voxel,  $V_P$ :

$$\mathcal{H}_L = \frac{\text{SA}_{G_L}}{\text{SA}_{G_P}} \quad (\text{B.5.5})$$

$$\mathcal{H}_R = \frac{\text{SA}_{G_R}}{\text{SA}_{G_P}}. \quad (\text{B.5.6})$$

- SRDH E: ground truth SRDH which uses ray sampling for evaluating the hit probabilities,  $\mathcal{H}_L$  and  $\mathcal{H}_R$ , involved in the SRDH formulation (3.23). Each of these probabilities is sampled with 4096 rays satisfying the associated ray distributions. We need to ensure for  $\mathcal{H}_L$  ( $\mathcal{H}_R$ ) that if a ray hits a geometric primitive, that geometric primitive is contained in the left (right) child voxel. Therefore, the ray sampling cannot be accelerated via an additional preconstructed ADS.
- SRDH APSA|APE: sweeping plane SRDH approximations as described in the main text.
- SRDH APE2: binned SRDH approximation as described in the main text.

Note that we can use a sweeping plane build for most approximations since no geometric primitive clipping is required as opposed to the RTSAH (see Equations (4.14) and (4.15)). Both our EP and APE approximations can be used in a SRDH sweeping plane build algorithm, since both the mean and standard deviation can be updated incrementally and decrementally in  $\mathcal{O}(1)$  time [Fin09], which is not possible for the median and MAD in our EP2 and APE2 approximations.

## B.6. Voxel traversal order heuristics

The optimal voxel traversal order in an ADS for closest-hit ray queries is a spatial front-to-back order. For any-hit ray queries, the traversal can be terminated as soon as a geometric primitive is found which occludes the ray. Finding the optimal traversal order in an arbitrary ADS for each any-hit ray query is an expensive operation. Therefore, voxel traversal order heuristics, which reorder the voxels to traverse, are proposed to quickly find occluding geometric primitives. Besides comparing differently constructed BVHs dedicated to the tracing of shadow rays, we also compare against BVHs constructed with SAH (SP) that use different voxel traversal order heuristics for tracing shadow rays:

- SAH + OB (*Origin Based*): variable traversal kernel that traverses the left (right) child voxel first if the ray direction is non-negative (negative) in the dimension of the split axis [BH06, PH10, PWH16].
- SAH + IO (*In Order*): variable traversal kernel that traverses the closest child voxel to the ray origin first.
- SAH + UDF<sup>5</sup> (*Uniform Depth First*): stochastic traversal kernel that has an equal probability of traversing the left and right child voxel first.
- SAH + LDF (*Left Depth First*): constant traversal kernel that always traverses the left child voxel first.
- SAH + RDF (*Right Depth First*): constant traversal kernel that always traverses the right child voxel first.
- SAH + CCF (*Closest Centroid First*): variable traversal kernel that always traverses the child voxel whose centroid is the closest to the ray origin first (a.k.a. *front-to-back* traversal order [FLF12]).
- SAH + FCF (*Furthest Centroid First*): variable traversal kernel that always traverses the child voxel whose centroid is the furthest to the ray origin first (a.k.a. *back-to-front* traversal order [FLF12]).
- SAH + NodeSATO (*Node Surface Area Traversal Order*): constant traversal kernel that always traverses the child voxel whose AABB's surface area is the largest first [NM14].

Furthermore, we also define:

- OMS + NodeSATO (*Object Median Split* + NodeSATO): BVH constructed with object median splitting [Hec82] using NodeSATO for tracing shadow rays.
- SMS + NodeSATO (*Spatial Median Split* + NodeSATO): BVH constructed with spatial median splitting [Kap85] using NodeSATO for tracing shadow rays.

---

<sup>5</sup>In the remainder of the text, we use the notation  $\langle \text{UDF} \rangle$  to indicate that we averaged the results of five UDF runs with different seeds.

Our BVHs dedicated to the tracing of shadow rays (built with our SRDH or SRDH') use a constant traversal kernel per intermediate node that is determined during the ADS construction. For constant traversal kernels, the voxel traversal order can be precomputed (e.g., a one bit flag specifying which child voxel to traverse first), resulting in a similar cost per traversed node. Our traversal heuristics (SAH + OB|CCF|FCF) that use a variable traversal kernel, will result in a slightly higher cost per traversed node. The SAH + IO will result in the highest cost per traversed node, since the ray-AABB intersection test of the child voxels will be performed while traversing the parent voxel (instead of right before traversing the child voxels themselves). This results in an unnecessary ray-AABB intersection test for the second child voxel, in case the ray terminates while traversing the first child voxel.

## B.7. Tree depth

Both kd-trees and SBVHs allow the duplication of geometric primitive references (i.e. in case the associated geometric primitives straddle the splitting plane) as opposed to BIHs and BVHs. In order to preallocate certain resources in the ADS build, we use a fixed tree depth based on the total number of geometric primitives to partition [HB02, PH10] for kd-trees and SBVHs, and a maximum tree depth (64) equal to the size of the node traversal stack for all ADSs. Once the depth is equal to the lower of these two values, a leaf node is created (independent of any cost metric).

## B.8. Tree termination

Given the optimal candidate partition for a voxel according to one of the build heuristics, a decision has to be made whether to apply (i.e. create an intermediate node) or not apply (i.e. create a leaf node) that candidate partition on the ADS under construction:

1. If the optimal candidate partition is invalid (i.e. empty leaf voxels for BVHs), a leaf node is created.
2. If the cost of splitting is lower than the cost of not splitting, an intermediate node is created.
3. Otherwise, we allow the forced creation of an intermediate node if its cost does not exceed four times the cost of not splitting and the number of geometric primitives involved is less than sixteen [HB02, PH10]. Furthermore, this action is only allowed at most three times for kd-trees and BIHs and at most two times for (S)BVHs (since the latter are more tight, the cost of splitting is more likely to be lower than the cost of not splitting) along each ADS tree path.

## C. Results

Table 3 shows an overview of the tables containing statistics about our ADSs, built with our RTSAH and SRDH approximations, with regard to the ray tracing and the tree structure for our artificial and realistic test scenes. For our RTSAH approximations, we consider closest-hit primary (camera) rays, closest-hit shadow (ambient) rays and any-hit shadow (ambient) rays. The closest-hit primary rays are directionally distributed in space, whereas the closest-hit shadow rays will be much more uniformly distributed in space. For our SRDH approximations, we only consider any-hit shadow (ambient) rays. We summarized the results for the realistic test scenes in Tables 4 to 5.

Statistics				
	Artificial Test Scenes		Realistic Test Scenes	
Approximations	Ray Tracing	Tree Structure	Ray Tracing	Tree Structure
RTSAH	Tables 6 to 13	Tables 14 to 17	Tables 18 to 29	Tables 30 to 33
SRDH	Table 34	Table 35	Table 36	Table 37

Table 3: An overview of the tables containing statistics about our ADSs, built with our RTSAH and SRDH approximations, with regard to the ray tracing and the tree structure for our artificial and realistic test scenes.

## C.1. Kd-trees

RTSAH Z|N and RTSAH SA to a lesser extent are all very poor RTSAH approximations of no real use in practice. Their main purpose is to illustrate the capacity of the more general RTSAH (i.e. the SAH is a constrained version of the RTSAH) to differ from the SAH. On the one hand, RTSAH Z is smaller than SAH by some constant ( $1/2 p_{L \leftrightarrow R} (|G_L| + |G_R|)$ ) and illustrates how large and deep the kd-tree can potentially become by including local ray termination in the SAH. For the realistic test scenes, we notice increases of the average tree depth by 0.5 to 1 level and increases in the number of leaf nodes by a factor of 2 to 5 compared to SAH. The RTSAH has the potential to provide a better termination criterion in the cost metric itself as opposed to the SAH or a heuristical, add-on termination criterion [HB02]. On the other hand, RTSAH SA has a much smaller effect on the tree growth, but illustrates the way including local ray termination in the SAH (i.e. generalizing the SAH) can result in fundamentally different trees by selecting different candidate partitions. The RTSAH favours cutting off child voxels which are not or hardly visible to each other, resulting in a different ranking among the candidate partitions as opposed to the SAH. RTSAH N is somewhere in between, resulting in deeply balanced trees.

For RTSAH Z|N and RTSAH SA to a lesser extent, the kd-tree characteristics as well as the performance of the ray tracing queries are very poor. In contrast, the kd-trees built with all our more subtle RTSAH approximations (see main text), are more similar to the kd-trees built with the SAH than to these extremes.

For BIHs and BVHs, a binned build considers only a subset of the candidate partitions considered in a full sweeping plane build, since the associated candidate splitting planes become tight after partitioning the geometric primitives. For kd-trees, the position of a candidate splitting plane remains unchanged after partitioning the geometric primitives. Therefore, a binned build can consider candidate partitions not considered by a full sweeping plane build and vice versa. Assuming the SAH is an accurate measure of the ray tracing cost, binned builds should always be inferior to full sweeping plane builds. For the SAH, only a finite number of candidate splitting planes needs to be considered to find the optimal candidate partition according to this cost metric. Between these candidate splitting planes, the SAH cost function increases or decreases monotonically. This is generally not true for the RTSAH due to the distribution of and occlusion caused by the scene's geometry. In most of our tests scenes,<sup>6</sup> however, we notice a discrepancy in the SAH cost metric, since SAH results in far less intersection tests than SAH (SP). In the remainder of our discussion for kd-trees, we will therefore mainly focus on a comparison against SAH (instead of against SAH (SP)).

In our artificial test scenes, SAH has a small advantage over RTSAH E for uniformly (**Icosahedron** and **Icosahedron2**) and non-uniformly (**Icosahedron3**) distributed geometric primitives with equal surface area by only considering the number of geometric primitives and the voxels' surface area, and by not considering occlusion at all (as is the case for RTSAH E). In order to illustrate the benefits of RTSAH E, we needed to construct **Icosahedron4**<sup>7</sup> which is even artificial among artificial test scenes. Here, RTSAH E results in some small gains with regard to the number of ray-triangle intersection tests of 1% (camera) and 3% (ambient) compared to SAH, and 55% (camera) and 52% (ambient) compared to SAH (SP). With regard to our different approximations, RTSAH (WC)HAPSA|HAPE(2)|(WN(WC))HANPSA are inferior to RTSAH (WN(WC))HANPSA2, since they consider all geometric primitives irrelevant of their orientation, whereas RTSAH (WN(WC))HANPSA2 culls the single-sided geometric primitives according to their normal. Furthermore, the assumption of normally distributed geometry vertices is generally not true for all scenes and candidate partitions, making the constant ( $k \approx 1.4826$ ) relating the MAD to the standard deviation, too large and arbitrary. So, although, MAD is more robust to outliers, RTSAH EP2|(H)APE2 consider large non-solid ellipsoids, resulting in low visibility probabilities. RTSAH APSA|(WN(WC))HANPSA2|EP|APE achieve results close to RTSAH E despite considering only the surface area domain or projected hemispherical domain (but not both). Based on the results obtained for the artificial test scenes, we only consider RTSAH APSA|(WN(WC))HANPSA2|EP|APE for our realistic test scenes.

In our realistic test scenes, the average number of ADS node traversal steps for our RTSAH approximations is 2 to 6% (camera), and 2 to 10% (ambient) larger as opposed to the SAH as expected. Since the RTSAH cost of a candidate partition could not be larger than the corresponding SAH cost, kd-trees constructed with the RTSAH, will be less compact compared to kd-trees constructed with the SAH. The gains in the number of

<sup>6</sup>Empty Box is an exception. At the root node of **Empty Box**, the SAH cost function is constant between the planes of the box along two axes. Due to the axis-aligned symmetry of the scene's geometry, the visibility probability functions behave symmetrically resulting in a constant RTSAH cost function along the same two axes as well. In both cases of a different kind, a binned build will consider and favour splitting planes which do not coincide with a geometric primitive of this scene.

<sup>7</sup>It took more than six days to build a kd-tree for the **Icosahedron4** scene (9080 geometric primitives) with a single-threaded RTSAH E build, using 4096 rays accelerated with a preconstructed ADS for each candidate partition.

ray-triangle intersection tests as opposed to SAH vary on average between -3 and 0.45% (camera), and -2 and 2% (ambient). Notable exceptions are RTSAH APSA|EP|APE for the first and third viewpoint of **Bedroom**. All these approximations use some parallel projection, making them very capable capturing the occlusion near the window and closest door. Furthermore, we notice larger losses of our approximations for few viewpoints in **Crytek Sponza** and **Museum Hall**. None of the results, however, indicate a structural inefficiency in the constructed trees for a single or all scenes. The tree statistics of our RTSAH approximations are close to each other. Their average depth is close to SAH and their number of leaf nodes is even in the extreme cases below twice the number of leaf nodes of SAH. Although having more leaf nodes, leaf nodes are more populated due to higher geometric primitive reference duplications. Compared to SAH (SP), however, one clearly observes the less populated leaf nodes of SAH and our RTSAH approximations.

Havran [Hav00] introduced the *General Cost Model* (GCM)<sup>8</sup>, a build heuristic for kd-trees similar to the RTSAH [IH11, MBD15]. The difference lies in the wrong calculation of  $p_{jL}$  ( $p_{jR}$ ) as  $\frac{SA_L - SA_S}{SA_P}$  ( $\frac{SA_R - SA_S}{SA_P}$ ) [Hav00] instead of the correct  $\frac{SA_L - 2SA_S}{SA_P}$  ( $\frac{SA_R - 2SA_S}{SA_P}$ ) [IH11] which impacts all the related piercing probabilities (3.13). Their obtained kd-trees improved the rendering performance on average by 1%. We mainly focus on the difference in the number of ray-triangle intersection tests and ADS node traversal steps, since both are targeted directly in the cost metric and since rendering performance is subject to various factors not included in the cost metric<sup>9</sup>. However, due to the small differences in the number of ray-triangle intersection tests and ADS node traversal steps, we obtain similar results to the GCM [Hav00] (without using ray sampling per candidate partition).

**Error distributions.** For our artificial test scenes, we also gathered statistics of the differences between our RTSAH build heuristics and the ground truth RTSAH E on a per candidate partition basis. For each scene, a kd-tree is constructed using RTSAH E as before, but instead of only evaluating the ground truth visibility probabilities and the ground truth RTSAH cost function, all our approximated visibility probabilities and our approximated RTSAH cost functions are evaluated as well for the same set of candidate partitions. Note that the latter evaluations do not necessarily correspond to some evaluations performed during the construction of kd-trees using our RTSAH approximations.<sup>10</sup> More concretely, we define and sample<sup>11</sup> the following errors:

- A *visibility probability error* is defined as the difference between the approximated and ground truth visibility probability:

$$\Delta \mathcal{V}_{L \rightarrow R}^{RTSAH i} = \mathcal{V}_{L \rightarrow R}^{RTSAH i} - \mathcal{V}_{L \rightarrow R}^{RTSAH E} \quad (C.1.1)$$

$$\Delta \mathcal{V}_{R \rightarrow L}^{RTSAH i} = \mathcal{V}_{R \rightarrow L}^{RTSAH i} - \mathcal{V}_{R \rightarrow L}^{RTSAH E} \quad (C.1.2)$$

$$\Delta \mathcal{V}_{RTSAH i} := \Delta \mathcal{V}_{L \rightarrow R}^{RTSAH i} | \Delta \mathcal{V}_{R \rightarrow L}^{RTSAH i}, \quad (C.1.3)$$

and ranges from -1 to 1. Note that both  $\mathcal{V}_{L \rightarrow R}$  and  $\mathcal{V}_{R \rightarrow L}$  samples are included (i.e. two samples per candidate partition).

- A *cost error* is defined as the (normalized) difference between the approximated and ground truth RTSAH cost:

$$\Delta C_{RTSAH i} := \frac{\mathcal{C}_{RTSAH i} - \mathcal{C}_{RTSAH E}}{|G_L| + |G_R|} = \frac{p_{L \rightarrow R} \Delta \mathcal{V}_{L \rightarrow R}^{RTSAH i} |G_R| + p_{R \rightarrow L} \Delta \mathcal{V}_{R \rightarrow L}^{RTSAH i} |G_L|}{|G_L| + |G_R|}, \quad (C.1.4)$$

and ranges from -1 to 1. Note that the RTSAH cost function includes two visibility probability components,  $\mathcal{V}_{L \rightarrow R}$  and  $\mathcal{V}_{R \rightarrow L}$ , whose associated visibility probability errors,  $\Delta \mathcal{V}_{L \rightarrow R}^{RTSAH i}$  and  $\Delta \mathcal{V}_{R \rightarrow L}^{RTSAH i}$ , can have a positive or negative impact on the cost error when combined. Furthermore,  $p_{L \rightarrow R} \equiv p_{R \rightarrow L} \equiv 1/2$   $p_{L \leftrightarrow R} \equiv \frac{SA_S}{SA_P}$  is a measure of the surface area of the splitting plane relative to the surface area of the AABB of the parent voxel. To analyse the contribution of each of these components, we will consider the following

<sup>8</sup>Here, we actually refer to a variant of the GCM [Hav00] which only uses ray sampling to calculate the visibility probabilities as opposed to the standard GCM which uses ray sampling to calculate both the piercing and visibility probabilities.

<sup>9</sup>In a multi-threaded rendering system, the local difference in the number of ray-triangle intersection tests and ADS node traversal steps can have a larger impact than the global difference as the time to render image chunks will vary spatially.

<sup>10</sup>Different candidate partitions can be considered optimal according to some RTSAH approximation, resulting in different sets of candidate partitions to consider at the lower levels of the tree. Only the candidate partitions for the root voxel are guaranteed to be considered, independent of the used cost function.

<sup>11</sup>Candidate partitions with  $p_{L \leftrightarrow R} \leq 0.05$  are not considered, since the impact of the visibility probabilities on the RTSAH cost function will be negligible, independent of their values. Furthermore, note that  $p_{L \leftrightarrow R} = \frac{2SA_S}{SA_P}$  is a constant value for all candidate partitions for the same parent voxel,  $V_P$ , for a fixed split axis. Therefore, the cost function (including its extrema) will be completely determined by the piercing probabilities,  $p_{jL}$  and  $p_{jR}$ , in these cases.

modified cost errors instead:

$$\Delta C'_{\text{RTSAH } i} := \frac{\Delta \mathcal{V}_{\text{L} \rightarrow \text{R}}^{\text{RTSAH } i} |G_{\text{R}}| + \Delta \mathcal{V}_{\text{R} \rightarrow \text{L}}^{\text{RTSAH } i} |G_{\text{L}}|}{|G_{\text{L}}| + |G_{\text{R}}|} \quad (\text{C.1.5})$$

$$\Delta C''_{\text{RTSAH } i} := p_{\text{L} \leftrightarrow \text{R}} \Delta C'_{\text{RTSAH } i} = 1/2 \Delta C_{\text{RTSAH } i}. \quad (\text{C.1.6})$$

- A *split position error* is defined as the absolute difference between the optimal normalized split position, according to the approximated (discretized) RTSAH cost, and the optimal normalized split position, according to the ground truth (discretized) RTSAH cost for the same split axis. Here, split positions are normalized over the spatial extent of the AABB of the parent voxel along the split axis. Note that split positions are only compared for the same split axis. The distribution of split position errors, however, includes samples for all three primary axes.

Furthermore, we also compute the percentage of cases where the optimal split axis, according to the approximated (discretized) RTSAH cost, is equal to the optimal split axis, according to the ground truth (discretized) RTSAH cost. The error distributions are shown in Tables 39 to 68.

Given the top-down construction of our kd-trees, not all candidate partitions have the same impact on the final shape of the kd-trees. Our different error distributions do not differentiate between the levels of the tree. Since the number of splitting planes (and thus candidate partitions) for our artificial test scenes is chosen linear in the number of the geometric primitives to partition, an equal number of candidate partitions would be considered for each level of a balanced tree in case of no duplication of references to geometric primitives. The actual duplication of references to geometric primitives, however, is high for kd-trees, resulting in a bias towards the lower levels of the tree (i.e. less populated candidate partitions).

The SAH always assumes both empty and non-empty child voxels to be completely non-blocking, resulting in only non-negative visibility probability and cost errors. The RTSAH Z always assumes non-empty child voxels to be completely blocking, resulting in only non-positive visibility probability and cost errors. The other RTSAH approximations are in between these two extremes.

The visibility error probability distributions for all our RTSAH approximations (except for RTSAH Z|N) have a large peak near zero due to two recurring cases:

1. Empty child voxels (i.e.  $|G_i| = 0$ ). For an empty child voxel the visibility probability error will be zero for all our RTSAH approximations (including RTSAH Z|N). Such empty child voxels are common in **Empty Box** and **Cornell Box**. In these scenes, both RTSAH Z|N (which are only count based) have a large peak near zero.
2. Non-empty child voxels (i.e.  $|G_i| \neq 0$ ) of which the AABBs ( $B_i$ ) overlap with a negligible part of the contained geometric primitives or overlap not at all. Kd-trees are generally built by partitioning the AABBs of the geometric primitives instead of the geometric primitives themselves.<sup>12</sup> Since the geometric primitives in our test scenes are triangles, their AABBs are not very tight bounding volumes. The surface area of the AABB for both axis-aligned and non-axis-aligned triangles is substantially larger than the surface area of the contained triangle. Therefore,  $B_i$  can overlap the AABB without overlapping the contained geometric primitive. Furthermore, our icosahedra (20 triangles) are edge-connected, watertight, manifold meshes of which some AABBs overlap. Due to the empty space contained in these overlaps,  $B_i$  can overlap multiple AABBs without overlapping any contained geometric primitive. For  $1 < |G_p|$ , we will consider 20  $G_p$  candidate partitions for each primary axis.<sup>13</sup> Our clipping based visibility probability approximations, our ray-tracing based ground truth, and even the SAH all handle such cases correctly, whereas our count based visibility probability approximations (RTSAH Z|N)<sup>14</sup> will result in underestimations.

The  $\Delta C'_{\text{RTSAH } i}$  distribution is similar to our  $\Delta \mathcal{V}_{\text{RTSAH } i}$  distribution, but with a smaller deviation from the mean. If  $|G_{\text{L}}| > |G_{\text{R}}|$ , then  $\Delta \mathcal{V}_{\text{L} \rightarrow \text{R}}^{\text{RTSAH } i}$  tends to be higher than  $\Delta \mathcal{V}_{\text{R} \rightarrow \text{L}}^{\text{RTSAH } i}$  and vice versa, but since  $\Delta \mathcal{V}_{\text{L} \rightarrow \text{R}}^{\text{RTSAH } i}$  ( $\Delta \mathcal{V}_{\text{R} \rightarrow \text{L}}^{\text{RTSAH } i}$ ) is multiplied by  $|G_{\text{R}}|$  ( $|G_{\text{L}}|$ ), the cost error,  $\Delta C'_{\text{RTSAH } i}$ , becomes smaller. For the  $\Delta C''_{\text{RTSAH } i}$

<sup>12</sup>Split clipping [HB02] is an optimization for building kd-trees by partitioning the geometric primitives (instead of their AABBs) relative to the splitting plane by using clipping.

<sup>13</sup>Note that the optimal candidate partition can still be rejected (see Subsection B.8). Though, the maximum fixed tree depth, based on the total number of geometric primitives in the scene, is always reached along some tree branches for our artificial test scenes (see Table 14).

<sup>14</sup>A possible optimization consists of evaluating RTSAH Z|N for the remaining geometric primitives after clipping, at the expense of a higher build time.

distribution the deviation decreases further due to the multiplication by  $p_{L \leftrightarrow R}$ . For  $p_{L \leftrightarrow R} \rightarrow 0$ , the contribution of the visibility probabilities becomes negligible with respect to the cost function, which will be completely determined by the less conditional piercing probabilities,  $p_{j_L}$  and  $p_{j_R}$ .

The cost error distribution is not necessarily representative for the split position error distribution. A constant cost error, does not change the course of the cost function or the positions of its extrema.<sup>15</sup> The split position error distribution has a peak near zero for all approximations including the SAH and RTSAH Z, which use a constant visibility probability, and RTSAH N|SA, which gradually adapt the visibility probability to the number of geometric primitives and the total clipped surface area of these geometric primitives, respectively. Furthermore, the piercing probabilities,  $p_{j_L}$  and  $p_{j_R}$ , are less conditional than the visibility probabilities, resulting in a larger impact on all our RTSAH cost functions in general. Apart from this peak, all split position error distributions have a small tail towards one, of which the impact on the tree quality is difficult to measure. The higher the level of the tree affected by a split position error, the larger the impact on the ray traversal will be for a scene-exterior isotropic ray distribution. This scene-exterior isotropic ray distribution, however, does neither correspond to our assumed parent-exterior isotropic ray distribution nor to the actual ray distribution. Furthermore, a split position error will indirectly impact the considered candidate partitions and split positions for the levels beneath. So split position errors on the lower levels have less impact on the ray traversal than split position errors on the higher levels, but the impact of the latter can be reduced by its complete subtree underneath. Finally, the impact itself can go both ways (i.e. positive or negative) due to the greedy construction of the kd-trees according to a local instead of global RTSAH cost function.

For the split axis error distribution, the SAH and RTSAH APSA|APE|EP are the closest to RTSAH E. These cost functions select a different split axis in less than 7% of the cases for our **Icosahedron** scenes of which the impact on the tree quality is difficult to measure (similar to the split position error).

## C.2. BIHs

We build our BIHs by explicitly considering multiple (locally adapted) candidate partitions for every voxel to partition, and a cost metric such as SAH or RTSAH to chose among these candidate partitions whereas Wächter and Keller [WK06] greedily refine a global regular grid.

We see similar results as for kd-trees and similar differences between the various build heuristics. RTSAH Z|N still have a destructing impact on the tree quality and the ray tracing performance. RTSAH E is only capable of outperforming SAH (SP) for **Icosahedron1** and **Icosahedron3** with gains in the number of ray-triangle intersection tests of up to 6% (camera) and 8% (ambient). The differences in the number of ray-triangle intersection tests and ADS node traversal steps as opposed to SAH (SP) (superset of candidate partitions) and SAH (same candidate partitions) is, however, much larger as is the case for kd-trees over the whole range of artificial and realistic test scenes. Remarkably, all our RTSAH approximations result in gains ranging from 89 to 121% (camera) and 61 to 78% (ambient) for our largest test scene, **Museum Hall** (Viewpoint 1). Here, both SAH (SP) and SAH (but also RTSAH APSA) have some heavily populated ( $|G_i| > 750$ ) leaf nodes. With regard to the remaining tree statistics, the constructed BIHs are very similar.

**Error distributions.** Since we use the explicit RTSAH cost function (3.4) for constructing both kd-trees and BIHs, we sample the same errors for our BIHs as for our kd-trees. The error distributions are shown in Tables 69 to 98.

The visibility error probability distributions for all our RTSAH approximations (except for RTSAH Z|N) have a large peak near zero due to two recurring cases:

1. Empty child voxels (i.e.  $|G_i| = 0$ ). For an empty child voxel the visibility probability error will be zero for all our RTSAH approximations (including RTSAH Z|N). A candidate partition containing such an empty child voxel,  $V_i$ , is explicitly considered if the AABB of the other child voxel is strictly smaller than the AABB of the parent voxel (i.e.  $p_{j_i} = 0$  and  $p_{j_e} \neq 0$ ).
2. Non-empty child voxels (i.e.  $|G_i| \neq 0$ ) of which the non-overlapping parts of their AABBs (i.e.  $B_L \setminus B_R$  or  $B_R \setminus B_L$ ) overlap with a negligible part of the contained geometric primitives or overlap not at all.

---

<sup>15</sup>To decide on tree termination (see Subsection B.8), however, a constant cost error may not be arbitrarily large.

The part of the geometric primitives that spatially overlaps with both  $B_L$  and  $B_R$  has no effect on the visibility probabilities, since rays cannot be terminated upon intersection before traversing both child voxels. Since only one out of six (instead of all six) planes of the AABBs of the child voxels is tight,  $B_L \setminus B_R$  and/or  $B_R \setminus B_L$  can overlap no geometric primitives<sup>16</sup>. Furthermore, it is possible to have  $p_{j_\varepsilon} = 0$  and  $p_{j_L} = 0$  ( $p_{j_R} = 0$ ), indicating that  $B_L$  ( $B_R$ ) and all of the contained geometric primitives,  $G_L$  ( $G_R$ ), are completely overlapped by  $B_R$  ( $B_L$ ), resulting in  $\mathcal{V}_{L \rightarrow R} = 1$  ( $\mathcal{V}_{R \rightarrow L} = 1$ ). Our clipping based visibility probability approximations, our ray-tracing based ground truth, and even the SAH all handle such cases correctly, whereas our count based visibility probability approximations (RTSAH Z|N)<sup>17</sup> will result in underestimations.

The conclusions for the  $\Delta C'_{\text{RTSAH } i}$  and  $\Delta C''_{\text{RTSAH } i}$  distributions are similar to those for kd-trees. Note that RTSAH APSA generally results in substantially better approximations than SAH for the ground truth RTSAH E. Due to the impact of the less conditional piercing probabilities and the importance of the positions of the cost function's extrema as opposed to the cost function errors, however, the SAH still remains very competitive with regard to the selection of the optimal split position and split axis. Furthermore, since at most  $|G_P|+1$  candidate partitions are considered per split axis for a voxel,  $V_P$ , to partition, selecting the optimal candidate partition is less difficult for less populated voxels, which are ubiquitous at the lower levels of the tree. Additionally, the spatial extent of the centroids of the geometric primitives contained in  $V_P$ , is often smaller than the spatial extent of the AABB of  $V_P$ . This explains the smaller deviations and tails in the split position error distributions for BIHs compared to those for kd-trees.

The SAH and RTSAH APSA cost functions select a different split axis in less than 10% of the cases for our **Icosahedron** scenes of which the impact on the tree quality is difficult to measure (similar to the split position error).

### C.3. BVHs

In our artificial test scenes, RTSAH E generally outperforms SAH (SP) and SAH with gains in the number of ray-triangle intersection tests of at most 5%.

In our realistic test scenes, the average number of ADS node traversal steps for our RTSAH approximations is slightly smaller on average compared to the SAH. The gains in the number of ray-triangle intersection tests as opposed to SAH (SP) (superset of candidate partitions) varies on average between 0 and 1% (camera and ambient), which is close to the already low (e.g., compared to kd-trees) absolute number of ray-triangle intersection tests. With regard to the tree statistics, the constructed BVHs are very similar, although we notice few deep branches (**Conference Room**, **Carnival** and **Crytek Sponza** which for the latter results in some geometric primitive residues at the maximum tree depth).

**Error distributions.** Since we use the implicit RTSAH cost function (3.18) for constructing BVHs, we cannot sample the visibility probability errors (C.1.3). Therefore, we define the *combined piercing and visibility probability error* as the difference between the approximated and ground truth combined piercing and visibility probability:

$$\Delta p_{vL}^{\text{RTSAH } i} = p_{vL}^{\text{RTSAH } i} - p_{vL}^{\text{RTSAH E}} \quad (\text{C.3.1})$$

$$\Delta p_{vR}^{\text{RTSAH } i} = p_{vR}^{\text{RTSAH } i} - p_{vR}^{\text{RTSAH E}} \quad (\text{C.3.2})$$

$$\Delta p_v^{\text{RTSAH } i} := \Delta p_{vL}^{\text{RTSAH } i} | \Delta p_{vR}^{\text{RTSAH } i}, \quad (\text{C.3.3})$$

which ranges from -1 to 1. Note that both  $p_{vL}$  and  $p_{vR}$  samples are included (i.e. two samples per candidate partition). The error distributions are shown in Tables 99 to 122.

Since all six planes of the AABBs of the child voxels are tight, candidate partitions with empty child voxels are not considered. Similar to BIHs, the part of the geometric primitives that spatially overlaps with both  $B_L$  and  $B_R$  has no effect on the combined piercing and visibility probabilities, since rays cannot be terminated upon intersection before traversing both child voxels.

<sup>16</sup>This is not possible for the candidate partitions of the root voxel.

<sup>17</sup>A possible optimization consists of setting  $\mathcal{V}_{L \rightarrow R} = 1$  ( $\mathcal{V}_{R \rightarrow L} = 1$ ) if  $p_{jL} = 0$  ( $p_{jR} = 0$ ). Or the more general optimization of evaluating RTSAH Z|N for the remaining geometric primitives after clipping, can be used.

The combined piercing and visibility probability error distributions for all our RTSAH approximations have a large peak near zero.  $p_{vL}$  and  $p_{vR}$  are determined by the transfer matrices of each grid cell (4.13) and our assumed parent-exterior isotropic ray distribution (3.22). For the planes of the AABB of a child voxel coinciding with the AABB of the parent voxel, the incoming ray fractions (from outside) are calculated exactly. In case of three such planes, these incoming ray fractions contribute for at least 50% of  $p_{vi}$ . For the planes of the AABB of a child voxel not coinciding with the AABB of the parent voxel, the incoming ray fractions (from outside) first traversed part of the parent voxel not belonging to this child voxel. This part is either empty space (i.e. belongs to none of the child voxels), in which case the traversal is determined by the plane-to-plane form factors (A.2)–(A.3) (i.e. no occlusion), or belongs to the other child voxel, in which case the traversal is (approximately) determined by the plane-to-plane form factors (A.2)–(A.3) and the plane visibility probabilities (4.1). To obtain  $\Delta p_v^{\text{RTSAH}i} = -1$ , a necessary (but not sufficient) condition requires the AABB of one child voxel to be strictly overlapped by the AABB of the other child voxel. Some  $\Delta p_v^{\text{RTSAH}i} > 0.5$  are obtained for **Empty Box**, **Cornell Box** and **Icosahedron4** due to their large axis-aligned triangles. Generally for our test scenes, however, the impact of the more conditional visibility probabilities, after accumulating all incoming ray fractions to obtain  $p_{vL}$  and  $p_{vR}$ , is small compared to the plane-to-plane form factors and assumed parent-exterior isotropic ray distribution.

The  $\Delta C_{\text{RTSAH}i}$  distribution is similar to our  $\Delta p_v^{\text{RTSAH}i}$  distribution, but with a smaller deviation from the mean. If  $|G_L| > |G_R|$ , then  $\Delta p_{vL}^{\text{RTSAH}i}$  tends to be higher than  $\Delta p_{vR}^{\text{RTSAH}i}$  and vice versa, but since  $\Delta p_{vR}^{\text{RTSAH}i}$  ( $\Delta p_{vL}^{\text{RTSAH}i}$ ) is multiplied by  $|G_R|$  ( $|G_L|$ ), the cost error,  $\Delta C_{\text{RTSAH}i}$ , becomes smaller. Due to the impact of the plane-to-plane form factors and the importance of the positions of the cost function's extrema as opposed to the cost function errors, however, the SAH still remains very competitive with regard to the selection of the optimal split position and split axis. Furthermore, since at most  $|G_p|-1$  candidate partitions are considered per split axis for a voxel,  $V_p$ , to partition, selecting the optimal candidate partition is less difficult for less populated voxels, which are ubiquitous at the lower levels of the tree. Additionally, the spatial extent of the centroids of the geometric primitives contained in  $V_p$ , is often smaller than the spatial extent of the AABB of  $V_p$ . This explains the smaller deviations and tails in the split position error distributions for BVHs compared to those for kd-trees.

All approximated RTSAH cost functions select a different split axis compared to RTSAH E in between 40 and 50% of the cases. These percentages are higher compared to those obtained for kd-trees and BIHs. Due to the tightness of the six planes of the AABBs of the child voxels, the RTSAH cost function has no constant components depending on the split axis. The candidate partitions for the same voxel to partition for the same split axis for kd-trees and BIHs, on the other hand, use splitting planes with a constant surface area (impacting the piercing probabilities and thus the cost functions).<sup>18</sup>

## C.4. SBVHs

In our artificial test scenes, RTSAH E always selects a BVH candidate partition and thus constructs a pure BVH (i.e. no spatial splits) in the end. For these scenes, the BVH contribution considers all possible candidate splitting planes (independent of the number of geometric primitives to partition), whereas our GK-BVH contribution generally considers a subset of all possible candidate splitting planes. This strategy works out for the geometrically more difficult **Icosahedron3** and **Icosahedron4** scenes, is similar for **Icosahedron2** (which is easier to partition due to its uniformly distributed geometry), and does not work out for **Icosahedron1** as opposed to SAH.

In our realistic test scenes, the average number of ADS node traversal steps for our RTSAH approximations is 2 to 11% (camera and ambient) larger than SAH as expected, since the RTSAH cost of a candidate partition could not be larger than the corresponding SAH cost and since the average tree depth is small (e.g., compared to kd-trees). The gains in the number of ray-triangle intersection tests as opposed to SAH vary on average between 0 and 5% (camera) with exception of RTSAH APSA|EP. The difference occurs in **Conference Room**. Here, RTSAH (WN(WC))HANPSA2|APE result in gains ranging from 15 to 38% (camera), whereas RTSAH APSA|EP suffer losses down to 53% (camera). The latter are less capable of capturing the occlusion due to large non-axis-aligned interior planes. For the third viewpoint of **Bedroom**, our RTSAH approximations perform notably worse than SAH. This viewpoint is, however, a very specific viewpoint illuminating only a small part of the scene. In **Museum-Hall**, RTSAH HANPSA2 is outperformed by RTSAH WNHANPSA2 which explicitly weights the geometric normals. With regard to the tree statistics, the SBVHs constructed with

<sup>18</sup>After partitioning a parent voxel into child voxels, given a splitting plane, that splitting plane is not explicitly present any more between the AABBs of the child voxels for BVHs as is the case for kd-trees and BIHs.

RTSAH APSA|APE have a larger number of leaf nodes and higher reference duplication compared to SAH and RTSAH (WN(WC))HANPSA2. The SBVs constructed with RTSAH (WN(WC))HANPSA2 are closer to SAH. For *Carnival*, RTSAH APSA|HANPSA2|APE and SAH result in some heavily populated leaf nodes (although having no very deep branches) which is not reflected in the number of ray-triangle intersection tests.

## C.5. BVHs dedicated to shadow ray traversal

NodeSATO [NM14] outperforms, as expected, all the naive voxel traversal orders for shadow rays (OB, IO, (L|R|U)DF, and (C|F)CF) [IH11, NM14] in the same BVHs constructed with the SAH. The BVHs constructed with SRDH Z|N|SA|APE(2) result in very deep and skewed trees with heavily populated leaf nodes at the maximum tree depth. The number of ray-triangle intersection tests and ADS node traversal steps is much larger than for the naive voxel traversal orders. Since a comparison provides no added value, we do not tabulate the results of those build heuristics. Similarly, all the BVHs constructed with SRDH' APSA|APE(2) result in very skewed trees with one heavily populated leaf node at the maximum tree depth. At every partition step, only a small number of geometric primitives is cut off in one of the child voxels due to the clamping operator that needs to ensure that the AABB hit probabilities (5.19) lie in  $[0, 1]$ .<sup>19</sup>

The number of ray-triangle intersection tests for SRDH E and SRDH' E is very close to NodeSATO, but the number of ADS node traversal steps increased by a factor up to seven (SRDH' E) and sixteen (SRDH E) for our artificial test scenes. Also note that the SRDH' which is derived from the SRDH by assuming worst-case behaviour ( $p_L \equiv p_R \equiv 1$ ), results in a similar number of ray-triangle intersection tests but smaller number of ADS traversal steps compared to the SRDH. SRDH APSA reduces the number of ray-triangle intersection tests on average by 22% with peaks up to 61% compared to NodeSATO while performing 86% more ADS node traversal steps. SRDH' N and SRDH' SA have a more balancing impact on the constructed BVHs. SRDH' N is generally outperformed by NodeSATO with regard to the number of ray-triangle intersection tests and leads to a huge increase in the number of ADS node traversal steps. The structure of the constructed BVHs is closer to OMS than SAH (i.e. shallow and perfectly balanced). Due to their balancing, leaf nodes occur far from the root node. The number of ADS node traversal steps, however, is exceptionally high and not close to any of our approaches. SRDH' SA reduces the number of ray-triangle intersection tests on average by 22% with peaks up to 113% compared to NodeSATO while performing 71% more ADS node traversal steps. Furthermore, this *geometric primitive surface area - count* balancing of SRDH' SA (which results on average in less deep trees than SAH) cannot be achieved with OMS or SMS which all result in considerably more ray-triangle intersection tests.

## C.6. Discussion

The RTSAH generalizes the SAH by including local ray termination in the cost function. Therefore, the (local) RTSAH cost function (3.4) results in the exact cost if candidate partitions are considered in isolation (i.e. not as part of a tree) and if the actual ray distribution corresponds to the assumed parent-exterior isotropic ray distribution. The RTSAH exploits the occlusion between voxels resulting in smaller and different costs compared to the SAH, leading to different split decisions and allowing further refinement. The SAH cost function (3.1) results in a less accurate cost prediction in the presence of geometric primitives. Though, due to the impact of the less conditional piercing probabilities (which do not take occlusion into account and are thus part of both the RTSAH and SAH cost functions) and the importance of the positions of the cost function's extrema as opposed to the cost function errors, the SAH is still competitive in selecting optimal candidate partitions close to those selected by the RTSAH.

When the local RTSAH cost function is used for greedily constructing a complete tree, we notice larger ADS trees resulting in more ray-triangle intersection tests and/or ADS node traversal steps for certain scenes and their associated actual ray distributions compared to the SAH. On the one hand, the actual ray distribution over the entire scene, does not correspond to a parent-exterior isotropic ray distribution for each parent voxel in the ADS tree. On the other hand, the local RTSAH cost function misses a component that properly takes care of the recursive traversal cost of the actual ray tracing through the ADS trees. The SAH, however, is used in a greedy way as well to construct the ADS trees, but due to its worst-case assumptions the refinement of tree branches can be terminated more early. Using a greedy divide-and-conquer approach is not guaranteed to

---

<sup>19</sup>We use a similar clamping operator for the plane visibility probabilities in the RTSAH. Here, this operator is less critical due to the presence of the (less conditional) piercing probabilities. Of course, the operator can become critical (degenerating to RTSAH Z) for some RTSAH approximations in scenes with many overlapping geometric primitives.

behave well for the RTSAH as is the case for the SAH. ADS construction can get stuck in local minima of the global RTSAH cost function. Furthermore, a greedy divide-and-conquer approach does not guarantee that the obtained ADSs are close to the global optimal ADS (of which the construction is *NP-hard*) according to the global RTSAH cost metric.

The largest drawback, however, for using the RTSAH is the built time. The workload per voxel,  $V_p$ , to partition can be expressed in the number of triangle-AABB clipping operations. A single kd-tree and BIH candidate partition require  $|G_p|$  clipping operations whereas a BVH and GK-BVH candidate partition require worst-case 27  $|G_p|$  clipping operations (since the maximal grid size is  $3 \times 3 \times 3$  voxels). Considering 3 axes and 256 candidate partitions per axis, results in 768  $|G_p|$  clipping operations for kd-trees and BIHs, 20736  $|G_p|$  clipping operations for BVHs and 41472  $|G_p|$  clipping operations for SBVHs (without restricting spatial splits), per voxel to partition. The complete ADS construction, can therefore take up to several hours<sup>20</sup> for large numbers of geometric primitives (e.g., primitive duplication in BSPs and SBVHs), which could not be compensated by the slight gains in rendering time.

Using ray sampling with 4096 rays in a preconstructed ADS, would require the tracing of 3 M rays for kd-trees and BIHs, 85 M rays for BVHs and 170 M rays for SBVHs (without restricting spatial splits), per voxel to partition. A closest-hit ray query using a preconstructed tree ADS has an average time complexity of  $\mathcal{O}(\log|G_s|)$  with  $|G_s|$  the total number of geometric primitives in the scene. So the number of rays traced during the ADS construction will be much higher than the number of rays traced during the actual ray tracing, which goes against the purpose of an ADS in the first place. The complete ADS construction, can therefore take up to multiple weeks for large numbers of geometric primitives.

The build time performance differences for our realistic test scenes are shown in Table 38. SAH (SP) builds are faster than binned (RT)SAH builds without triangle-AABB clipping operations (e.g., SAH, RTSAH Z|N). This difference is primarily due to the modular software design used for our implementation. To ease the integration and experimentation with a wide variety of heuristics at different levels of the ADS construction, our binned build algorithms are decomposed into several logical steps (candidate partition selection, creation, visibility evaluation and cost evaluation), resulting in multiple passes over the contained geometric primitives per candidate partition. Removing and collapsing these different abstraction levels and per heuristic optimizations, can improve build time performance of our binned builds, but are not the focus of our study.<sup>21</sup> For more information about the design of our implementation, see our other supplementary material. The remaining binned builds, perform worse due to the large number of triangle-AABB clipping operations involved. The build time performance differences are the largest for BVHs, since the contained geometric primitives are clipped against the irregular grid cells constituting each candidate partition. For SBVHs, additional clipping is always required for creating the candidate partitions, resulting in smaller differences compared to the reference (SAH). Kd-trees require less clipping operations per candidate partition, but contain more tree nodes and result in large primitive duplication factors.

The rendering time performance differences for our realistic test scenes are shown in Table 38 and include, among other factors, both the ray-triangle intersection tests and ADS node traversal steps, which were discussed before in more depth and detail. As expected, the overall impact on the rendering time is in general small due to the small differences in the number of ray-triangle intersection tests and ADS node traversal steps. Furthermore, gains in ray-triangle intersection tests are often compensated by losses in ADS node traversal steps, resulting in rendering times close to the references.

In the case of SRDH and SRDH' for constructing dedicated BVHs for any-hit ray queries, no triangle-AABB clipping operations are required, since all geometric primitives are fully contained inside a single child voxel. The build time is comparable to SAH (SP) (with the difference of having two separate ADSs instead of one). SRDH' SA reduces the number of ray-triangle intersection tests on average by 22%, but due to its balancing effect on the tree construction, geometric primitives occur on lower tree levels compared to SAH (SP), resulting in an average increase of the number of ADS node traversal steps (which includes a ray-AABB intersection test for BVHs) by 71% compared to NodeSATO. The latter has generally a negative impact on the rendering performance (see Table 38).

---

<sup>20</sup>For our experiments, we use a single-threaded build.

<sup>21</sup>Furthermore, both our single-threaded sweeping plane and binned builds can be parallelized. The efficiency of the parallelization depends, among other factors, on the optimality of the load balancing which is more straightforward to account for in binned builds.

Kd-tree												
Build heuristic	Average case				Best case				Worst case			
	$\Delta I_c$	$\Delta T_c$	$\Delta I'_s$	$\Delta T'_s$	$\Delta I_c$	$\Delta T_c$	$\Delta I'_s$	$\Delta T'_s$	$\Delta I_c$	$\Delta T_c$	$\Delta I'_s$	$\Delta T'_s$
SAH (SP)	-14.43%	7.84%	-10.68%	14.71%	6.74%	18.89%	4.99%	28.66%	-53.54%	-0.72%	-29.74%	5.89%
SAH		Reference			Reference				Reference			
RTSAH Z	-73.09%	-41.04%	-72.69%	-45.73%	-50.26%	-9.64%	-51.53%	-20.05%	-97.92%	-95.19%	-94.14%	-88.76%
RTSAH N	-56.94%	-22.88%	-54.94%	-24.26%	-20.66%	-2.30%	-20.01%	-5.86%	-84.70%	-66.89%	-81.69%	-61.85%
RTSAH SA	-6.78%	-7.95%	-3.94%	-8.09%	21.18%	9.60%	21.23%	-2.17%	-37.21%	-25.66%	-25.13%	-16.46%
RTSAH APSA	0.45%	-1.67%	2.26%	-2.33%	11.94%	14.19%	17.96%	1.52%	-10.02%	-12.30%	-2.41%	-7.25%
RTSAH HANPSA2	-3.20%	-5.73%	-1.46%	-8.54%	3.60%	13.35%	8.75%	-3.47%	-15.45%	-17.93%	-8.97%	-14.48%
RTSAH WNHANPSA2	-1.57%	-5.73%	-0.63%	-8.41%	5.91%	16.04%	10.18%	-3.07%	-8.98%	-36.96%	-8.52%	-21.81%
RTSAH WNWCHANPSA2	-3.08%	-6.43%	-2.30%	-9.58%	3.75%	18.17%	5.98%	-2.85%	-15.87%	-47.95%	-9.99%	-31.00%
RTSAH EP	-0.36%	-5.42%	-0.86%	-5.46%	15.05%	4.06%	19.48%	-1.48%	-13.97%	-22.43%	-14.72%	-15.20%
RTSAH APE	0.22%	-3.94%	2.31%	-3.19%	18.58%	6.65%	13.45%	-0.74%	-21.26%	-18.95%	-1.98%	-8.68%
BIH												
Build heuristic	Average case				Best case				Worst case			
	$\Delta I_c$	$\Delta T_c$	$\Delta I'_s$	$\Delta T'_s$	$\Delta I_c$	$\Delta T_c$	$\Delta I'_s$	$\Delta T'_s$	$\Delta I_c$	$\Delta T_c$	$\Delta I'_s$	$\Delta T'_s$
SAH (SP)		Reference			Reference				Reference			
SAH	-0.33%	1.54%	-1.07%	0.43%	8.22%	18.12%	12.96%	13.45%	-7.80%	-9.07%	-12.66%	-7.25%
RTSAH Z	-83.05%	-62.33%	-78.55%	-58.16%	-66.62%	-41.22%	-57.25%	-36.38%	-95.44%	-86.07%	-90.33%	-71.33%
RTSAH N	-25.18%	-30.34%	-24.66%	-26.07%	53.60%	11.22%	26.97%	12.83%	-68.33%	-63.99%	-57.13%	-51.63%
RTSAH SA	3.33%	-4.15%	-0.55%	-6.88%	98.42%	12.87%	60.57%	3.36%	-40.26%	-17.87%	-32.27%	-15.63%
RTSAH APSA	1.09%	-6.03%	-2.49%	-7.48%	88.38%	20.95%	61.16%	4.53%	-39.33%	-44.22%	-28.23%	-20.15%
RTSAH HANPSA2	-2.81%	-17.30%	-1.01%	-15.62%	102.95%	5.37%	67.08%	0.20%	-47.58%	-40.30%	-41.03%	-35.22%
RTSAH WNHANPSA2	-3.55%	-18.35%	-2.74%	-16.97%	108.36%	6.37%	68.65%	-1.35%	-47.05%	-48.71%	-37.47%	-38.44%
RTSAH WNWCHANPSA2	-6.18%	-17.85%	-3.66%	-15.61%	120.97%	13.23%	75.07%	-0.73%	-50.67%	-60.06%	-35.85%	-37.80%
RTSAH EP	-13.54%	-8.01%	-8.67%	-5.82%	89.27%	15.88%	62.21%	7.87%	-59.89%	-43.57%	-44.26%	-31.52%
RTSAH APE	-7.80%	-9.73%	-4.80%	-7.47%	115.82%	9.74%	77.65%	8.39%	-61.54%	-44.59%	-45.32%	-32.78%
BVH												
Build heuristic	Average case				Best case				Worst case			
	$\Delta I_c$	$\Delta T_c$	$\Delta I'_s$	$\Delta T'_s$	$\Delta I_c$	$\Delta T_c$	$\Delta I'_s$	$\Delta T'_s$	$\Delta I_c$	$\Delta T_c$	$\Delta I'_s$	$\Delta T'_s$
SAH (SP)		Reference			Reference				Reference			
SAH	0.22%	2.97%	0.15%	0.33%	2.10%	24.03%	2.08%	13.36%	-3.61%	-6.95%	-1.07%	-5.69%
RTSAH APSA	0.75%	1.12%	0.50%	-1.04%	3.32%	23.29%	3.27%	12.25%	-1.48%	-11.08%	-0.93%	-8.06%
RTSAH HANPSA2	0.76%	2.08%	0.64%	-0.98%	3.24%	27.46%	3.09%	14.03%	-1.80%	-13.94%	-0.31%	-9.11%
RTSAH WNHANPSA2	0.52%	1.51%	0.46%	-1.26%	3.32%	22.04%	3.28%	11.71%	-2.19%	-14.66%	-0.36%	-8.83%
RTSAH WNWCHANPSA2	0.38%	0.45%	0.38%	-1.75%	2.96%	22.01%	3.16%	11.19%	-3.07%	-12.66%	-0.43%	-10.10%
RTSAH EP	-0.15%	0.46%	0.26%	-0.94%	12.14%	15.14%	2.28%	8.87%	-14.99%	-11.28%	-4.75%	-9.90%
RTSAH APE	0.27%	-0.57%	0.62%	-0.97%	5.34%	13.55%	3.39%	10.62%	-7.58%	-6.21%	-0.64%	-8.07%
SBVH												
Build heuristic	Average case				Best case				Worst case			
	$\Delta I_c$	$\Delta T_c$	$\Delta I'_s$	$\Delta T'_s$	$\Delta I_c$	$\Delta T_c$	$\Delta I'_s$	$\Delta T'_s$	$\Delta I_c$	$\Delta T_c$	$\Delta I'_s$	$\Delta T'_s$
SAH		Reference			Reference				Reference			
RTSAH APSA	-5.67%	-5.16%	0.43%	-5.35%	7.67%	5.34%	16.44%	0.91%	-52.64%	-23.75%	-17.83%	-19.50%
RTSAH HANPSA2	1.43%	-10.10%	-0.58%	-10.48%	35.22%	10.12%	21.59%	-3.78%	-32.36%	-38.05%	-20.15%	-17.97%
RTSAH WNHANPSA2	3.05%	-11.01%	0.74%	-10.67%	38.84%	9.41%	20.98%	-3.44%	-17.47%	-44.67%	-15.99%	-22.52%
RTSAH WNWCHANPSA2	0.53%	-2.82%	-2.10%	-6.47%	35.49%	14.59%	19.44%	3.59%	-18.87%	-17.98%	-27.79%	-13.73%
RTSAH EP	-9.74%	-11.43%	-8.45%	-11.29%	19.53%	3.23%	-0.32%	-2.53%	-30.35%	-32.28%	-23.35%	-24.05%
RTSAH APE	4.59%	-9.90%	1.93%	-8.50%	38.14%	6.58%	17.14%	-1.48%	-6.69%	-24.81%	-5.98%	-16.97%

Table 4: A summary of the gains in the number of ray-triangle intersection tests to perform for primary (camera),  $\Delta I_c$ , and closest-hit shadow (ambient),  $\Delta I'_s$ , rays and the gains in the number of ADS node traversal steps to perform for primary (camera),  $\Delta T_c$ , and closest-hit shadow (ambient),  $\Delta T'_s$ , rays, for different ADSs built with various build heuristics, for a variety of realistic test scenes rendered as ambient occlusion images of resolution 512×512 pixels using 512 primary rays per pixel and 1 shadow ray per primary ray which is not limited to a fixed, finite, maximum distance.

BVH						
Build heuristic	Average case		Best case		Worst case	
	$\Delta I_s$	$\Delta T_s$	$\Delta I_s$	$\Delta T_s$	$\Delta I_s$	$\Delta T_s$
SAH + OB	-40.64%	-47.01%	-25.29%	-29.29%	-59.03%	-60.48%
SAH + IO	-38.06%	-23.93%	-18.45%	18.91%	-68.73%	-73.53%
SAH + <UDF>	-17.37%	-25.79%	10.30%	1.00%	-32.70%	-79.47%
SAH + LDF	-15.46%	-20.90%	28.93%	7.47%	-38.19%	-51.19%
SAH + RDF	-20.68%	-20.78%	11.57%	13.87%	-43.80%	-40.83%
SAH + CCF	-29.08%	-33.27%	-1.40%	-4.20%	-57.26%	-54.22%
SAH + FCF	5.65%	5.07%	79.18%	63.89%	-28.64%	-48.30%
SAH + NodeSATO		Reference		Reference		Reference
OMS + NodeSATO	1.04%	-74.16%	56.96%	-48.50%	-32.92%	-83.36%
SMS + NodeSATO	-14.02%	-46.72%	3.04%	-17.67%	-42.46%	-65.47%
SRDH APSA	11.09%	-86.24%	60.54%	-72.39%	-21.89%	-99.06%
SRDH' N	-23.20%	-98.76%	19.06%	-96.51%	-54.72%	-99.76%
SRDH' SA	22.36%	-71.01%	112.83%	-40.33%	-23.65%	-96.09%

Table 5: A summary of the gains in the number of ray-triangle intersection tests,  $\Delta I_s$ , and the gains in the number of ADS node traversal steps,  $\Delta T_s$ , to perform for any-hit shadow (ambient) rays, for a BVH ADS built with various build heuristics, for a variety of realistic test scenes rendered as ambient occlusion images of resolution 512×512 pixels using 512 primary rays per pixel and 1 shadow ray per primary ray which is not limited to a fixed, finite, maximum distance.

Build heuristic	Kd-tree											
	I <sub>c</sub>	ΔI <sub>c</sub>	T <sub>c</sub>	ΔT <sub>c</sub>	I' <sub>s</sub>	ΔI' <sub>s</sub>	T' <sub>s</sub>	ΔT' <sub>s</sub>	I <sub>s</sub>	ΔI <sub>s</sub>	T <sub>s</sub>	ΔT <sub>s</sub>
	Empty Box											
SAH (SP)	10.59	-81.11%	3.44	267.71%	10.49	-80.08%	3.37	428.83%	6.44	-73.54%	3.00	493.27%
SAH	2.00	Ref.	12.64	Ref.	2.09	Ref.	17.80	Ref.	1.70	Ref.	17.80	Ref.
RTSAH E	2.00	-0.17%	14.88	-15.05%	1.56	34.02%	18.81	-5.39%	1.17	46.09%	18.79	-5.26%
RTSAH Z	2.00	0.00%	14.81	-14.68%	1.55	35.19%	18.82	-5.41%	1.16	46.89%	18.82	-5.41%
RTSAH N	2.00	0.00%	14.85	-14.87%	1.55	35.17%	19.07	-6.64%	1.16	46.87%	19.07	-6.65%
RTSAH SA	2.00	0.00%	14.85	-14.90%	1.55	35.17%	18.93	-5.99%	1.16	46.88%	18.93	-5.99%
RTSAH APSA	2.00	0.00%	14.89	-15.14%	1.55	35.09%	19.08	-6.71%	1.16	46.75%	19.08	-6.71%
RTSAH HAPSA	2.00	0.00%	14.95	-15.48%	1.55	34.91%	20.90	-14.82%	1.16	46.50%	20.90	-14.82%
RTSAH WCHAPSA	2.00	0.00%	14.95	-15.49%	1.55	35.02%	20.24	-12.08%	1.16	46.65%	20.24	-12.08%
RTSAH HANPSA	2.00	0.00%	14.81	-14.66%	1.55	35.18%	18.83	-5.46%	1.16	46.89%	18.83	-5.47%
RTSAH WNHANPSA	2.00	0.00%	14.81	-14.67%	1.55	35.08%	18.91	-5.87%	1.16	46.74%	18.91	-5.87%
RTSAH WNWCHANPSA	2.00	0.00%	14.82	-14.75%	1.55	35.18%	18.85	-5.56%	1.16	46.90%	18.85	-5.56%
RTSAH HANPSA2	2.00	0.00%	14.74	-14.28%	1.55	35.22%	20.94	-15.02%	1.16	46.94%	20.94	-15.02%
RTSAH WNHANPSA2	2.00	0.00%	14.74	-14.28%	1.55	35.22%	20.94	-15.02%	1.16	46.94%	20.94	-15.02%
RTSAH WNWCHANPSA2	2.00	0.00%	14.29	-11.58%	1.55	35.24%	20.32	-12.40%	1.16	46.97%	20.32	-12.40%
RTSAH EP	2.00	0.00%	14.70	-14.05%	1.54	35.24%	18.75	-5.05%	1.16	46.98%	18.75	-5.05%
RTSAH APE	2.00	0.00%	14.52	-12.97%	1.54	35.24%	18.57	-4.16%	1.16	46.98%	18.57	-4.16%
RTSAH HAPE	2.00	0.00%	14.81	-14.69%	1.54	35.26%	20.90	-14.85%	1.16	47.00%	20.90	-14.85%
RTSAH EP2	2.00	0.00%	16.55	-23.63%	1.55	35.13%	21.09	-15.61%	1.16	46.82%	21.09	-15.61%
RTSAH APE2	2.00	0.00%	17.59	-28.15%	1.55	35.22%	21.25	-16.24%	1.16	46.94%	21.25	-16.24%
RTSAH HAPE2	2.00	0.00%	15.10	-16.30%	1.78	17.35%	19.84	-10.31%	1.39	22.15%	19.84	-10.31%
Cornell Box												
SAH (SP)	7.20	-57.36%	9.83	59.85%	8.25	-55.54%	11.74	82.06%	5.84	-53.85%	10.96	92.55%
SAH	3.07	Ref.	15.71	Ref.	3.67	Ref.	21.37	Ref.	2.69	Ref.	21.11	Ref.
RTSAH E	2.27	35.15%	19.72	-20.35%	2.58	42.16%	24.92	-14.23%	1.99	35.31%	23.54	-10.32%
RTSAH Z	2.48	23.76%	16.52	-4.91%	2.76	32.76%	22.90	-6.69%	2.08	29.57%	22.50	-6.18%
RTSAH N	2.49	23.20%	16.66	-5.71%	2.71	35.40%	22.90	-6.66%	2.03	32.80%	22.47	-6.07%
RTSAH SA	2.30	33.68%	16.63	-5.56%	2.52	45.57%	22.97	-6.98%	1.92	40.35%	22.59	-6.55%
RTSAH APSA	2.31	32.79%	16.68	-5.83%	2.54	44.29%	23.08	-7.40%	1.92	40.45%	22.67	-6.90%
RTSAH HAPSA	2.35	30.62%	17.25	-8.94%	2.66	38.21%	24.33	-12.14%	1.98	36.36%	23.87	-11.55%
RTSAH WCHAPSA	2.47	24.35%	16.84	-6.73%	2.78	32.15%	24.20	-11.69%	2.06	30.66%	23.70	-10.92%
RTSAH HANPSA	2.36	29.93%	16.59	-5.35%	2.55	44.06%	22.78	-6.20%	1.91	40.95%	22.41	-5.81%
RTSAH WNHANPSA	2.37	29.52%	16.64	-5.64%	2.60	41.20%	22.96	-6.91%	1.94	38.54%	22.55	-6.40%
RTSAH WNWCHANPSA	2.49	23.05%	16.70	-5.98%	2.83	29.52%	23.06	-7.33%	2.09	29.04%	22.58	-6.52%
RTSAH HANPSA2	2.38	29.23%	16.67	-5.78%	2.67	37.25%	23.44	-8.82%	2.02	33.20%	23.06	-8.46%
RTSAH WNHANPSA2	2.38	28.79%	16.70	-5.94%	2.77	32.67%	23.48	-8.96%	2.08	29.34%	23.08	-8.53%
RTSAH WNWCHANPSA2	2.43	26.17%	16.75	-6.25%	2.74	33.92%	23.70	-9.81%	2.04	32.23%	23.29	-9.38%
RTSAH EP	2.35	30.86%	16.75	-6.25%	2.52	45.45%	22.68	-5.77%	1.92	40.38%	22.33	-5.47%
RTSAH APE	2.31	33.14%	16.57	-5.22%	2.50	46.52%	22.75	-6.07%	1.89	42.58%	22.38	-5.68%
RTSAH HAPE	2.55	20.23%	17.55	-10.49%	2.86	28.16%	24.37	-12.30%	2.15	25.45%	23.80	-11.32%
RTSAH EP2	2.38	29.16%	17.13	-8.31%	2.68	36.98%	23.80	-10.22%	2.04	32.06%	23.39	-9.75%
RTSAH APE2	2.46	24.70%	17.09	-8.09%	2.75	33.23%	23.84	-10.36%	2.07	29.84%	23.40	-9.81%
RTSAH HAPE2	2.34	31.07%	17.04	-7.82%	2.69	36.31%	23.79	-10.16%	2.02	33.35%	23.36	-9.63%
Icosahderon1												
SAH (SP)	4.57	-1.01%	39.33	12.64%	6.08	-2.40%	50.39	15.45%	4.76	-0.85%	49.00	16.00%
SAH	4.53	Ref.	44.30	Ref.	5.94	Ref.	58.17	Ref.	4.72	Ref.	56.84	Ref.
RTSAH E	4.60	-1.59%	46.38	-4.48%	6.03	-1.52%	60.87	-4.44%	4.76	-0.91%	58.87	-3.45%
RTSAH Z	9.36	-51.65%	55.51	-20.21%	10.47	-43.29%	72.29	-19.53%	7.99	-40.94%	68.32	-16.81%
RTSAH N	7.42	-39.04%	49.91	-11.25%	8.41	-29.41%	65.52	-11.22%	6.43	-26.63%	62.57	-9.17%
RTSAH SA	4.82	-6.18%	46.87	-5.49%	6.33	-6.13%	62.18	-6.44%	5.01	-5.75%	60.07	-5.39%
RTSAH APSA	4.56	-0.69%	44.98	-1.53%	5.96	-0.35%	59.44	-2.14%	4.74	-0.36%	57.82	-1.70%
RTSAH HAPSA	4.95	-8.64%	49.15	-9.88%	6.58	-9.69%	64.17	-9.34%	5.13	-7.99%	61.89	-8.17%
RTSAH WCHAPSA	5.11	-11.46%	50.80	-12.81%	6.77	-12.29%	64.30	-9.53%	5.27	-10.43%	61.91	-8.19%
RTSAH HANPSA	5.20	-12.94%	49.85	-11.15%	6.89	-13.80%	66.07	-11.95%	5.37	-12.05%	63.53	-10.54%
RTSAH WNHANPSA	5.24	-13.62%	49.78	-11.01%	6.96	-14.71%	66.08	-11.97%	5.43	-13.00%	63.53	-10.53%
RTSAH WNWCHANPSA	5.40	-16.13%	50.12	-11.63%	7.16	-17.08%	66.51	-12.54%	5.57	-15.19%	63.85	-10.99%
RTSAH HANPSA2	4.59	-1.32%	46.86	-5.47%	6.00	-1.00%	62.07	-6.28%	4.76	-0.86%	60.23	-5.63%
RTSAH WNHANPSA2	4.63	-2.17%	46.74	-5.24%	6.07	-2.12%	61.96	-6.12%	4.82	-2.08%	60.11	-5.45%
RTSAH WNWCHANPSA2	4.62	-2.01%	47.15	-6.06%	6.14	-3.30%	62.43	-6.82%	4.90	-3.64%	60.56	-6.15%
RTSAH EP	4.62	-2.00%	45.46	-2.57%	6.04	-1.68%	60.41	-3.71%	4.78	-1.33%	58.56	-2.95%
RTSAH APE	4.59	-1.48%	45.66	-2.98%	5.99	-0.91%	60.10	-3.21%	4.75	-0.67%	58.32	-2.55%
RTSAH HAPE	5.55	-18.40%	61.78	-28.30%	7.33	-18.97%	68.27	-14.79%	5.67	-16.69%	65.58	-13.34%
RTSAH EP2	6.73	-32.78%	49.08	-9.75%	8.40	-29.29%	64.64	-10.00%	6.50	-27.42%	61.86	-8.12%
RTSAH APE2	6.18	-26.79%	47.88	-7.48%	7.73	-23.17%	63.55	-8.47%	5.99	-21.24%	60.99	-6.81%
RTSAH HAPE2	5.02	-9.90%	49.76	-10.98%	6.66	-10.77%	64.96	-10.44%	5.20	-9.29%	62.75	-9.43%

Table 6: The average number of ray-triangle intersection tests to perform per primary (camera), I<sub>c</sub>, closest-hit shadow (ambient), I'<sub>s</sub>, and any-hit shadow (ambient), I<sub>s</sub>, ray and the average number of ADS node traversal steps to perform per primary (camera), T<sub>c</sub>, closest-hit shadow (ambient), T'<sub>s</sub>, and any-hit shadow (ambient), T<sub>s</sub>, ray for a **kd-tree** ADS, built with various build heuristics, for a variety of artificial test scenes rendered as ambient occlusion images of resolution 512×512 pixels using 512 primary rays per pixel and 1 shadow ray per primary ray which is not limited to a fixed, finite, maximum distance.





Build heuristic	BIH											
	I <sub>c</sub>	ΔI <sub>c</sub>	T <sub>c</sub>	ΔT <sub>c</sub>	I' <sub>s</sub>	ΔI' <sub>s</sub>	T' <sub>s</sub>	ΔT' <sub>s</sub>	I <sub>s</sub>	ΔI <sub>s</sub>	T <sub>s</sub>	ΔT <sub>s</sub>
	Icosahderon2											
SAH	2.63	Ref.	31.71	Ref.	1.81	Ref.	14.62	Ref.	1.67	Ref.	14.12	Ref.
RTSAH E	2.72	-3.43%	33.23	-4.57%	1.84	-1.76%	14.94	-2.08%	1.69	-1.43%	14.38	-1.81%
RTSAH Z	10.30	-74.47%	53.65	-40.89%	4.81	-62.43%	21.41	-31.70%	4.48	-62.76%	20.32	-30.54%
RTSAH N	3.89	-32.49%	35.87	-11.59%	2.27	-20.24%	15.62	-6.35%	2.10	-20.60%	15.02	-6.02%
RTSAH SA	3.00	-12.32%	32.96	-3.77%	1.94	-6.74%	14.84	-1.43%	1.79	-6.90%	14.31	-1.39%
RTSAH APSA	2.72	-3.21%	32.39	-2.09%	1.83	-1.32%	14.72	-0.66%	1.69	-1.36%	14.20	-0.62%
RTSAH HAPSA	3.06	-13.98%	45.21	-29.84%	2.02	-10.71%	16.83	-13.10%	1.84	-9.26%	15.98	-11.65%
RTSAH WCHAPSA	2.90	-9.42%	48.10	-34.06%	1.99	-9.39%	16.72	-12.56%	1.80	-7.58%	15.88	-11.09%
RTSAH HANPSA	4.08	-35.51%	47.88	-33.76%	2.38	-23.95%	19.13	-23.55%	2.18	-23.40%	18.19	-22.40%
RTSAH WNHANPSA	4.29	-38.70%	46.85	-32.30%	2.45	-26.26%	18.92	-22.69%	2.24	-25.75%	17.99	-21.56%
RTSAH WNWCHANPSA	4.34	-39.38%	47.34	-33.00%	2.45	-26.11%	18.88	-22.54%	2.24	-25.65%	17.96	-21.42%
RTSAH HANPSA2	3.02	-12.90%	45.94	-30.96%	2.03	-10.89%	17.54	-16.60%	1.84	-9.41%	16.64	-15.15%
RTSAH WNHANPSA2	3.02	-12.95%	45.92	-30.93%	2.02	-10.72%	17.46	-16.26%	1.83	-9.17%	16.57	-14.81%
RTSAH WNWCHANPSA2	3.01	-12.75%	43.80	-27.60%	2.01	-10.30%	17.06	-14.28%	1.83	-8.87%	16.19	-12.80%
RTSAH EP	2.72	-3.40%	33.70	-5.90%	1.85	-2.18%	14.75	-0.88%	1.70	-2.06%	14.22	-0.71%
RTSAH APE	2.77	-5.26%	33.33	-4.84%	1.85	-2.07%	14.73	-0.74%	1.70	-1.97%	14.19	-0.56%
RTSAH HAPE	3.43	-23.42%	75.29	-57.88%	2.28	-20.61%	20.73	-29.46%	2.05	-18.81%	19.60	-27.99%
RTSAH EP2	3.01	-12.64%	33.87	-6.36%	1.98	-8.80%	15.14	-3.42%	1.82	-8.46%	14.57	-3.10%
RTSAH APE2	2.93	-10.20%	33.32	-4.81%	1.92	-5.86%	15.01	-2.58%	1.77	-5.77%	14.46	-2.38%
RTSAH HAPE2	2.94	-10.45%	50.93	-37.73%	1.99	-9.34%	17.60	-16.89%	1.81	-7.81%	16.68	-15.36%
Icosahderon3												
SAH	1.78	Ref.	20.06	Ref.	1.35	Ref.	9.08	Ref.	1.15	Ref.	8.19	Ref.
RTSAH E	1.70	4.97%	21.35	-6.02%	1.38	-2.12%	9.23	-1.58%	1.16	-0.86%	8.22	-0.45%
RTSAH Z	6.47	-72.50%	32.13	-37.56%	3.26	-58.53%	14.01	-35.18%	2.81	-58.87%	12.42	-34.09%
RTSAH N	2.31	-22.97%	22.35	-10.26%	1.64	-17.33%	9.51	-4.48%	1.38	-16.38%	8.44	-3.03%
RTSAH SA	1.81	-1.52%	21.58	-7.05%	1.43	-5.74%	9.29	-2.21%	1.21	-4.98%	8.30	-1.35%
RTSAH APSA	1.69	5.63%	20.90	-4.01%	1.37	-1.02%	9.31	-2.49%	1.15	0.05%	8.31	-1.45%
RTSAH HAPSA	1.99	-10.47%	23.49	-14.59%	1.54	-12.22%	10.78	-15.76%	1.30	-11.05%	9.60	-14.71%
RTSAH WCHAPSA	1.90	-6.26%	23.26	-13.76%	1.50	-9.85%	10.53	-13.70%	1.26	-8.68%	9.39	-12.84%
RTSAH HANPSA	2.53	-29.51%	27.37	-26.71%	1.81	-25.32%	12.08	-24.84%	1.52	-24.01%	10.72	-23.67%
RTSAH WNHANPSA	2.60	-31.65%	27.08	-25.93%	1.86	-27.23%	11.98	-24.17%	1.56	-25.94%	10.63	-22.97%
RTSAH WNWCHANPSA	2.65	-32.78%	27.40	-26.78%	1.89	-28.41%	12.07	-24.77%	1.59	-27.25%	10.72	-23.66%
RTSAH HANPSA2	1.86	-4.16%	23.87	-15.97%	1.48	-8.71%	10.65	-14.68%	1.24	-6.98%	9.45	-13.37%
RTSAH WNHANPSA2	1.89	-5.65%	23.93	-16.15%	1.49	-9.45%	10.62	-14.51%	1.25	-7.54%	9.43	-13.17%
RTSAH WNWCHANPSA2	1.93	-7.75%	23.69	-15.31%	1.50	-10.08%	10.52	-13.66%	1.26	-8.28%	9.33	-12.29%
RTSAH EP	1.81	-1.59%	21.02	-4.57%	1.40	-3.73%	9.22	-1.53%	1.19	-2.79%	8.26	-0.93%
RTSAH APE	1.74	2.12%	20.96	-4.28%	1.38	-2.18%	9.22	-1.51%	1.17	-1.04%	8.26	-0.92%
RTSAH HAPE	2.25	-20.74%	26.27	-23.64%	1.69	-19.80%	11.26	-19.30%	1.40	-17.39%	9.82	-16.68%
RTSAH EP2	1.90	-6.44%	21.25	-5.62%	1.49	-9.48%	9.39	-3.23%	1.25	-7.96%	8.36	-2.08%
RTSAH APE2	1.85	-3.69%	20.92	-4.12%	1.43	-5.26%	9.19	-1.17%	1.21	-4.30%	8.23	-0.57%
RTSAH HAPE2	1.96	-9.08%	24.29	-17.41%	1.52	-10.98%	10.73	-15.32%	1.27	-9.13%	9.45	-13.39%
Icosahderon4												
SAH	4.81	Ref.	29.38	Ref.	3.67	Ref.	26.64	Ref.	2.42	Ref.	24.31	Ref.
RTSAH E	5.35	-10.10%	32.97	-10.88%	4.09	-10.29%	29.43	-9.50%	2.83	-14.34%	25.82	-5.86%
RTSAH Z	17.96	-73.21%	71.46	-58.88%	16.18	-77.30%	65.55	-59.37%	11.82	-79.51%	51.58	-52.87%
RTSAH N	5.60	-14.02%	31.82	-7.66%	4.38	-16.16%	28.80	-7.51%	3.07	-21.18%	25.58	-4.96%
RTSAH SA	5.46	-11.87%	30.19	-2.67%	4.51	-18.59%	27.51	-3.19%	3.17	-23.70%	24.83	-2.09%
RTSAH APSA	5.11	-5.91%	33.77	-12.98%	4.25	-13.56%	31.22	-14.67%	2.92	-17.13%	26.81	-9.32%
RTSAH HAPSA	5.49	-12.30%	46.09	-36.26%	4.31	-14.82%	40.08	-33.55%	2.75	-11.85%	32.51	-25.23%
RTSAH WCHAPSA	5.60	-14.08%	45.81	-35.86%	4.52	-18.70%	40.03	-33.47%	2.94	-17.78%	32.74	-25.75%
RTSAH HANPSA	7.01	-31.35%	51.64	-43.10%	5.65	-35.04%	44.67	-40.37%	3.74	-35.33%	35.90	-32.29%
RTSAH WNHANPSA	7.37	-34.71%	49.88	-41.09%	6.13	-40.07%	43.08	-38.17%	4.11	-41.09%	34.41	-29.36%
RTSAH WNWCHANPSA	7.17	-32.92%	51.21	-42.62%	5.77	-36.30%	44.27	-39.84%	3.83	-36.74%	35.59	-31.70%
RTSAH HANPSA2	5.64	-14.74%	43.33	-32.19%	4.65	-20.95%	37.98	-29.88%	3.00	-19.35%	31.26	-22.23%
RTSAH WNHANPSA2	5.61	-14.25%	43.47	-32.42%	4.58	-19.81%	38.16	-30.20%	2.94	-17.59%	31.36	-22.50%
RTSAH WNWCHANPSA2	5.72	-15.85%	43.15	-31.91%	4.64	-20.91%	37.76	-29.46%	3.02	-19.91%	31.18	-22.03%
RTSAH EP	5.19	-7.38%	30.78	-4.54%	4.04	-9.10%	28.07	-5.12%	2.85	-15.11%	25.01	-2.80%
RTSAH APE	4.75	1.32%	31.35	-6.27%	3.49	5.16%	28.02	-4.93%	2.33	3.68%	24.99	-2.71%
RTSAH HAPE	5.65	-14.80%	50.85	-42.22%	4.19	-12.42%	45.23	-41.11%	2.72	-10.93%	37.33	-34.89%
RTSAH EP2	4.74	1.42%	36.09	-18.58%	3.37	8.88%	31.86	-16.39%	2.13	13.40%	27.84	-12.70%
RTSAH APE2	4.23	13.87%	33.52	-12.35%	2.87	28.04%	29.72	-10.39%	1.73	39.74%	26.31	-7.59%
RTSAH HAPE2	4.39	9.59%	42.24	-30.43%	2.86	28.29%	38.22	-30.31%	1.68	43.67%	32.26	-24.65%

Table 9: The average number of ray-triangle intersection tests to perform per primary (camera), I<sub>c</sub>, closest-hit shadow (ambient), I'<sub>s</sub>, and any-hit shadow (ambient), I<sub>s</sub>, ray and the average number of ADS node traversal steps to perform per primary (camera), T<sub>c</sub>, closest-hit shadow (ambient), T'<sub>s</sub>, and any-hit shadow (ambient), T<sub>s</sub>, ray for a BIH ADS, built with various build heuristics, for a variety of artificial test scenes rendered as ambient occlusion images of resolution 512×512 pixels using 512 primary rays per pixel and 1 shadow ray per primary ray which is not limited to a fixed, finite, maximum distance.

BVH												
Build heuristic	$I_c$	$\Delta I_c$	$T_c$	$\Delta T_c$	$I'_s$	$\Delta I'_s$	$T'_s$	$\Delta T'_s$	$I_s$	$\Delta I_s$	$T_s$	$\Delta T_s$
Empty Box												
SAH	1.74	Ref.	11.00	Ref.	1.31	Ref.	10.54	Ref.	1.15	Ref.	9.60	Ref.
RTSAH E	1.76	-1.15%	11.00	0.00%	1.32	-0.41%	10.54	0.00%	1.15	-0.19%	9.59	0.05%
RTSAH APSA	1.74	0.00%	11.00	0.00%	1.31	0.00%	10.54	0.00%	1.15	0.00%	9.58	0.14%
RTSAH HAPSA	1.73	0.27%	11.00	0.00%	1.30	0.61%	10.54	0.00%	1.15	0.02%	9.60	0.00%
RTSAH WCHAPSA	1.73	0.27%	11.00	0.00%	1.30	0.61%	10.54	0.00%	1.15	0.02%	9.60	0.00%
RTSAH HANPSA	1.73	0.27%	11.00	0.00%	1.30	0.61%	10.54	0.00%	1.15	0.02%	9.60	0.00%
RTSAH WNCHANPSA	1.73	0.27%	11.00	0.00%	1.30	0.61%	10.54	0.00%	1.15	0.02%	9.60	0.00%
RTSAH HANPSA2	1.74	0.00%	11.00	0.00%	1.31	0.00%	10.54	0.00%	1.15	0.00%	9.58	0.14%
RTSAH WNCHANPSA2	1.74	0.00%	11.00	0.00%	1.31	0.00%	10.54	0.00%	1.15	0.00%	9.58	0.14%
RTSAH EP	1.73	0.27%	11.00	0.00%	1.30	0.61%	10.54	0.00%	1.15	0.02%	9.60	-0.01%
RTSAH APE	1.73	0.27%	11.00	0.00%	1.30	0.61%	10.54	0.00%	1.15	0.02%	9.60	0.00%
RTSAH HAPE	1.73	0.27%	11.00	0.00%	1.30	0.61%	10.54	0.00%	1.15	0.02%	9.60	-0.01%
RTSAH EP2	1.73	0.27%	11.00	0.00%	1.30	0.61%	10.54	0.00%	1.15	0.02%	9.60	0.00%
RTSAH APE2	1.73	0.27%	11.00	0.00%	1.30	0.61%	10.54	0.00%	1.15	0.02%	9.60	0.00%
RTSAH HAPE2	1.74	0.00%	11.00	0.00%	1.31	0.00%	10.54	0.00%	1.15	0.00%	9.58	0.14%
Cornell Box												
SAH	2.11	Ref.	19.02	Ref.	1.87	Ref.	21.00	Ref.	1.53	Ref.	17.25	Ref.
RTSAH E	2.07	1.87%	17.01	11.80%	1.85	0.82%	18.76	11.98%	1.57	-2.56%	15.81	9.10%
RTSAH APSA	2.17	-2.87%	17.05	11.51%	1.84	1.48%	18.80	11.73%	1.56	-2.06%	15.83	8.94%
RTSAH HAPSA	2.15	-1.70%	18.04	5.42%	1.84	1.59%	19.91	5.50%	1.59	-3.68%	16.81	2.63%
RTSAH WCHAPSA	2.14	-1.55%	18.02	5.50%	1.84	1.57%	19.91	5.50%	1.59	-3.67%	16.81	2.63%
RTSAH HANPSA	2.13	-0.96%	18.66	1.91%	1.84	1.39%	20.90	0.52%	1.59	-3.52%	17.53	-1.59%
RTSAH WNCHANPSA	2.13	-0.96%	18.66	1.91%	1.84	1.39%	20.90	0.52%	1.59	-3.52%	17.53	-1.59%
RTSAH WNWCHANPSA	2.13	-0.96%	18.66	1.91%	1.84	1.39%	20.90	0.52%	1.59	-3.52%	17.53	-1.59%
RTSAH HANPSA2	2.15	-1.77%	19.47	-2.34%	1.85	1.18%	20.95	0.27%	1.56	-1.89%	17.68	-2.44%
RTSAH WNCHANPSA2	2.15	-1.77%	19.47	-2.34%	1.85	1.18%	20.95	0.27%	1.56	-1.89%	17.68	-2.44%
RTSAH WNWCHANPSA2	2.08	1.54%	20.12	-5.51%	1.87	0.06%	22.01	-4.55%	1.53	0.03%	18.13	-4.86%
RTSAH EP	2.14	-1.42%	17.04	11.62%	1.85	1.27%	18.91	11.08%	1.56	-2.12%	15.96	8.10%
RTSAH APE	2.11	-0.15%	17.61	8.00%	1.86	0.73%	19.70	6.61%	1.57	-2.39%	16.51	4.48%
RTSAH HAPE	2.16	-2.19%	17.75	7.15%	1.85	0.95%	19.72	6.52%	1.57	-2.27%	16.56	4.15%
RTSAH EP2	2.15	-1.64%	16.90	12.53%	1.84	1.80%	18.67	12.53%	1.56	-1.86%	15.66	10.17%
RTSAH APE2	2.11	-0.01%	18.06	5.27%	1.84	1.73%	20.07	4.63%	1.59	-3.59%	16.98	1.58%
RTSAH HAPE2	2.17	-2.87%	17.10	11.20%	1.84	1.83%	18.83	11.58%	1.56	-1.83%	15.81	9.07%
Icosahderon1												
SAH	2.79	Ref.	50.02	Ref.	2.99	Ref.	62.62	Ref.	2.46	Ref.	51.81	Ref.
RTSAH E	2.65	5.28%	52.77	-5.21%	3.01	-0.47%	67.07	-6.63%	2.51	-2.08%	56.46	-8.23%
RTSAH APSA	2.80	-0.05%	50.64	-1.23%	2.99	0.03%	64.17	-2.40%	2.47	-0.18%	53.40	-2.97%
RTSAH HAPSA	2.85	-1.98%	52.50	-4.72%	3.01	-0.58%	69.64	-10.07%	2.50	-1.53%	58.86	-11.98%
RTSAH WCHAPSA	2.89	-3.36%	51.48	-2.84%	3.01	-0.75%	68.26	-8.26%	2.51	-1.81%	57.47	-9.85%
RTSAH HANPSA	2.77	0.78%	56.05	-10.76%	2.99	0.01%	73.79	-15.13%	2.48	-0.88%	62.77	-17.46%
RTSAH WNCHANPSA	2.78	0.57%	56.02	-10.72%	2.99	0.01%	73.82	-15.17%	2.48	-0.89%	62.80	-17.50%
RTSAH WNWCHANPSA	2.78	0.47%	56.16	-10.93%	2.99	-0.07%	73.19	-14.44%	2.49	-0.96%	62.24	-16.75%
RTSAH HANPSA2	2.82	-0.81%	53.52	-6.54%	3.00	-0.35%	70.20	-10.79%	2.49	-1.26%	59.34	-12.69%
RTSAH WNCHANPSA2	2.84	-1.46%	50.77	-1.49%	3.00	-0.26%	67.44	-7.15%	2.48	-0.92%	55.70	-6.98%
RTSAH WNWCHANPSA2	2.76	1.42%	51.69	-3.24%	3.00	-0.41%	66.49	-5.82%	2.49	-1.01%	56.83	-8.82%
RTSAH EP	2.79	0.26%	51.70	-3.25%	2.99	-0.01%	66.59	-5.96%	2.47	-0.42%	55.82	-7.17%
RTSAH APE	2.77	0.77%	50.76	-1.47%	2.99	0.03%	65.00	-3.65%	2.47	-0.26%	54.24	-4.47%
RTSAH HAPE	2.87	-2.65%	51.90	-3.64%	3.01	-0.63%	66.66	-6.05%	2.49	-1.00%	55.87	-7.26%
RTSAH EP2	2.59	7.82%	53.72	-6.90%	3.03	-1.28%	65.69	-4.66%	2.36	4.25%	52.03	-0.41%
RTSAH APE2	2.59	7.83%	52.33	-4.42%	3.03	-1.24%	63.59	-1.52%	2.36	4.41%	49.96	3.72%
RTSAH HAPE2	2.83	-1.37%	53.15	-5.89%	2.98	0.35%	69.60	-10.02%	2.52	-2.17%	59.51	-12.94%

Table 10: The average number of ray-triangle intersection tests to perform per primary (camera),  $I_c$ , closest-hit shadow (ambient),  $I'_s$ , and any-hit shadow (ambient),  $I_s$ , ray and the average number of ADS node traversal steps to perform per primary (camera),  $T_c$ , closest-hit shadow (ambient),  $T'_s$ , and any-hit shadow (ambient),  $T_s$ , ray for a **BVH** ADS, built with various build heuristics, for a variety of artificial test scenes rendered as ambient occlusion images of resolution 512×512 pixels using 512 primary rays per pixel and 1 shadow ray per primary ray which is not limited to a fixed, finite, maximum distance.

BVH												
Build heuristic	$I_c$	$\Delta I_c$	$T_c$	$\Delta T_c$	$I'_s$	$\Delta I'_s$	$T'_s$	$\Delta T'_s$	$I_s$	$\Delta I_s$	$T_s$	$\Delta T_s$
Icosahderon2												
SAH	1.41	Ref.	33.83	Ref.	1.09	Ref.	16.95	Ref.	1.04	Ref.	16.20	Ref.
RTSAH E	1.42	-0.38%	35.12	-3.68%	1.09	-0.12%	17.49	-3.08%	1.04	-0.09%	16.70	-3.01%
RTSAH APSA	1.42	-0.23%	33.89	-0.19%	1.09	-0.01%	16.96	-0.05%	1.04	-0.01%	16.20	-0.05%
RTSAH HAPSA	1.50	-5.72%	34.99	-3.31%	1.10	-0.52%	19.53	-13.22%	1.05	-0.34%	18.68	-13.28%
RTSAH WCHAPSA	1.51	-6.09%	34.84	-2.92%	1.10	-0.55%	19.48	-13.01%	1.05	-0.36%	18.63	-13.05%
RTSAH HANPSA	1.43	-1.41%	35.68	-5.20%	1.10	-0.20%	17.82	-4.89%	1.04	-0.14%	17.03	-4.92%
RTSAH WNCHANPSA	1.44	-1.69%	35.01	-3.37%	1.10	-0.17%	17.70	-4.25%	1.04	-0.12%	16.92	-4.27%
RTSAH WNWCHANPSA	1.45	-2.76%	34.98	-3.30%	1.10	-0.23%	17.71	-4.30%	1.04	-0.15%	16.93	-4.33%
RTSAH HANPSA2	1.47	-3.56%	34.03	-0.61%	1.10	-0.31%	18.41	-7.95%	1.04	-0.22%	17.60	-7.99%
RTSAH WNHANPSA2	1.46	-3.36%	33.72	0.31%	1.10	-0.31%	18.12	-6.47%	1.04	-0.22%	17.32	-6.51%
RTSAH WNWCHANPSA2	1.46	-3.34%	33.88	-0.16%	1.10	-0.29%	18.24	-7.07%	1.04	-0.21%	17.44	-7.13%
RTSAH EP	1.43	-1.29%	35.19	-3.88%	1.09	-0.11%	17.28	-1.90%	1.04	-0.08%	16.50	-1.84%
RTSAH APE	1.42	-0.61%	35.06	-3.52%	1.09	-0.08%	17.26	-1.83%	1.04	-0.05%	16.49	-1.77%
RTSAH HAPE	1.51	-6.26%	36.18	-6.49%	1.10	-0.62%	20.04	-15.43%	1.05	-0.43%	19.16	-15.48%
RTSAH EP2	1.43	-0.89%	35.02	-3.40%	1.09	-0.12%	17.43	-2.77%	1.04	-0.09%	16.65	-2.72%
RTSAH APE2	1.42	-0.12%	35.38	-4.38%	1.09	-0.03%	17.30	-2.03%	1.04	-0.03%	16.52	-1.96%
RTSAH HAPE2	1.46	-2.84%	35.48	-4.66%	1.10	-0.20%	19.50	-13.10%	1.04	-0.14%	18.64	-13.13%
Icosahderon3												
SAH	0.74	Ref.	18.67	Ref.	0.68	Ref.	9.99	Ref.	0.63	Ref.	9.18	Ref.
RTSAH E	0.74	0.83%	19.14	-2.48%	0.68	-0.16%	10.26	-2.61%	0.63	-0.23%	9.42	-2.58%
RTSAH APSA	0.74	0.20%	18.62	0.27%	0.68	-0.07%	10.00	-0.04%	0.63	-0.15%	9.17	0.04%
RTSAH HAPSA	0.77	-3.05%	18.76	-0.51%	0.68	-0.34%	10.70	-6.58%	0.63	-0.27%	9.81	-6.46%
RTSAH WCHAPSA	0.77	-3.37%	18.76	-0.47%	0.68	-0.43%	10.62	-5.90%	0.63	-0.38%	9.75	-5.88%
RTSAH HANPSA	0.75	-1.09%	19.40	-3.79%	0.68	-0.28%	10.66	-6.20%	0.63	-0.19%	9.76	-6.02%
RTSAH WNCHANPSA	0.75	-1.53%	18.96	-1.53%	0.68	-0.20%	10.57	-5.48%	0.63	-0.21%	9.71	-5.47%
RTSAH WNWCHANPSA	0.75	-1.58%	18.89	-1.16%	0.68	-0.16%	10.55	-5.23%	0.63	-0.17%	9.68	-5.23%
RTSAH HANPSA2	0.76	-1.82%	18.84	-0.91%	0.68	-0.28%	10.45	-4.32%	0.63	-0.29%	9.60	-4.39%
RTSAH WNHANPSA2	0.75	-1.63%	18.85	-0.96%	0.68	-0.24%	10.44	-4.25%	0.63	-0.29%	9.60	-4.36%
RTSAH WNWCHANPSA2	0.76	-2.03%	18.78	-0.61%	0.68	-0.26%	10.42	-4.07%	0.63	-0.29%	9.58	-4.18%
RTSAH EP	0.74	-0.21%	18.64	0.17%	0.68	-0.13%	9.98	0.17%	0.63	-0.13%	9.16	0.20%
RTSAH APE	0.74	0.09%	18.42	1.36%	0.68	-0.05%	9.94	0.56%	0.63	-0.14%	9.12	0.56%
RTSAH HAPE	0.77	-4.15%	18.80	-0.68%	0.68	-0.65%	10.82	-7.64%	0.63	-0.48%	9.90	-7.27%
RTSAH EP2	0.74	0.47%	18.96	-1.54%	0.68	-0.18%	10.12	-1.26%	0.63	-0.27%	9.30	-1.31%
RTSAH APE2	0.74	0.65%	18.91	-1.31%	0.68	-0.12%	10.10	-1.00%	0.63	-0.22%	9.27	-0.99%
RTSAH HAPE2	0.75	-0.51%	19.07	-2.13%	0.68	-0.14%	10.61	-5.79%	0.63	-0.18%	9.72	-5.63%
Icosahderon4												
SAH	2.84	0.00%	33.70	0.00%	1.89	0.00%	31.76	0.00%	1.11	0.00%	28.34	0.00%
RTSAH E	2.76	2.91%	33.78	-0.23%	1.82	3.43%	32.44	-2.10%	1.10	0.28%	28.86	-1.80%
RTSAH APSA	2.74	3.83%	34.48	-2.25%	1.83	3.16%	32.56	-2.45%	1.11	-0.55%	28.95	-2.09%
RTSAH HAPSA	2.76	3.12%	34.64	-2.69%	1.83	3.00%	33.24	-4.45%	1.12	-1.24%	29.58	-4.18%
RTSAH WCHAPSA	2.76	3.09%	34.72	-2.91%	1.83	3.03%	33.30	-4.61%	1.12	-1.18%	29.63	-4.36%
RTSAH HANPSA	2.74	3.79%	35.24	-4.36%	1.83	3.02%	33.61	-5.51%	1.12	-1.38%	29.92	-5.28%
RTSAH WNCHANPSA	2.74	3.65%	34.94	-3.54%	1.83	3.00%	33.39	-4.88%	1.12	-1.45%	29.72	-4.62%
RTSAH WNWCHANPSA	2.74	3.69%	35.22	-4.30%	1.83	3.00%	33.59	-5.46%	1.12	-1.41%	29.92	-5.28%
RTSAH HANPSA2	2.72	4.35%	34.73	-2.97%	1.83	2.96%	33.41	-4.94%	1.12	-1.28%	29.78	-4.84%
RTSAH WNHANPSA2	2.73	4.31%	34.71	-2.89%	1.83	2.95%	33.39	-4.88%	1.12	-1.30%	29.77	-4.79%
RTSAH WNWCHANPSA2	2.73	4.19%	34.91	-3.45%	1.83	2.85%	33.64	-5.58%	1.12	-1.33%	30.00	-5.52%
RTSAH EP	2.74	3.68%	33.93	-0.65%	1.83	3.22%	32.11	-1.10%	1.11	-0.31%	28.49	-0.51%
RTSAH APE	2.74	3.57%	33.88	-0.52%	1.83	3.13%	32.21	-1.40%	1.12	-0.76%	28.60	-0.91%
RTSAH HAPE	2.75	3.36%	35.41	-4.82%	1.83	2.82%	35.68	-10.98%	1.13	-1.61%	31.84	-10.99%
RTSAH EP2	2.74	3.93%	34.48	-2.26%	1.83	3.07%	32.82	-3.22%	1.13	-1.68%	29.12	-2.68%
RTSAH APE2	2.74	3.68%	34.29	-1.72%	1.83	3.10%	32.65	-2.72%	1.12	-0.94%	29.00	-2.28%
RTSAH HAPE2	2.73	3.96%	35.81	-5.89%	1.83	2.86%	35.82	-11.32%	1.13	-1.71%	31.92	-11.21%

Table 11: The average number of ray-triangle intersection tests to perform per primary (camera),  $I_c$ , closest-hit shadow (ambient),  $I'_s$ , and any-hit shadow (ambient),  $I_s$ , ray and the average number of ADS node traversal steps to perform per primary (camera),  $T_c$ , closest-hit shadow (ambient),  $T'_s$ , and any-hit shadow (ambient),  $T_s$ , ray for a **BVH** ADS, built with various build heuristics, for a variety of artificial test scenes rendered as ambient occlusion images of resolution 512×512 pixels using 512 primary rays per pixel and 1 shadow ray per primary ray which is not limited to a fixed, finite, maximum distance.

Build heuristic	SBVH											
	I <sub>c</sub>	ΔI <sub>c</sub>	T <sub>c</sub>	ΔT <sub>c</sub>	I' <sub>s</sub>	ΔI' <sub>s</sub>	T' <sub>s</sub>	ΔT' <sub>s</sub>	I <sub>s</sub>	ΔI <sub>s</sub>	T <sub>s</sub>	ΔT <sub>s</sub>
	Empty Box											
SAH	1.96	Ref.	11.00	Ref.	1.51	Ref.	10.54	Ref.	1.16	Ref.	9.59	Ref.
RTSAH E	1.76	11.52%	11.00	0.00%	1.32	14.65%	10.54	0.00%	1.15	0.28%	9.59	-0.02%
RTSAH APSA	1.92	2.30%	10.63	3.45%	1.44	5.07%	10.21	3.22%	1.16	-0.15%	9.34	2.65%
RTSAH HAPSA	1.90	3.48%	11.35	-3.06%	1.43	5.67%	11.93	-11.61%	1.14	1.13%	10.97	-12.61%
RTSAH WCHAPSA	1.92	2.30%	10.63	3.45%	1.44	5.07%	10.21	3.22%	1.15	0.56%	9.35	2.58%
RTSAH HANPSA	1.88	4.06%	11.51	-4.41%	1.41	7.13%	11.82	-10.85%	1.14	1.57%	10.79	-11.14%
RTSAH WNCHANPSA	1.88	4.06%	11.51	-4.41%	1.41	7.13%	11.82	-10.85%	1.14	1.57%	10.79	-11.14%
RTSAH WNWCHANPSA	1.85	5.97%	11.44	-3.83%	1.39	8.96%	12.09	-12.84%	1.12	2.97%	11.11	-13.68%
RTSAH HANPSA2	1.92	2.30%	10.63	3.45%	1.44	5.07%	10.21	3.22%	1.16	-0.15%	9.33	2.73%
RTSAH WNHANPSA2	1.92	2.30%	10.63	3.45%	1.44	5.07%	10.21	3.22%	1.16	-0.15%	9.33	2.73%
RTSAH EP	1.92	2.30%	10.63	3.45%	1.44	5.07%	10.21	3.22%	1.15	0.56%	9.35	2.57%
RTSAH APE	1.92	2.30%	10.63	3.45%	1.44	5.07%	10.21	3.22%	1.15	0.56%	9.35	2.50%
RTSAH HAPE	1.92	2.30%	10.63	3.45%	1.44	5.07%	10.21	3.22%	1.15	0.56%	9.35	2.57%
RTSAH EP2	1.92	2.30%	10.63	3.45%	1.44	5.07%	10.21	3.22%	1.15	0.56%	9.35	2.58%
RTSAH APE2	1.92	2.30%	10.63	3.45%	1.44	5.07%	10.21	3.22%	1.15	0.56%	9.34	2.61%
RTSAH HAPE2	1.92	2.30%	10.63	3.45%	1.44	5.07%	10.21	3.22%	1.16	-0.15%	9.33	2.73%
Cornell Box												
SAH	1.92	Ref.	16.91	Ref.	1.78	Ref.	21.31	Ref.	1.33	Ref.	17.60	Ref.
RTSAH E	2.07	-7.53%	17.01	-0.58%	1.85	-4.28%	18.76	13.60%	1.57	-15.28%	15.81	11.31%
RTSAH APSA	1.78	7.61%	15.27	10.76%	1.54	15.55%	20.07	6.17%	1.29	2.99%	18.03	-2.40%
RTSAH HAPSA	2.12	-9.38%	14.79	14.33%	2.13	-16.68%	20.19	5.57%	1.73	-23.19%	18.14	-2.99%
RTSAH WCHAPSA	2.16	-11.41%	14.82	14.08%	2.14	-17.16%	20.21	5.42%	1.76	-24.43%	18.19	-3.26%
RTSAH HANPSA	1.80	6.32%	15.51	9.02%	1.63	8.75%	20.80	2.43%	1.37	-3.00%	18.38	-4.25%
RTSAH WNCHANPSA	2.01	-4.72%	15.19	11.31%	1.98	-10.14%	20.22	5.40%	1.61	-17.47%	17.89	-1.63%
RTSAH WNWCHANPSA	1.82	5.54%	15.50	9.13%	1.63	8.89%	20.67	3.09%	1.37	-2.90%	18.27	-3.68%
RTSAH HANPSA2	1.83	4.74%	14.11	19.84%	1.61	10.10%	18.85	13.07%	1.35	-1.23%	17.00	3.53%
RTSAH WNHANPSA2	1.75	9.75%	14.80	14.22%	1.51	17.49%	19.94	6.88%	1.27	4.72%	17.80	-1.15%
RTSAH WNWCHANPSA2	1.81	5.62%	14.19	19.19%	1.58	12.13%	19.01	12.09%	1.32	0.50%	17.10	2.90%
RTSAH EP	2.26	-15.21%	15.84	6.76%	2.09	-15.00%	19.60	8.71%	1.67	-20.51%	16.62	5.86%
RTSAH APE	1.73	10.78%	15.25	10.91%	1.52	16.61%	20.37	4.59%	1.23	8.11%	17.86	-1.48%
RTSAH HAPE	1.85	3.61%	14.39	17.52%	1.62	9.92%	19.55	9.01%	1.32	1.04%	17.28	1.84%
RTSAH EP2	1.72	11.22%	14.81	14.19%	1.49	19.13%	19.50	9.28%	1.24	7.05%	17.42	1.00%
RTSAH APE2	1.87	2.39%	16.96	-0.27%	1.59	11.35%	20.68	3.03%	1.31	1.52%	18.00	-2.23%
RTSAH HAPE2	1.88	2.02%	14.50	16.64%	1.57	12.85%	18.98	12.25%	1.29	2.86%	16.48	6.77%
Icosahderon1												
SAH	2.27	Ref.	38.88	Ref.	2.75	Ref.	51.81	Ref.	2.40	Ref.	46.63	Ref.
RTSAH E	2.65	-14.39%	52.77	-26.31%	3.01	-8.67%	67.07	-22.75%	2.51	-4.48%	56.46	-17.40%
RTSAH APSA	2.26	0.71%	38.57	0.82%	2.72	1.06%	52.39	-1.11%	2.38	0.98%	47.24	-1.30%
RTSAH HAPSA	2.30	-1.28%	38.00	2.31%	2.74	0.27%	54.83	-5.51%	2.38	0.88%	49.58	-5.94%
RTSAH WCHAPSA	2.32	-2.07%	38.10	2.04%	2.74	0.24%	53.70	-3.53%	2.39	0.47%	48.51	-3.88%
RTSAH HANPSA	2.26	0.64%	41.12	-5.44%	2.71	1.21%	54.64	-5.19%	2.35	2.28%	48.88	-4.60%
RTSAH WNCHANPSA	2.27	0.28%	40.14	-3.14%	2.72	0.96%	54.06	-4.16%	2.37	1.35%	48.61	-4.07%
RTSAH WNWCHANPSA	2.28	-0.38%	40.09	-3.02%	2.73	0.73%	54.02	-4.10%	2.37	1.13%	48.57	-4.00%
RTSAH HANPSA2	2.26	0.40%	38.78	0.25%	2.73	0.63%	54.93	-5.69%	2.39	0.59%	49.64	-6.06%
RTSAH WNCHANPSA2	2.27	-0.06%	38.79	0.24%	2.73	0.61%	54.91	-5.66%	2.39	0.50%	49.65	-6.08%
RTSAH WNWCHANPSA2	2.27	0.23%	37.85	2.71%	2.73	0.47%	54.90	-5.63%	2.37	1.50%	49.60	-5.98%
RTSAH EP	2.22	2.18%	38.81	0.18%	2.74	0.37%	51.66	0.28%	2.37	1.33%	46.20	0.95%
RTSAH APE	2.21	2.70%	38.97	-0.24%	2.71	1.41%	51.79	0.03%	2.34	2.53%	46.29	0.75%
RTSAH HAPE	2.30	-1.16%	37.99	2.34%	2.75	-0.02%	58.05	-10.75%	2.38	0.71%	52.74	-11.59%
RTSAH EP2	2.25	1.21%	39.18	-0.77%	2.78	-1.36%	51.94	-0.26%	2.40	-0.06%	46.47	0.34%
RTSAH APE2	2.27	0.03%	39.98	-2.75%	2.77	-0.83%	52.25	-0.85%	2.37	1.30%	46.71	-0.17%
RTSAH HAPE2	2.30	-0.99%	37.54	3.57%	2.76	-0.41%	55.42	-6.52%	2.41	-0.29%	50.20	-7.10%

Table 12: The average number of ray-triangle intersection tests to perform per primary (camera), I<sub>c</sub>, closest-hit shadow (ambient), I'<sub>s</sub>, and any-hit shadow (ambient), I<sub>s</sub>, ray and the average number of ADS node traversal steps to perform per primary (camera), T<sub>c</sub>, closest-hit shadow (ambient), T'<sub>s</sub>, and any-hit shadow (ambient), T<sub>s</sub>, ray for a SBVH ADS, built with various build heuristics, for a variety of artificial test scenes rendered as ambient occlusion images of resolution 512×512 pixels using 512 primary rays per pixel and 1 shadow ray per primary ray which is not limited to a fixed, finite, maximum distance.

SBVH												
Build heuristic	$I_c$	$\Delta I_c$	$T_c$	$\Delta T_c$	$I'_s$	$\Delta I'_s$	$T'_s$	$\Delta T'_s$	$I_s$	$\Delta I_s$	$T_s$	$\Delta T_s$
Icosahderon2												
SAH	1.41	Ref.	33.83	Ref.	1.10	Ref.	16.95	Ref.	1.04	Ref.	16.20	Ref.
RTSAH E	1.42	-0.63%	35.12	-3.66%	1.09	0.02%	17.49	-3.07%	1.04	-0.03%	16.70	-2.98%
RTSAH APSA	1.40	1.13%	33.68	0.47%	1.09	0.45%	16.98	-0.21%	1.04	0.52%	16.24	-0.24%
RTSAH HAPSA	1.47	-4.11%	34.84	-2.90%	1.10	-0.31%	19.60	-13.51%	1.04	-0.09%	18.74	-13.55%
RTSAH WCHAPSA	1.47	-4.09%	34.93	-3.15%	1.10	-0.13%	19.49	-13.06%	1.04	0.10%	18.64	-13.09%
RTSAH HANPSA	1.40	0.80%	35.90	-5.75%	1.08	0.95%	17.91	-5.37%	1.03	1.12%	17.12	-5.38%
RTSAH WNHANPSA	1.41	0.38%	36.64	-7.67%	1.09	0.92%	17.50	-3.16%	1.03	1.06%	16.74	-3.21%
RTSAH WNWCHANPSA	1.41	0.00%	36.68	-7.76%	1.08	1.22%	17.54	-3.39%	1.03	1.39%	16.78	-3.45%
RTSAH HANPSA2	1.43	-1.34%	33.35	1.45%	1.09	0.43%	18.23	-7.03%	1.04	0.63%	17.44	-7.11%
RTSAH WNHANPSA2	1.43	-1.63%	33.25	1.75%	1.09	0.41%	18.20	-6.88%	1.04	0.57%	17.41	-6.96%
RTSAH WNWCHANPSA2	1.43	-1.55%	32.86	2.95%	1.09	0.31%	17.95	-5.55%	1.04	0.51%	17.17	-5.63%
RTSAH EP	1.41	0.35%	35.17	-3.80%	1.09	0.22%	17.32	-2.14%	1.04	0.34%	16.54	-2.08%
RTSAH APE	1.39	1.79%	35.12	-3.66%	1.08	1.15%	17.38	-2.45%	1.03	1.23%	16.60	-2.39%
RTSAH HAPE	1.48	-4.76%	35.96	-5.91%	1.10	-0.34%	19.77	-14.28%	1.04	-0.11%	18.91	-14.33%
RTSAH EP2	1.41	0.40%	34.80	-2.78%	1.09	0.08%	17.30	-2.02%	1.04	0.25%	16.53	-1.97%
RTSAH APE2	1.40	0.64%	35.20	-3.90%	1.10	-0.36%	17.26	-1.81%	1.05	-0.25%	16.49	-1.73%
RTSAH HAPE2	1.42	-0.89%	35.28	-4.10%	1.10	-0.14%	19.24	-11.91%	1.04	0.04%	18.39	-11.91%
Icosahderon3												
SAH	0.74	Ref.	18.60	Ref.	0.68	Ref.	9.94	Ref.	0.63	Ref.	9.13	Ref.
RTSAH E	0.74	0.75%	19.14	-2.84%	0.68	-0.22%	10.26	-3.12%	0.63	-0.37%	9.42	-3.06%
RTSAH APSA	0.72	2.91%	18.55	0.29%	0.67	1.47%	9.94	0.05%	0.62	1.41%	9.14	-0.06%
RTSAH HAPSA	0.75	-1.43%	18.62	-0.11%	0.68	0.18%	10.63	-6.44%	0.63	0.38%	9.76	-6.44%
RTSAH WCHAPSA	0.75	-1.26%	18.68	-0.46%	0.68	0.45%	10.56	-5.86%	0.62	0.57%	9.71	-5.94%
RTSAH HANPSA	0.74	0.16%	19.38	-4.01%	0.68	0.17%	10.61	-6.31%	0.63	0.37%	9.73	-6.13%
RTSAH WNHANPSA	0.74	-0.38%	18.91	-1.65%	0.68	0.66%	10.50	-5.34%	0.62	0.78%	9.65	-5.41%
RTSAH WNWCHANPSA	0.75	-0.53%	18.84	-1.29%	0.67	0.78%	10.49	-5.23%	0.62	0.97%	9.64	-5.29%
RTSAH HANPSA2	0.74	-0.04%	18.99	-2.04%	0.68	0.43%	10.37	-4.16%	0.62	0.52%	9.54	-4.32%
RTSAH WNHANPSA2	0.75	-0.62%	19.00	-2.13%	0.68	0.21%	10.33	-3.75%	0.63	0.21%	9.51	-4.00%
RTSAH WNWCHANPSA2	0.75	-0.65%	18.65	-0.30%	0.68	0.42%	10.35	-3.90%	0.62	0.47%	9.52	-4.07%
RTSAH EP	0.74	0.27%	18.60	-0.01%	0.68	-0.13%	9.95	-0.07%	0.63	-0.11%	9.14	-0.07%
RTSAH APE	0.74	0.37%	18.41	1.00%	0.68	-0.23%	9.95	-0.13%	0.63	-0.29%	9.14	-0.11%
RTSAH HAPE	0.77	-3.62%	18.88	-1.50%	0.69	-1.07%	10.91	-8.86%	0.63	-0.78%	9.99	-8.61%
RTSAH EP2	0.73	1.48%	18.88	-1.49%	0.68	-0.54%	10.09	-1.44%	0.63	-0.39%	9.27	-1.46%
RTSAH APE2	0.73	1.57%	18.87	-1.42%	0.68	-0.20%	10.03	-0.88%	0.63	-0.12%	9.21	-0.90%
RTSAH HAPE2	0.73	2.03%	19.26	-3.45%	0.68	-0.27%	10.45	-4.87%	0.63	-0.11%	9.58	-4.72%
Icosahderon4												
SAH	3.35	Ref.	32.56	Ref.	2.42	Ref.	31.13	Ref.	1.41	Ref.	28.01	Ref.
RTSAH E	2.76	21.16%	33.78	-3.62%	1.82	32.59%	32.44	-4.06%	1.10	27.77%	28.86	-2.95%
RTSAH APSA	3.88	-13.73%	32.87	-0.95%	2.57	-6.08%	31.80	-2.12%	1.52	-7.22%	28.72	-2.47%
RTSAH HAPSA	3.85	-13.09%	33.17	-1.86%	2.38	1.71%	32.40	-3.93%	1.36	3.89%	29.23	-4.19%
RTSAH WCHAPSA	3.91	-14.33%	33.27	-2.14%	2.46	-1.72%	32.32	-3.68%	1.40	0.83%	29.18	-4.02%
RTSAH HANPSA	3.95	-15.34%	33.65	-3.24%	2.58	-6.39%	32.51	-4.25%	1.52	-7.16%	29.37	-4.62%
RTSAH WNHANPSA	3.83	-12.63%	33.43	-2.60%	2.40	0.55%	32.46	-4.10%	1.38	2.30%	29.30	-4.39%
RTSAH WNWCHANPSA	4.17	-19.80%	33.44	-2.63%	2.86	-15.50%	32.23	-3.44%	1.71	-17.32%	29.13	-3.83%
RTSAH HANPSA2	3.81	-12.15%	33.08	-1.59%	2.58	-6.28%	32.51	-4.25%	1.52	-7.17%	29.41	-4.77%
RTSAH WNHANPSA2	3.81	-12.09%	33.09	-1.61%	2.58	-6.46%	32.48	-4.18%	1.53	-7.58%	29.39	-4.70%
RTSAH WNWCHANPSA2	3.95	-15.36%	33.17	-1.85%	2.80	-13.76%	32.55	-4.39%	1.71	-17.66%	29.46	-4.93%
RTSAH EP	3.55	-5.84%	32.51	0.15%	2.46	-1.74%	31.41	-0.92%	1.44	-2.26%	28.35	-1.20%
RTSAH APE	3.75	-10.81%	33.06	-1.53%	2.73	-11.50%	31.76	-2.01%	1.64	-13.82%	28.64	-2.21%
RTSAH HAPE	4.17	-19.72%	33.80	-3.66%	2.93	-17.65%	34.54	-9.90%	1.78	-20.94%	31.23	-10.31%
RTSAH EP2	3.63	-7.78%	32.92	-1.11%	2.32	4.31%	32.06	-2.90%	1.35	4.23%	28.90	-3.07%
RTSAH APE2	3.70	-9.56%	32.97	-1.27%	2.42	-0.22%	32.00	-2.73%	1.43	-1.29%	28.84	-2.89%
RTSAH HAPE2	3.74	-10.59%	33.98	-4.18%	2.44	-1.13%	34.63	-10.12%	1.38	1.87%	31.30	-10.52%

Table 13: The average number of ray-triangle intersection tests to perform per primary (camera),  $I_c$ , closest-hit shadow (ambient),  $I'_s$ , and any-hit shadow (ambient),  $I_s$ , ray and the average number of ADS node traversal steps to perform per primary (camera),  $T_c$ , closest-hit shadow (ambient),  $T'_s$ , and any-hit shadow (ambient),  $T_s$ , ray for a SBVH ADS, built with various build heuristics, for a variety of artificial test scenes rendered as ambient occlusion images of resolution 512×512 pixels using 512 primary rays per pixel and 1 shadow ray per primary ray which is not limited to a fixed, finite, maximum distance.

Build heuristic	Kd-tree											
	D <sub>max</sub>	D <sub>avg</sub>	L <sub>tot</sub>	RD%	G <sub>max</sub> /L	G <sub>avg</sub> /L	D <sub>max</sub>	D <sub>avg</sub>	L <sub>tot</sub>	RD%	G <sub>max</sub> /L	G <sub>avg</sub> /L
	Empty Box					Cornell Box						
SAH (SP)	2	2.00	4	40%	10	3.50	<b>13</b>	9.13	115	1150%	8	3.26
SAH	<b>12</b>	9.80	397	5320%	6	1.37	<b>13</b>	11.35	917	4563%	8	1.53
RTSAH E	<b>12</b>	10.31	513	6600%	6	1.31	<b>13</b>	11.56	1056	5263%	6	1.52
RTSAH Z	<b>12</b>	10.58	604	7960%	6	1.33	<b>13</b>	11.84	1210	6337%	6	1.60
RTSAH N	<b>12</b>	10.42	565	7360%	6	1.32	<b>13</b>	11.73	1181	6130%	6	1.58
RTSAH SA	<b>12</b>	10.41	553	7000%	6	1.28	<b>13</b>	11.69	1130	5957%	6	1.61
RTSAH APSA	<b>12</b>	10.31	540	8800%	6	1.65	<b>13</b>	11.65	1113	6833%	6	1.87
RTSAH HAPSA	<b>12</b>	10.55	588	6940%	6	1.20	<b>13</b>	11.75	1160	6090%	6	1.60
RTSAH WCHAPSA	<b>12</b>	10.51	582	6940%	6	1.21	<b>13</b>	11.77	1158	5977%	6	1.57
RTSAH HANPSA	<b>12</b>	10.48	567	7260%	6	1.30	<b>13</b>	11.69	1116	5593%	6	1.53
RTSAH WNHANPSA	<b>12</b>	10.47	569	7020%	6	1.25	<b>13</b>	11.73	1141	5733%	6	1.53
RTSAH WNCHANPSA	<b>12</b>	10.55	594	7880%	6	1.34	<b>13</b>	11.74	1143	6020%	6	1.61
RTSAH HANPSA2	<b>12</b>	10.47	574	6640%	6	1.17	<b>13</b>	11.57	1002	5133%	6	1.57
RTSAH WNHANPSA2	<b>12</b>	10.44	567	7060%	6	1.26	<b>13</b>	11.55	995	5343%	6	1.64
RTSAH WNWCHANPSA2	<b>12</b>	10.46	570	7080%	6	1.26	<b>13</b>	11.56	1015	5480%	6	1.65
RTSAH EP	<b>12</b>	10.37	544	7160%	6	1.33	<b>13</b>	11.66	1102	5857%	6	1.62
RTSAH APE	<b>12</b>	10.37	557	9000%	6	1.63	<b>13</b>	11.60	1088	6340%	6	1.78
RTSAH HAPE	<b>12</b>	10.49	570	6920%	6	1.23	<b>13</b>	11.81	1231	6993%	6	1.73
RTSAH EP2	<b>12</b>	10.51	581	6080%	6	1.06	<b>13</b>	11.80	1269	6617%	6	1.59
RTSAH APE2	<b>12</b>	10.61	609	7520%	6	1.25	<b>13</b>	11.85	1266	6663%	6	1.60
RTSAH HAPE2	<b>12</b>	10.17	463	5460%	6	1.20	<b>13</b>	11.72	1259	6660%	6	1.61
Icosahedron1												
SAH (SP)	<b>24</b>	21.05	61 k	2984%	12	2.61	<b>24</b>	21.18	58 k	2848%	10	2.59
SAH	<b>24</b>	22.48	137 k	5727%	12	2.19	<b>24</b>	22.65	126 k	5403%	10	2.22
RTSAH E	<b>24</b>	22.67	255 k	10538%	9	2.14	<b>24</b>	22.71	233 k	9706%	9	2.15
RTSAH Z	<b>24</b>	23.16	491 k	17818%	9	1.87	<b>24</b>	23.15	516 k	18749%	8	1.86
RTSAH N	<b>24</b>	23.21	497 k	18684%	9	1.94	<b>24</b>	23.24	478 k	18042%	8	1.94
RTSAH SA	<b>24</b>	23.01	348 k	14362%	9	2.13	<b>24</b>	23.04	333 k	13746%	9	2.12
RTSAH APSA	<b>24</b>	22.68	222 k	9397%	9	2.19	<b>24</b>	22.74	204 k	8642%	11	2.19
RTSAH HAPSA	<b>24</b>	22.64	322 k	13155%	9	2.11	<b>24</b>	22.60	300 k	12336%	9	2.11
RTSAH WCHAPSA	<b>24</b>	22.73	337 k	13835%	10	2.12	<b>24</b>	22.72	318 k	13121%	9	2.12
RTSAH HANPSA	<b>24</b>	22.78	376 k	15276%	9	2.10	<b>24</b>	22.74	376 k	15312%	9	2.09
RTSAH WNHANPSA	<b>24</b>	22.79	383 k	15496%	9	2.09	<b>24</b>	22.76	386 k	15667%	9	2.09
RTSAH WNCHANPSA	<b>24</b>	22.82	395 k	15981%	9	2.09	<b>24</b>	22.78	397 k	16116%	9	2.09
RTSAH HANPSA2	<b>24</b>	22.51	283 k	11849%	11	2.16	<b>24</b>	22.50	274 k	11515%	9	2.16
RTSAH WNHANPSA2	<b>24</b>	22.52	281 k	11743%	11	2.16	<b>24</b>	22.52	273 k	11484%	11	2.16
RTSAH WNWCHANPSA2	<b>24</b>	22.58	300 k	12636%	9	2.18	<b>24</b>	22.59	284 k	12016%	9	2.18
RTSAH EP	<b>24</b>	22.87	249 k	10454%	11	2.18	<b>24</b>	22.91	238 k	10038%	11	2.18
RTSAH APE	<b>24</b>	22.84	236 k	10088%	9	2.21	<b>24</b>	22.89	225 k	9631%	9	2.21
RTSAH HAPE	<b>24</b>	22.76	381 k	15407%	9	2.09	<b>24</b>	22.78	366 k	14871%	9	2.08
RTSAH EP2	<b>24</b>	23.01	341 k	13287%	10	2.01	<b>24</b>	23.06	325 k	12702%	10	2.01
RTSAH APE2	<b>24</b>	23.08	318 k	12555%	11	2.04	<b>24</b>	23.11	315 k	12527%	9	2.04
RTSAH HAPE2	<b>24</b>	22.56	292 k	11613%	10	2.06	<b>24</b>	22.60	276 k	11015%	9	2.05
Icosahedron3												
SAH (SP)	<b>24</b>	20.37	78 k	4372%	27	2.94	<b>25</b>	20.46	110 k	3804%	24	3.24
SAH	<b>24</b>	22.00	171 k	8054%	27	2.44	<b>25</b>	22.36	333 k	8506%	24	2.35
RTSAH E	<b>24</b>	22.19	322 k	16626%	18	2.66	<b>25</b>	22.86	560 k	16445%	20	2.69
RTSAH Z	<b>24</b>	23.25	793 k	36495%	18	2.36	<b>25</b>	24.00	1124 k	29256%	28	2.37
RTSAH N	<b>24</b>	23.27	953 k	49544%	16	2.67	<b>25</b>	23.96	1359 k	40789%	20	2.73
RTSAH SA	<b>24</b>	22.73	531 k	28109%	17	2.72	<b>25</b>	23.35	774 k	22991%	20	2.71
RTSAH APSA	<b>24</b>	22.17	289 k	14975%	17	2.67	<b>25</b>	22.85	548 k	17430%	20	2.91
RTSAH HAPSA	<b>24</b>	22.47	415 k	22762%	18	2.82	<b>25</b>	23.13	678 k	20783%	24	2.80
RTSAH WCHAPSA	<b>24</b>	22.57	466 k	25821%	19	2.85	<b>25</b>	23.25	729 k	22666%	24	2.84
RTSAH HANPSA	<b>24</b>	22.64	506 k	26694%	18	2.71	<b>25</b>	23.27	776 k	23363%	24	2.75
RTSAH WNHANPSA	<b>24</b>	22.65	519 k	27373%	18	2.71	<b>25</b>	23.30	786 k	23640%	24	2.74
RTSAH WNWCHANPSA	<b>24</b>	22.69	539 k	28435%	18	2.71	<b>25</b>	23.35	815 k	24607%	24	2.75
RTSAH HANPSA2	<b>24</b>	22.20	348 k	18387%	19	2.72	<b>25</b>	22.84	565 k	16207%	20	2.62
RTSAH WNHANPSA2	<b>24</b>	22.24	353 k	18769%	20	2.74	<b>25</b>	22.84	572 k	16521%	20	2.64
RTSAH WNCHANPSA2	<b>24</b>	22.30	375 k	20131%	19	2.76	<b>25</b>	22.93	598 k	17714%	20	2.71
RTSAH EP	<b>24</b>	22.53	341 k	17625%	20	2.66	<b>25</b>	23.04	556 k	16033%	20	2.63
RTSAH APE	<b>24</b>	22.49	319 k	16528%	20	2.67	<b>25</b>	23.02	556 k	17201%	20	2.83
RTSAH HAPE	<b>24</b>	22.80	522 k	28693%	18	2.82	<b>25</b>	23.40	851 k	26667%	20	2.85
RTSAH EP2	<b>24</b>	22.98	518 k	25527%	29	2.53	<b>25</b>	23.59	724 k	19683%	21	2.48
RTSAH APE2	<b>24</b>	22.98	517 k	26096%	22	2.60	<b>25</b>	23.60	789 k	23256%	20	2.69
RTSAH HAPE2	<b>24</b>	22.45	380 k	20254%	21	2.74	<b>25</b>	22.91	635 k	18580%	20	2.67

Table 14: The maximum (average) tree depth, D<sub>max</sub> (D<sub>avg</sub>) (in **bold** if equal to the fixed tree depth), the total number of leaf nodes, L<sub>tot</sub>, The geometric primitive reference duplication percentage, RD%, and the maximum (average) number of geometric primitives per leaf node, G<sub>max</sub>/L (G<sub>avg</sub>/L) for constructing the **kd-tree** ADSs with various build heuristics for a variety of artificial test scenes.

Build heuristic	BIH											
	D <sub>max</sub>	D <sub>avg</sub>	L <sub>tot</sub>	RD%	G <sub>max/L</sub>	G <sub>avg/L</sub>	D <sub>max</sub>	D <sub>avg</sub>	L <sub>tot</sub>	RD%	G <sub>max/L</sub>	G <sub>avg/L</sub>
	Empty Box						Cornell Box					
SAH	6	4.50	14	0%	1	0.71	11	6.94	53	0%	1	0.57
RTSAH E	4	3.50	10	0%	1	1.00	11	6.60	40	0%	1	0.75
RTSAH Z	7	4.20	10	0%	1	1.00	8	5.57	30	0%	1	1.00
RTSAH N	4	3.40	10	0%	1	1.00	7	5.28	32	0%	1	0.94
RTSAH SA	6	4.09	11	0%	1	0.91	10	6.38	42	0%	1	0.71
RTSAH APSA	6	4.09	11	0%	1	0.91	9	6.00	41	0%	1	0.73
RTSAH HAPSA	5	3.80	10	0%	1	1.00	9	6.02	42	0%	1	0.71
RTSAH WCHAPSA	5	3.80	10	0%	1	1.00	10	6.23	44	0%	1	0.68
RTSAH HANPSA	6	4.09	11	0%	1	0.91	9	5.88	40	0%	1	0.75
RTSAH WNCHANPSA	6	4.09	11	0%	1	0.91	9	5.88	40	0%	1	0.75
RTSAH WNWCHANPSA	6	4.09	11	0%	1	0.91	9	5.88	40	0%	1	0.75
RTSAH HANPSA2	6	4.09	11	0%	1	0.91	10	6.47	43	0%	1	0.70
RTSAH WNCHANPSA2	6	4.09	11	0%	1	0.91	10	6.27	41	0%	1	0.73
RTSAH WNWCHANPSA2	6	4.09	11	0%	1	0.91	9	5.86	37	0%	1	0.81
RTSAH EP	5	3.80	10	0%	1	1.00	11	7.20	40	0%	1	0.75
RTSAH APE	5	3.80	10	0%	1	1.00	9	6.00	41	0%	1	0.73
RTSAH HAPE	5	3.80	10	0%	1	1.00	10	6.41	39	0%	1	0.77
RTSAH EP2	5	3.80	10	0%	1	1.00	11	6.51	37	0%	1	0.81
RTSAH APE2	5	3.80	10	0%	1	1.00	11	6.97	39	0%	1	0.77
RTSAH HAPE2	6	4.17	12	0%	1	0.83	10	6.50	46	0%	1	0.65
Icosahedron1												
SAH	21	14.75	6456	0%	4	0.79	19	14.29	6338	0%	1	0.80
RTSAH E	20	14.72	6571	0%	1	0.78	18	13.91	6360	0%	1	0.80
RTSAH Z	19	14.23	5467	0%	1	0.94	17	13.25	5370	0%	1	0.95
RTSAH N	18	13.75	6147	0%	1	0.83	16	13.38	5924	0%	1	0.86
RTSAH SA	20	14.23	6396	0%	4	0.80	18	13.78	6183	0%	1	0.82
RTSAH APSA	20	14.60	6456	0%	4	0.79	19	14.11	6339	0%	1	0.80
RTSAH HAPSA	20	14.09	6562	0%	4	0.78	19	13.77	6439	0%	1	0.79
RTSAH WCHAPSA	20	14.56	6608	0%	4	0.78	17	13.74	6465	0%	1	0.79
RTSAH HANPSA	20	14.43	6681	0%	4	0.77	17	13.47	6612	0%	1	0.77
RTSAH WNCHANPSA	20	14.25	6408	0%	4	0.80	17	13.41	6399	0%	1	0.80
RTSAH WNWCHANPSA	21	14.09	6351	0%	4	0.81	17	13.41	6409	0%	1	0.80
RTSAH HANPSA2	21	14.14	6801	0%	4	0.75	18	13.78	6751	0%	1	0.76
RTSAH WNCHANPSA2	21	14.13	6750	0%	4	0.76	18	13.77	6710	0%	1	0.76
RTSAH WNWCHANPSA2	21	14.39	6732	0%	4	0.76	18	13.76	6673	0%	1	0.76
RTSAH EP	21	15.38	6324	0%	1	0.81	18	13.96	6232	0%	1	0.82
RTSAH APE	20	14.48	6376	0%	4	0.80	18	14.02	6226	0%	1	0.82
RTSAH HAPE	20	13.91	6498	0%	4	0.79	18	13.51	6310	0%	1	0.81
RTSAH EP2	22	15.95	6280	0%	1	0.82	18	13.92	6204	0%	1	0.82
RTSAH APE2	22	15.98	6292	0%	1	0.82	19	13.98	6247	0%	1	0.82
RTSAH HAPE2	21	14.24	6777	0%	4	0.76	18	13.92	6711	0%	1	0.76
Icosahedron3												
SAH	19	14.39	6258	0%	1	0.82	23	14.88	11828	0%	10	0.77
RTSAH E	19	13.97	6145	0%	1	0.83	22	14.72	11609	0%	10	0.78
RTSAH Z	17	13.62	5309	0%	1	0.96	28	14.96	9423	0%	1	0.96
RTSAH N	16	13.37	5547	0%	1	0.92	17	13.88	10483	0%	1	0.87
RTSAH SA	18	13.80	5981	0%	1	0.86	23	14.60	11143	0%	10	0.81
RTSAH APSA	19	14.09	6198	0%	1	0.83	23	14.80	11764	0%	10	0.77
RTSAH HAPSA	20	13.87	6219	0%	1	0.82	22	14.79	12122	0%	10	0.75
RTSAH WCHAPSA	19	13.90	6184	0%	1	0.83	24	14.76	11886	0%	10	0.76
RTSAH HANPSA	19	13.73	6094	0%	1	0.84	22	14.71	11992	0%	10	0.76
RTSAH WNCHANPSA	19	13.66	5882	0%	1	0.87	22	14.61	11596	0%	10	0.78
RTSAH WNWCHANPSA	19	13.64	5843	0%	1	0.88	21	14.65	11729	0%	10	0.77
RTSAH HANPSA2	19	14.00	6386	0%	1	0.80	25	14.87	12217	0%	10	0.74
RTSAH WNCHANPSA2	19	13.97	6347	0%	1	0.81	25	14.85	12149	0%	10	0.75
RTSAH WNWCHANPSA2	20	13.97	6328	0%	1	0.81	23	14.84	12095	0%	10	0.75
RTSAH EP	19	14.08	6016	0%	1	0.85	21	14.56	11635	0%	3	0.78
RTSAH APE	20	14.17	5966	0%	1	0.86	22	14.68	12003	0%	3	0.76
RTSAH HAPE	20	14.01	5998	0%	1	0.85	21	14.80	12397	0%	6	0.73
RTSAH EP2	20	14.11	5921	0%	1	0.86	24	14.87	12627	0%	4	0.72
RTSAH APE2	19	14.13	6051	0%	1	0.85	22	14.82	12817	0%	4	0.71
RTSAH HAPE2	20	14.16	6382	0%	1	0.80	22	15.00	13301	0%	6	0.68

Table 15: The maximum (average) tree depth, D<sub>max</sub> (D<sub>avg</sub>) (in **bold** if equal to the fixed tree depth), the total number of leaf nodes, L<sub>tot</sub>, The geometric primitive reference duplication percentage, RD%, and the maximum (average) number of geometric primitives per leaf node, G<sub>max/L</sub> (G<sub>avg/L</sub>) for constructing the BIH ADSs with various build heuristics for a variety of artificial test scenes.

BVH												
Build heuristic	D <sub>max</sub>	D <sub>avg</sub>	L <sub>tot</sub>	RD%	G <sub>max</sub> /L	G <sub>avg</sub> /L	D <sub>max</sub>	D <sub>avg</sub>	L <sub>tot</sub>	RD%	G <sub>max</sub> /L	G <sub>avg</sub> /L
	Empty Box						Cornell Box					
SAH	5	3.80	10	0%	1	1.00	8	5.47	30	0%	1	1.00
RTSAH E	5	3.80	10	0%	1	1.00	8	5.53	30	0%	1	1.00
RTSAH APSA	5	3.80	10	0%	1	1.00	8	5.53	30	0%	1	1.00
RTSAH HAPSA	5	3.80	10	0%	1	1.00	8	5.50	30	0%	1	1.00
RTSAH WCHAPSA	5	3.80	10	0%	1	1.00	8	5.50	30	0%	1	1.00
RTSAH HANPSA	5	3.80	10	0%	1	1.00	7	5.37	30	0%	1	1.00
RTSAH WNHNPSA	5	3.80	10	0%	1	1.00	7	5.37	30	0%	1	1.00
RTSAH WNWCHANPSA	5	3.80	10	0%	1	1.00	7	5.37	30	0%	1	1.00
RTSAH HANPSA2	5	3.80	10	0%	1	1.00	9	5.67	30	0%	1	1.00
RTSAH WNHNPSA2	5	3.80	10	0%	1	1.00	9	5.73	30	0%	1	1.00
RTSAH EP	5	3.80	10	0%	1	1.00	8	5.63	30	0%	1	1.00
RTSAH APE	5	3.80	10	0%	1	1.00	8	5.50	30	0%	1	1.00
RTSAH HAPE	5	3.80	10	0%	1	1.00	8	5.50	30	0%	1	1.00
RTSAH EP2	5	3.80	10	0%	1	1.00	8	5.63	30	0%	1	1.00
RTSAH APE2	5	3.80	10	0%	1	1.00	8	5.57	30	0%	1	1.00
RTSAH HAPE2	5	3.80	10	0%	1	1.00	8	5.53	30	0%	1	1.00
	Icosahedron1						Icosahedron2					
SAH	17	13.15	5130	0%	1	1.00	16	12.78	5100	0%	1	1.00
RTSAH E	17	13.13	5130	0%	1	1.00	16	12.76	5100	0%	1	1.00
RTSAH APSA	17	13.12	5130	0%	1	1.00	16	12.77	5100	0%	1	1.00
RTSAH HAPSA	18	13.01	5130	0%	1	1.00	16	12.78	5100	0%	1	1.00
RTSAH WCHAPSA	17	13.03	5130	0%	1	1.00	16	12.76	5100	0%	1	1.00
RTSAH HANPSA	17	12.94	5130	0%	1	1.00	16	12.72	5100	0%	1	1.00
RTSAH WNHNPSA	17	12.94	5130	0%	1	1.00	16	12.72	5100	0%	1	1.00
RTSAH WNWCHANPSA	17	12.95	5130	0%	1	1.00	16	12.73	5100	0%	1	1.00
RTSAH HANPSA2	18	13.03	5130	0%	1	1.00	16	12.79	5100	0%	1	1.00
RTSAH WNHNPSA2	18	13.26	5130	0%	1	1.00	16	12.78	5100	0%	1	1.00
RTSAH WNWCHANPSA2	18	13.06	5130	0%	1	1.00	16	12.78	5100	0%	1	1.00
RTSAH EP	17	13.06	5130	0%	1	1.00	16	12.75	5100	0%	1	1.00
RTSAH APE	17	13.09	5130	0%	1	1.00	16	12.76	5100	0%	1	1.00
RTSAH HAPE	18	13.14	5130	0%	1	1.00	16	12.76	5100	0%	1	1.00
RTSAH EP2	17	13.09	5130	0%	1	1.00	16	12.76	5100	0%	1	1.00
RTSAH APE2	17	13.10	5130	0%	1	1.00	16	12.76	5100	0%	1	1.00
RTSAH HAPE2	17	13.09	5130	0%	1	1.00	16	12.77	5100	0%	1	1.00
	Icosahedron3						Icosahedron4					
SAH	17	13.05	5120	0%	1	1.00	19	13.69	7661	0%	3	1.19
RTSAH E	17	12.93	5120	0%	1	1.00	19	13.78	8302	0%	3	1.09
RTSAH APSA	17	12.97	5120	0%	1	1.00	31	13.79	8296	0%	3	1.09
RTSAH HAPSA	16	12.95	5120	0%	1	1.00	31	13.76	8306	0%	3	1.09
RTSAH WCHAPSA	16	12.93	5120	0%	1	1.00	31	13.77	8313	0%	3	1.09
RTSAH HANPSA	16	12.91	5120	0%	1	1.00	31	13.71	8312	0%	3	1.09
RTSAH WNHNPSA	16	12.98	5120	0%	1	1.00	31	13.72	8312	0%	3	1.09
RTSAH WNWCHANPSA	16	12.98	5120	0%	1	1.00	31	13.71	8313	0%	3	1.09
RTSAH HANPSA2	17	12.96	5120	0%	1	1.00	31	13.76	8294	0%	3	1.09
RTSAH WNHNPSA2	17	12.96	5120	0%	1	1.00	31	13.78	8294	0%	3	1.09
RTSAH WNWCHANPSA2	17	12.95	5120	0%	1	1.00	31	13.76	8294	0%	3	1.09
RTSAH EP	17	13.03	5120	0%	1	1.00	23	13.86	8298	0%	3	1.09
RTSAH APE	17	13.07	5120	0%	1	1.00	23	13.87	8286	0%	3	1.10
RTSAH HAPE	17	13.04	5120	0%	1	1.00	33	13.78	8302	0%	3	1.09
RTSAH EP2	16	13.02	5120	0%	1	1.00	23	13.88	8337	0%	3	1.09
RTSAH APE2	18	13.06	5120	0%	1	1.00	21	13.86	8305	0%	3	1.09
RTSAH HAPE2	18	13.02	5120	0%	1	1.00	36	13.82	8336	0%	3	1.09

Table 16: The maximum (average) tree depth, D<sub>max</sub> (D<sub>avg</sub>) (in **bold** if equal to the fixed tree depth), the total number of leaf nodes, L<sub>tot</sub>, The geometric primitive reference duplication percentage, RD%, and the maximum (average) number of geometric primitives per leaf node, G<sub>max</sub>/L (G<sub>avg</sub>/L) for constructing the **BVH** ADSs with various build heuristics for a variety of artificial test scenes.

SBVH												
Build heuristic	D <sub>max</sub>	D <sub>avg</sub>	L <sub>tot</sub>	RD%	G <sub>max</sub> /L	G <sub>avg</sub> /L	D <sub>max</sub>	D <sub>avg</sub>	L <sub>tot</sub>	RD%	G <sub>max</sub> /L	G <sub>avg</sub> /L
	Empty Box						Cornell Box					
SAH	5	3.80	10	80%	2	1.80	10	6.65	52	117%	2	1.25
RTSAH E	5	3.80	10	0%	1	1.00	8	5.53	30	0%	1	1.00
RTSAH APSA	5	3.89	9	40%	2	1.56	<b>13</b>	9.47	131	437%	2	1.23
RTSAH HAPSA	6	4.60	15	130%	2	1.53	<b>13</b>	8.98	110	370%	4	1.28
RTSAH WCHAPSA	5	3.67	9	40%	2	1.56	<b>13</b>	8.82	116	367%	4	1.21
RTSAH HANPSA	6	4.82	17	130%	2	1.35	<b>13</b>	8.92	106	310%	2	1.16
RTSAH WNCHANPSA	6	4.82	17	130%	2	1.35	<b>13</b>	9.25	109	350%	3	1.24
RTSAH WNWCHANPSA	6	4.82	17	130%	2	1.35	<b>13</b>	9.08	107	330%	2	1.21
RTSAH HANPSA2	5	3.89	9	40%	2	1.56	11	7.78	76	190%	2	1.14
RTSAH WNCHANPSA2	5	3.89	9	40%	2	1.56	<b>13</b>	9.16	125	377%	2	1.14
RTSAH WNWCHANPSA2	5	3.89	9	40%	2	1.56	<b>13</b>	8.81	96	277%	2	1.18
RTSAH EP	5	3.67	9	40%	2	1.56	9	6.37	46	80%	3	1.17
RTSAH APE	5	3.67	9	40%	2	1.56	<b>13</b>	10.27	117	390%	2	1.26
RTSAH HAPE	5	3.67	9	40%	2	1.56	<b>13</b>	9.32	105	317%	2	1.19
RTSAH EP2	5	3.67	9	40%	2	1.56	<b>13</b>	10.23	188	650%	2	1.20
RTSAH APE2	5	3.67	9	40%	2	1.56	<b>13</b>	10.08	114	390%	2	1.29
RTSAH HAPE2	5	3.89	9	40%	2	1.56	12	7.93	84	200%	2	1.07
	Icosahedron1						Icosahedron2					
SAH	23	13.81	7041	0%	2	1.01	22	13.11	5631	10%	2	1.00
RTSAH E	17	13.13	5130	0%	1	1.00	16	12.76	5100	0%	1	1.00
RTSAH APSA	<b>24</b>	15.51	10559	110%	2	1.02	<b>24</b>	14.83	7939	58%	2	1.02
RTSAH HAPSA	<b>24</b>	15.05	10306	103%	2	1.00	<b>24</b>	14.13	7152	41%	2	1.01
RTSAH WCHAPSA	<b>24</b>	15.46	10995	119%	2	1.02	<b>24</b>	14.82	8182	63%	2	1.01
RTSAH HANPSA	<b>24</b>	16.23	13731	171%	2	1.01	<b>24</b>	15.59	10316	104%	2	1.01
RTSAH WNCHANPSA	<b>24</b>	16.19	13203	162%	2	1.02	<b>24</b>	15.50	9877	97%	2	1.02
RTSAH WNWCHANPSA	<b>24</b>	16.32	13072	162%	2	1.03	<b>24</b>	15.73	10205	105%	2	1.03
RTSAH HANPSA2	<b>24</b>	14.78	9380	85%	2	1.01	<b>24</b>	13.96	7303	44%	2	1.00
RTSAH WNCHANPSA2	<b>24</b>	14.51	8787	72%	2	1.01	<b>24</b>	13.72	6856	34%	2	1.00
RTSAH WNWCHANPSA2	<b>24</b>	14.92	9708	90%	2	1.01	<b>24</b>	14.05	7306	43%	2	1.00
RTSAH EP	<b>24</b>	14.78	9249	82%	2	1.01	<b>24</b>	14.31	7582	50%	2	1.01
RTSAH APE	<b>24</b>	16.92	13675	182%	2	1.06	<b>24</b>	16.54	10740	123%	2	1.06
RTSAH HAPE	<b>24</b>	15.77	11797	137%	2	1.03	<b>24</b>	14.25	7120	42%	2	1.02
RTSAH EP2	<b>24</b>	14.17	8665	70%	3	1.01	<b>24</b>	13.47	6806	34%	2	1.00
RTSAH APE2	<b>24</b>	14.12	8261	63%	2	1.01	<b>24</b>	13.45	6466	27%	2	1.00
RTSAH HAPE2	<b>24</b>	14.49	10037	97%	2	1.00	<b>24</b>	13.60	7003	37%	2	1.00
	Icosahedron3						Icosahedron4					
SAH	23	13.33	5617	10%	1	1.00	<b>25</b>	14.18	8401	47%	12	1.59
RTSAH E	17	12.93	5120	0%	1	1.00	19	13.78	8302	0%	3	1.09
RTSAH APSA	<b>24</b>	15.30	8789	75%	4	1.02	<b>25</b>	16.55	14524	139%	24	1.50
RTSAH HAPSA	<b>24</b>	14.40	7458	46%	3	1.01	24	17.11	16325	167%	24	1.48
RTSAH WCHAPSA	<b>24</b>	14.77	8006	59%	3	1.02	<b>25</b>	17.32	16860	179%	24	1.50
RTSAH HANPSA	<b>24</b>	14.68	8028	58%	2	1.01	<b>25</b>	16.34	13415	132%	24	1.57
RTSAH WNCHANPSA	<b>24</b>	14.67	7712	53%	4	1.01	<b>25</b>	16.16	12748	120%	24	1.57
RTSAH WNWCHANPSA	<b>24</b>	15.11	8227	64%	2	1.02	<b>25</b>	16.48	13343	132%	24	1.58
RTSAH HANPSA2	<b>24</b>	14.11	7042	38%	2	1.01	<b>25</b>	16.34	13550	111%	24	1.41
RTSAH WNCHANPSA2	<b>24</b>	14.04	7023	37%	2	1.00	<b>25</b>	16.24	12804	101%	24	1.43
RTSAH WNWCHANPSA2	<b>24</b>	14.36	7356	44%	3	1.00	<b>25</b>	16.53	14057	121%	24	1.43
RTSAH EP	<b>24</b>	13.65	6091	19%	2	1.00	<b>25</b>	15.78	12019	89%	16	1.43
RTSAH APE	<b>24</b>	14.91	7234	45%	2	1.03	<b>25</b>	16.58	13955	124%	16	1.46
RTSAH HAPE	<b>24</b>	13.98	6345	25%	2	1.01	<b>25</b>	15.51	10918	91%	24	1.59
RTSAH EP2	<b>24</b>	13.55	6294	23%	2	1.00	<b>25</b>	14.84	9412	49%	12	1.44
RTSAH APE2	<b>24</b>	13.66	6268	23%	2	1.00	<b>25</b>	14.92	9695	62%	13	1.52
RTSAH HAPE2	<b>24</b>	13.86	6937	36%	2	1.00	<b>25</b>	15.62	11424	81%	28	1.44

Table 17: The maximum (average) tree depth, D<sub>max</sub> (D<sub>avg</sub>) (in **bold** if equal to the fixed tree depth), the total number of leaf nodes, L<sub>tot</sub>, The geometric primitive reference duplication percentage, RD%, and the maximum (average) number of geometric primitives per leaf node, G<sub>max</sub>/L (G<sub>avg</sub>/L) for constructing the **SBVH** ADSs with various build heuristics for a variety of artificial test scenes.

Build heuristic	Kd-tree											
	I <sub>c</sub>	ΔI <sub>c</sub>	T <sub>c</sub>	ΔT <sub>c</sub>	I' <sub>s</sub>	ΔI' <sub>s</sub>	T' <sub>s</sub>	ΔT' <sub>s</sub>	I <sub>s</sub>	ΔI <sub>s</sub>	T <sub>s</sub>	ΔT <sub>s</sub>
	Kitchen - Viewpoint 1											
SAH (SP)	5.24	-6.86%	59.32	7.70%	6.42	-13.81%	47.66	20.99%	5.17	-11.05%	46.98	21.51%
SAH	4.88	Ref.	63.88	Ref.	5.53	Ref.	57.66	Ref.	4.60	Ref.	57.09	Ref.
RTSAH Z	10.68	-54.34%	71.89	-11.14%	14.45	-61.73%	76.80	-24.92%	12.17	-62.23%	74.76	-23.64%
RTSAH N	6.76	-27.87%	65.38	-2.30%	8.51	-34.99%	62.26	-7.38%	7.15	-35.71%	61.16	-6.67%
RTSAH SA	5.09	-4.11%	63.45	0.67%	5.74	-3.72%	60.22	-4.25%	4.79	-3.92%	59.48	-4.03%
RTSAH APSA	4.89	-0.21%	63.68	0.31%	5.58	-0.88%	57.62	0.07%	4.64	-0.94%	57.01	0.13%
RTSAH HANPSA2	4.80	1.57%	56.36	13.35%	5.67	-2.51%	60.12	-4.10%	4.73	-2.72%	59.44	-3.96%
RTSAH WNHANPSA2	4.83	0.91%	55.84	14.41%	5.60	-1.20%	60.21	-4.24%	4.66	-1.24%	59.53	-4.10%
RTSAH WNWCHANPSA2	4.83	1.08%	56.34	13.39%	5.73	-3.45%	61.55	-6.32%	4.79	-3.93%	60.85	-6.19%
RTSAH EP	5.10	-4.37%	62.40	2.38%	5.72	-3.30%	58.96	-2.20%	4.77	-3.63%	58.27	-2.03%
RTSAH APE	4.85	0.50%	62.16	2.77%	5.58	-0.94%	58.09	-0.74%	4.65	-1.11%	57.47	-0.67%
Kitchen - Viewpoint 2												
SAH (SP)	5.80	-17.60%	49.81	10.81%	5.52	-16.82%	43.24	23.70%	4.18	-14.22%	42.57	24.11%
SAH	4.78	Ref.	55.20	Ref.	4.59	Ref.	53.49	Ref.	3.58	Ref.	52.83	Ref.
RTSAH Z	15.20	-68.53%	80.96	-31.82%	10.90	-57.87%	66.90	-20.05%	8.57	-58.18%	64.78	-18.44%
RTSAH N	8.31	-42.47%	61.64	-10.46%	6.46	-28.98%	57.50	-6.97%	5.12	-30.01%	56.30	-6.16%
RTSAH SA	5.49	-12.92%	59.62	-7.43%	4.64	-0.98%	55.90	-4.31%	3.61	-0.83%	55.02	-3.99%
RTSAH APSA	4.72	1.28%	57.83	-4.55%	4.51	1.83%	54.56	-1.97%	3.50	2.33%	53.85	-1.89%
RTSAH HANPSA2	4.82	-0.72%	61.20	-9.82%	4.52	1.59%	55.41	-3.47%	3.53	1.44%	54.68	-3.38%
RTSAH WNHANPSA2	4.84	-1.24%	62.32	-11.44%	4.50	2.09%	56.49	-5.32%	3.51	1.96%	55.75	-5.23%
RTSAH WNWCHANPSA2	4.90	-2.48%	59.43	-7.12%	4.53	1.27%	55.75	-4.05%	3.56	0.47%	55.03	-4.00%
RTSAH EP	4.96	-3.67%	59.66	-7.49%	4.61	-0.46%	55.09	-2.91%	3.61	-0.75%	54.30	-2.70%
RTSAH APE	4.82	-0.79%	60.30	-8.47%	4.49	2.24%	54.22	-1.36%	3.51	1.96%	53.48	-1.21%
Kitchen - Viewpoint 3												
SAH (SP)	6.86	-11.29%	63.81	2.29%	7.90	-12.19%	53.19	19.57%	6.25	-9.02%	52.24	20.08%
SAH	6.08	Ref.	65.27	Ref.	6.94	Ref.	63.60	Ref.	5.68	Ref.	62.73	Ref.
RTSAH Z	16.10	-62.23%	85.03	-23.25%	17.16	-59.58%	83.31	-23.67%	14.13	-59.79%	80.81	-22.37%
RTSAH N	10.62	-42.73%	75.66	-13.74%	10.75	-35.46%	69.68	-8.73%	8.87	-35.93%	68.06	-7.83%
RTSAH SA	6.34	-4.07%	66.60	-2.01%	7.12	-2.62%	65.80	-3.35%	5.84	-2.63%	64.69	-3.03%
RTSAH APSA	6.02	0.01%	64.72	0.85%	6.91	0.42%	62.82	1.23%	5.66	0.49%	61.90	1.34%
RTSAH HANPSA2	6.34	-4.16%	74.65	-12.58%	7.15	-2.97%	66.69	-4.64%	5.86	-3.02%	65.64	-4.42%
RTSAH WNHANPSA2	6.11	-0.50%	72.89	-10.46%	6.99	-0.73%	65.61	-3.07%	5.73	-0.75%	64.62	-2.92%
RTSAH WNWCHANPSA2	6.18	-1.63%	70.15	-6.97%	7.05	-1.65%	65.47	-2.85%	5.80	-1.93%	64.51	-2.75%
RTSAH EP	6.19	-1.81%	66.18	-1.38%	7.02	-1.15%	65.48	-2.87%	5.75	-1.15%	64.46	-2.68%
RTSAH APE	6.08	0.09%	65.47	-0.31%	6.91	0.33%	64.61	-1.57%	5.65	0.63%	63.64	-1.43%
Crytek Sponza - Viewpoint 1												
SAH (SP)	4.70	-20.15%	61.27	7.26%	7.08	-18.43%	60.88	15.77%	5.37	-17.49%	59.34	16.34%
SAH	3.76	Ref.	65.71	Ref.	5.77	Ref.	70.49	Ref.	4.43	Ref.	69.03	Ref.
RTSAH Z	7.55	-50.26%	76.72	-14.35%	12.08	-52.22%	89.23	-21.00%	9.00	-50.74%	85.20	-18.98%
RTSAH N	4.73	-20.66%	71.25	-7.77%	7.32	-21.17%	74.87	-5.86%	5.47	-19.02%	72.57	-4.88%
RTSAH SA	3.78	-0.56%	71.91	-8.61%	5.72	0.87%	72.83	-3.22%	4.39	0.91%	71.17	-3.01%
RTSAH APSA	3.75	0.13%	62.30	5.48%	5.65	2.10%	73.20	-3.71%	4.31	2.75%	71.67	-3.68%
RTSAH HANPSA2	3.78	-0.67%	72.50	-9.36%	5.42	6.56%	76.84	-8.27%	4.10	8.18%	75.23	-8.24%
RTSAH WNHANPSA2	3.74	0.44%	71.39	-7.96%	5.48	5.31%	76.06	-7.33%	4.16	6.63%	74.46	-7.29%
RTSAH WNWCHANPSA2	3.72	0.93%	69.10	-4.90%	5.45	5.98%	77.92	-9.54%	4.14	7.10%	76.31	-9.54%
RTSAH EP	3.84	-2.29%	66.98	-1.89%	5.59	3.20%	71.99	-2.09%	4.25	4.37%	70.32	-1.83%
RTSAH APE	3.73	0.65%	68.50	-4.07%	5.65	2.25%	71.88	-1.94%	4.31	2.74%	70.33	-1.84%
Crytek Sponza - Viewpoint 2												
SAH (SP)	4.17	-17.12%	46.49	12.82%	6.10	-21.69%	49.99	20.25%	4.75	-22.41%	48.94	20.71%
SAH	3.46	Ref.	52.46	Ref.	4.78	Ref.	60.11	Ref.	3.68	Ref.	59.07	Ref.
RTSAH Z	7.71	-55.15%	72.60	-27.74%	10.72	-55.41%	77.61	-22.55%	7.76	-52.53%	74.00	-20.18%
RTSAH N	4.41	-21.72%	56.26	-6.76%	5.98	-20.01%	64.74	-7.15%	4.53	-18.68%	63.16	-6.47%
RTSAH SA	3.48	-0.84%	55.43	-5.37%	4.76	0.35%	63.08	-4.71%	3.70	-0.35%	61.92	-4.60%
RTSAH APSA	3.42	1.06%	57.05	-8.05%	4.75	0.71%	62.60	-3.97%	3.68	-0.01%	61.55	-4.02%
RTSAH HANPSA2	3.38	2.19%	63.91	-17.93%	4.64	3.12%	64.83	-7.28%	3.61	2.14%	63.75	-7.33%
RTSAH WNHANPSA2	3.38	2.37%	63.47	-17.36%	4.61	3.63%	64.42	-6.70%	3.59	2.60%	63.36	-6.76%
RTSAH WNWCHANPSA2	3.33	3.75%	55.58	-5.61%	4.59	4.18%	64.39	-6.65%	3.58	2.94%	63.36	-6.77%
RTSAH EP	3.71	-6.87%	56.35	-6.91%	4.95	-3.44%	61.01	-1.48%	3.84	-3.96%	59.76	-1.15%
RTSAH APE	3.40	1.59%	55.20	-4.96%	4.71	1.54%	62.07	-3.16%	3.65	1.01%	61.02	-3.19%
Crytek Sponza - Viewpoint 3												
SAH (SP)	5.99	-10.55%	80.26	-0.49%	9.06	-18.89%	64.16	12.65%	6.96	-21.04%	62.18	13.03%
SAH	5.36	Ref.	79.86	Ref.	7.35	Ref.	72.27	Ref.	5.49	Ref.	70.28	Ref.
RTSAH Z	10.84	-50.57%	88.38	-9.64%	15.15	-51.53%	97.69	-26.02%	11.39	-51.77%	92.54	-24.05%
RTSAH N	7.43	-27.86%	90.96	-12.20%	9.83	-25.30%	78.19	-7.56%	7.29	-24.63%	75.03	-6.33%
RTSAH SA	7.53	-28.80%	89.79	-11.05%	7.62	-3.60%	76.52	-5.55%	5.75	-4.43%	74.16	-5.23%
RTSAH APSA	5.96	-10.02%	88.27	-9.53%	7.23	1.59%	74.36	-2.81%	5.38	2.02%	72.25	-2.73%
RTSAH HANPSA2	6.34	-15.45%	86.65	-7.84%	7.37	-0.30%	80.01	-9.67%	5.54	-0.78%	77.77	-9.63%
RTSAH WNHANPSA2	5.06	5.91%	80.71	-1.05%	7.45	-1.36%	82.01	-11.87%	5.61	-2.04%	79.72	-11.84%
RTSAH WNWCHANPSA2	5.21	2.92%	78.93	1.18%	7.47	-1.66%	80.97	-10.74%	5.65	-2.71%	78.70	-10.70%
RTSAH EP	4.91	9.23%	91.03	-12.27%	7.40	-0.70%	75.00	-3.64%	5.53	-0.71%	72.72	-3.36%
RTSAH APE	5.37	-0.15%	85.69	-6.80%	7.17	2.47%	72.87	-0.82%	5.33	3.12%	70.76	-0.67%

Table 18: The average number of ray-triangle intersection tests to perform per primary (camera), I<sub>c</sub>, closest-hit shadow (ambient), I'<sub>s</sub>, and any-hit shadow (ambient), I<sub>s</sub>, ray and the average number of ADS node traversal steps to perform per primary (camera), T<sub>c</sub>, closest-hit shadow (ambient), T'<sub>s</sub>, and any-hit shadow (ambient), T<sub>s</sub>, ray for a kd-tree ADS, built with various build heuristics, for a variety of realistic test scenes rendered as ambient occlusion images of resolution 512×512 pixels using 512 primary rays per pixel and 1 shadow ray per primary ray which is not limited to a fixed, finite, maximum distance.











BVH												
Build heuristic	$I_c$	$\Delta I_c$	$T_c$	$\Delta T_c$	$I'_s$	$\Delta I'_s$	$T'_s$	$\Delta T'_s$	$I_s$	$\Delta I_s$	$T_s$	$\Delta T_s$
Kitchen - Viewpoint 1												
SAH (SP)	3.07	Ref.	61.18	Ref.	3.68	Ref.	61.55	Ref.	3.07	Ref.	53.46	Ref.
SAH	3.19	-3.61%	58.86	3.95%	3.72	-1.07%	65.26	-5.69%	3.08	-0.38%	56.47	-5.33%
RTSAH APSA	3.06	0.40%	68.80	-11.08%	3.67	0.37%	64.74	-4.92%	3.06	0.37%	56.63	-5.59%
RTSAH HANPSA2	3.08	-0.18%	69.40	-11.85%	3.68	0.10%	64.95	-5.23%	3.07	0.23%	56.69	-5.69%
RTSAH WNHANPSA2	3.14	-2.19%	69.45	-11.91%	3.68	0.12%	64.52	-4.60%	3.07	0.16%	56.34	-5.10%
RTSAH WNWCHANPSA2	3.17	-3.07%	67.69	-9.62%	3.67	0.13%	66.73	-7.76%	3.07	-0.05%	58.72	-8.95%
RTSAH EP	3.04	0.95%	65.24	-6.23%	3.67	0.39%	61.74	-0.31%	3.05	0.66%	53.63	-0.30%
RTSAH APE	3.05	0.68%	65.05	-5.96%	3.67	0.31%	62.65	-1.75%	3.07	0.12%	54.63	-2.14%
Kitchen - Viewpoint 2												
SAH (SP)	3.34	Ref.	75.02	Ref.	3.14	Ref.	64.21	Ref.	2.49	Ref.	54.41	Ref.
SAH	3.36	-0.73%	78.07	-3.91%	3.16	-0.55%	64.21	-0.01%	2.50	-0.11%	54.35	0.11%
RTSAH APSA	3.31	0.89%	78.46	-4.39%	3.11	0.96%	67.28	-4.57%	2.49	0.16%	57.62	-5.58%
RTSAH HANPSA2	3.35	-0.24%	78.47	-4.40%	3.13	0.20%	68.59	-6.39%	2.49	0.02%	58.37	-6.79%
RTSAH WNHANPSA2	3.35	-0.24%	78.22	-4.09%	3.13	0.24%	68.33	-6.03%	2.49	0.01%	58.14	-6.42%
RTSAH WNWCHANPSA2	3.39	-1.38%	82.18	-8.71%	3.13	0.24%	71.42	-10.10%	2.50	-0.20%	60.96	-10.75%
RTSAH EP	3.30	1.19%	71.68	4.66%	3.12	0.53%	65.53	-2.02%	2.50	-0.02%	56.20	-3.20%
RTSAH APE	3.32	0.44%	77.33	-2.99%	3.12	0.73%	67.48	-4.86%	2.50	-0.10%	57.97	-6.14%
Kitchen - Viewpoint 3												
SAH (SP)	3.39	Ref.	91.54	Ref.	4.04	Ref.	77.28	Ref.	3.18	Ref.	65.56	Ref.
SAH	3.35	1.35%	95.41	-4.06%	4.05	-0.27%	80.78	-4.34%	3.19	-0.20%	68.69	-4.57%
RTSAH APSA	3.32	2.08%	95.23	-3.88%	4.02	0.39%	79.54	-2.84%	3.18	0.12%	67.76	-3.25%
RTSAH HANPSA2	3.33	1.96%	93.71	-2.32%	4.04	0.05%	80.83	-4.39%	3.18	-0.04%	68.89	-4.84%
RTSAH WNHANPSA2	3.32	2.04%	93.40	-2.00%	4.04	0.06%	80.32	-3.79%	3.18	-0.11%	68.41	-4.18%
RTSAH WNWCHANPSA2	3.33	1.93%	97.59	-6.21%	4.05	-0.14%	83.46	-7.41%	3.19	-0.16%	71.52	-8.34%
RTSAH EP	3.33	1.82%	94.17	-2.80%	4.03	0.23%	78.47	-1.52%	3.18	0.00%	66.65	-1.64%
RTSAH APE	3.33	1.94%	95.07	-3.72%	4.04	0.02%	79.31	-2.56%	3.18	-0.05%	67.51	-2.90%
Crytek Sponza - Viewpoint 1												
SAH (SP)	2.55	Ref.	84.29	Ref.	3.67	Ref.	97.56	Ref.	2.74	Ref.	72.87	Ref.
SAH	2.50	1.71%	84.30	-0.01%	3.66	0.39%	99.72	-2.17%	2.71	1.16%	74.88	-2.68%
RTSAH APSA	2.50	1.99%	83.44	1.02%	3.65	0.59%	99.53	-1.99%	2.76	-0.62%	75.69	-3.73%
RTSAH HANPSA2	2.49	2.41%	88.56	-4.82%	3.67	0.15%	102.91	-5.20%	2.76	-0.69%	78.08	-6.68%
RTSAH WNHANPSA2	2.51	1.50%	88.16	-4.39%	3.67	0.03%	103.39	-5.64%	2.76	-0.71%	78.38	-7.04%
RTSAH WNWCHANPSA2	2.50	1.86%	85.79	-1.75%	3.65	0.50%	102.55	-4.87%	2.76	-0.68%	77.93	-6.50%
RTSAH EP	3.00	-14.99%	95.00	-11.28%	3.66	0.30%	108.27	-9.90%	2.75	-0.30%	82.14	-11.29%
RTSAH APE	2.74	-7.18%	85.84	-1.81%	3.68	-0.14%	100.08	-2.52%	2.74	0.03%	74.89	-2.70%
Crytek Sponza - Viewpoint 2												
SAH (SP)	2.65	Ref.	88.97	Ref.	3.51	Ref.	90.66	Ref.	2.79	Ref.	65.61	Ref.
SAH	2.66	-0.50%	75.12	18.44%	3.51	0.21%	84.98	6.68%	2.79	0.05%	63.28	3.68%
RTSAH APSA	2.65	-0.18%	72.17	23.29%	3.49	0.69%	87.87	3.17%	2.79	0.10%	64.23	2.15%
RTSAH HANPSA2	2.66	-0.37%	75.08	18.51%	3.50	0.37%	87.14	4.03%	2.79	0.30%	64.82	1.21%
RTSAH WNHANPSA2	2.63	0.64%	75.18	18.35%	3.50	0.47%	86.90	4.32%	2.78	0.32%	64.44	1.82%
RTSAH WNWCHANPSA2	2.66	-0.51%	75.57	17.74%	3.51	0.15%	90.81	-0.16%	2.79	0.05%	66.25	-0.97%
RTSAH EP	2.36	12.14%	77.27	15.14%	3.55	-1.00%	88.02	2.99%	2.82	-0.86%	67.51	-2.81%
RTSAH APE	2.65	0.01%	86.89	2.40%	3.53	-0.43%	89.10	1.74%	2.80	-0.15%	64.95	1.02%
Crytek Sponza - Viewpoint 3												
SAH (SP)	2.96	Ref.	116.12	Ref.	4.61	Ref.	112.79	Ref.	3.31	Ref.	79.82	Ref.
SAH	2.95	0.45%	110.99	4.63%	4.57	1.00%	114.44	-1.44%	3.24	2.06%	81.33	-1.86%
RTSAH APSA	2.96	0.08%	121.08	-4.10%	4.54	1.51%	113.70	-0.79%	3.24	2.20%	80.76	-1.17%
RTSAH HANPSA2	2.92	1.33%	109.83	5.73%	4.56	1.09%	117.65	-4.12%	3.23	2.33%	83.90	-4.86%
RTSAH WNHANPSA2	2.93	1.03%	109.38	6.17%	4.56	1.06%	117.34	-3.88%	3.23	2.32%	83.75	-4.69%
RTSAH WNWCHANPSA2	2.93	1.02%	123.07	-5.65%	4.56	1.11%	115.02	-1.94%	3.24	2.29%	81.88	-2.52%
RTSAH EP	3.43	-13.80%	129.65	-10.44%	4.64	-0.53%	121.80	-7.39%	3.19	3.81%	83.98	-4.95%
RTSAH APE	3.20	-7.58%	120.34	-3.51%	4.64	-0.64%	115.45	-2.30%	3.18	4.15%	78.73	1.39%

Table 24: The average number of ray-triangle intersection tests to perform per primary (camera),  $I_c$ , closest-hit shadow (ambient),  $I'_s$ , and any-hit shadow (ambient),  $I_s$ , ray and the average number of ADS node traversal steps to perform per primary (camera),  $T_c$ , closest-hit shadow (ambient),  $T'_s$ , and any-hit shadow (ambient),  $T_s$ , ray for a **BVH** ADS, built with various build heuristics, for a variety of realistic test scenes rendered as ambient occlusion images of resolution 512×512 pixels using 512 primary rays per pixel and 1 shadow ray per primary ray which is not limited to a fixed, finite, maximum distance.

BVH												
Build heuristic	$I_c$	$\Delta I_c$	$T_c$	$\Delta T_c$	$I'_s$	$\Delta I'_s$	$T'_s$	$\Delta T'_s$	$I_s$	$\Delta I_s$	$T_s$	$\Delta T_s$
Conference Room - Viewpoint 1												
SAH (SP)	4.61	Ref.	57.34	Ref.	5.10	Ref.	59.37	Ref.	3.95	Ref.	47.67	Ref.
SAH	4.60	0.22%	57.08	0.46%	5.09	0.11%	59.76	-0.65%	3.94	0.06%	48.27	-1.25%
RTSAH APSA	4.62	-0.04%	54.25	5.70%	5.15	-0.93%	61.28	-3.12%	3.91	0.85%	47.96	-0.60%
RTSAH HANPSA2	4.60	0.29%	51.49	11.38%	5.07	0.61%	59.19	0.29%	3.90	1.17%	46.81	1.83%
RTSAH WNHANPSA2	4.61	0.03%	51.72	10.88%	5.08	0.35%	59.65	-0.48%	3.90	1.25%	47.05	1.31%
RTSAH WNWCHANPSA2	4.62	-0.20%	51.43	11.51%	5.08	0.33%	59.22	0.25%	3.90	1.15%	46.81	1.82%
RTSAH EP	4.58	0.83%	60.84	-5.75%	5.02	1.61%	64.09	-7.38%	3.92	0.63%	52.27	-8.81%
RTSAH APE	4.56	1.11%	60.15	-4.66%	5.01	1.68%	63.93	-7.14%	3.92	0.70%	52.18	-8.64%
Conference Room - Viewpoint 2												
SAH (SP)	3.83	Ref.	57.98	Ref.	5.05	Ref.	66.04	Ref.	4.01	Ref.	54.93	Ref.
SAH	3.81	0.52%	55.81	3.88%	5.03	0.30%	65.26	1.20%	4.00	0.17%	54.41	0.95%
RTSAH APSA	3.89	-1.48%	54.30	6.77%	5.05	-0.08%	64.67	2.11%	4.02	-0.35%	52.85	3.93%
RTSAH HANPSA2	3.80	0.76%	52.99	9.40%	5.01	0.63%	64.05	3.11%	4.01	-0.14%	52.58	4.46%
RTSAH WNHANPSA2	3.81	0.57%	52.94	9.51%	5.03	0.39%	64.46	2.45%	4.02	-0.22%	52.84	3.96%
RTSAH WNWCHANPSA2	3.80	0.74%	53.20	8.97%	5.02	0.50%	64.05	3.11%	4.01	-0.14%	52.68	4.28%
RTSAH EP	3.64	5.23%	60.28	-3.83%	4.99	1.17%	70.06	-5.74%	4.01	-0.13%	58.96	-6.84%
RTSAH APE	3.64	5.34%	60.90	-4.80%	4.99	1.05%	71.84	-8.07%	4.01	-0.09%	60.72	-9.54%
Conference Room - Viewpoint 3												
SAH (SP)	5.67	Ref.	63.50	Ref.	6.17	Ref.	69.17	Ref.	5.10	Ref.	57.61	Ref.
SAH	5.64	0.51%	63.09	0.64%	6.16	0.11%	69.65	-0.70%	5.10	0.04%	58.29	-1.18%
RTSAH APSA	5.59	1.51%	64.99	-2.30%	6.20	-0.57%	68.87	0.44%	5.04	1.06%	56.39	2.15%
RTSAH HANPSA2	5.60	1.37%	62.66	1.34%	6.15	0.30%	68.32	1.24%	5.02	1.46%	56.08	2.73%
RTSAH WNHANPSA2	5.65	0.41%	62.38	1.79%	6.17	-0.08%	68.11	1.56%	5.03	1.45%	55.86	3.12%
RTSAH WNWCHANPSA2	5.64	0.58%	62.38	1.79%	6.17	-0.03%	68.03	1.68%	5.02	1.46%	55.87	3.10%
RTSAH EP	5.54	2.46%	67.55	-6.00%	6.03	2.28%	72.51	-4.60%	5.01	1.80%	60.99	-5.54%
RTSAH APE	5.51	2.94%	67.70	-6.21%	6.03	2.37%	74.09	-6.65%	5.00	1.89%	62.46	-7.77%
Bedroom - Viewpoint 1												
SAH (SP)	15.56	Ref.	103.09	Ref.	16.82	Ref.	96.61	Ref.	13.99	Ref.	81.12	Ref.
SAH	15.56	0.01%	102.76	0.32%	16.82	0.01%	96.37	0.25%	13.99	-0.01%	80.98	0.16%
RTSAH APSA	15.52	0.25%	105.68	-2.45%	16.84	-0.11%	99.12	-2.53%	13.92	0.53%	83.12	-2.41%
RTSAH HANPSA2	15.63	-0.45%	103.24	-0.14%	16.64	1.07%	97.40	-0.81%	13.54	3.35%	81.04	0.09%
RTSAH WNHANPSA2	15.65	-0.57%	104.21	-1.07%	16.65	1.04%	97.30	-0.71%	13.51	3.58%	80.62	0.62%
RTSAH WNWCHANPSA2	15.53	0.21%	104.34	-1.20%	16.77	0.33%	97.97	-1.39%	13.87	0.91%	81.87	-0.91%
RTSAH EP	15.68	-0.79%	101.53	1.54%	16.67	0.94%	94.88	1.82%	13.63	2.65%	78.93	2.77%
RTSAH APE	15.65	-0.62%	103.00	0.08%	16.71	0.68%	96.72	-0.12%	13.65	2.49%	80.51	0.75%
Bedroom - Viewpoint 2												
SAH (SP)	8.48	Ref.	149.39	Ref.	8.89	Ref.	130.49	Ref.	6.47	Ref.	93.42	Ref.
SAH	8.51	-0.34%	140.70	6.18%	8.90	-0.03%	126.79	2.92%	6.58	-1.67%	92.28	1.23%
RTSAH APSA	8.46	0.19%	135.21	10.49%	8.88	0.19%	125.15	4.27%	6.58	-1.61%	91.74	1.83%
RTSAH HANPSA2	8.34	1.72%	151.60	-1.46%	8.80	1.13%	131.29	-0.60%	6.82	-5.13%	101.58	-8.04%
RTSAH WNHANPSA2	8.44	0.53%	149.62	-0.15%	8.88	0.12%	130.06	0.33%	6.48	-0.13%	94.21	-0.84%
RTSAH WNWCHANPSA2	8.46	0.24%	155.54	-3.95%	8.89	0.06%	130.01	0.38%	6.47	0.05%	93.93	-0.55%
RTSAH EP	8.46	0.30%	137.16	8.91%	8.89	0.07%	127.07	2.70%	6.51	-0.64%	92.53	0.96%
RTSAH APE	8.51	-0.35%	142.55	4.80%	8.86	0.35%	127.42	2.41%	6.58	-1.69%	93.16	0.27%
Bedroom - Viewpoint 3												
SAH (SP)	6.23	Ref.	57.72	Ref.	8.33	Ref.	69.32	Ref.	6.04	Ref.	48.62	Ref.
SAH	6.25	-0.22%	57.23	0.86%	8.33	-0.01%	68.90	0.61%	6.00	0.65%	48.26	0.75%
RTSAH APSA	6.31	-1.22%	61.26	-5.78%	8.27	0.71%	73.38	-5.53%	5.94	1.56%	51.20	-5.04%
RTSAH HANPSA2	6.35	-1.80%	54.88	5.18%	8.18	1.83%	66.92	3.59%	6.82	-11.51%	51.66	-5.88%
RTSAH WNHANPSA2	6.33	-1.56%	59.01	-2.18%	8.36	-0.36%	71.73	-3.35%	6.01	0.51%	50.29	-3.31%
RTSAH WNWCHANPSA2	6.37	-2.16%	58.67	-1.61%	8.36	-0.38%	70.83	-2.13%	6.02	0.36%	50.13	-3.02%
RTSAH EP	6.27	-0.55%	57.22	0.89%	8.20	1.62%	67.06	3.37%	6.86	-11.93%	52.12	-6.72%
RTSAH APE	6.20	0.54%	57.57	0.26%	8.32	0.18%	71.02	-2.39%	6.00	0.56%	49.59	-1.96%

Table 25: The average number of ray-triangle intersection tests to perform per primary (camera),  $I_c$ , closest-hit shadow (ambient),  $I'_s$ , and any-hit shadow (ambient),  $I_s$ , ray and the average number of ADS node traversal steps to perform per primary (camera),  $T_c$ , closest-hit shadow (ambient),  $T'_s$ , and any-hit shadow (ambient),  $T_s$ , ray for a **BVH** ADS, built with various build heuristics, for a variety of realistic test scenes rendered as ambient occlusion images of resolution 512×512 pixels using 512 primary rays per pixel and 1 shadow ray per primary ray which is not limited to a fixed, finite, maximum distance.

BVH													
Build heuristic	$I_c$	$\Delta I_c$	$T_c$	$\Delta T_c$	$I'_s$	$\Delta I'_s$	$T'_s$	$\Delta T'_s$	$I_s$	$\Delta I_s$	$T_s$	$\Delta T_s$	
Carnival - Viewpoint 1													
SAH (SP)	9.04	Ref.	126.87	Ref.	12.39	Ref.	129.13	Ref.	9.71	Ref.	105.42	Ref.	
SAH	8.97	0.85%	102.29	24.03%	12.35	0.34%	113.91	13.36%	10.00	-2.92%	96.64	9.08%	
RTSAH APSA	8.95	1.01%	103.27	22.84%	12.34	0.43%	115.04	12.25%	9.99	-2.81%	97.72	7.88%	
RTSAH HANPSA2	8.96	0.90%	99.53	27.46%	12.33	0.47%	113.24	14.03%	10.00	-2.86%	96.03	9.78%	
RTSAH WNHANPSA2	8.95	1.07%	103.95	22.04%	12.33	0.45%	115.59	11.71%	10.01	-3.02%	98.43	7.10%	
RTSAH WNWCHANPSA2	8.96	0.90%	103.98	22.01%	12.32	0.53%	116.14	11.19%	9.98	-2.71%	98.62	6.89%	
RTSAH EP	9.02	0.28%	111.94	13.34%	12.33	0.53%	118.61	8.87%	10.03	-3.16%	100.76	4.62%	
RTSAH APE	9.11	-0.76%	111.73	13.55%	12.45	-0.45%	116.73	10.62%	9.94	-2.34%	98.39	7.14%	
Carnival - Viewpoint 2													
SAH (SP)	41.97	Ref.	175.76	Ref.	25.82	Ref.	115.97	Ref.	23.26	Ref.	104.50	Ref.	
SAH	41.95	0.03%	175.30	0.26%	25.83	-0.04%	115.03	0.82%	23.25	0.04%	103.65	0.82%	
RTSAH APSA	41.95	0.04%	174.88	0.50%	25.82	-0.02%	114.70	1.10%	23.25	0.03%	103.38	1.09%	
RTSAH HANPSA2	42.47	-1.19%	178.83	-1.72%	25.83	-0.05%	116.17	-0.18%	23.26	-0.02%	104.71	-0.20%	
RTSAH WNHANPSA2	42.47	-1.19%	178.74	-1.67%	25.84	-0.07%	116.19	-0.19%	23.27	-0.03%	104.73	-0.22%	
RTSAH WNWCHANPSA2	42.29	-0.76%	179.21	-1.93%	25.81	0.03%	115.98	-0.01%	23.28	-0.11%	104.60	-0.10%	
RTSAH EP	41.95	0.03%	175.50	0.15%	25.83	-0.05%	115.12	0.74%	23.22	0.18%	103.54	0.93%	
RTSAH APE	41.94	0.06%	175.45	0.18%	25.83	-0.04%	115.18	0.68%	23.21	0.20%	103.61	0.86%	
Carnival - Viewpoint 3													
SAH (SP)	12.12	Ref.	109.69	Ref.	24.17	Ref.	142.00	Ref.	22.12	Ref.	127.26	Ref.	
SAH	12.02	0.79%	104.02	5.45%	24.27	-0.44%	138.41	2.60%	22.03	0.40%	122.29	4.06%	
RTSAH APSA	11.99	1.00%	103.35	6.13%	24.24	-0.32%	137.80	3.05%	22.06	0.27%	122.04	4.28%	
RTSAH HANPSA2	11.99	1.01%	104.68	4.78%	24.24	-0.31%	138.62	2.44%	22.07	0.21%	122.89	3.56%	
RTSAH WNHANPSA2	12.00	0.92%	104.83	4.64%	24.25	-0.35%	137.43	3.32%	22.08	0.17%	121.77	4.50%	
RTSAH WNWCHANPSA2	12.05	0.52%	101.25	8.34%	24.27	-0.43%	135.11	5.10%	22.07	0.22%	119.49	6.50%	
RTSAH EP	12.54	-3.40%	105.77	3.71%	25.37	-4.75%	138.57	2.48%	22.63	-2.27%	119.76	6.26%	
RTSAH APE	12.15	-0.25%	105.46	4.01%	24.21	-0.17%	137.52	3.26%	21.87	1.12%	119.31	6.66%	
Museum Hall - Viewpoint 1													
SAH (SP)	6.65	Ref.	110.43	Ref.	9.91	Ref.	136.68	Ref.	7.17	Ref.	103.07	Ref.	
SAH	6.51	2.10%	118.68	-6.95%	9.84	0.76%	141.45	-3.37%	7.11	0.78%	107.12	-3.78%	
RTSAH APSA	6.44	3.32%	118.88	-7.11%	9.76	1.49%	147.74	-7.49%	7.12	0.63%	115.40	-10.69%	
RTSAH HANPSA2	6.44	3.24%	116.05	-4.84%	9.80	1.10%	147.06	-7.06%	7.21	-0.63%	115.13	-10.48%	
RTSAH WNHANPSA2	6.44	3.32%	114.98	-3.96%	9.79	1.27%	146.04	-6.41%	7.20	-0.45%	114.19	-9.74%	
RTSAH WNWCHANPSA2	6.46	2.96%	117.02	-5.63%	9.82	0.92%	146.30	-6.58%	7.17	0.04%	113.56	-9.24%	
RTSAH EP	6.51	2.10%	105.18	4.99%	9.88	0.32%	144.49	-5.41%	7.18	-0.20%	111.50	-7.56%	
RTSAH APE	6.39	4.01%	108.81	1.49%	9.75	1.62%	141.36	-3.31%	7.13	0.50%	111.10	-7.23%	
Museum Hall - Viewpoint 2													
SAH (SP)	10.84	Ref.	186.80	Ref.	7.17	Ref.	137.97	Ref.	5.29	Ref.	107.27	Ref.	
SAH	10.78	0.55%	194.19	-3.81%	7.03	2.08%	142.90	-3.45%	5.19	1.75%	111.42	-3.73%	
RTSAH APSA	10.65	1.79%	197.34	-5.35%	6.95	3.27%	142.55	-3.21%	5.19	1.91%	114.89	-6.63%	
RTSAH HANPSA2	10.61	2.17%	188.52	-0.91%	6.96	3.09%	142.71	-3.32%	5.26	0.47%	116.16	-7.65%	
RTSAH WNHANPSA2	10.61	2.18%	186.94	-0.08%	6.95	3.28%	141.55	-2.53%	5.27	0.34%	115.06	-6.77%	
RTSAH WNWCHANPSA2	10.61	2.18%	193.11	-3.27%	6.95	3.16%	140.82	-2.03%	5.23	1.12%	113.47	-5.47%	
RTSAH EP	10.70	1.30%	183.88	1.59%	7.11	0.87%	139.69	-1.23%	5.21	1.52%	108.87	-1.47%	
RTSAH APE	10.60	2.29%	192.28	-2.85%	6.94	3.39%	138.23	-0.19%	5.20	1.65%	111.02	-3.38%	
Museum Hall - Viewpoint 3													
SAH (SP)	22.76	Ref.	158.08	Ref.	12.71	Ref.	152.35	Ref.	9.52	Ref.	113.38	Ref.	
SAH	22.71	0.21%	153.43	3.03%	12.73	-0.15%	153.37	-0.66%	9.47	0.48%	114.03	-0.57%	
RTSAH APSA	22.36	1.78%	176.13	-10.25%	12.64	0.51%	165.70	-8.06%	9.61	-0.92%	129.35	-12.34%	
RTSAH HANPSA2	22.59	0.79%	183.69	-13.94%	12.74	-0.22%	167.63	-9.11%	9.59	-0.78%	129.55	-12.48%	
RTSAH WNHANPSA2	22.55	0.94%	185.25	-14.66%	12.68	0.20%	167.11	-8.83%	9.59	-0.75%	128.84	-12.00%	
RTSAH WNWCHANPSA2	22.36	1.82%	181.00	-12.66%	12.72	-0.09%	167.08	-8.82%	9.57	-0.56%	128.56	-11.80%	
RTSAH EP	22.26	2.24%	158.53	-0.28%	12.68	0.22%	144.16	5.68%	9.50	0.16%	111.32	1.85%	
RTSAH APE	22.27	2.20%	159.07	-0.62%	12.63	0.59%	144.13	5.70%	9.47	0.57%	112.16	1.09%	

Table 26: The average number of ray-triangle intersection tests to perform per primary (camera),  $I_c$ , closest-hit shadow (ambient),  $I'_s$ , and any-hit shadow (ambient),  $I_s$ , ray and the average number of ADS node traversal steps to perform per primary (camera),  $T_c$ , closest-hit shadow (ambient),  $T'_s$ , and any-hit shadow (ambient),  $T_s$ , ray for a **BVH** ADS, built with various build heuristics, for a variety of realistic test scenes rendered as ambient occlusion images of resolution 512×512 pixels using 512 primary rays per pixel and 1 shadow ray per primary ray which is not limited to a fixed, finite, maximum distance.

SBVH												
Build heuristic	$I_c$	$\Delta I_c$	$T_c$	$\Delta T_c$	$I'_s$	$\Delta I'_s$	$T'_s$	$\Delta T'_s$	$I_s$	$\Delta I_s$	$T_s$	$\Delta T_s$
Kitchen - Viewpoint 1												
SAH	2.13	Ref.	62.69	Ref.	2.86	Ref.	56.42	Ref.	2.35	Ref.	50.37	Ref.
RTSAH APSA	2.16	-1.60%	65.99	-5.00%	2.81	1.73%	59.80	-5.65%	2.33	0.52%	53.71	-6.23%
RTSAH HANPSA2	2.15	-1.23%	61.69	1.62%	2.90	-1.68%	60.12	-6.16%	2.39	-2.04%	53.73	-6.25%
RTSAH WNHANPSA2	2.11	1.06%	62.47	0.34%	2.89	-1.16%	60.77	-7.16%	2.37	-1.05%	54.39	-7.39%
RTSAH WNWCHANPSA2	2.21	-3.81%	61.81	1.42%	2.89	-1.02%	58.43	-3.45%	2.38	-1.48%	52.42	-3.91%
RTSAH EP	2.30	-7.60%	73.77	-15.02%	3.01	-5.02%	70.50	-19.98%	2.28	3.01%	59.19	-14.90%
RTSAH APE	2.22	-4.27%	65.64	-4.50%	2.83	0.97%	60.78	-7.18%	2.29	2.57%	53.67	-6.15%
Kitchen - Viewpoint 2												
SAH	2.21	Ref.	59.03	Ref.	2.62	Ref.	50.70	Ref.	2.00	Ref.	44.61	Ref.
RTSAH APSA	2.07	6.52%	59.38	-0.59%	2.39	9.40%	54.99	-7.79%	1.89	6.21%	48.85	-8.67%
RTSAH HANPSA2	2.19	0.65%	64.43	-8.38%	2.50	4.76%	54.28	-6.58%	1.96	2.00%	47.81	-6.69%
RTSAH WNHANPSA2	2.38	-7.37%	64.74	-8.82%	2.68	-2.41%	56.51	-10.27%	2.11	-4.86%	50.15	-11.04%
RTSAH WNWCHANPSA2	2.14	3.13%	60.40	-2.26%	2.50	4.77%	55.43	-8.53%	1.95	2.66%	49.33	-9.55%
RTSAH EP	2.46	-10.41%	67.93	-13.10%	2.66	-1.59%	62.62	-19.03%	1.99	0.61%	51.99	-14.18%
RTSAH APE	2.27	-2.93%	61.45	-3.93%	2.64	-0.89%	54.95	-7.73%	2.00	0.19%	47.45	-5.98%
Kitchen - Viewpoint 3												
SAH	2.55	Ref.	56.19	Ref.	3.28	Ref.	61.16	Ref.	2.63	Ref.	54.63	Ref.
RTSAH APSA	2.47	3.10%	69.47	-19.12%	3.11	5.51%	66.23	-7.66%	2.51	4.90%	59.55	-8.26%
RTSAH HANPSA2	2.44	4.31%	61.55	-8.71%	3.16	3.72%	68.27	-10.41%	2.50	5.15%	59.59	-8.33%
RTSAH WNHANPSA2	2.47	3.18%	61.70	-8.94%	3.20	2.29%	69.00	-11.37%	2.53	3.90%	60.31	-9.41%
RTSAH WNWCHANPSA2	2.55	-0.01%	68.14	-17.54%	3.22	1.93%	64.60	-5.32%	2.57	2.43%	57.98	-5.78%
RTSAH EP	2.93	-12.98%	81.81	-31.32%	3.36	-2.44%	80.53	-24.05%	2.51	4.83%	66.69	-18.09%
RTSAH APE	2.45	4.08%	67.59	-16.87%	3.25	0.79%	70.54	-13.29%	2.49	5.78%	60.58	-9.82%
Crytek Sponza - Viewpoint 1												
SAH	2.19	Ref.	61.46	Ref.	2.81	Ref.	69.08	Ref.	2.32	Ref.	60.21	Ref.
RTSAH APSA	2.39	-8.24%	69.03	-10.96%	2.68	4.78%	74.24	-6.94%	2.21	4.98%	64.85	-7.15%
RTSAH HANPSA2	2.43	-9.79%	78.76	-21.96%	2.84	-1.15%	82.15	-15.91%	2.33	-0.21%	72.81	-17.31%
RTSAH WNHANPSA2	2.47	-11.38%	78.85	-22.05%	2.86	-1.79%	82.07	-15.82%	2.34	-0.85%	72.69	-17.17%
RTSAH WNWCHANPSA2	2.50	-12.48%	70.52	-12.84%	2.87	-2.36%	77.66	-11.04%	2.37	-1.81%	68.62	-12.26%
RTSAH EP	2.29	-4.20%	76.65	-19.81%	3.06	-8.29%	83.57	-17.33%	2.33	-0.35%	69.05	-12.80%
RTSAH APE	2.21	-0.89%	72.74	-15.51%	2.74	2.25%	77.01	-10.29%	2.22	4.61%	65.39	-7.92%
Crytek Sponza - Viewpoint 2												
SAH	1.99	Ref.	62.15	Ref.	2.67	Ref.	62.88	Ref.	2.22	Ref.	54.08	Ref.
RTSAH APSA	1.85	7.15%	63.04	-1.41%	2.46	8.76%	67.20	-6.43%	2.10	5.98%	58.17	-7.03%
RTSAH HANPSA2	1.91	3.88%	67.64	-8.12%	2.61	2.28%	69.75	-9.84%	2.22	0.30%	60.34	-10.38%
RTSAH WNHANPSA2	2.16	-8.11%	73.83	-15.81%	2.71	-1.48%	69.59	-9.63%	2.26	-1.54%	60.06	-9.96%
RTSAH WNWCHANPSA2	2.09	-4.80%	65.41	-4.98%	2.67	0.20%	68.13	-7.70%	2.25	-1.30%	59.26	-8.75%
RTSAH EP	2.03	-2.12%	74.75	-16.85%	2.71	-1.53%	70.78	-11.16%	2.11	5.33%	58.21	-7.10%
RTSAH APE	1.79	10.81%	73.01	-14.87%	2.47	8.28%	70.62	-10.95%	2.08	6.92%	59.95	-9.80%
Crytek Sponza - Viewpoint 3												
SAH	2.20	Ref.	89.52	Ref.	3.32	Ref.	71.39	Ref.	2.79	Ref.	61.80	Ref.
RTSAH APSA	2.24	-2.04%	93.40	-4.16%	3.12	6.34%	74.55	-4.24%	2.52	10.88%	64.64	-4.38%
RTSAH HANPSA2	2.15	2.31%	81.29	10.12%	3.27	1.55%	86.08	-17.07%	2.74	2.10%	76.58	-19.30%
RTSAH WNHANPSA2	2.16	2.03%	81.82	9.41%	3.26	1.96%	86.84	-17.79%	2.73	2.37%	77.28	-20.03%
RTSAH WNWCHANPSA2	2.33	-5.51%	78.12	14.59%	3.27	1.44%	80.72	-11.56%	2.71	3.24%	71.27	-13.28%
RTSAH EP	2.50	-11.93%	109.95	-18.58%	3.77	-11.84%	89.05	-19.84%	2.59	7.82%	65.42	-5.53%
RTSAH APE	2.34	-5.91%	83.99	6.58%	3.24	2.63%	78.67	-9.25%	2.58	8.44%	64.52	-4.20%

Table 27: The average number of ray-triangle intersection tests to perform per primary (camera),  $I_c$ , closest-hit shadow (ambient),  $I'_s$ , and any-hit shadow (ambient),  $I_s$ , ray and the average number of ADS node traversal steps to perform per primary (camera),  $T_c$ , closest-hit shadow (ambient),  $T'_s$ , and any-hit shadow (ambient),  $T_s$ , ray for a **SBVH** ADS, built with various build heuristics, for a variety of realistic test scenes rendered as ambient occlusion images of resolution 512×512 pixels using 512 primary rays per pixel and 1 shadow ray per primary ray which is not limited to a fixed, finite, maximum distance.

SBVH												
Build heuristic	$I_c$	$\Delta I_c$	$T_c$	$\Delta T_c$	$I'_s$	$\Delta I'_s$	$T'_s$	$\Delta T'_s$	$I_s$	$\Delta I_s$	$T_s$	$\Delta T_s$
Conference Room - Viewpoint 1												
SAH	2.70	Ref.	51.82	Ref.	3.02	Ref.	49.04	Ref.	1.94	Ref.	41.72	Ref.
RTSAH APSA	3.86	-29.94%	49.67	4.32%	3.67	-17.83%	49.46	-0.84%	1.98	-1.82%	42.65	-2.18%
RTSAH HANPSA2	2.12	27.65%	51.77	0.09%	2.48	21.59%	56.64	-13.41%	2.00	-2.76%	48.66	-14.26%
RTSAH WNHANPSA2	2.12	27.49%	52.00	-0.36%	2.50	20.98%	56.72	-13.54%	2.00	-3.06%	48.78	-14.47%
RTSAH WNWCHANPSA2	2.34	15.41%	46.79	10.76%	2.53	19.44%	53.35	-8.09%	2.06	-5.72%	44.81	-6.89%
RTSAH EP	3.04	-11.01%	50.20	3.23%	3.03	-0.32%	54.46	-9.95%	2.08	-6.69%	42.54	-1.94%
RTSAH APE	2.39	12.99%	66.50	-22.08%	2.58	17.14%	53.93	-9.07%	1.99	-2.19%	45.26	-7.82%
Conference Room - Viewpoint 2												
SAH	2.69	Ref.	46.62	Ref.	2.81	Ref.	52.54	Ref.	2.06	Ref.	46.02	Ref.
RTSAH APSA	3.36	-19.90%	48.41	-3.69%	3.16	-11.15%	54.29	-3.22%	2.04	0.92%	47.98	-4.09%
RTSAH HANPSA2	2.01	33.99%	59.32	-21.40%	2.46	14.27%	61.00	-13.88%	2.05	0.55%	53.84	-14.53%
RTSAH WNHANPSA2	2.02	33.36%	59.21	-21.25%	2.49	12.62%	61.06	-13.95%	2.07	-0.51%	53.90	-14.63%
RTSAH WNWCHANPSA2	1.98	35.49%	47.47	-1.77%	2.58	8.80%	58.95	-10.88%	2.11	-2.45%	50.32	-8.55%
RTSAH EP	2.25	19.53%	47.62	-2.09%	2.97	-5.32%	55.37	-5.12%	2.01	2.52%	46.77	-1.62%
RTSAH APE	2.18	23.01%	62.01	-24.81%	2.51	11.95%	60.14	-12.63%	1.92	7.55%	51.21	-10.15%
Conference Room - Viewpoint 3												
SAH	3.03	Ref.	55.78	Ref.	2.89	Ref.	53.51	Ref.	1.99	Ref.	45.85	Ref.
RTSAH APSA	6.41	-52.64%	52.95	5.34%	3.45	-16.26%	53.88	-0.68%	2.08	-4.09%	47.39	-3.25%
RTSAH HANPSA2	2.24	35.22%	66.54	-16.16%	2.52	14.56%	61.69	-13.26%	2.09	-4.68%	54.38	-15.69%
RTSAH WNHANPSA2	2.19	38.84%	66.35	-15.93%	2.53	14.06%	61.60	-13.13%	2.09	-4.68%	54.29	-15.55%
RTSAH WNWCHANPSA2	2.50	21.29%	48.87	14.14%	2.56	12.70%	59.16	-9.55%	2.13	-6.48%	49.83	-7.98%
RTSAH EP	3.50	-13.36%	54.48	2.38%	3.19	-9.41%	58.02	-7.76%	2.13	-6.72%	48.63	-5.72%
RTSAH APE	2.40	26.32%	58.51	-4.67%	2.62	10.16%	58.09	-7.88%	1.97	1.10%	48.66	-5.78%
Bedroom - Viewpoint 1												
SAH	2.71	Ref.	67.98	Ref.	3.28	Ref.	63.46	Ref.	2.79	Ref.	55.96	Ref.
RTSAH APSA	2.62	3.38%	68.21	-0.34%	3.14	4.41%	64.36	-1.40%	2.68	4.27%	56.71	-1.32%
RTSAH HANPSA2	2.66	1.94%	109.73	-38.05%	3.22	1.90%	77.36	-17.97%	2.74	2.14%	70.37	-20.47%
RTSAH WNHANPSA2	2.63	3.22%	122.86	-44.67%	3.29	-0.27%	81.91	-22.52%	2.77	0.71%	75.10	-25.48%
RTSAH WNWCHANPSA2	2.67	1.32%	82.89	-17.98%	3.48	-5.73%	67.61	-6.13%	2.93	-4.65%	60.82	-7.99%
RTSAH EP	3.89	-30.35%	100.39	-32.28%	3.76	-12.84%	77.87	-18.50%	3.21	-13.06%	68.62	-18.44%
RTSAH APE	2.73	-0.86%	75.70	-10.20%	3.30	-0.64%	68.37	-7.18%	2.76	1.26%	59.52	-5.98%
Bedroom - Viewpoint 2												
SAH	3.09	Ref.	101.54	Ref.	3.98	Ref.	89.16	Ref.	3.42	Ref.	79.37	Ref.
RTSAH APSA	2.87	7.67%	103.81	-2.18%	3.80	4.71%	88.36	0.91%	3.28	4.53%	78.92	0.57%
RTSAH HANPSA2	3.14	-1.61%	109.24	-7.05%	3.96	0.33%	92.67	-3.78%	3.40	0.72%	82.93	-4.29%
RTSAH WNHANPSA2	3.08	0.28%	106.99	-5.09%	3.96	0.47%	92.34	-3.44%	3.41	0.30%	82.83	-4.17%
RTSAH WNWCHANPSA2	3.02	2.08%	114.85	-11.59%	3.97	0.16%	92.54	-3.64%	3.40	0.83%	83.01	-4.38%
RTSAH EP	3.40	-9.23%	117.69	-13.72%	4.18	-4.89%	94.41	-5.56%	3.48	-1.48%	81.63	-2.77%
RTSAH APE	2.97	4.01%	112.76	-9.94%	3.99	-0.38%	93.92	-5.06%	3.33	2.82%	81.51	-2.62%
Bedroom - Viewpoint 3												
SAH	2.70	Ref.	53.49	Ref.	3.86	Ref.	64.55	Ref.	3.28	Ref.	54.72	Ref.
RTSAH APSA	2.95	-8.75%	61.99	-13.71%	3.93	-1.62%	68.12	-5.23%	3.46	-5.16%	58.66	-6.72%
RTSAH HANPSA2	2.91	-7.23%	59.88	-10.66%	4.32	-10.50%	69.53	-7.16%	3.60	-8.83%	59.47	-8.00%
RTSAH WNHANPSA2	3.27	-17.47%	58.10	-7.93%	4.60	-15.99%	67.79	-4.78%	3.84	-14.52%	58.37	-6.26%
RTSAH WNWCHANPSA2	3.32	-18.87%	53.11	0.72%	4.58	-15.57%	64.86	-0.48%	3.92	-16.31%	55.85	-2.02%
RTSAH EP	3.34	-19.28%	58.37	-8.35%	4.66	-17.03%	66.88	-3.48%	3.92	-16.37%	55.51	-1.43%
RTSAH APE	2.89	-6.69%	58.03	-7.82%	4.11	-5.98%	65.98	-2.16%	3.55	-7.59%	55.83	-2.00%

Table 28: The average number of ray-triangle intersection tests to perform per primary (camera),  $I_c$ , closest-hit shadow (ambient),  $I'_s$ , and any-hit shadow (ambient),  $I_s$ , ray and the average number of ADS node traversal steps to perform per primary (camera),  $T_c$ , closest-hit shadow (ambient),  $T'_s$ , and any-hit shadow (ambient),  $T_s$ , ray for a **SBVH** ADS, built with various build heuristics, for a variety of realistic test scenes rendered as ambient occlusion images of resolution  $512 \times 512$  pixels using 512 primary rays per pixel and 1 shadow ray per primary ray which is not limited to a fixed, finite, maximum distance.

SBVH												
Build heuristic	$I_c$	$\Delta I_c$	$T_c$	$\Delta T_c$	$I'_s$	$\Delta I'_s$	$T'_s$	$\Delta T'_s$	$I_s$	$\Delta I_s$	$T_s$	$\Delta T_s$
Carnival - Viewpoint 1												
SAH	4.08	Ref.	74.67	Ref.	5.26	Ref.	82.09	Ref.	4.54	Ref.	72.61	Ref.
RTSAH APSA	4.09	-0.29%	79.96	-6.62%	5.34	-1.60%	87.04	-5.69%	4.59	-1.00%	77.06	-5.78%
RTSAH HANPSA2	4.27	-4.42%	82.66	-9.66%	5.55	-5.32%	89.54	-8.32%	4.76	-4.49%	79.18	-8.30%
RTSAH WNHANPSA2	4.26	-4.14%	83.47	-10.55%	5.48	-4.10%	89.66	-8.45%	4.70	-3.40%	79.55	-8.72%
RTSAH WNWCHANPSA2	4.26	-4.26%	74.91	-0.32%	5.51	-4.54%	82.54	-0.54%	4.71	-3.50%	74.33	-2.32%
RTSAH EP	4.49	-9.04%	88.30	-15.44%	5.68	-7.53%	93.30	-12.02%	4.84	-6.22%	81.64	-11.06%
RTSAH APE	4.19	-2.65%	84.17	-11.29%	5.36	-1.98%	92.00	-10.77%	4.57	-0.54%	80.39	-9.69%
Carnival - Viewpoint 2												
SAH	3.64	Ref.	66.83	Ref.	3.90	Ref.	54.16	Ref.	3.44	Ref.	49.84	Ref.
RTSAH APSA	3.96	-8.05%	87.65	-23.75%	4.35	-10.25%	67.28	-19.50%	3.55	-3.26%	56.84	-12.31%
RTSAH HANPSA2	3.76	-2.98%	65.63	1.84%	4.16	-6.13%	58.32	-7.13%	3.58	-4.01%	52.08	-4.30%
RTSAH WNHANPSA2	3.72	-2.08%	65.46	2.10%	4.11	-4.95%	58.09	-6.77%	3.55	-3.23%	51.93	-4.03%
RTSAH WNWCHANPSA2	3.64	0.16%	62.74	6.53%	3.98	-1.94%	54.48	-0.59%	3.51	-2.05%	50.20	-0.71%
RTSAH EP	3.75	-2.79%	67.53	-1.03%	4.06	-3.88%	55.72	-2.79%	3.58	-4.06%	51.55	-3.31%
RTSAH APE	3.66	-0.48%	84.18	-20.61%	3.97	-1.78%	65.23	-16.97%	3.46	-0.54%	57.44	-13.23%
Carnival - Viewpoint 3												
SAH	4.29	Ref.	67.64	Ref.	5.63	Ref.	73.40	Ref.	4.73	Ref.	63.38	Ref.
RTSAH APSA	4.48	-4.12%	76.06	-11.08%	6.06	-7.10%	77.73	-5.57%	5.13	-7.76%	66.91	-5.27%
RTSAH HANPSA2	4.52	-5.01%	79.75	-15.19%	5.88	-4.37%	76.79	-4.41%	4.91	-3.59%	66.00	-3.97%
RTSAH WNHANPSA2	4.52	-4.99%	79.75	-15.19%	5.88	-4.23%	76.17	-3.63%	4.90	-3.46%	65.41	-3.10%
RTSAH WNWCHANPSA2	4.55	-5.71%	70.41	-3.94%	5.84	-3.57%	70.86	3.59%	4.86	-2.56%	61.51	3.04%
RTSAH EP	4.80	-10.63%	70.47	-4.02%	6.36	-11.46%	75.31	-2.53%	5.36	-11.77%	65.48	-3.20%
RTSAH APE	4.48	-4.15%	70.30	-3.79%	5.85	-3.85%	74.51	-1.48%	4.91	-3.65%	64.48	-1.70%
Museum Hall - Viewpoint 1												
SAH	3.11	Ref.	72.05	Ref.	4.16	Ref.	84.71	Ref.	3.23	Ref.	73.37	Ref.
RTSAH APSA	3.13	-0.84%	71.95	0.14%	3.84	8.27%	92.79	-8.70%	3.04	6.01%	81.86	-10.37%
RTSAH HANPSA2	3.60	-13.70%	85.37	-15.60%	4.83	-13.98%	97.94	-13.50%	3.71	-13.12%	86.11	-14.79%
RTSAH WNHANPSA2	3.45	-9.83%	82.96	-13.16%	4.31	-3.56%	95.44	-11.24%	3.36	-4.05%	84.21	-12.87%
RTSAH WNWCHANPSA2	3.70	-15.92%	78.83	-8.60%	5.76	-27.79%	96.31	-12.04%	4.01	-19.47%	85.18	-13.86%
RTSAH EP	3.63	-14.41%	76.12	-5.35%	4.85	-14.26%	92.04	-7.96%	3.70	-12.68%	77.03	-4.74%
RTSAH APE	3.28	-5.30%	77.99	-7.62%	4.27	-2.59%	92.74	-8.65%	3.19	1.08%	77.68	-5.54%
Museum Hall - Viewpoint 2												
SAH	7.32	Ref.	130.75	Ref.	4.69	Ref.	90.06	Ref.	3.76	Ref.	78.73	Ref.
RTSAH APSA	6.95	5.22%	134.73	-2.96%	4.54	3.23%	93.46	-3.64%	3.66	2.92%	82.54	-4.62%
RTSAH HANPSA2	7.78	-5.94%	144.29	-9.38%	5.34	-12.17%	102.56	-12.18%	4.17	-9.67%	90.66	-13.16%
RTSAH WNHANPSA2	6.54	11.94%	154.12	-15.17%	4.79	-1.95%	101.76	-11.50%	3.82	-1.36%	90.28	-12.79%
RTSAH WNWCHANPSA2	7.28	0.55%	155.80	-16.08%	5.94	-21.08%	104.40	-13.73%	4.38	-14.14%	93.20	-15.52%
RTSAH EP	7.26	0.72%	145.15	-9.92%	5.28	-11.07%	98.20	-8.29%	4.09	-8.09%	83.10	-5.26%
RTSAH APE	5.30	38.14%	134.62	-2.87%	4.71	-0.32%	94.88	-5.08%	3.62	4.06%	80.17	-1.79%
Museum Hall - Viewpoint 3												
SAH	3.23	Ref.	71.27	Ref.	3.77	Ref.	82.38	Ref.	2.82	Ref.	70.77	Ref.
RTSAH APSA	3.19	1.32%	69.31	2.82%	3.24	16.44%	85.86	-4.05%	2.55	10.50%	74.89	-5.51%
RTSAH HANPSA2	4.78	-32.36%	75.20	-5.23%	4.73	-20.15%	89.17	-7.61%	3.69	-23.54%	77.21	-8.35%
RTSAH WNHANPSA2	3.27	-1.06%	75.15	-5.17%	3.67	2.83%	88.60	-7.02%	2.76	2.28%	76.93	-8.01%
RTSAH WNWCHANPSA2	3.19	1.45%	72.03	-1.06%	3.91	-3.55%	88.44	-6.85%	3.03	-6.93%	77.27	-8.41%
RTSAH EP	4.38	-26.14%	74.53	-4.38%	4.92	-23.35%	89.39	-7.84%	3.71	-23.91%	73.73	-4.02%
RTSAH APE	3.32	-2.55%	73.79	-3.41%	3.81	-1.00%	88.91	-7.34%	2.82	0.08%	73.91	-4.26%

Table 29: The average number of ray-triangle intersection tests to perform per primary (camera),  $I_c$ , closest-hit shadow (ambient),  $I'_s$ , and any-hit shadow (ambient),  $I_s$ , ray and the average number of ADS node traversal steps to perform per primary (camera),  $T_c$ , closest-hit shadow (ambient),  $T'_s$ , and any-hit shadow (ambient),  $T_s$ , ray for a SBVH ADS, built with various build heuristics, for a variety of realistic test scenes rendered as ambient occlusion images of resolution 512×512 pixels using 512 primary rays per pixel and 1 shadow ray per primary ray which is not limited to a fixed, finite, maximum distance.

Kd-tree						
Build heuristic	D <sub>max</sub>	D <sub>avg</sub>	L <sub>tot</sub>	RD%	G <sub>max/L</sub>	G <sub>avg/L</sub>
Kitchen						
SAH (SP)	<b>29</b>	26.70	1147 k	2678%	118	2.91
SAH	<b>29</b>	27.24	2349 k	4409%	126	2.31
RTSAH Z	<b>29</b>	27.70	4261 k	8044%	133	2.30
RTSAH N	<b>29</b>	27.71	4838 k	10457%	125	2.62
RTSAH SA	<b>29</b>	27.52	3741 k	7481%	127	2.44
RTSAH APSA	<b>29</b>	27.33	2880 k	5752%	129	2.44
RTSAH HANPSA2	<b>29</b>	27.37	3032 k	5992%	128	2.42
RTSAH WNHANPSA2	<b>29</b>	27.23	2530 k	4724%	125	2.29
RTSAH WNWCHANPSA2	<b>29</b>	27.20	2615 k	4982%	127	2.34
RTSAH EP	<b>29</b>	27.40	2739 k	5208%	126	2.33
RTSAH APE	<b>29</b>	27.35	2671 k	5293%	126	2.43
Crytek Sponza						
SAH (SP)	<b>31</b>	27.69	3896 k	3860%	39	2.67
SAH	<b>31</b>	29.10	10279 k	8466%	44	2.19
RTSAH Z	<b>31</b>	29.69	21232 k	18116%	161	2.25
RTSAH N	<b>31</b>	29.60	26386 k	25789%	28	2.57
RTSAH SA	<b>31</b>	29.35	16630 k	15412%	28	2.45
RTSAH APSA	<b>31</b>	29.21	12892 k	11876%	28	2.44
RTSAH HANPSA2	<b>31</b>	29.18	13447 k	11989%	28	2.36
RTSAH WNHANPSA2	<b>31</b>	29.12	13610 k	12106%	28	2.35
RTSAH WNWCHANPSA2	<b>31</b>	29.12	13912 k	12514%	28	2.38
RTSAH EP	<b>31</b>	29.25	13336 k	12090%	28	2.40
RTSAH APE	<b>31</b>	29.22	13270 k	12393%	28	2.47
Conference Room						
SAH (SP)	<b>31</b>	28.68	1730 k	3114%	156	6.15
SAH	<b>31</b>	28.96	2708 k	3611%	157	4.54
RTSAH Z	<b>31</b>	29.94	15928 k	39294%	113	8.19
RTSAH N	<b>31</b>	29.88	20526 k	88443%	106	14.29
RTSAH SA	<b>31</b>	29.29	6848 k	12065%	118	5.88
RTSAH APSA	<b>31</b>	29.12	4772 k	8057%	140	5.66
RTSAH HANPSA2	<b>31</b>	29.06	5125 k	9216%	142	6.02
RTSAH WNHANPSA2	<b>31</b>	28.76	4230 k	5943%	144	4.73
RTSAH WNWCHANPSA2	<b>31</b>	28.66	4353 k	5905%	155	4.57
RTSAH EP	<b>31</b>	29.14	3974 k	5909%	151	5.01
RTSAH APE	<b>31</b>	29.16	3517 k	5481%	168	5.26
Bedroom						
SAH (SP)	<b>31</b>	27.97	4640 k	4060%	208	3.24
SAH	<b>31</b>	29.02	8860 k	6204%	204	2.57
RTSAH Z	<b>31</b>	29.85	23829 k	24362%	427	3.71
RTSAH N	<b>31</b>	29.72	30343 k	43090%	166	5.15
RTSAH SA	<b>31</b>	29.29	16369 k	13518%	175	3.01
RTSAH APSA	<b>31</b>	29.08	11786 k	9106%	199	2.83
RTSAH HANPSA2	<b>31</b>	29.09	12631 k	9960%	190	2.88
RTSAH WNHANPSA2	<b>31</b>	28.88	10294 k	7334%	198	2.61
RTSAH WNWCHANPSA2	<b>31</b>	28.87	10356 k	7538%	208	2.67
RTSAH EP	<b>31</b>	29.17	12095 k	9089%	182	2.75
RTSAH APE	<b>31</b>	29.16	11916 k	9327%	196	2.86
Carnival						
SAH (SP)	<b>31</b>	29.19	2478 k	2301%	148	4.36
SAH	<b>31</b>	29.51	3638 k	2909%	148	3.72
RTSAH Z	<b>31</b>	30.00	12434 k	19917%	113	7.24
RTSAH N	<b>31</b>	30.00	16076 k	30613%	104	8.59
RTSAH SA	<b>31</b>	29.77	7407 k	7186%	120	4.43
RTSAH APSA	<b>31</b>	29.65	4891 k	4479%	155	4.21
RTSAH HANPSA2	<b>31</b>	29.71	5940 k	5618%	148	4.33
RTSAH WNHANPSA2	<b>31</b>	29.65	5826 k	5400%	148	4.25
RTSAH WNWCHANPSA2	<b>31</b>	29.64	5671 k	5460%	173	4.41
RTSAH EP	<b>31</b>	29.67	4986 k	4479%	148	4.13
RTSAH APE	<b>31</b>	29.69	4604 k	4262%	148	4.26
Museum Hall						
SAH (SP)	<b>34</b>	30.65	18515 k	3830%	100	3.12
SAH	<b>34</b>	31.96	48182 k	7682%	100	2.37
RTSAH Z	<b>34</b>	32.49	104099 k	17407%	223	2.47
RTSAH N	<b>34</b>	32.15	112073 k	21999%	96	2.90
RTSAH SA	<b>34</b>	32.11	78145 k	14228%	96	2.69
RTSAH APSA	<b>34</b>	31.92	59432 k	10371%	96	2.59
RTSAH HANPSA2	<b>34</b>	31.98	63990 k	10509%	96	2.43
RTSAH WNHANPSA2	<b>34</b>	31.90	52072 k	8289%	100	2.37
RTSAH WNWCHANPSA2	<b>34</b>	31.88	52785 k	8373%	100	2.36
RTSAH EP	<b>34</b>	32.06	61650 k	10441%	100	2.51
RTSAH APE	<b>34</b>	32.03	58945 k	10539%	100	2.65

Table 30: The maximum (average) tree depth, D<sub>max</sub> (D<sub>avg</sub>) (in **bold** if equal to the fixed tree depth), the total number of leaf nodes, L<sub>tot</sub>, The geometric primitive reference duplication percentage, RD%, and the maximum (average) number of geometric primitives per leaf node, G<sub>max/L</sub> (G<sub>avg/L</sub>) for constructing the **kd-tree** ADSs with various build heuristics for a variety of realistic test scenes.

Build heuristic	BIH					
	D <sub>max</sub>	D <sub>avg</sub>	L <sub>tot</sub>	RD%	G <sub>max/L</sub>	G <sub>avg/L</sub>
Kitchen						
SAH (SP)	42	25.51	208 k	0%	8	0.58
SAH	44	25.72	208 k	0%	8	0.58
RTSAH Z	40	25.50	131 k	0%	1	0.92
RTSAH N	35	22.71	147 k	0%	1	0.82
RTSAH SA	40	24.92	199 k	0%	11	0.61
RTSAH APSA	46	25.53	203 k	0%	8	0.59
RTSAH HANPSA2	42	25.57	208 k	0%	3	0.58
RTSAH WNHANPSA2	45	25.94	208 k	0%	9	0.58
RTSAH WNWCHANPSA2	47	26.40	208 k	0%	8	0.58
RTSAH EP	42	25.20	185 k	0%	11	0.65
RTSAH APE	42	25.24	189 k	0%	11	0.64
Crytek Sponza						
SAH (SP)	37	24.78	453 k	0%	4	0.58
SAH	37	24.85	454 k	0%	4	0.58
RTSAH Z	47	27.85	285 k	0%	1	0.92
RTSAH N	30	21.86	323 k	0%	1	0.81
RTSAH SA	36	23.62	431 k	0%	4	0.61
RTSAH APSA	37	24.09	435 k	0%	2	0.60
RTSAH HANPSA2	39	24.97	445 k	0%	2	0.59
RTSAH WNHANPSA2	40	24.69	442 k	0%	2	0.59
RTSAH WNWCHANPSA2	39	24.78	449 k	0%	2	0.58
RTSAH EP	41	24.78	384 k	0%	2	0.68
RTSAH APE	40	25.19	397 k	0%	2	0.66
Conference Room						
SAH (SP)	38	27.26	522 k	0%	2	0.63
SAH	39	27.37	523 k	0%	2	0.63
RTSAH Z	41	27.85	353 k	0%	1	0.94
RTSAH N	34	25.71	385 k	0%	1	0.86
RTSAH SA	38	27.09	500 k	0%	2	0.66
RTSAH APSA	38	27.52	516 k	0%	2	0.64
RTSAH HANPSA2	39	27.48	523 k	0%	2	0.63
RTSAH WNHANPSA2	38	27.56	523 k	0%	2	0.63
RTSAH WNWCHANPSA2	40	27.61	523 k	0%	2	0.63
RTSAH EP	37	27.09	455 k	0%	2	0.73
RTSAH APE	36	26.89	475 k	0%	2	0.70
Bedroom						
SAH (SP)	47	27.01	628 k	0%	11	0.58
SAH	48	27.26	628 k	0%	12	0.58
RTSAH Z	44	26.81	391 k	0%	1	0.92
RTSAH N	35	23.64	435 k	0%	1	0.83
RTSAH SA	50	26.23	610 k	0%	12	0.59
RTSAH APSA	50	27.00	614 k	0%	12	0.59
RTSAH HANPSA2	50	26.81	629 k	0%	12	0.57
RTSAH WNHANPSA2	48	26.97	626 k	0%	12	0.58
RTSAH WNWCHANPSA2	46	26.81	630 k	0%	12	0.57
RTSAH EP	51	26.84	553 k	0%	12	0.65
RTSAH APE	49	26.90	565 k	0%	12	0.64
Carnival						
SAH (SP)	49	29.44	724 k	0%	21	0.62
SAH	47	29.47	724 k	0%	21	0.62
RTSAH Z	42	28.05	490 k	0%	1	0.92
RTSAH N	37	26.53	548 k	0%	1	0.82
RTSAH SA	48	28.37	697 k	0%	18	0.65
RTSAH APSA	47	29.22	714 k	0%	18	0.63
RTSAH HANPSA2	46	28.83	722 k	0%	21	0.62
RTSAH WNHANPSA2	47	28.83	723 k	0%	21	0.62
RTSAH WNWCHANPSA2	47	29.02	724 k	0%	21	0.62
RTSAH EP	45	29.00	667 k	0%	18	0.67
RTSAH APE	49	30.92	679 k	0%	18	0.66
Museum Hall						
SAH (SP)	46	28.81	2550 k	0%	775	0.58
SAH	46	28.84	2557 k	0%	766	0.57
RTSAH Z	43	28.05	1573 k	0%	1	0.93
RTSAH N	34	25.05	1830 k	0%	1	0.80
RTSAH SA	45	27.17	2488 k	0%	58	0.59
RTSAH APSA	44	27.81	2497 k	0%	766	0.59
RTSAH HANPSA2	46	27.48	2553 k	0%	59	0.58
RTSAH WNHANPSA2	46	27.86	2545 k	0%	58	0.58
RTSAH WNWCHANPSA2	45	28.13	2547 k	0%	60	0.58
RTSAH EP	44	27.78	2157 k	0%	4	0.68
RTSAH APE	50	28.44	2244 k	0%	6	0.65

Table 31: The maximum (average) tree depth, D<sub>max</sub> (D<sub>avg</sub>) (in **bold** if equal to the fixed tree depth), the total number of leaf nodes, L<sub>tot</sub>, The geometric primitive reference duplication percentage, RD%, and the maximum (average) number of geometric primitives per leaf node, G<sub>max/L</sub> (G<sub>avg/L</sub>) for constructing the **BIH** ADSs with various build heuristics for a variety of realistic test scenes.

BVH						
Build heuristic	D <sub>max</sub>	D <sub>avg</sub>	L <sub>tot</sub>	RD%	G <sub>max</sub> /L	G <sub>avg</sub> /L
Kitchen						
SAH (SP)	32	20.41	120k	0%	6	1.00
SAH	31	20.14	120k	0%	6	1.00
RTSAH APSA	31	20.18	120k	0%	6	1.00
RTSAH HANPSA2	32	20.37	120k	0%	6	1.00
RTSAH WNHANPSA2	32	20.31	120k	0%	6	1.00
RTSAH WNWCHANPSA2	31	20.27	120k	0%	6	1.00
RTSAH EP	31	20.39	120k	0%	6	1.00
RTSAH APE	31	20.39	120k	0%	6	1.00
Crytek Sponza						
SAH (SP)	29	20.64	262k	0%	2	1.00
SAH	29	20.85	262k	0%	2	1.00
RTSAH APSA	<b>64</b>	20.66	262k	0%	31	1.00
RTSAH HANPSA2	<b>64</b>	20.73	262k	0%	27	1.00
RTSAH WNHANPSA2	<b>64</b>	20.71	262k	0%	27	1.00
RTSAH WNWCHANPSA2	<b>64</b>	20.75	262k	0%	27	1.00
RTSAH EP	<b>64</b>	21.40	262k	0%	24	1.00
RTSAH APE	<b>64</b>	20.94	262k	0%	25	1.00
Conference Room						
SAH (SP)	29	22.08	331k	0%	2	1.00
SAH	29	22.02	331k	0%	2	1.00
RTSAH APSA	52	21.74	331k	0%	2	1.00
RTSAH HANPSA2	51	21.63	331k	0%	2	1.00
RTSAH WNHANPSA2	51	21.71	331k	0%	2	1.00
RTSAH WNWCHANPSA2	34	21.65	331k	0%	2	1.00
RTSAH EP	<b>64</b>	21.98	331k	0%	29	1.00
RTSAH APE	53	22.03	331k	0%	1	1.00
Bedroom						
SAH (SP)	36	21.43	362k	0%	3	1.00
SAH	36	21.54	362k	0%	3	1.00
RTSAH APSA	37	21.62	362k	0%	3	1.00
RTSAH HANPSA2	37	21.63	362k	0%	3	1.00
RTSAH WNHANPSA2	37	21.99	362k	0%	3	1.00
RTSAH WNWCHANPSA2	36	22.11	362k	0%	3	1.00
RTSAH EP	36	21.64	362k	0%	3	1.00
RTSAH APE	36	21.55	362k	0%	3	1.00
Carnival						
SAH (SP)	37	23.20	450k	0%	3	1.00
SAH	35	22.17	450k	0%	3	1.00
RTSAH APSA	54	22.13	450k	0%	3	1.00
RTSAH HANPSA2	53	22.04	450k	0%	3	1.00
RTSAH WNHANPSA2	53	22.10	450k	0%	3	1.00
RTSAH WNWCHANPSA2	53	22.10	450k	0%	3	1.00
RTSAH EP	53	22.51	450k	0%	3	1.00
RTSAH APE	53	22.50	450k	0%	3	1.00
Museum Hall						
SAH (SP)	34	23.14	1466k	0%	3	1.00
SAH	35	23.18	1466k	0%	3	1.00
RTSAH APSA	36	23.03	1467k	0%	3	1.00
RTSAH HANPSA2	35	23.06	1466k	0%	3	1.00
RTSAH WNHANPSA2	34	23.10	1466k	0%	3	1.00
RTSAH WNWCHANPSA2	35	23.07	1466k	0%	3	1.00
RTSAH EP	35	23.58	1468k	0%	3	1.00
RTSAH APE	36	23.48	1467k	0%	3	1.00

Table 32: The maximum (average) tree depth, D<sub>max</sub> (D<sub>avg</sub>) (in **bold** if equal to the fixed tree depth), the total number of leaf nodes, L<sub>tot</sub>, The geometric primitive reference duplication percentage, RD%, and the maximum (average) number of geometric primitives per leaf node, G<sub>max</sub>/L (G<sub>avg</sub>/L) for constructing the **BVH** ADSSs with various build heuristics for a variety of realistic test scenes.

SBVH						
Build heuristic	D <sub>max</sub>	D <sub>avg</sub>	L <sub>tot</sub>	RD%	G <sub>max/L</sub>	G <sub>avg/L</sub>
Kitchen						
SAH	<b>29</b>	22.71	264 k	128%	59	1.04
RTSAH APSA	<b>29</b>	22.92	396 k	260%	59	1.09
RTSAH HANPSA2	<b>29</b>	22.88	320 k	189%	60	1.09
RTSAH WNHANPSA2	<b>29</b>	22.58	277 k	140%	59	1.04
RTSAH WNWCHANPSA2	<b>29</b>	22.27	281 k	143%	59	1.04
RTSAH EP	<b>29</b>	22.79	283 k	144%	59	1.04
RTSAH APE	<b>29</b>	22.68	359 k	229%	59	1.10
Crytek Sponza						
SAH	<b>31</b>	22.64	778 k	203%	18	1.02
RTSAH APSA	<b>31</b>	23.90	1374 k	469%	56	1.09
RTSAH HANPSA2	<b>31</b>	23.79	1066 k	330%	81	1.06
RTSAH WNHANPSA2	<b>31</b>	23.79	1061 k	322%	79	1.04
RTSAH WNWCHANPSA2	<b>31</b>	23.86	1082 k	333%	88	1.05
RTSAH EP	<b>31</b>	22.79	867 k	237%	42	1.02
RTSAH APE	<b>31</b>	23.58	1218 k	402%	50	1.08
Conference Room						
SAH	<b>31</b>	24.55	1029 k	266%	41	1.18
RTSAH APSA	<b>31</b>	25.02	1458 k	473%	82	1.30
RTSAH HANPSA2	<b>31</b>	25.04	1283 k	428%	47	1.36
RTSAH WNHANPSA2	<b>31</b>	24.82	1193 k	333%	42	1.20
RTSAH WNWCHANPSA2	<b>31</b>	24.72	1203 k	341%	159	1.21
RTSAH EP	<b>31</b>	24.21	1086 k	294%	82	1.20
RTSAH APE	<b>31</b>	25.24	1253 k	401%	42	1.32
Bedroom						
SAH	<b>31</b>	24.27	1442 k	372%	49	1.18
RTSAH APSA	<b>31</b>	24.81	2037 k	625%	46	1.29
RTSAH HANPSA2	<b>31</b>	24.94	1813 k	553%	69	1.30
RTSAH WNHANPSA2	<b>31</b>	24.47	1565 k	412%	58	1.18
RTSAH WNWCHANPSA2	<b>31</b>	24.30	1579 k	416%	159	1.18
RTSAH EP	<b>31</b>	24.42	1541 k	415%	55	1.21
RTSAH APE	<b>31</b>	24.81	1906 k	585%	55	1.30
Carnival						
SAH	<b>31</b>	22.71	900 k	142%	2685	1.21
RTSAH APSA	<b>31</b>	23.05	1068 k	203%	651	1.28
RTSAH HANPSA2	<b>31</b>	23.46	1137 k	260%	3194	1.43
RTSAH WNHANPSA2	<b>31</b>	23.38	1139 k	243%	58	1.36
RTSAH WNWCHANPSA2	<b>31</b>	23.49	1149 k	252%	46	1.38
RTSAH EP	<b>31</b>	23.01	970 k	166%	2688	1.24
RTSAH APE	<b>31</b>	23.08	1011 k	193%	2688	1.30
Museum Hall						
SAH	<b>34</b>	25.03	3872 k	181%	130	1.07
RTSAH APSA	<b>34</b>	25.36	5049 k	290%	95	1.13
RTSAH HANPSA2	<b>34</b>	25.32	4494 k	237%	125	1.10
RTSAH WNHANPSA2	<b>34</b>	25.02	3944 k	187%	95	1.07
RTSAH WNWCHANPSA2	<b>34</b>	24.97	3960 k	188%	158	1.07
RTSAH EP	<b>34</b>	24.91	3766 k	171%	173	1.06
RTSAH APE	<b>34</b>	25.15	4484 k	250%	67	1.15

Table 33: The maximum (average) tree depth, D<sub>max</sub> (D<sub>avg</sub>) (in **bold** if equal to the fixed tree depth), the total number of leaf nodes, L<sub>tot</sub>, The geometric primitive reference duplication percentage, RD%, and the maximum (average) number of geometric primitives per leaf node, G<sub>max/L</sub> (G<sub>avg/L</sub>) for constructing the **SBVH** ADSs with various build heuristics for a variety of realistic test scenes.

Build heuristic	BVH								Icosahedron1								
	$I_s$	$\Delta I_s$	$T_s$	$\Delta T_s$	$I_s$	$\Delta I_s$	$T_s$	$\Delta T_s$	$I_s$	$\Delta I_s$	$T_s$	$\Delta T_s$					
			Empty Box				Cornell Box				Icosahedron1						
SAH + OB	1.15	1.77%	9.60	-9.53%	1.53	-5.37%	17.25	-12.69%	2.46	-24.13%	51.81	-34.70%					
SAH + IO	1.17	0.00%	5.94	46.07%	1.56	-7.31%	10.04	50.01%	2.27	-17.79%	26.35	28.41%					
SAH + <UDF>	1.16	1.40%	8.12	6.88%	1.49	-2.99%	14.68	2.57%	2.17	-14.11%	40.83	-17.13%					
SAH + LDF	1.17	0.00%	8.31	4.47%	1.55	-6.65%	14.95	0.73%	2.17	-13.95%	40.98	-17.45%					
SAH + RDF	1.14	2.83%	7.94	9.40%	1.45	-0.49%	14.51	3.76%	2.19	-14.64%	40.69	-16.85%					
SAH + CCF	1.17	0.00%	8.31	4.48%	1.53	-5.37%	14.72	2.33%	2.49	-25.09%	49.34	-31.42%					
SAH + FCF	1.17	0.00%	7.97	8.95%	1.43	0.94%	14.45	4.19%	1.70	9.96%	31.13	8.69%					
SAH + NodeSATO	1.17	Ref.	8.68	Ref.	1.45	Ref.	15.06	Ref.	1.87	Ref.	33.83	Ref.					
OMS + NodeSATO	0.86	36.89%	13.34	-34.92%	0.95	52.63%	22.62	-33.43%	1.47	27.41%	97.71	-65.37%					
SMS + NodeSATO	1.16	0.69%	13.44	-35.39%	1.44	0.25%	20.27	-25.73%	2.04	-8.37%	65.42	-48.28%					
SRDH E	1.16	0.77%	11.44	-24.12%	1.33	9.00%	18.54	-18.76%	1.85	0.85%	404.98	-91.65%					
SRDH APSA	1.15	2.11%	11.11	-21.85%	1.34	7.85%	18.56	-18.86%	1.84	1.40%	429.49	-92.12%					
SRDH' E	1.16	0.77%	11.06	-21.50%	1.32	9.26%	16.39	-8.14%	1.80	3.71%	186.93	-81.90%					
SRDH' N	1.16	1.43%	12.26	-29.19%	1.51	-3.96%	20.56	-26.75%	2.25	-17.09%	577.50	-94.14%					
SRDH' SA	1.16	1.43%	12.26	-29.19%	1.34	8.38%	18.44	-18.33%	1.78	4.70%	47.73	-29.12%					
Icosahedron2								Icosahedron3								Icosahedron4	
SAH + OB	1.04	-5.64%	16.20	-3.58%	0.63	-11.46%	9.18	-8.65%	1.11	-11.88%	28.34	-10.20%					
SAH + IO	1.03	-4.24%	9.11	71.31%	0.60	-7.34%	5.07	65.43%	1.07	-9.11%	15.79	61.17%					
SAH + <UDF>	0.97	1.16%	15.39	1.45%	0.56	-0.85%	8.41	-0.35%	1.03	-4.85%	25.83	-1.47%					
SAH + LDF	0.96	2.91%	15.20	2.75%	0.56	0.21%	8.26	1.47%	1.08	-9.71%	25.79	-1.32%					
SAH + RDF	0.99	-0.69%	15.65	-0.21%	0.58	-3.73%	8.74	-4.09%	1.00	-1.96%	26.48	-3.89%					
SAH + CCF	1.03	-4.51%	15.88	-1.68%	0.60	-6.46%	8.56	-2.02%	1.07	-8.85%	25.87	-1.61%					
SAH + FCF	0.88	11.43%	14.79	5.60%	0.52	7.82%	8.24	1.70%	1.03	-4.97%	25.42	0.13%					
SAH + NodeSATO	0.98	Ref.	15.61	Ref.	0.56	Ref.	8.38	Ref.	0.98	Ref.	25.45	Ref.					
OMS + NodeSATO	0.66	49.46%	21.45	-27.20%	0.38	45.58%	11.26	-25.56%	0.82	18.60%	47.07	-45.93%					
SMS + NodeSATO	0.98	0.27%	17.71	-11.82%	0.56	-0.86%	9.39	-10.77%	1.16	-15.69%	36.99	-31.19%					
SRDH E	1.00	-1.85%	257.23	-93.93%	0.57	-1.91%	93.04	-90.99%	0.95	2.45%	172.08	-85.21%					
SRDH APSA	0.97	1.65%	258.85	-93.97%	0.56	-0.79%	89.71	-90.66%	1.01	-3.30%	169.18	-84.96%					
SRDH' E	0.99	-0.93%	103.22	-84.87%	0.56	-0.80%	44.40	-81.12%	0.98	-0.51%	110.88	-77.05%					
SRDH' N	0.97	0.84%	226.66	-93.11%	0.57	-2.51%	84.64	-90.10%	1.06	-7.67%	168.81	-84.92%					
SRDH' SA	0.97	0.92%	30.34	-48.54%	0.56	-1.39%	14.76	-43.23%	1.02	-3.83%	101.50	-74.92%					

Table 34: The average number of ray-triangle intersection tests,  $I_s$ , and the average number of ADS node traversal steps,  $T_s$ , to perform per any-hit shadow (ambient) ray using various traversal heuristics for a **BVH** ADS, built with **SAH SP**, (and/or a dedicated **BVH** ADS for shadow ray traversal) for a variety of artificial test scenes rendered as ambient occlusion images of resolution  $512 \times 512$  pixels using 512 primary rays per pixel and 1 shadow ray per primary ray which is not limited to a fixed, finite, maximum distance.

BVH						
Build heuristic	D <sub>max</sub>	D <sub>avg</sub>	L <sub>tot</sub>	RD%	G <sub>max</sub> /L	G <sub>avg</sub> /L
Empty Box						
SAH	5	3.80	10	0%	1	1.00
OMS	4	3.40	10	0%	1	1.00
SMS	4	3.40	10	0%	1	1.00
SRDH E	4	3.40	10	0%	1	1.00
SRDH APSA	4	3.40	10	0%	1	1.00
SRDH' E	4	3.40	10	0%	1	1.00
SRDH' N	5	3.60	10	0%	1	1.00
SRDH' SA	5	3.60	10	0%	1	1.00
Cornell Box						
SAH	8	5.47	30	0%	1	1.00
OMS	5	4.93	30	0%	1	1.00
SMS	8	5.70	30	0%	1	1.00
SRDH E	8	6.13	30	0%	1	1.00
SRDH APSA	8	5.43	30	0%	1	1.00
SRDH' E	8	5.73	30	0%	1	1.00
SRDH' N	6	5.10	30	0%	1	1.00
SRDH' SA	7	5.30	30	0%	1	1.00
Icosahedron1						
SAH	17	13.15	5130	0%	1	1.00
OMS	13	12.40	5130	0%	1	1.00
SMS	16	12.81	5130	0%	1	1.00
SRDH E	19	14.64	5130	0%	1	1.00
SRDH APSA	17	14.03	5130	0%	1	1.00
SRDH' E	18	13.53	5130	0%	1	1.00
SRDH' N	14	12.54	5130	0%	1	1.00
SRDH' SA	15	13.40	5130	0%	1	1.00
Icosahedron2						
SAH	16	12.78	5100	0%	1	1.00
OMS	13	12.39	5100	0%	1	1.00
SMS	16	12.80	5100	0%	1	1.00
SRDH E	18	12.99	5100	0%	1	1.00
SRDH APSA	15	12.50	5100	0%	1	1.00
SRDH' E	16	12.64	5100	0%	1	1.00
SRDH' N	14	12.53	5100	0%	1	1.00
SRDH' SA	14	12.40	5100	0%	1	1.00
Icosahedron3						
SAH	17	13.05	5120	0%	1	1.00
OMS	13	12.40	5120	0%	1	1.00
SMS	20	14.37	5120	0%	1	1.00
SRDH E	22	13.45	5120	0%	1	1.00
SRDH APSA	16	12.59	5120	0%	1	1.00
SRDH' E	16	12.75	5120	0%	1	1.00
SRDH' N	14	12.53	5120	0%	1	1.00
SRDH' SA	14	12.41	5120	0%	1	1.00
Icosahedron4						
SAH	19	13.70	7661	0%	3	1.19
OMS	14	13.20	9080	0%	1	1.00
SMS	20	14.42	7100	0%	2	1.28
SRDH E	23	14.94	9080	0%	1	1.00
SRDH APSA	21	15.74	9080	0%	1	1.00
SRDH' E	18	14.00	9080	0%	1	1.00
SRDH' N	15	13.35	9080	0%	1	1.00
SRDH' SA	16	13.45	9080	0%	1	1.00

Table 35: The maximum (average) tree depth, D<sub>max</sub> (D<sub>avg</sub>) (in **bold** if equal to the fixed tree depth), the total number of leaf nodes, L<sub>tot</sub>, The geometric primitive reference duplication percentage, RD%, and the maximum (average) number of geometric primitives per leaf node, G<sub>max</sub>/L (G<sub>avg</sub>/L) for constructing the **BVH** ADSs with various build heuristics for a variety of artificial test scenes.

Build heuristic	BVH							
	$I_s$	$\Delta I_s$	$T_s$	$\Delta T_s$	$I_s$	$\Delta I_s$	$T_s$	$\Delta T_s$
			Kitchen - Viewpoint 1				Kitchen - Viewpoint 2	
SAH + OB	3.07	-34.06%	53.46	-41.87%	2.49	-25.29%	54.41	-36.99%
SAH + IO	3.02	-32.80%	30.92	0.51%	2.41	-22.80%	30.20	13.53%
SAH + <UDF>	2.25	-9.94%	36.22	-14.20%	2.01	-7.31%	38.30	-10.48%
SAH + LDF	2.62	-22.51%	43.64	-28.79%	2.14	-12.77%	39.68	-13.61%
SAH + RDF	2.02	0.12%	29.41	5.66%	1.96	-4.76%	37.10	-7.60%
SAH + CCF	2.86	-29.25%	45.78	-32.12%	2.27	-18.02%	45.62	-24.85%
SAH + FCF	1.65	22.91%	26.13	18.91%	1.74	7.28%	29.86	14.82%
SAH + NodeSATO	2.03	Ref.	31.08	Ref.	1.86	Ref.	34.28	Ref.
OMS + NodeSATO	1.80	12.32%	129.54	-76.01%	1.74	7.14%	134.03	-74.42%
SMS + NodeSATO	2.04	-0.67%	48.08	-35.36%	1.86	0.09%	46.36	-26.05%
SRDH APSA	1.85	9.63%	144.70	-78.52%	1.92	-3.17%	170.78	-79.93%
SRDH' N	2.35	-13.75%	1542.22	-97.98%	2.04	-8.61%	981.91	-96.51%
SRDH' SA	1.77	14.38%	60.69	-48.79%	1.67	11.51%	80.27	-57.29%
Crytek Sponza - Viewpoint 1								
SAH + OB	2.74	-31.95%	72.87	-50.04%	2.79	-28.19%	65.61	-49.42%
SAH + IO	2.55	-26.73%	84.29	-56.81%	2.65	-24.29%	88.97	-62.70%
SAH + <UDF>	2.36	-20.98%	44.69	-18.54%	2.46	-18.47%	43.15	-23.09%
SAH + LDF	2.02	-7.65%	43.20	-15.72%	2.09	-3.80%	34.72	-4.42%
SAH + RDF	2.82	-33.92%	49.57	-26.56%	3.02	-33.48%	50.69	-34.54%
SAH + CCF	2.58	-27.78%	63.95	-43.08%	2.55	-21.44%	58.02	-42.81%
SAH + FCF	2.26	-17.24%	30.16	20.71%	2.51	-20.03%	29.36	13.05%
SAH + NodeSATO	1.87	Ref.	36.40	Ref.	2.01	Ref.	33.19	Ref.
OMS + NodeSATO	2.31	-19.17%	146.59	-75.17%	2.99	-32.92%	174.70	-81.00%
SMS + NodeSATO	2.52	-25.80%	79.10	-53.98%	3.49	-42.46%	96.12	-65.47%
SRDH APSA	1.96	-4.78%	337.40	-89.21%	1.96	2.14%	217.55	-84.75%
SRDH' N	3.26	-42.75%	6471.15	-99.44%	2.66	-24.47%	1982.27	-98.33%
SRDH' SA	2.12	-11.86%	931.56	-96.09%	2.34	-14.20%	612.39	-94.58%
Conference Room - Viewpoint 1								
SAH + OB	3.95	-46.96%	47.67	-49.62%	4.01	-51.77%	54.93	-60.08%
SAH + IO	3.72	-43.67%	28.08	-14.47%	3.57	-45.91%	29.17	-24.83%
SAH + <UDF>	2.82	-25.82%	32.94	-27.09%	2.76	-30.05%	34.76	-36.92%
SAH + LDF	3.00	-30.18%	33.82	-29.00%	2.96	-34.72%	36.45	-39.85%
SAH + RDF	2.65	-21.14%	32.31	-25.69%	2.62	-26.33%	33.85	-35.24%
SAH + CCF	3.40	-38.38%	38.23	-37.19%	3.66	-47.19%	47.89	-54.22%
SAH + FCF	2.26	-7.34%	27.20	-11.72%	1.78	8.84%	20.91	4.86%
SAH + NodeSATO	2.09	Ref.	24.01	Ref.	1.93	Ref.	21.93	Ref.
OMS + NodeSATO	2.17	-3.72%	118.96	-79.81%	2.08	-7.27%	131.79	-83.36%
SMS + NodeSATO	2.30	-8.88%	45.73	-47.49%	2.70	-28.33%	46.91	-53.26%
SRDH APSA	2.68	-21.89%	124.74	-80.75%	1.67	15.95%	99.19	-77.90%
SRDH' N	3.20	-34.58%	1831.01	-98.69%	3.08	-37.31%	2456.25	-99.11%
SRDH' SA	1.99	5.00%	159.04	-84.90%	1.87	3.33%	121.79	-82.00%
Bedroom - Viewpoint 1								
SAH + OB	13.99	-36.77%	81.12	-29.29%	6.47	-59.03%	93.42	-57.68%
SAH + IO	15.56	-43.13%	103.09	-44.36%	8.48	-68.73%	149.39	-73.53%
SAH + <UDF>	8.14	8.69%	56.79	1.00%	3.94	-32.70%	57.97	-31.80%
SAH + LDF	6.86	28.93%	53.37	7.47%	4.21	-37.01%	62.83	-37.07%
SAH + RDF	10.84	-18.34%	64.52	-11.10%	4.06	-34.72%	56.23	-29.69%
SAH + CCF	11.96	-26.05%	68.84	-16.68%	6.21	-57.26%	81.05	-51.22%
SAH + FCF	6.04	46.55%	48.49	18.28%	2.42	9.48%	38.15	3.64%
SAH + NodeSATO	8.85	Ref.	57.36	Ref.	2.65	Ref.	39.54	Ref.
OMS + NodeSATO	5.64	56.96%	164.03	-65.03%	3.15	-15.73%	180.25	-78.07%
SMS + NodeSATO	8.88	-0.38%	97.11	-40.94%	3.26	-18.61%	77.62	-49.06%
SRDH APSA	6.06	46.04%	1033.31	-94.45%	1.87	41.45%	195.31	-79.76%
SRDH' N	12.34	-28.30%	5250.22	-98.91%	2.44	8.84%	1320.94	-97.01%
SRDH' SA	5.91	49.72%	415.86	-86.21%	1.91	38.65%	73.99	-46.56%
Carnival - Viewpoint 1								
SAH + OB	9.71	-50.64%	105.42	-57.46%	23.26	-41.68%	104.50	-39.42%
SAH + IO	8.28	-42.09%	58.72	-23.63%	22.14	-38.74%	73.00	-13.28%
SAH + <UDF>	5.83	-17.82%	67.42	-33.48%	17.42	-22.13%	81.03	-21.87%
SAH + LDF	5.47	-12.31%	63.71	-29.62%	13.44	0.90%	64.56	-1.94%
SAH + RDF	6.87	-30.27%	75.79	-40.83%	21.93	-38.13%	99.53	-36.40%
SAH + CCF	5.59	-14.30%	60.24	-25.56%	22.24	-39.01%	98.67	-35.84%
SAH + FCF	5.60	-14.35%	72.40	-38.06%	13.11	3.48%	64.89	-2.45%
SAH + NodeSATO	4.79	Ref.	44.85	Ref.	13.57	Ref.	63.31	Ref.
OMS + NodeSATO	4.39	9.25%	153.81	-70.84%	11.23	20.81%	176.65	-64.16%
SMS + NodeSATO	5.64	-15.03%	88.89	-49.55%	16.65	-18.51%	99.94	-36.65%
SRDH APSA	2.99	60.54%	4760.76	-99.06%	13.53	0.27%	5822.59	-98.91%
SRDH' N	8.78	-45.44%	16023.49	-99.72%	17.48	-22.41%	14982.77	-99.58%
SRDH' SA	3.80	25.99%	133.11	-66.31%	12.74	6.51%	218.33	-71.00%
Museum Hall - Viewpoint 1								
SAH + OB	7.17	-30.43%	103.07	-40.93%	5.29	-38.67%	107.27	-43.08%
SAH + IO	6.83	-26.99%	56.99	6.83%	5.14	-36.92%	53.63	13.85%
SAH + <UDF>	5.22	-4.42%	68.64	-11.31%	3.87	-16.32%	67.01	-8.89%
SAH + LDF	5.42	-7.96%	70.36	-13.47%	4.03	-19.53%	61.80	-1.21%
SAH + RDF	5.31	-6.00%	67.30	-9.54%	4.05	-19.96%	77.58	-21.31%
SAH + CCF	5.96	-16.40%	83.12	-26.75%	4.82	-32.76%	80.20	-23.87%
SAH + FCF	4.25	17.21%	51.88	17.36%	2.89	12.00%	52.46	16.37%
SAH + NodeSATO	4.99	Ref.	60.88	Ref.	3.24	Ref.	61.05	Ref.
OMS + NodeSATO	4.47	11.51%	213.44	-71.47%	3.55	-8.60%	221.18	-72.40%
SMS + NodeSATO	5.15	-3.18%	124.87	-51.24%	3.53	-8.14%	107.96	-43.45%
SRDH APSA	4.74	5.29%	817.32	-92.55%	2.90	11.73%	624.76	-90.23%
SRDH' N	4.53	10.03%	20690.61	-99.71%	3.60	-9.90%	25879.69	-99.76%
SRDH' SA	3.05	63.58%	253.90	-76.02%	2.45	32.43%	201.36	-69.68%

Table 36: The average number of ray-triangle intersection tests,  $I_s$ , and the average number of ADS node traversal steps,  $T_s$ , to perform per any-hit shadow (ambient) ray using various traversal heuristics for a **BVH** ADS, built with SAH SP, (and/or a dedicated **BVH** ADS for shadow ray traversal) for a variety of realistic test scenes and viewpoints rendered as ambient occlusion images of resolution 512×512 pixels using 512 primary rays per pixel and 1 shadow ray per primary ray which is not limited to a fixed, finite, maximum distance.

Build heuristic	BVH					
	D <sub>max</sub>	D <sub>avg</sub>	L <sub>tot</sub>	RD%	G <sub>max/L</sub>	G <sub>avg/L</sub>
Kitchen						
SAH (SP)	32	20.41	120 k	0%	6	1.00
OMS	17	16.91	120 k	0%	1	1.00
SMS	40	25.43	120 k	0%	3	1.00
SRDH APSA	<b>64</b>	23.50	120 k	0%	14	1.00
SRDH' N	18	17.06	120 k	0%	1	1.00
SRDH' SA	29	20.62	120 k	0%	7	1.00
Crytek Sponza						
SAH (SP)	29	20.64	262 k	0%	2	1.00
OMS	19	18.00	262 k	0%	1	1.00
SMS	32	21.88	262 k	0%	2	1.00
SRDH APSA	37	23.30	262 k	0%	1	1.00
SRDH' N	20	18.17	262 k	0%	1	1.00
SRDH' SA	27	20.18	262 k	0%	1	1.00
Conference Room						
SAH (SP)	29	22.08	331 k	0%	2	1.00
OMS	19	18.42	331 k	0%	1	1.00
SMS	35	26.15	331 k	0%	2	1.00
SRDH APSA	<b>64</b>	26.25	331 k	0%	39	1.00
SRDH' N	20	18.55	331 k	0%	1	1.00
SRDH' SA	29	22.20	331 k	0%	1	1.00
Bedroom						
SAH (SP)	36	21.43	362 k	0%	3	1.00
OMS	19	18.55	362 k	0%	1	1.00
SMS	41	25.07	362 k	0%	1	1.00
SRDH APSA	<b>64</b>	23.83	362 k	0%	73	1.00
SRDH' N	20	18.67	362 k	0%	1	1.00
SRDH' SA	30	21.68	362 k	0%	13	1.00
Carnival						
SAH (SP)	37	23.20	450 k	0%	3	1.00
OMS	19	18.83	450 k	0%	1	1.00
SMS	39	25.92	450 k	0%	2	1.00
SRDH APSA	<b>64</b>	24.88	450 k	0%	80	1.00
SRDH' N	20	18.98	450 k	0%	1	1.00
SRDH' SA	29	22.07	448 k	0%	14	1.00
Museum Hall						
SAH (SP)	34	23.14	1466 k	0%	3	1.00
OMS	21	20.57	1468 k	0%	1	1.00
SMS	40	25.02	1466 k	0%	2	1.00
SRDH APSA	<b>64</b>	25.13	1468 k	0%	68	1.00
SRDH' N	22	20.69	1468 k	0%	1	1.00
SRDH' SA	30	22.95	1468 k	0%	3	1.00

Table 37: The maximum (average) tree depth, D<sub>max</sub> (D<sub>avg</sub>) (in **bold** if equal to the fixed tree depth), the total number of leaf nodes, L<sub>tot</sub>, The geometric primitive reference duplication percentage, RD%, and the maximum (average) number of geometric primitives per leaf node, G<sub>max/L</sub> (G<sub>avg/L</sub>) for constructing the **BVH** ADSSs with various build heuristics for a variety of realistic test scenes.

Kd-tree						
Build heuristic	Build Time			Rendering Time		
	Avg.	Best	Worst	Avg.	Best	Worst
SAH (SP)	0.1	0.1	0.2	-0.1%	3.6%	-13.6%
SAH	Reference			Reference		
RTSAH Z	2.9	1.8	5.4	-49.6%	-14.9%	-96.5%
RTSAH N	4.8	2.2	11.0	-34.3%	-4.3%	-80.5%
RTSAH SA	162.6	118.6	248.2	-5.2%	2.7%	-19.5%
RTSAH APSA	94.1	74.2	141.8	-0.4%	5.6%	-4.2%
RTSAH HANPSA2	107.3	80.6	166.4	-4.0%	3.4%	-8.7%
RTSAH WNHANPSA2	91.4	67.4	124.3	-3.6%	4.4%	-11.4%
RTSAH WNWCHANPSA2	92.3	68.4	124.6	-4.3%	1.3%	-16.5%
RTSAH EP	87.2	68.3	113.1	-2.0%	5.3%	-9.6%
RTSAH APE	91.9	76.2	107.8	-1.5%	2.0%	-3.9%
BIH						
Build heuristic	Build Time			Rendering Time		
	Avg.	Best	Worst	Avg.	Best	Worst
SAH (SP)	Reference			Reference		
SAH	2.3	2.0	2.7	0.5%	9.9%	-9.0%
RTSAH Z	2.1	1.5	2.5	-61.6%	-41.5%	-78.4%
RTSAH N	1.9	1.5	2.2	-23.1%	5.1%	-46.0%
RTSAH SA	369.5	301.5	413.0	-4.7%	5.5%	-12.8%
RTSAH APSA	179.9	149.0	204.0	-4.9%	8.3%	-27.3%
RTSAH HANPSA2	183.7	155.5	200.7	-12.4%	1.0%	-25.3%
RTSAH WNHANPSA2	185.0	159.0	199.3	-13.9%	1.2%	-36.5%
RTSAH WNWCHANPSA2	186.0	161.8	205.6	-12.7%	7.1%	-40.3%
RTSAH EP	172.9	139.5	189.7	-5.2%	10.4%	-23.9%
RTSAH APE	174.8	137.5	209.1	-5.4%	9.4%	-25.3%
BVH						
Build heuristic	Build Time			Rendering Time		
	Avg.	Best	Worst	Avg.	Best	Worst
SAH (SP)	Reference			Reference		
SAH	10.4	8.5	11.7	0.8%	7.2%	-5.6%
RTSAH APSA	962.4	762.5	1163.3	0.5%	8.5%	-6.5%
RTSAH HANPSA2	999.2	803.0	1202.1	-0.7%	7.6%	-8.0%
RTSAH WNHANPSA2	996.1	783.5	1200.1	-0.3%	5.5%	-6.5%
RTSAH WNWCHANPSA2	991.1	780.5	1181.1	-0.9%	4.7%	-9.2%
RTSAH EP	936.4	715.5	1171.9	0.8%	11.0%	-5.1%
RTSAH APE	931.7	723.5	1154.1	0.6%	15.8%	-4.7%
SBVH						
Build heuristic	Build Time			Rendering Time		
	Avg.	Best	Worst	Avg.	Best	Worst
SAH	Reference			Reference		
RTSAH APSA	9.7	7.0	13.2	-3.4%	2.8%	-14.6%
RTSAH HANPSA2	10.3	6.9	15.3	-5.0%	-0.7%	-9.3%
RTSAH WNHANPSA2	10.1	7.1	14.6	-5.1%	-1.9%	-10.8%
RTSAH WNWCHANPSA2	10.0	6.8	14.8	-2.6%	1.4%	-10.5%
RTSAH EP	8.3	5.9	14.1	-4.7%	-0.8%	-11.4%
RTSAH APE	8.9	6.8	14.3	-3.4%	4.9%	-11.0%
BVH						
Build heuristic	Build Time			Rendering Time		
	Avg.	Best	Worst	Avg.	Best	Worst
SAH + NodeSATO	Reference			Reference		
SRDH APSA	1.6	1.5	1.7	-59.4%	-60.6%	-61.5%
SRDH' SA	1.3	1.0	1.5	-39.8%	-41.2%	-42.6%

Table 38: A summary of the number of times the build CPU time is increased (factor) and of the gains in the rendering CPU time (percentage), for different ADSs built with various build heuristics, for our realistic test scenes.

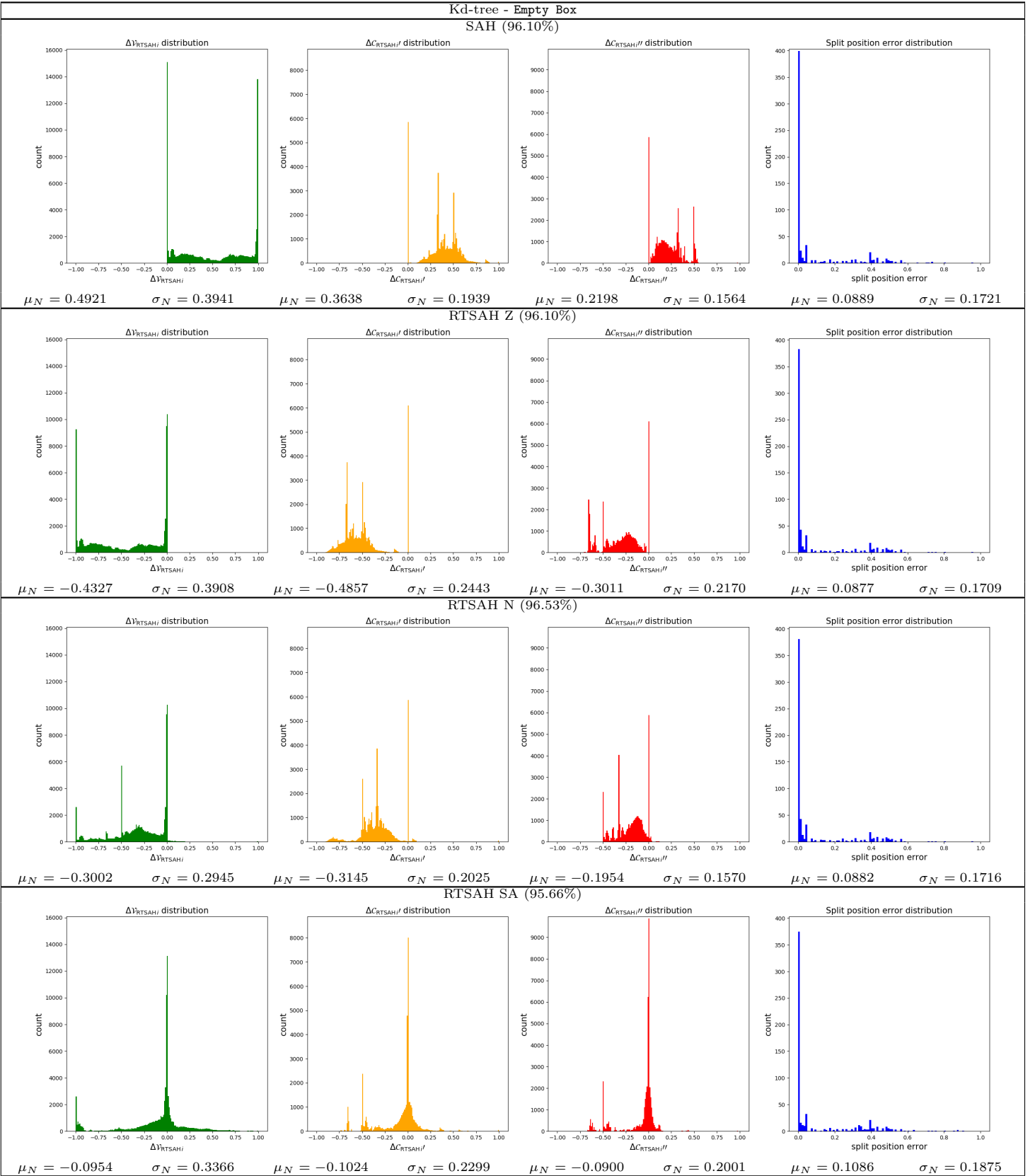


Table 39: The distributions (histogram, mean,  $\mu_N$ , standard deviation,  $\sigma_N$ ) of the visibility probability error,  $\Delta V_{\text{RTSAH}_i}$ , the modified cost errors,  $\Delta C'_{\text{RTSAH}_i}$  and  $\Delta C''_{\text{RTSAH}_i}$ , and the split position error, and the optimal axis selection percentage for a **kd-tree** ADS, built with various build heuristics, for the **Empty Box** scene.

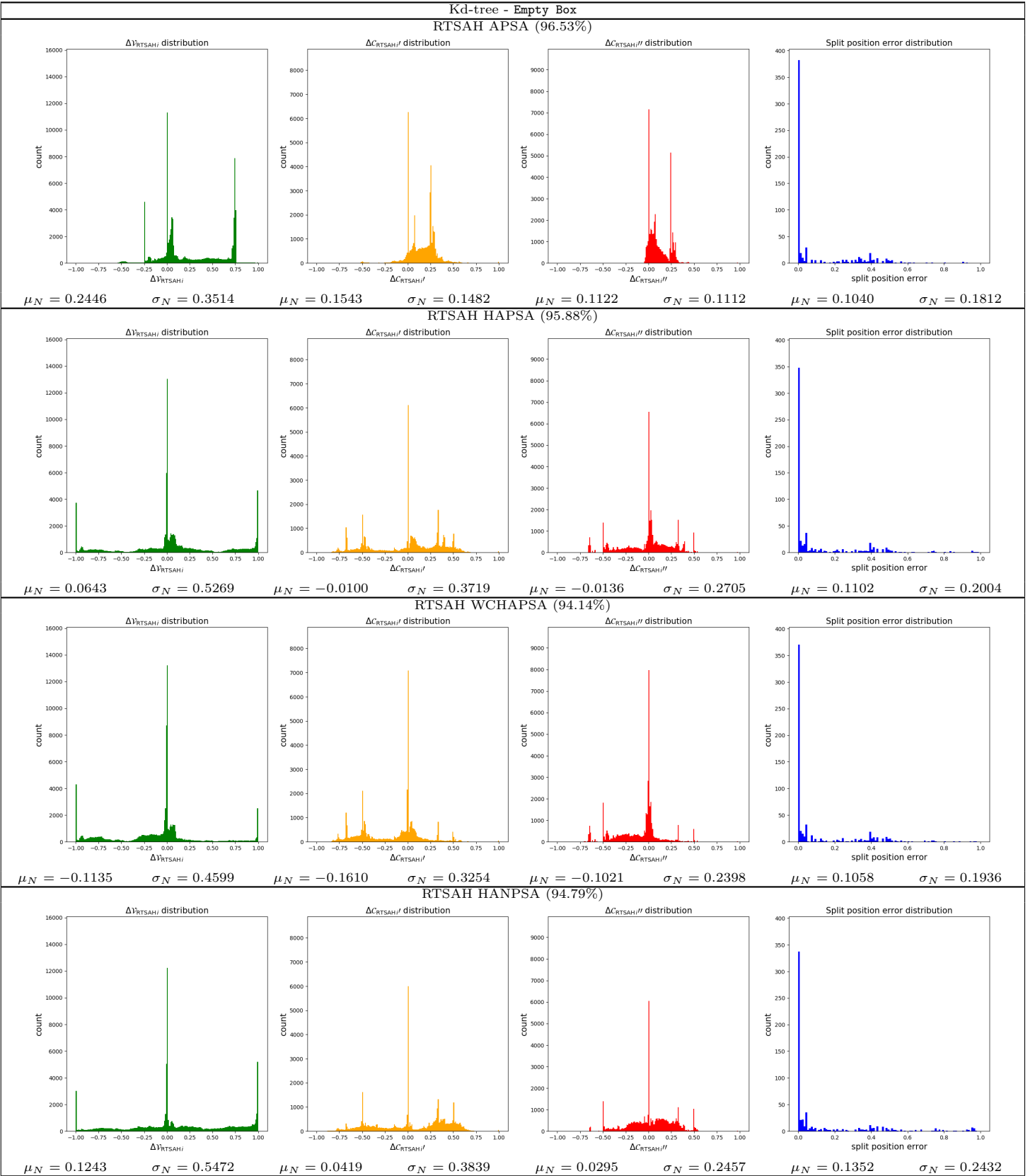


Table 40: The distributions (histogram, mean,  $\mu_N$ , standard deviation,  $\sigma_N$ ) of the visibility probability error,  $\Delta V_{\text{RTSAH}_i}$ , the modified cost errors,  $\Delta C'_{\text{RTSAH}_i}$  and  $\Delta C''_{\text{RTSAH}_i}$ , and the split position error, and the optimal axis selection percentage for a **kd-tree** ADS, built with various build heuristics, for the **Empty Box** scene.

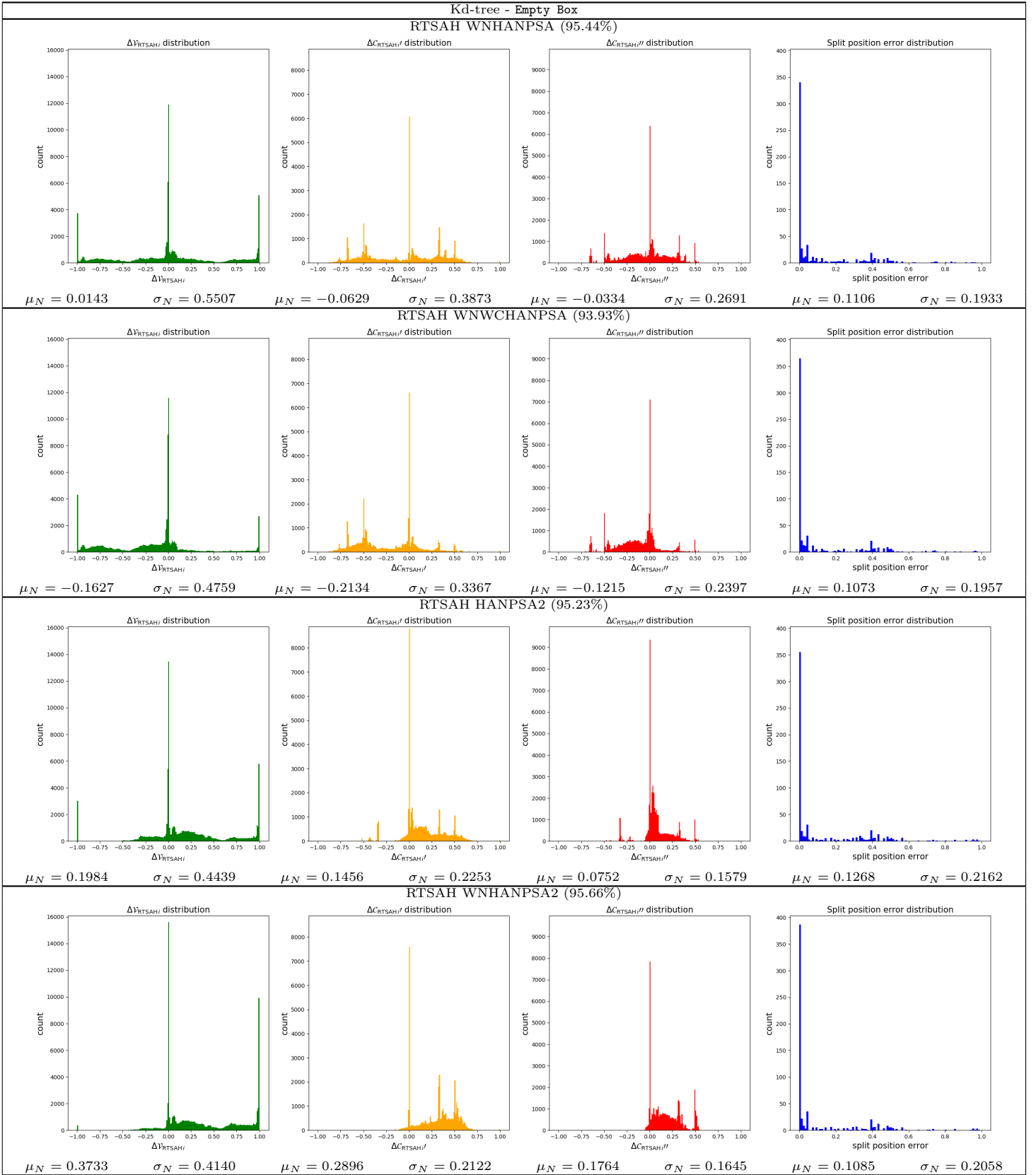


Table 41: The distributions (histogram, mean,  $\mu_N$ , standard deviation,  $\sigma_N$ ) of the visibility probability error,  $\Delta V_{\text{RTSAH}_i}$ , the modified cost errors,  $\Delta C'_{\text{RTSAH}_i}$  and  $\Delta C''_{\text{RTSAH}_i}$ , and the split position error, and the optimal axis selection percentage for a **kd-tree** ADS, built with various build heuristics, for the **Empty Box** scene.

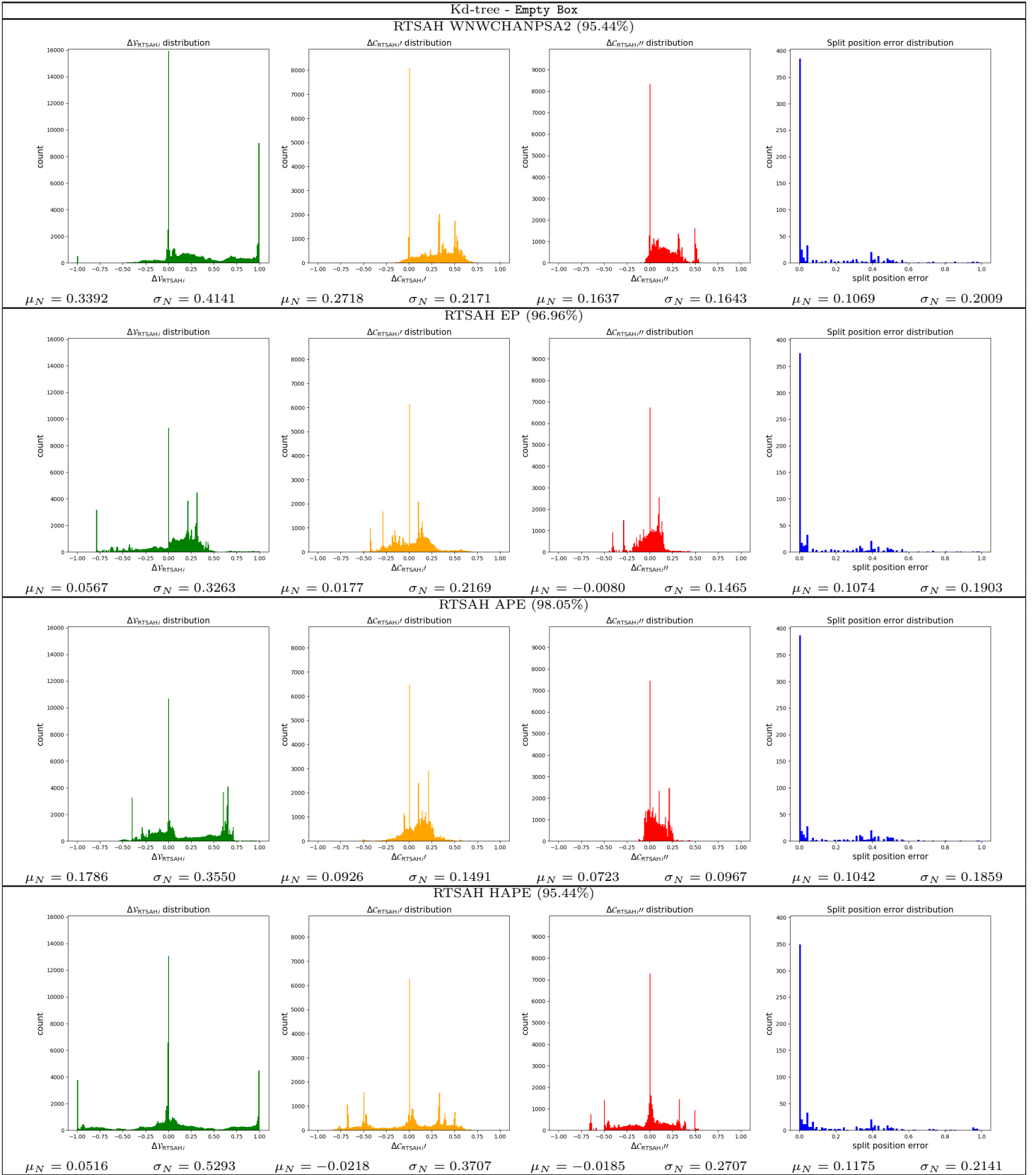


Table 42: The distributions (histogram, mean,  $\mu_N$ , standard deviation,  $\sigma_N$ ) of the visibility probability error,  $\Delta V_{RTSAH_i}$ , the modified cost errors,  $\Delta C'_{RTSAH_i}$  and  $\Delta C''_{RTSAH_i}$ , and the split position error, and the optimal axis selection percentage for a **kd-tree** ADS, built with various build heuristics, for the **Empty Box** scene.

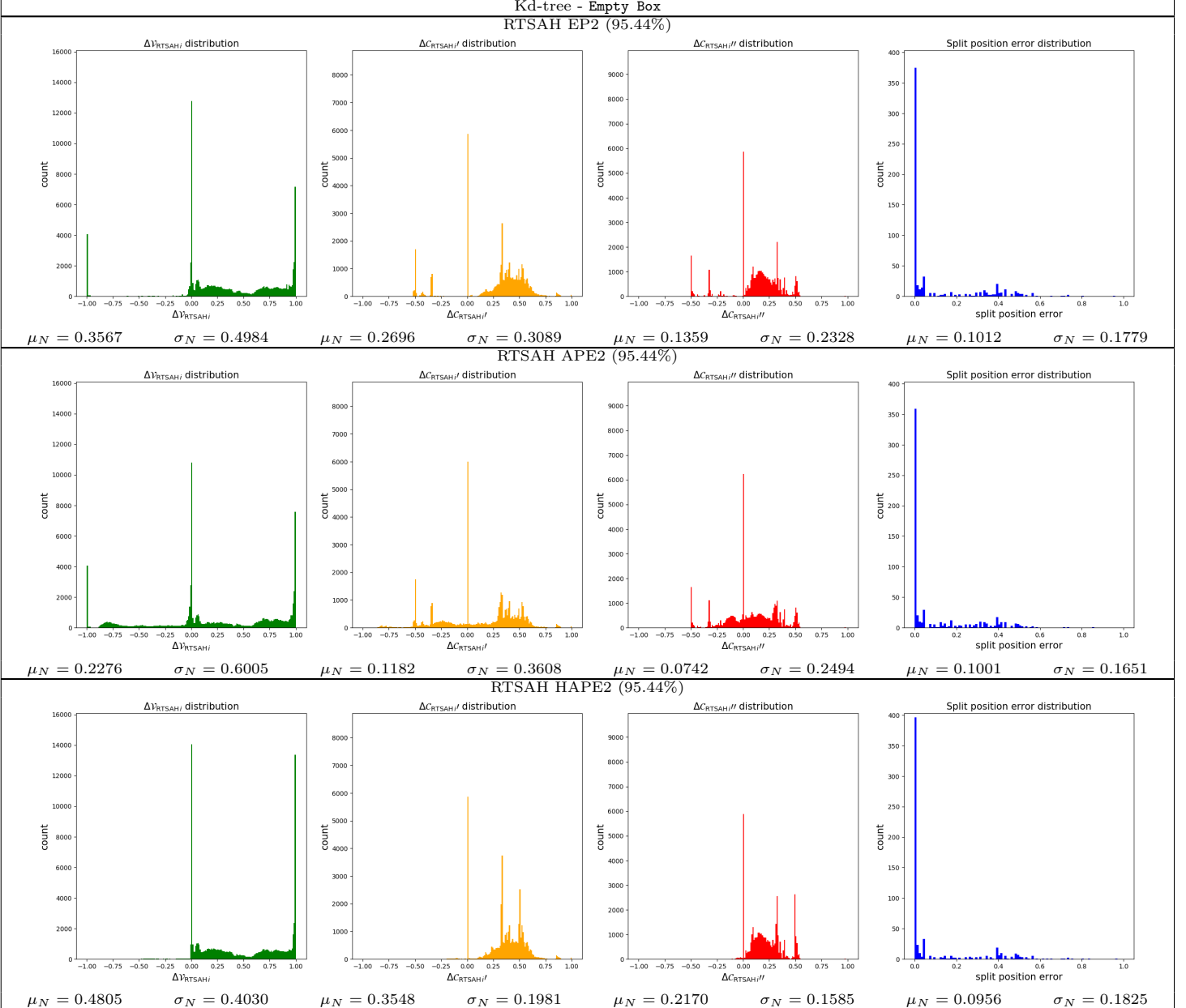


Table 43: The distributions (histogram, mean,  $\mu_N$ , standard deviation,  $\sigma_N$ ) of the visibility probability error,  $\Delta V_{\text{RTSAH}_i}$ , the modified cost errors,  $\Delta C'_{\text{RTSAH}_i}$  and  $\Delta C''_{\text{RTSAH}_i}$ , and the split position error, and the optimal axis selection percentage for a **kd-tree** ADS, built with various build heuristics, for the *Empty Box* scene.

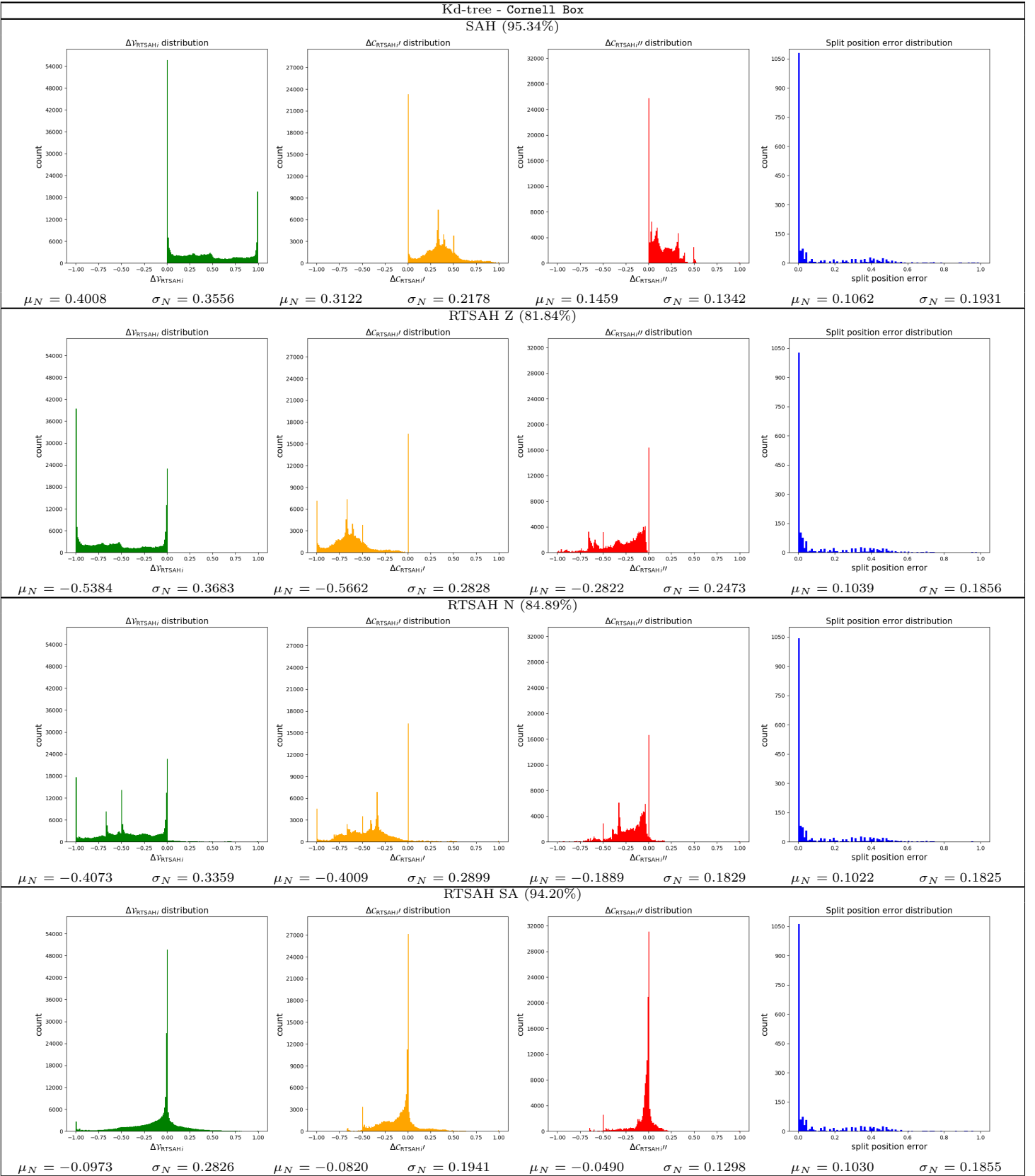


Table 44: The distributions (histogram, mean,  $\mu_N$ , standard deviation,  $\sigma_N$ ) of the visibility probability error,  $\Delta V_{\text{RTSAH}_i}$ , the modified cost errors,  $\Delta C'_{\text{RTSAH}_i}$  and  $\Delta C''_{\text{RTSAH}_i}$ , and the split position error, and the optimal axis selection percentage for a **kd-tree** ADS, built with various build heuristics, for the **Cornell Box** scene.

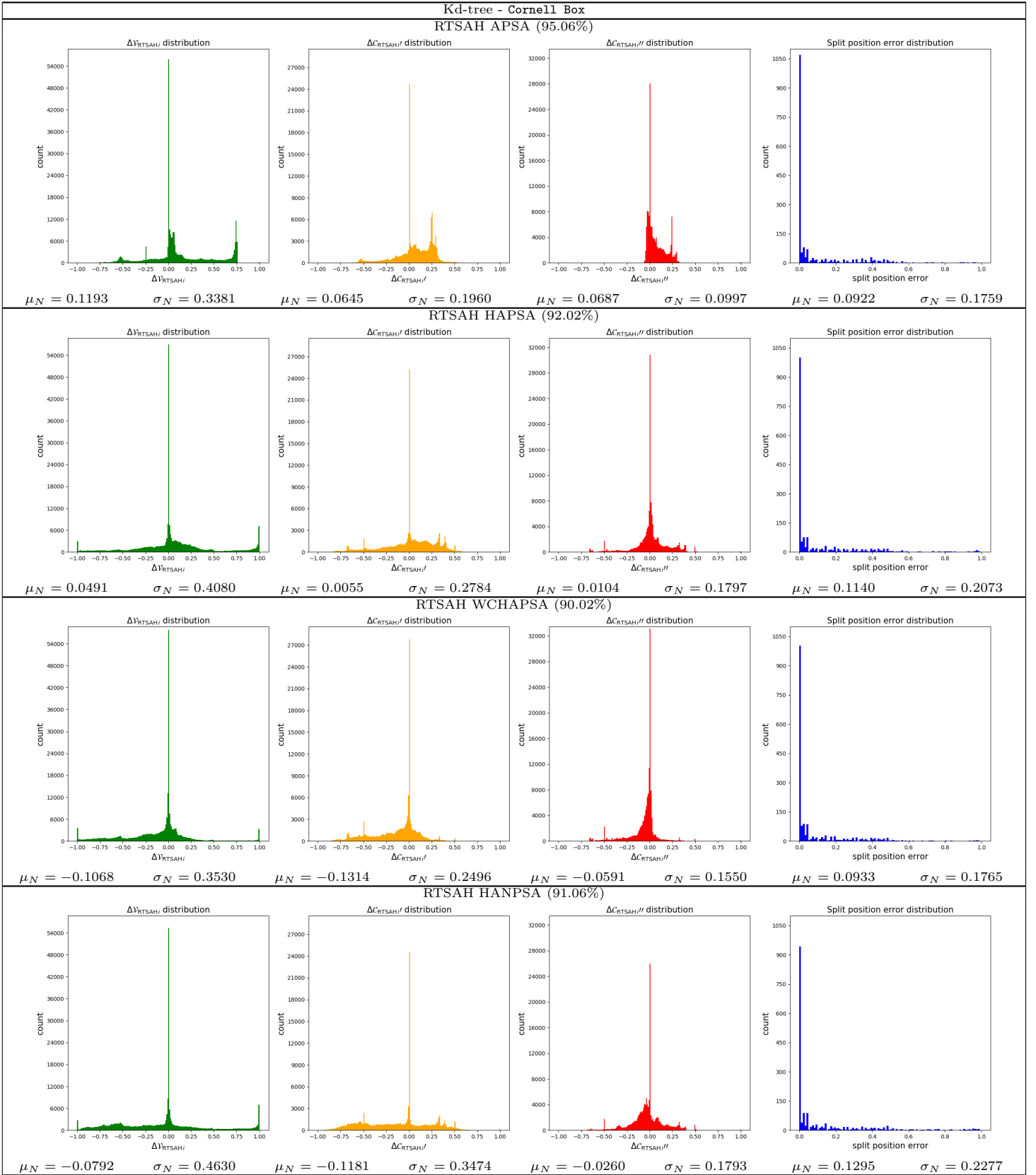


Table 45: The distributions (histogram, mean,  $\mu_N$ , standard deviation,  $\sigma_N$ ) of the visibility probability error,  $\Delta V_{\text{RTSAH}_i}$ , the modified cost errors,  $\Delta C'_{\text{RTSAH}_i}$  and  $\Delta C''_{\text{RTSAH}_i}$ , and the split position error, and the optimal axis selection percentage for a **kd-tree** ADS, built with various build heuristics, for the **Cornell Box** scene.

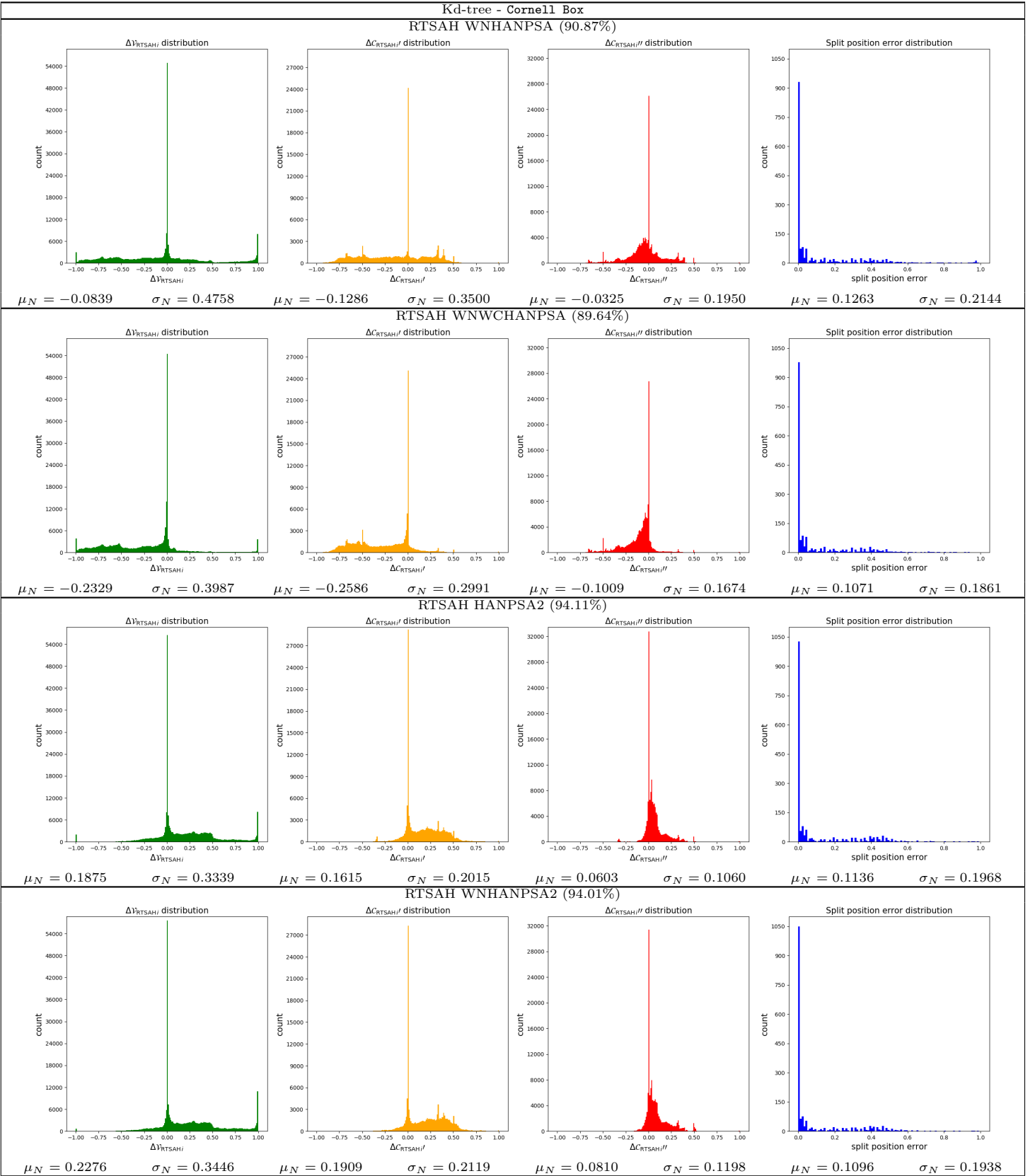


Table 46: The distributions (histogram, mean,  $\mu_N$ , standard deviation,  $\sigma_N$ ) of the visibility probability error,  $\Delta V_{\text{RTSAH}_i}$ , the modified cost errors,  $\Delta C'_{\text{RTSAH}_i}$  and  $\Delta C''_{\text{RTSAH}_i}$ , and the split position error, and the optimal axis selection percentage for a **kd-tree** ADS, built with various build heuristics, for the **Cornell Box** scene.

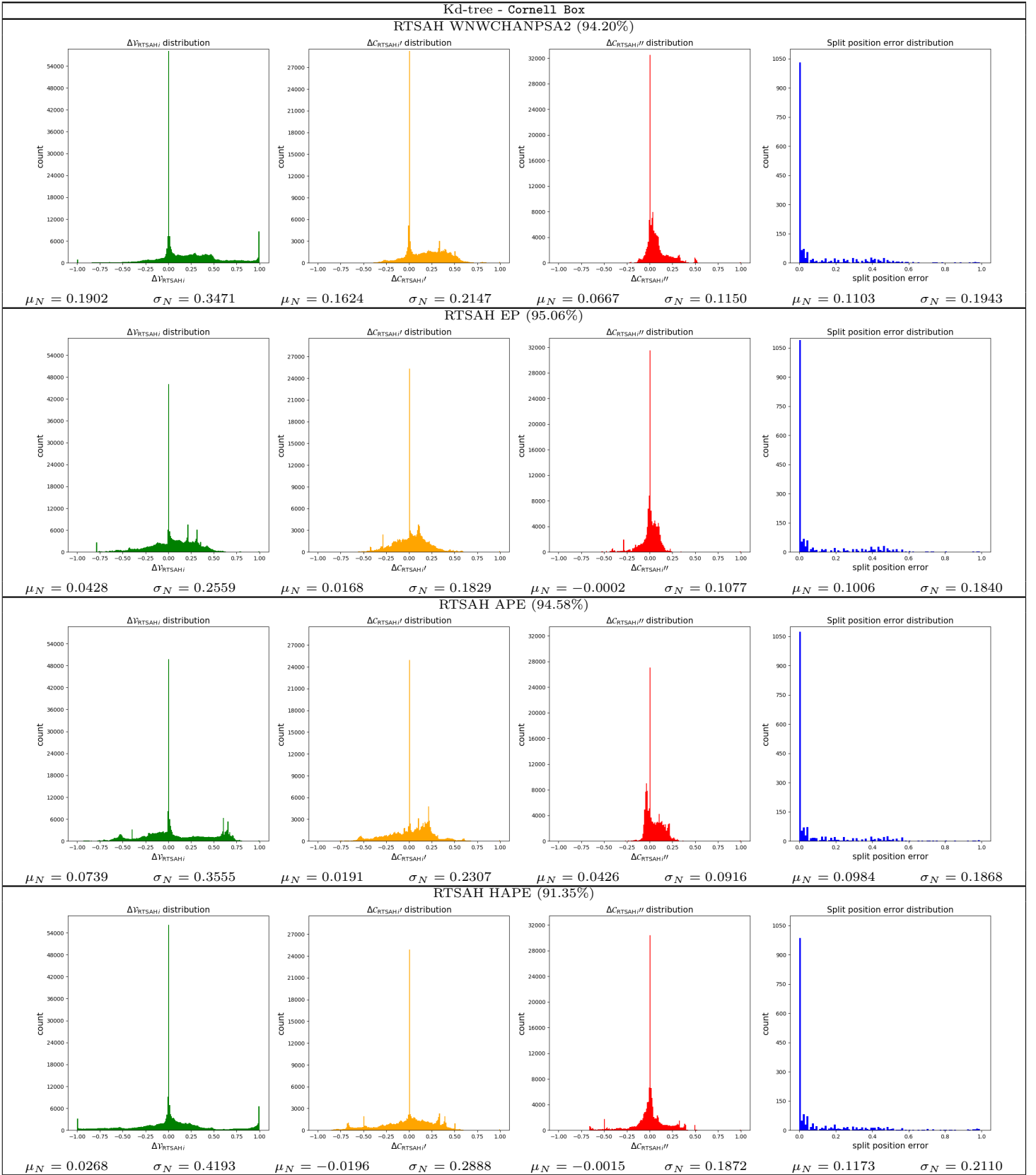


Table 47: The distributions (histogram, mean,  $\mu_N$ , standard deviation,  $\sigma_N$ ) of the visibility probability error,  $\Delta V_{\text{RTSAH}_i}$ , the modified cost errors,  $\Delta C'_{\text{RTSAH}_i}$  and  $\Delta C''_{\text{RTSAH}_i}$ , and the split position error, and the optimal axis selection percentage for a **kd-tree** ADS, built with various build heuristics, for the **Cornell Box** scene.

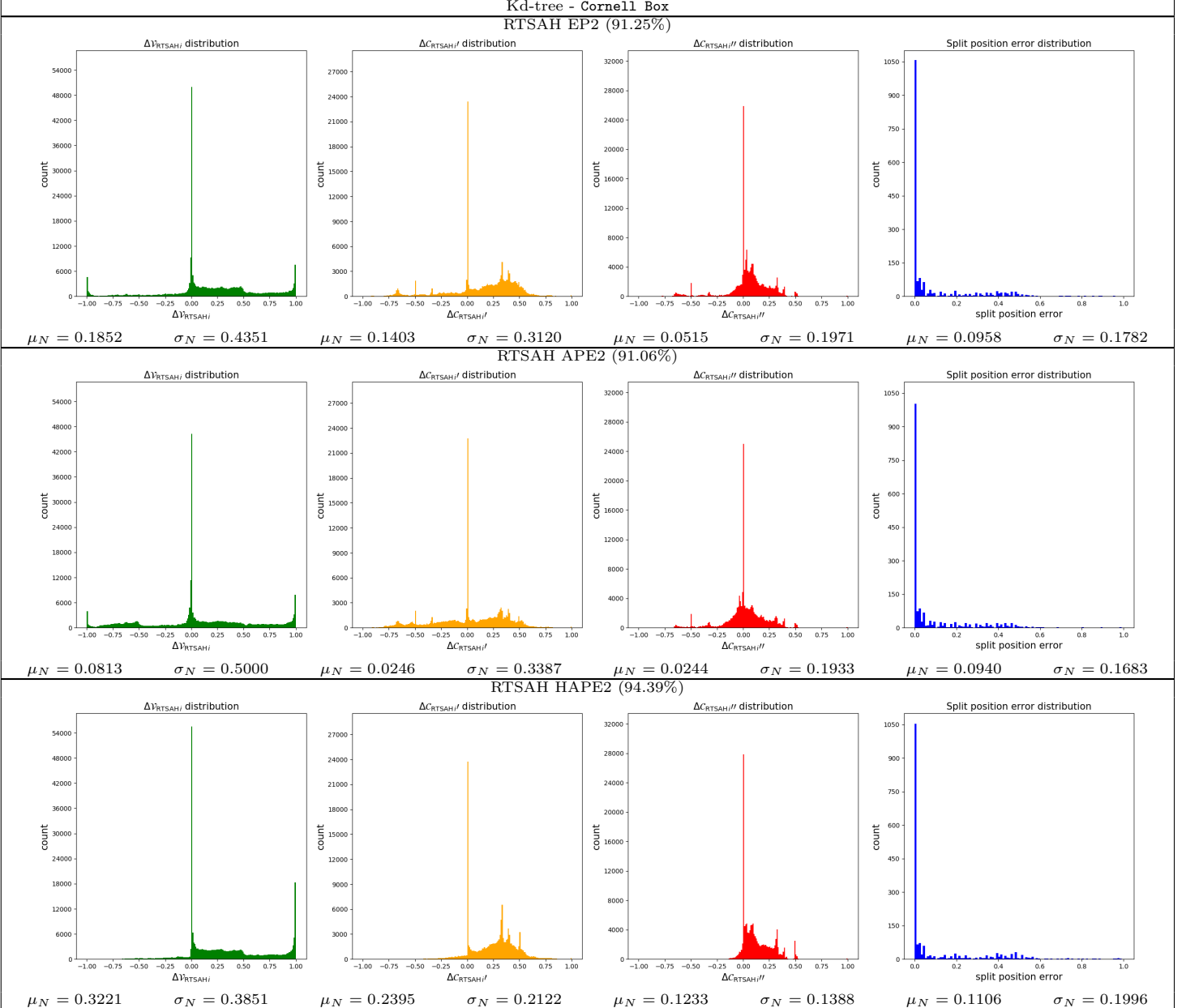


Table 48: The distributions (histogram, mean,  $\mu_N$ , standard deviation,  $\sigma_N$ ) of the visibility probability error,  $\Delta V_{\text{RTSAH}_i}$ , the modified cost errors,  $\Delta C'_{\text{RTSAH}_i}$  and  $\Delta C''_{\text{RTSAH}_i}$ , and the split position error, and the optimal axis selection percentage for a **kd-tree** ADS, built with various build heuristics, for the **Cornell Box** scene.

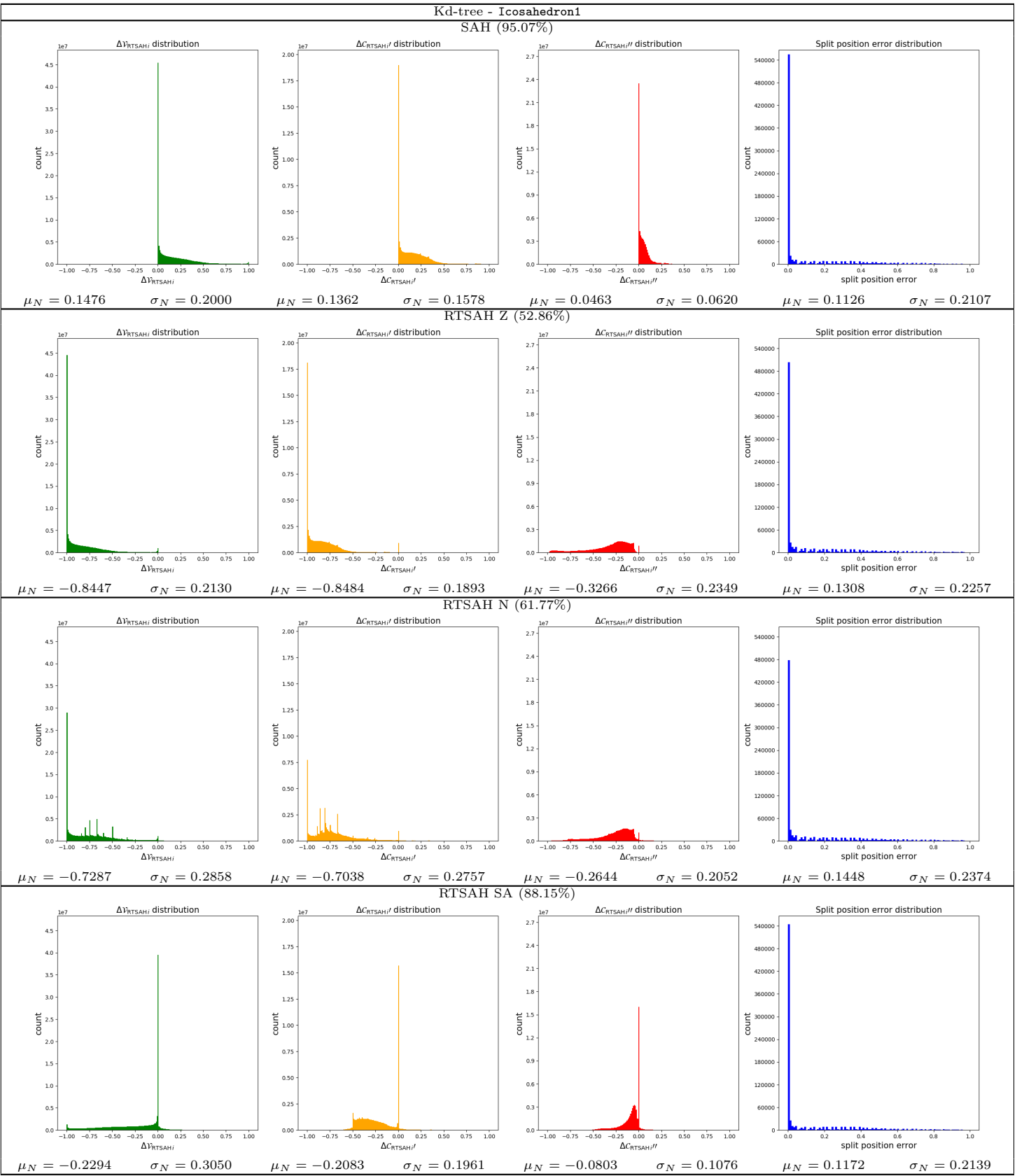


Table 49: The distributions (histogram, mean,  $\mu_N$ , standard deviation,  $\sigma_N$ ) of the visibility probability error,  $\Delta V_{\text{RTSAH}_i}$ , the modified cost errors,  $\Delta C'_{\text{RTSAH}_i}$  and  $\Delta C''_{\text{RTSAH}_i}$ , and the split position error, and the optimal axis selection percentage for a **kd-tree** ADS, built with various build heuristics, for the **Icosahedron1** scene.

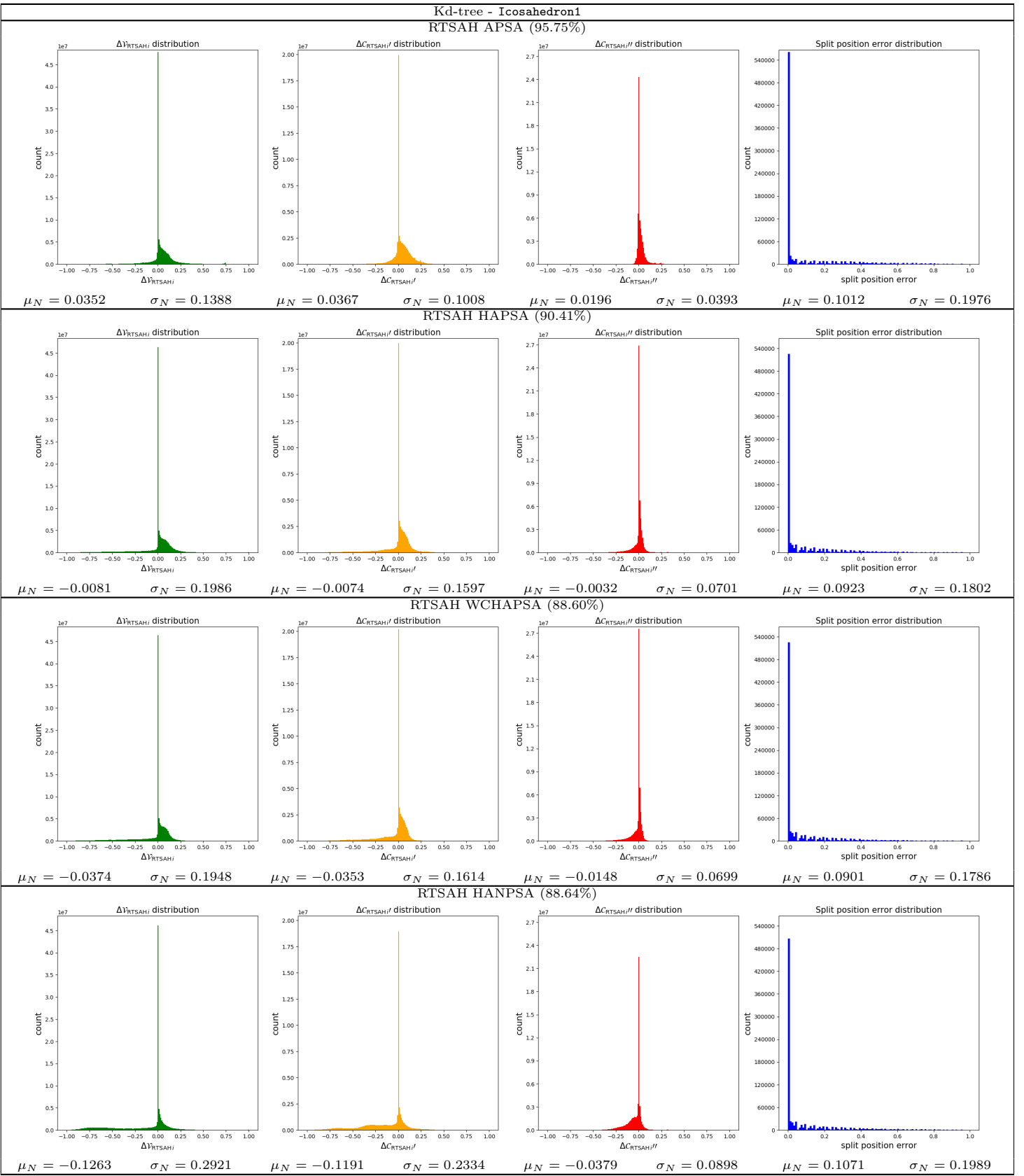


Table 50: The distributions (histogram, mean,  $\mu_N$ , standard deviation,  $\sigma_N$ ) of the visibility probability error,  $\Delta V_{\text{RTSAH}_i}$ , the modified cost errors,  $\Delta C'_{\text{RTSAH}_i}$  and  $\Delta C''_{\text{RTSAH}_i}$ , and the split position error, and the optimal axis selection percentage for a **kd-tree** ADS, built with various build heuristics, for the **Icosahedron1** scene.

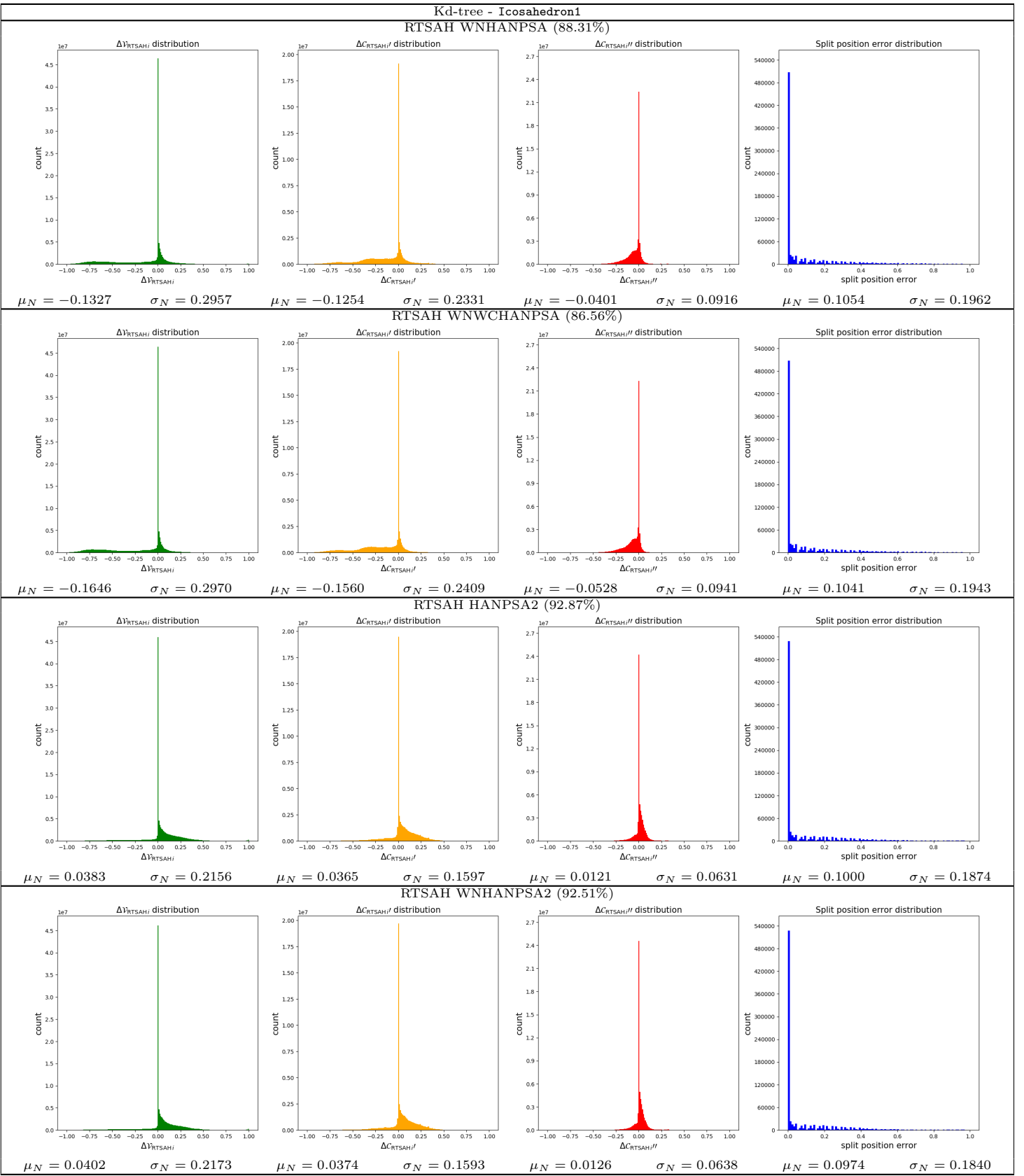


Table 51: The distributions (histogram, mean,  $\mu_N$ , standard deviation,  $\sigma_N$ ) of the visibility probability error,  $\Delta V_{\text{RTSAH}i}$ , the modified cost errors,  $\Delta C'_{\text{RTSAH}i}$  and  $\Delta C''_{\text{RTSAH}i}$ , and the split position error, and the optimal axis selection percentage for a **kd-tree** ADS, built with various build heuristics, for the **Icosahedron1** scene.

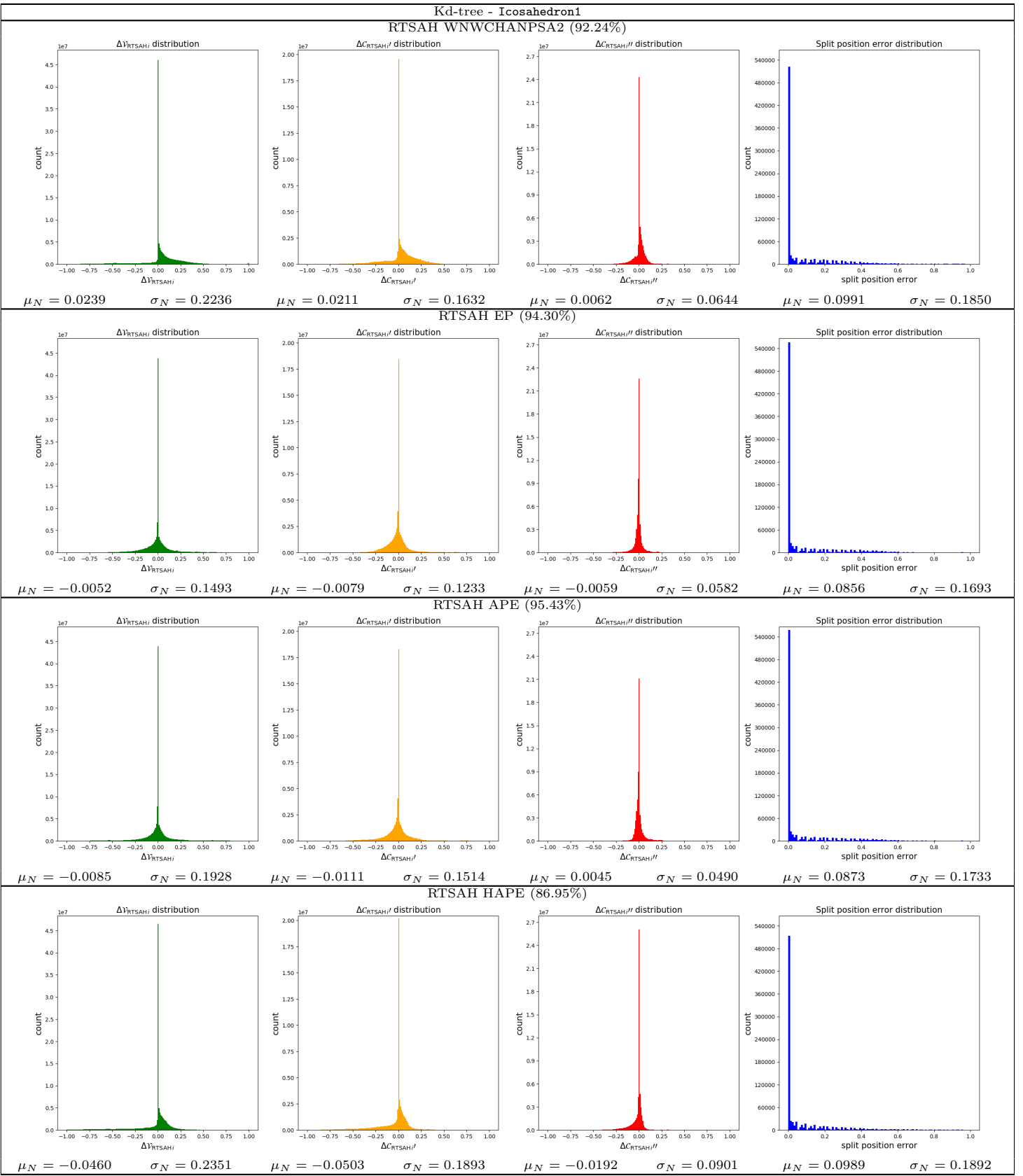


Table 52: The distributions (histogram, mean,  $\mu_N$ , standard deviation,  $\sigma_N$ ) of the visibility probability error,  $\Delta V_{\text{RTSAH}i}$ , the modified cost errors,  $\Delta C'_{\text{RTSAH}i}$  and  $\Delta C''_{\text{RTSAH}i}$ , and the split position error, and the optimal axis selection percentage for a **kd-tree** ADS, built with various build heuristics, for the **Icosahedron1** scene.

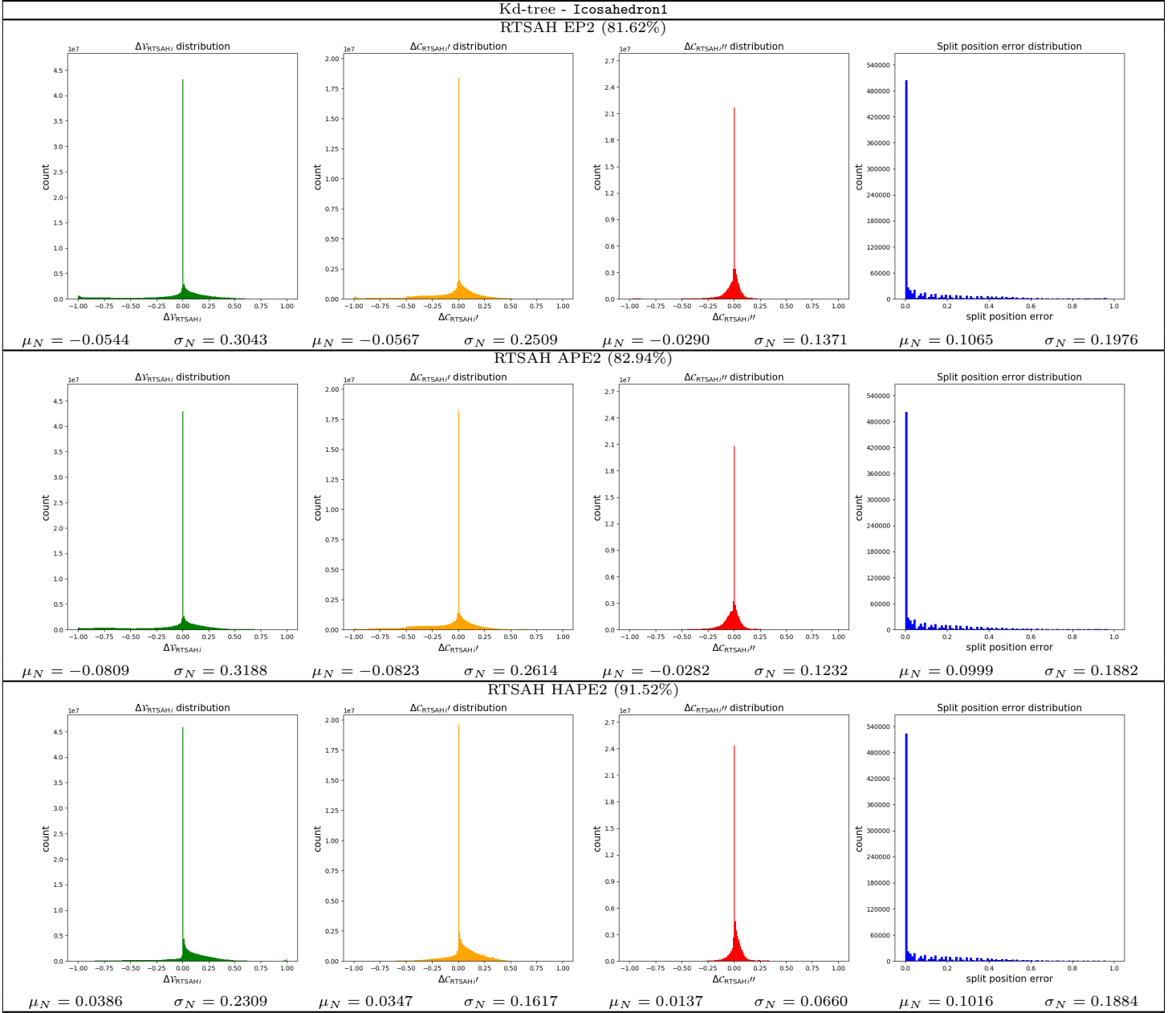


Table 53: The distributions (histogram, mean,  $\mu_N$ , standard deviation,  $\sigma_N$ ) of the visibility probability error,  $\Delta V_{\text{RTSAH}i}$ , the modified cost errors,  $\Delta C'_{\text{RTSAH}i}$  and  $\Delta C''_{\text{RTSAH}i}$ , and the split position error, and the optimal axis selection percentage for a **kd-tree** ADS, built with various build heuristics, for the **Icosahedron1** scene.

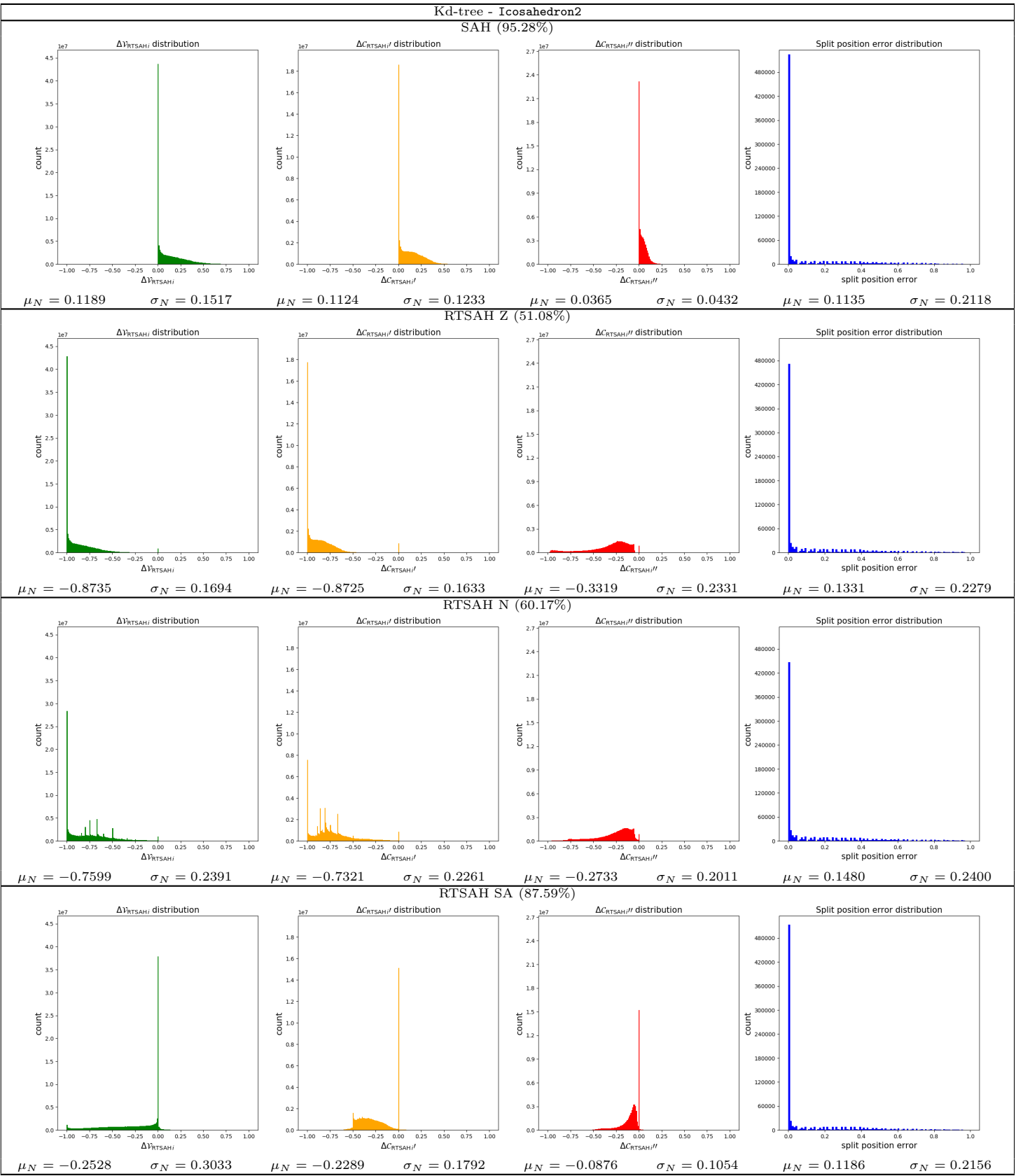


Table 54: The distributions (histogram, mean,  $\mu_N$ , standard deviation,  $\sigma_N$ ) of the visibility probability error,  $\Delta V_{RTSAH,i}$ , the modified cost errors,  $\Delta C'_{RTSAH,i}$  and  $\Delta C''_{RTSAH,i}$ , and the split position error, and the optimal axis selection percentage for a **kd-tree** ADS, built with various build heuristics, for the **Icosahedron2** scene.

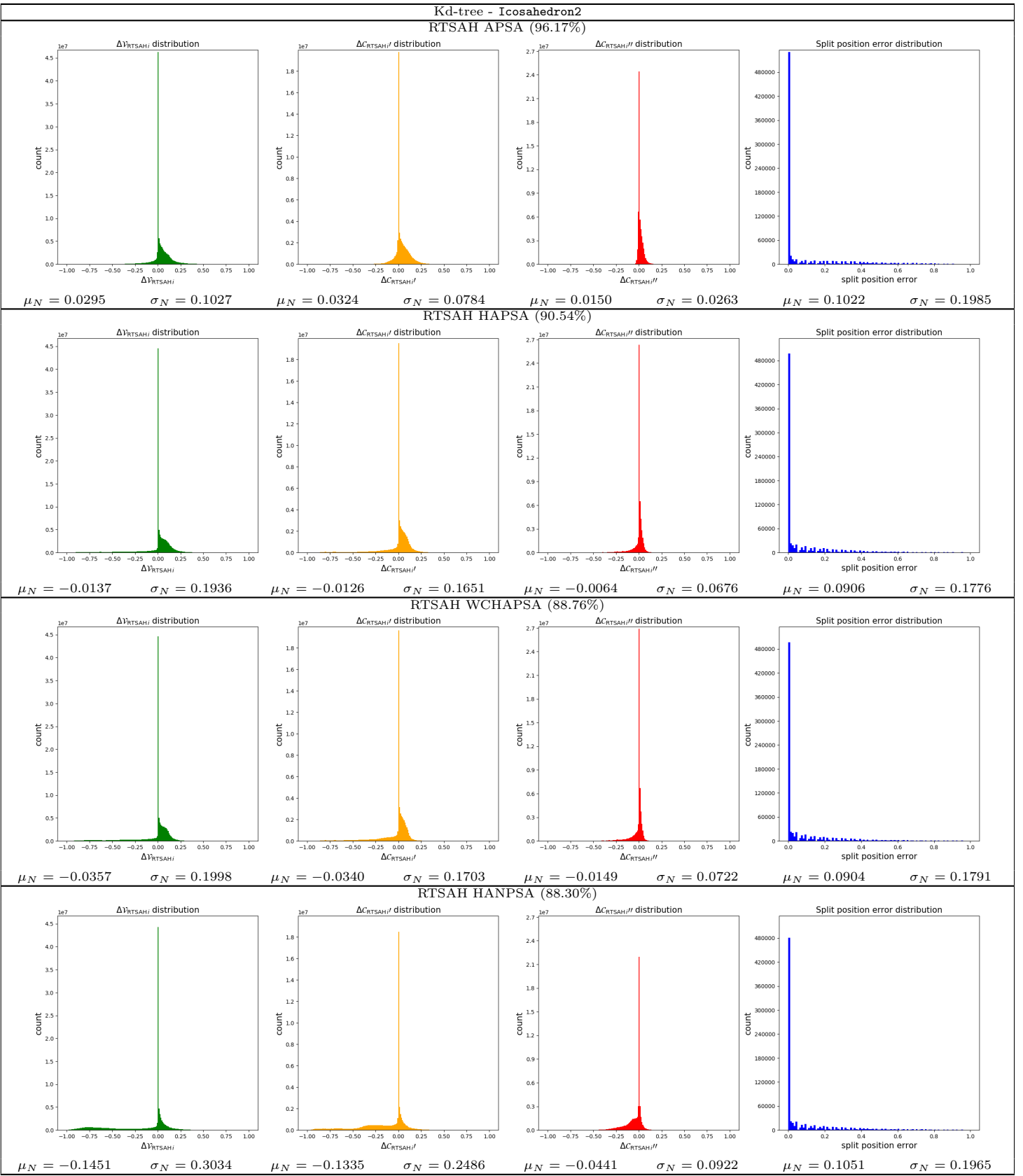


Table 55: The distributions (histogram, mean,  $\mu_N$ , standard deviation,  $\sigma_N$ ) of the visibility probability error,  $\Delta V_{\text{RTSAH}i}$ , the modified cost errors,  $\Delta C'_{\text{RTSAH}i}$  and  $\Delta C''_{\text{RTSAH}i}$ , and the split position error, and the optimal axis selection percentage for a **kd-tree** ADS, built with various build heuristics, for the **Icosahedron2** scene.

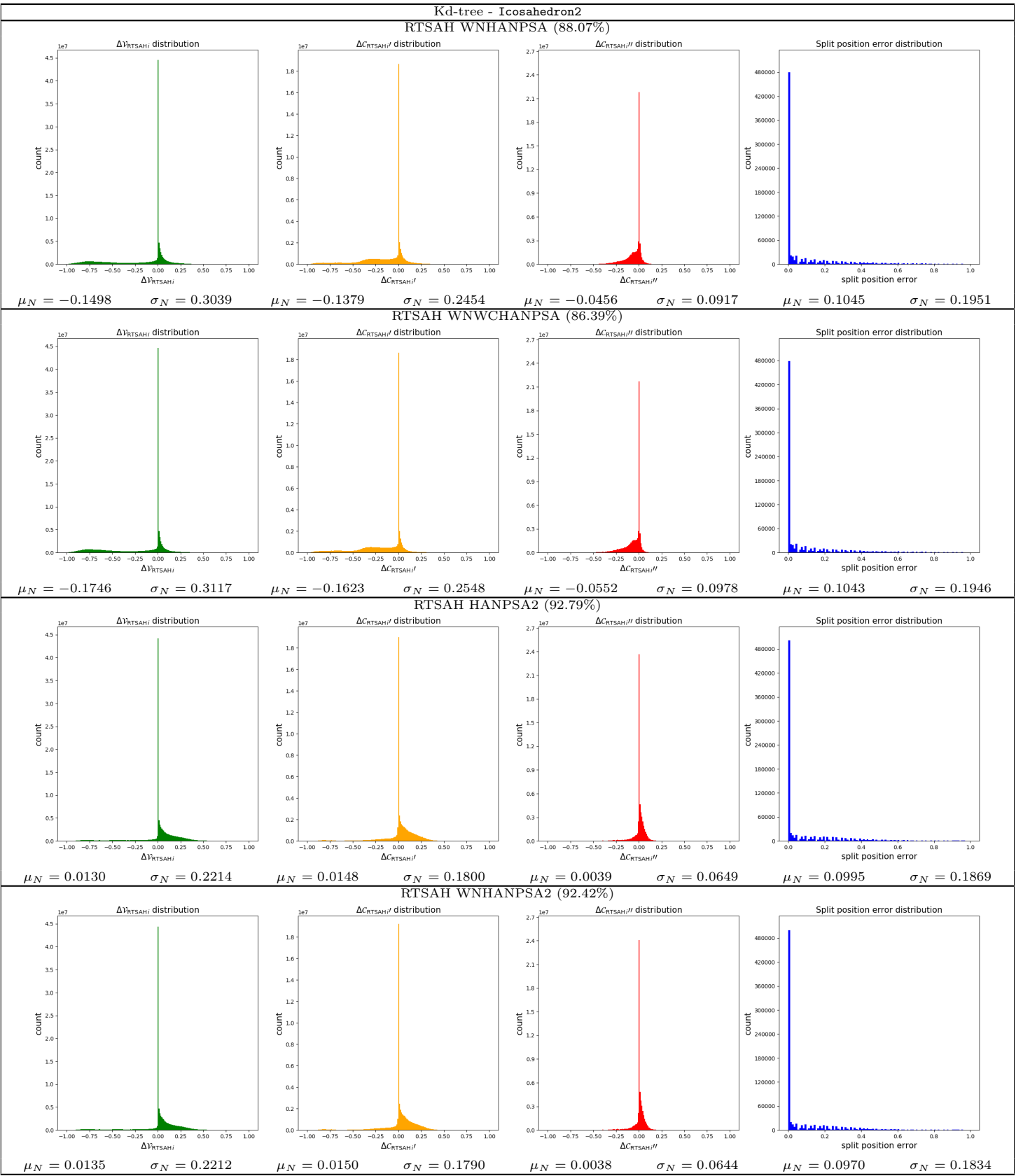


Table 56: The distributions (histogram, mean,  $\mu_N$ , standard deviation,  $\sigma_N$ ) of the visibility probability error,  $\Delta V_{\text{RTSAH}i}$ , the modified cost errors,  $\Delta C'_{\text{RTSAH}i}$  and  $\Delta C''_{\text{RTSAH}i}$ , and the split position error, and the optimal axis selection percentage for a **kd-tree** ADS, built with various build heuristics, for the **Icosahedron2** scene.

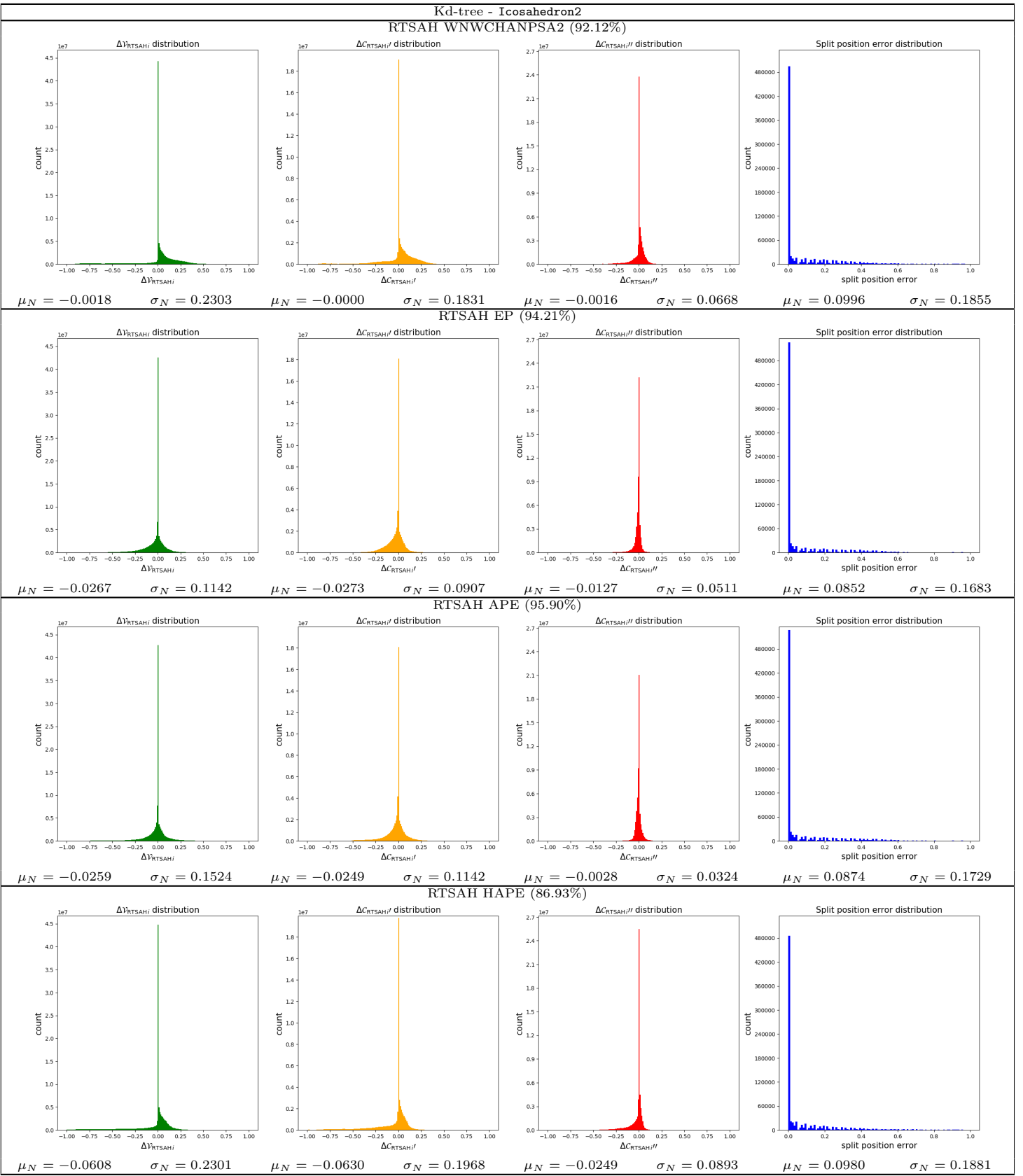


Table 57: The distributions (histogram, mean,  $\mu_N$ , standard deviation,  $\sigma_N$ ) of the visibility probability error,  $\Delta V_{RTSAH_i}$ , the modified cost errors,  $\Delta C'_{RTSAH_i}$  and  $\Delta C''_{RTSAH_i}$ , and the split position error, and the optimal axis selection percentage for a **kd-tree** ADS, built with various build heuristics, for the **Icosahedron2** scene.

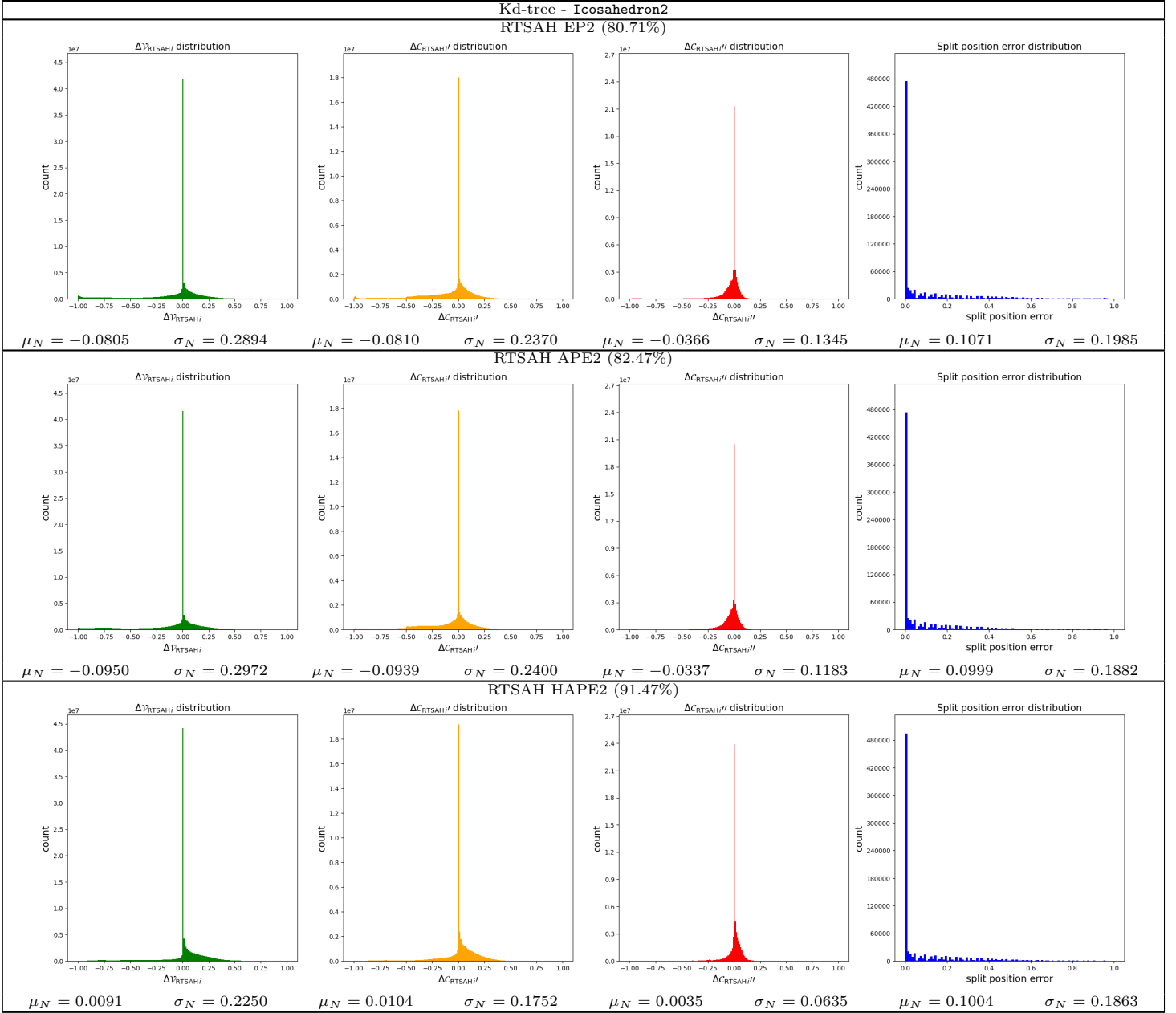


Table 58: The distributions (histogram, mean,  $\mu_N$ , standard deviation,  $\sigma_N$ ) of the visibility probability error,  $\Delta V_{\text{RTSAH}i}$ , the modified cost errors,  $\Delta C'_{\text{RTSAH}i}$  and  $\Delta C''_{\text{RTSAH}i}$ , and the split position error, and the optimal axis selection percentage for a **kd-tree** ADS, built with various build heuristics, for the **Icosahedron2** scene.

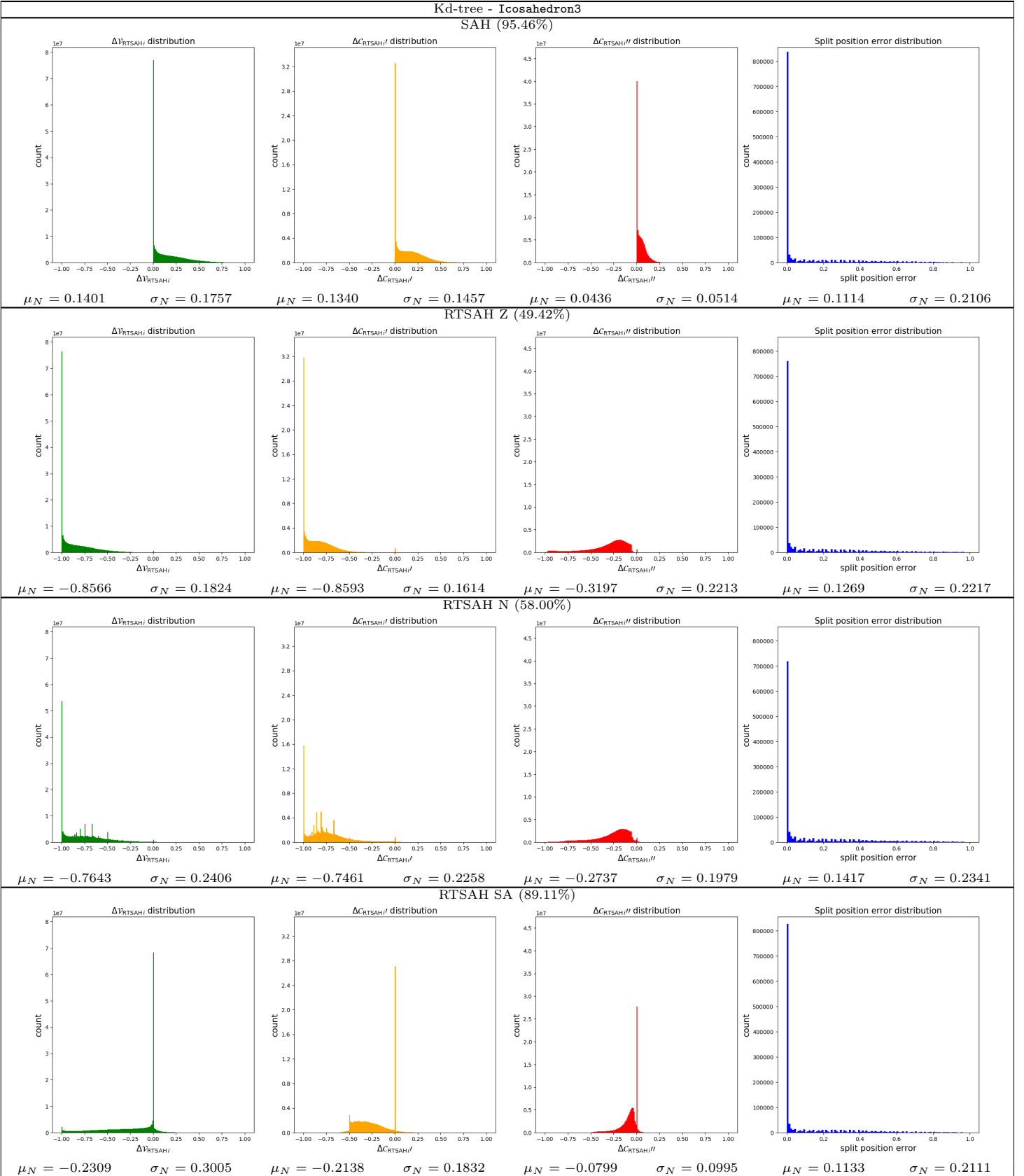


Table 59: The distributions (histogram, mean,  $\mu_N$ , standard deviation,  $\sigma_N$ ) of the visibility probability error,  $\Delta V_{\text{RTSAH}_i}$ , the modified cost errors,  $\Delta C'_{\text{RTSAH}_i}$  and  $\Delta C''_{\text{RTSAH}_i}$ , and the split position error, and the optimal axis selection percentage for a **kd-tree** ADS, built with various build heuristics, for the **Icosahedron3** scene.

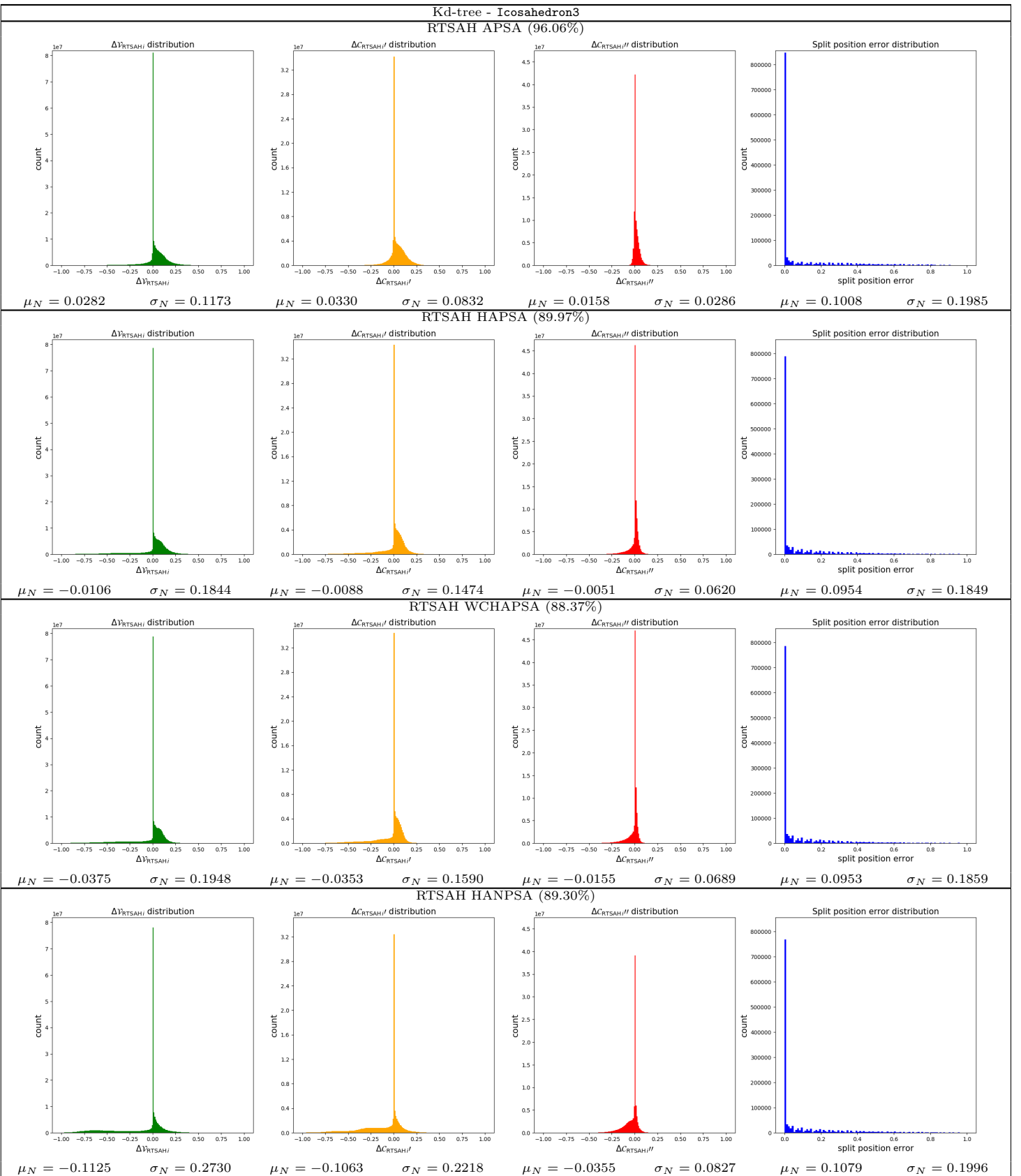


Table 60: The distributions (histogram, mean,  $\mu_N$ , standard deviation,  $\sigma_N$ ) of the visibility probability error,  $\Delta V_{\text{RTSAH}_i}$ , the modified cost errors,  $\Delta C'_{\text{RTSAH}_i}$  and  $\Delta C''_{\text{RTSAH}_i}$ , and the split position error, and the optimal axis selection percentage for a **kd-tree** ADS, built with various build heuristics, for the **Icosahedron3** scene.

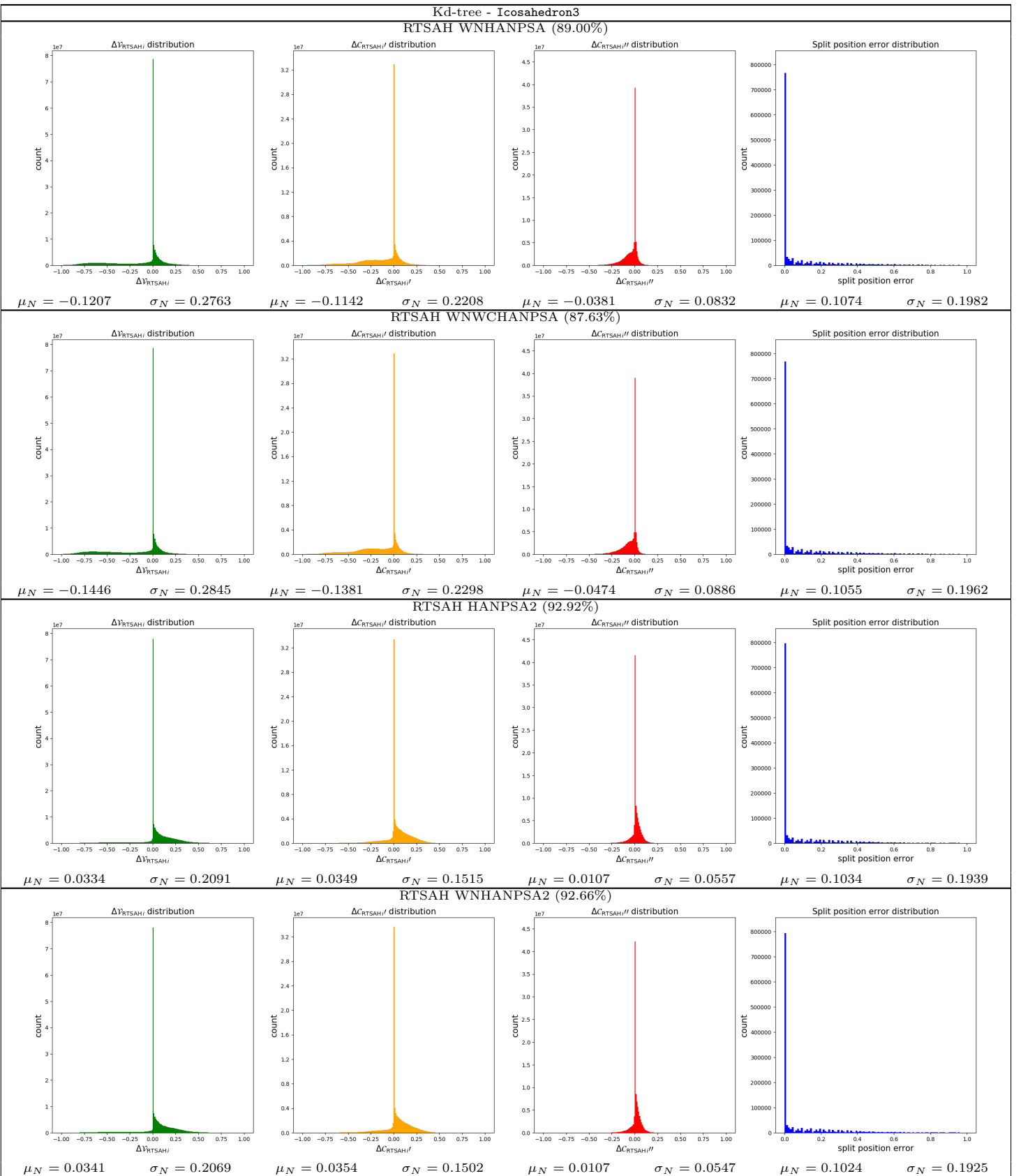


Table 61: The distributions (histogram, mean,  $\mu_N$ , standard deviation,  $\sigma_N$ ) of the visibility probability error,  $\Delta V_{\text{RTSAH}_i}$ , the modified cost errors,  $\Delta C'_{\text{RTSAH}_i}$  and  $\Delta C''_{\text{RTSAH}_i}$ , and the split position error, and the optimal axis selection percentage for a **kd-tree** ADS, built with various build heuristics, for the **Icosahedron3** scene.

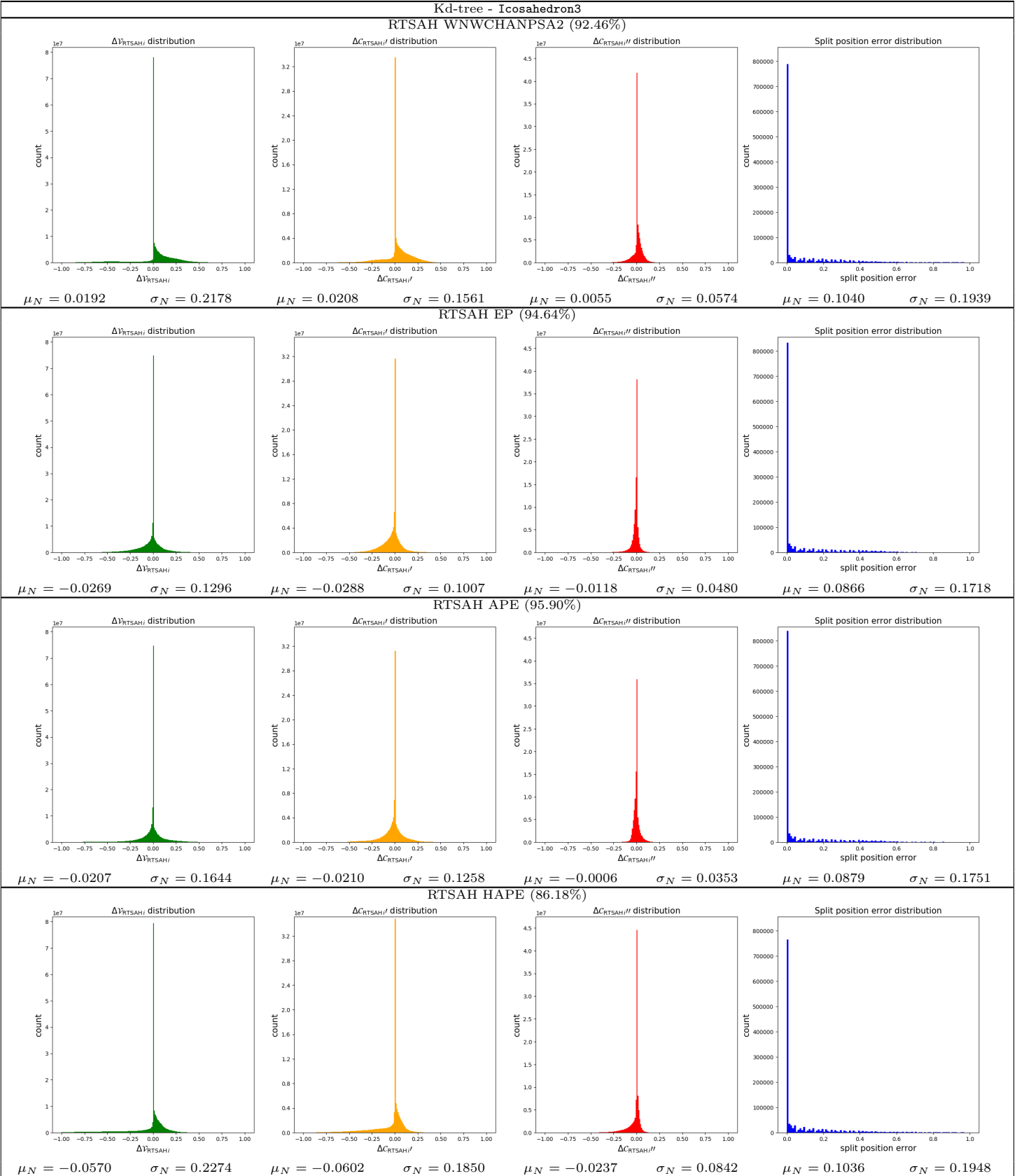


Table 62: The distributions (histogram, mean,  $\mu_N$ , standard deviation,  $\sigma_N$ ) of the visibility probability error,  $\Delta V_{\text{RTSAH}_i}$ , the modified cost errors,  $\Delta C'_{\text{RTSAH}_i}$  and  $\Delta C''_{\text{RTSAH}_i}$ , and the split position error, and the optimal axis selection percentage for a **kd-tree** ADS, built with various build heuristics, for the **Icosahedron3** scene.

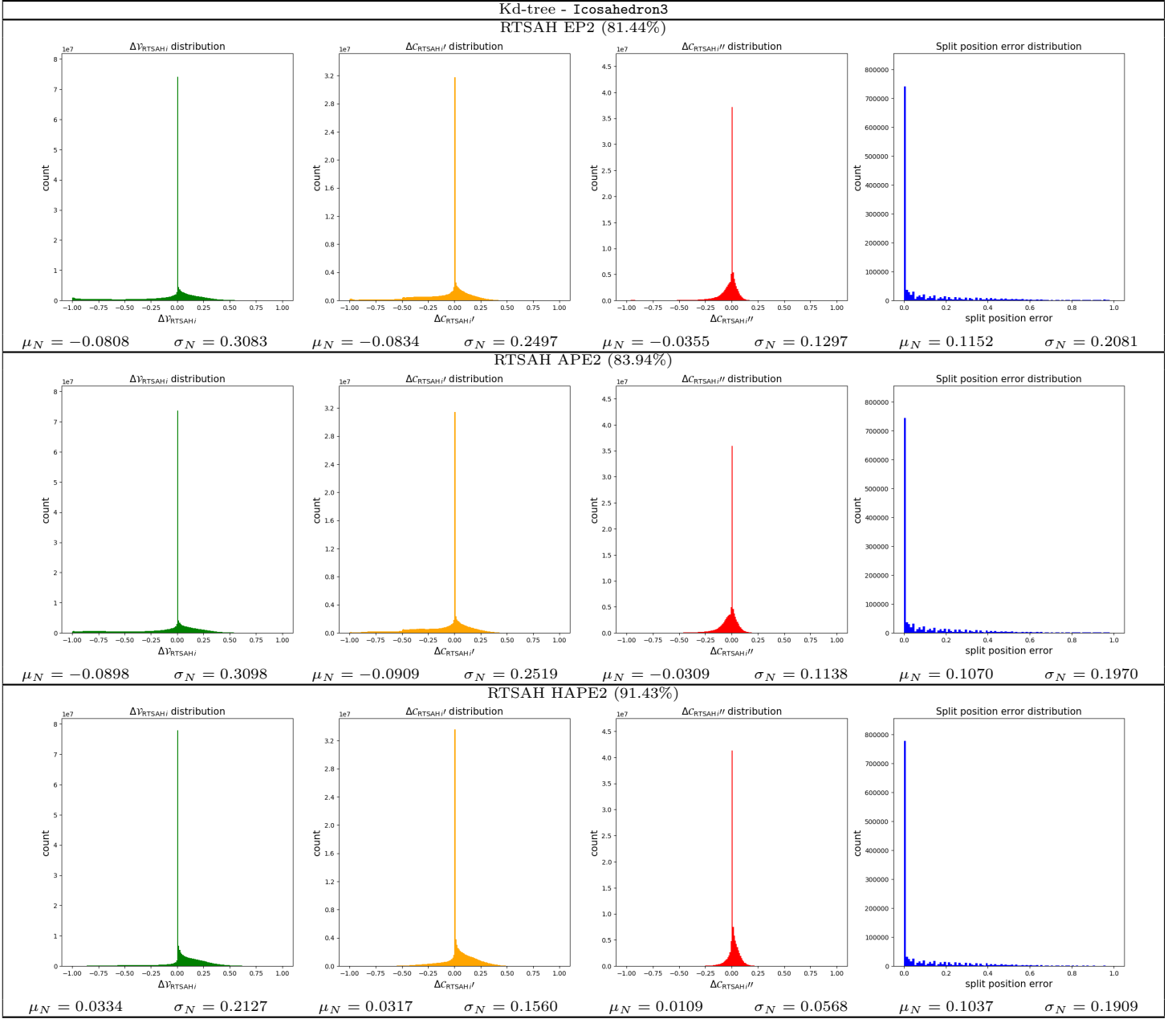


Table 63: The distributions (histogram, mean,  $\mu_N$ , standard deviation,  $\sigma_N$ ) of the visibility probability error,  $\Delta V_{\text{RTSAH}i}$ , the modified cost errors,  $\Delta C'_{\text{RTSAH}i}$  and  $\Delta C''_{\text{RTSAH}i}$ , and the split position error, and the optimal axis selection percentage for a **kd-tree** ADS, built with various build heuristics, for the **Icosahedron3** scene.

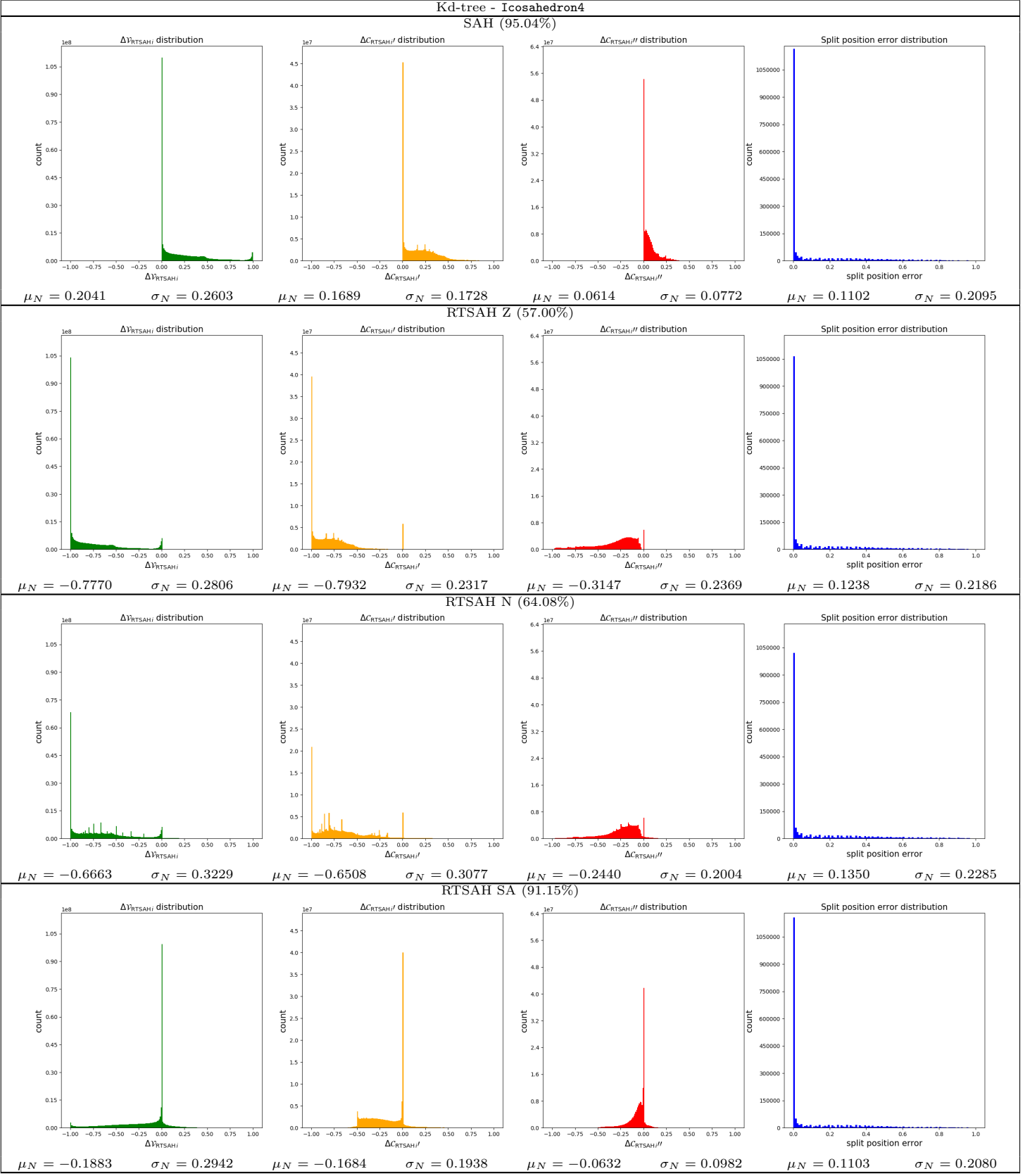


Table 64: The distributions (histogram, mean,  $\mu_N$ , standard deviation,  $\sigma_N$ ) of the visibility probability error,  $\Delta V_{\text{RTSAH}_i}$ , the modified cost errors,  $\Delta C'_{\text{RTSAH}_i}$  and  $\Delta C''_{\text{RTSAH}_i}$ , and the split position error, and the optimal axis selection percentage for a **kd-tree** ADS, built with various build heuristics, for the **Icosahedron4** scene.

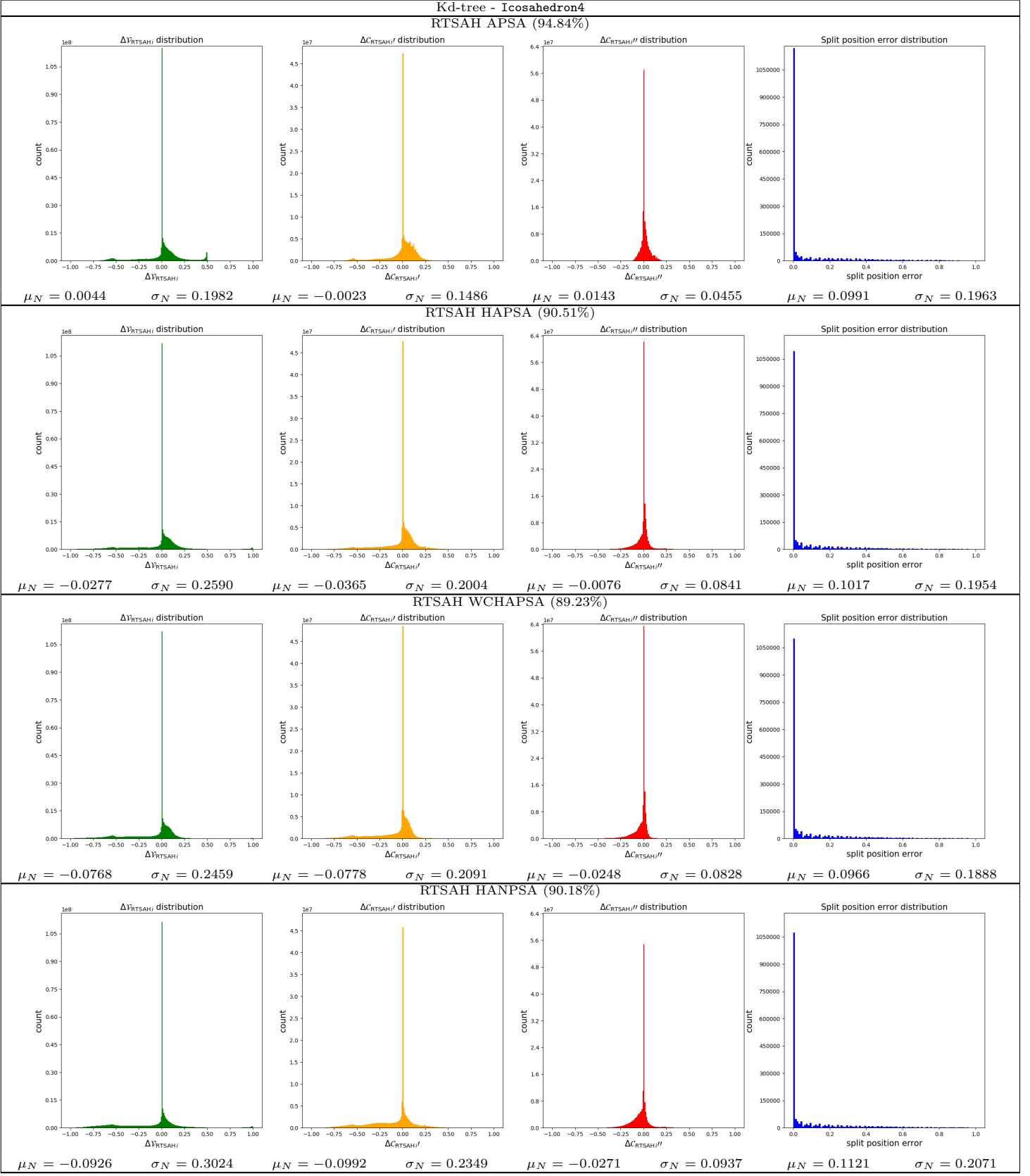


Table 65: The distributions (histogram, mean,  $\mu_N$ , standard deviation,  $\sigma_N$ ) of the visibility probability error,  $\Delta V_{\text{RTSAH}_i}$ , the modified cost errors,  $\Delta C'_{\text{RTSAH}_i}$  and  $\Delta C''_{\text{RTSAH}_i}$ , and the split position error, and the optimal axis selection percentage for a **kd-tree** ADS, built with various build heuristics, for the **Icosahedron4** scene.

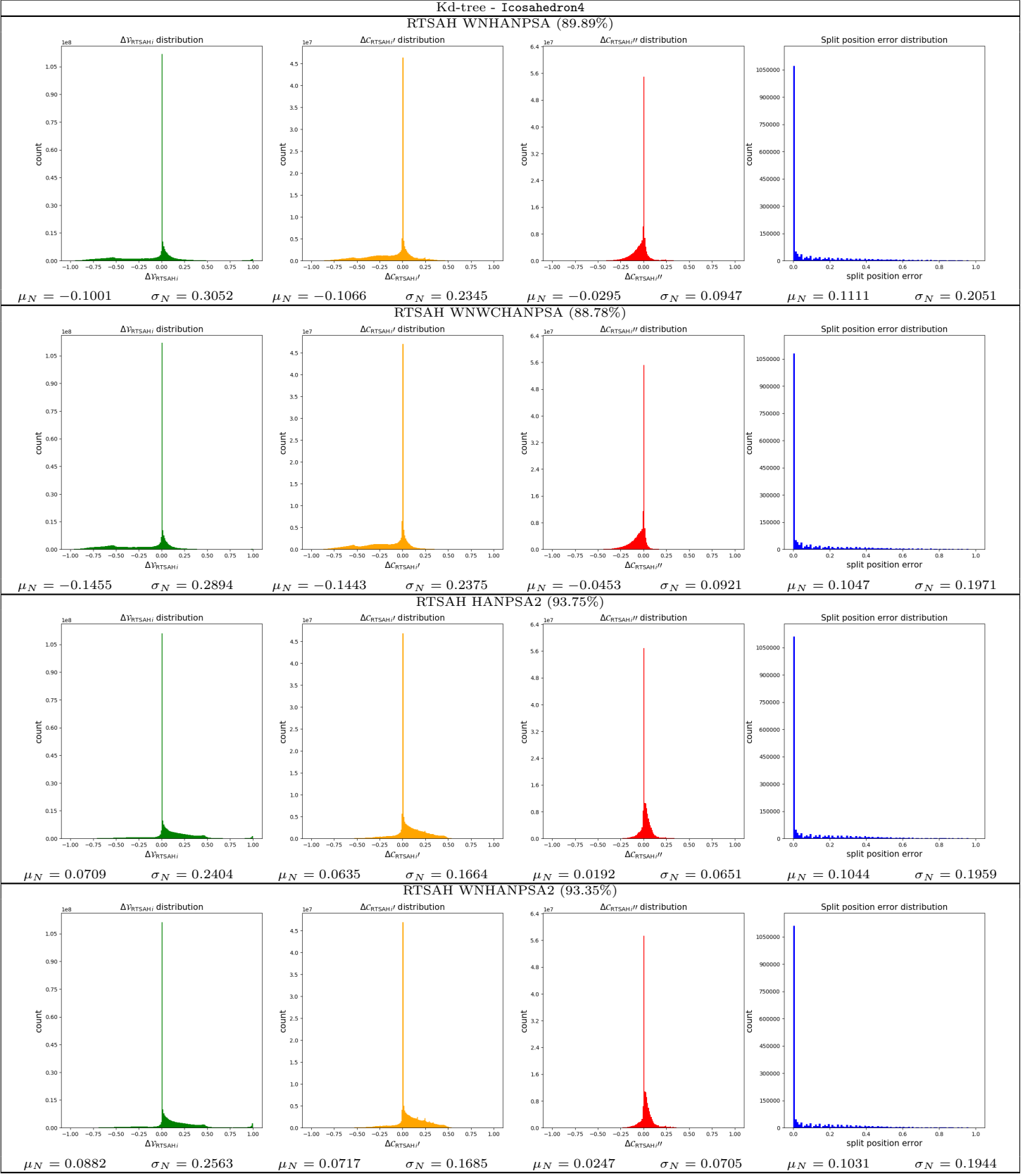


Table 66: The distributions (histogram, mean,  $\mu_N$ , standard deviation,  $\sigma_N$ ) of the visibility probability error,  $\Delta V_{\text{RTSAH}_i}$ , the modified cost errors,  $\Delta C'_{\text{RTSAH}_i}$  and  $\Delta C''_{\text{RTSAH}_i}$ , and the split position error, and the optimal axis selection percentage for a **kd-tree** ADS, built with various build heuristics, for the **Icosahedron4** scene.

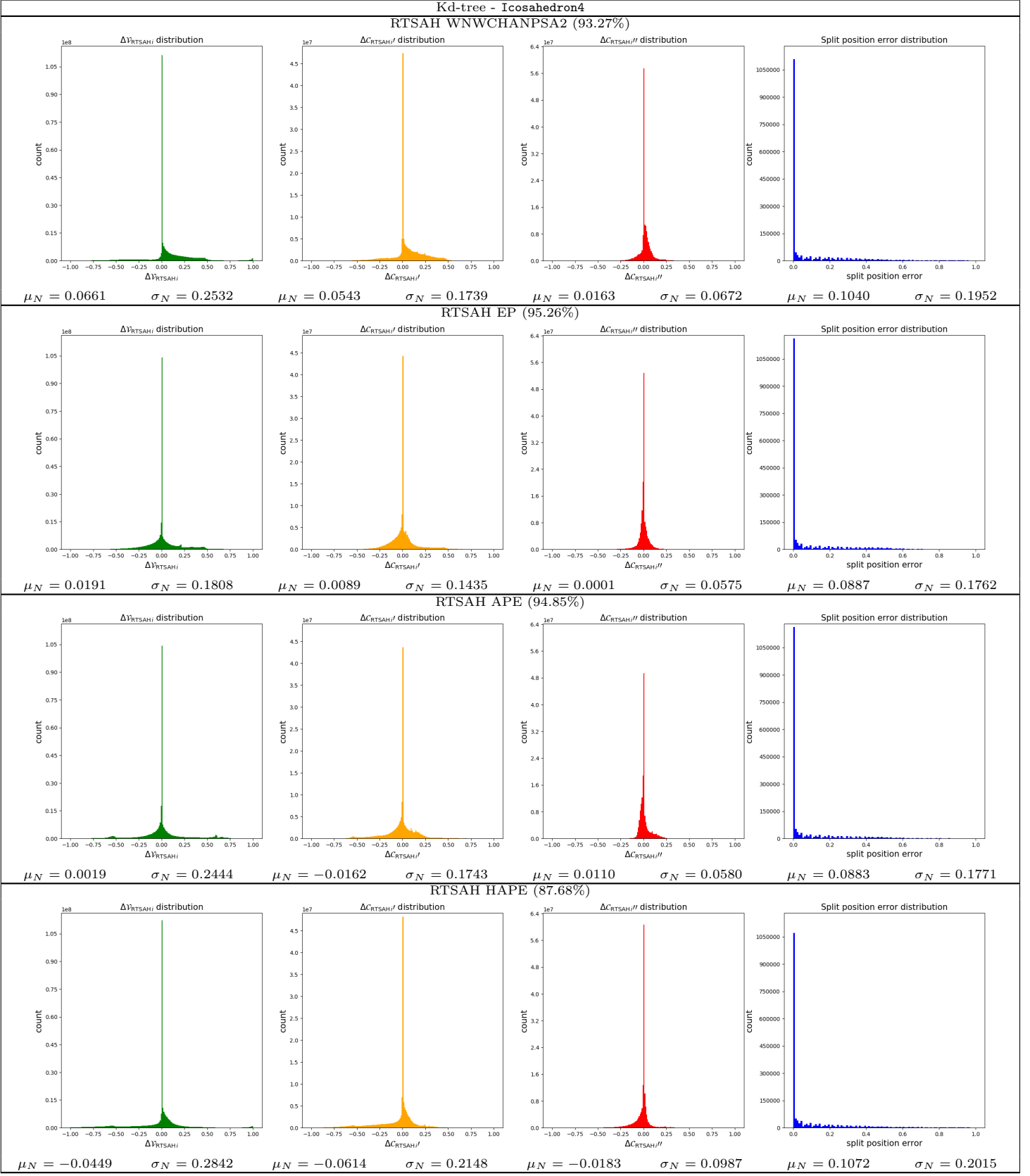


Table 67: The distributions (histogram, mean,  $\mu_N$ , standard deviation,  $\sigma_N$ ) of the visibility probability error,  $\Delta V_{\text{RTSAH}_i}$ , the modified cost errors,  $\Delta C'_{\text{RTSAH}_i}$  and  $\Delta C''_{\text{RTSAH}_i}$ , and the split position error, and the optimal axis selection percentage for a **kd-tree** ADS, built with various build heuristics, for the **Icosahedron4** scene.

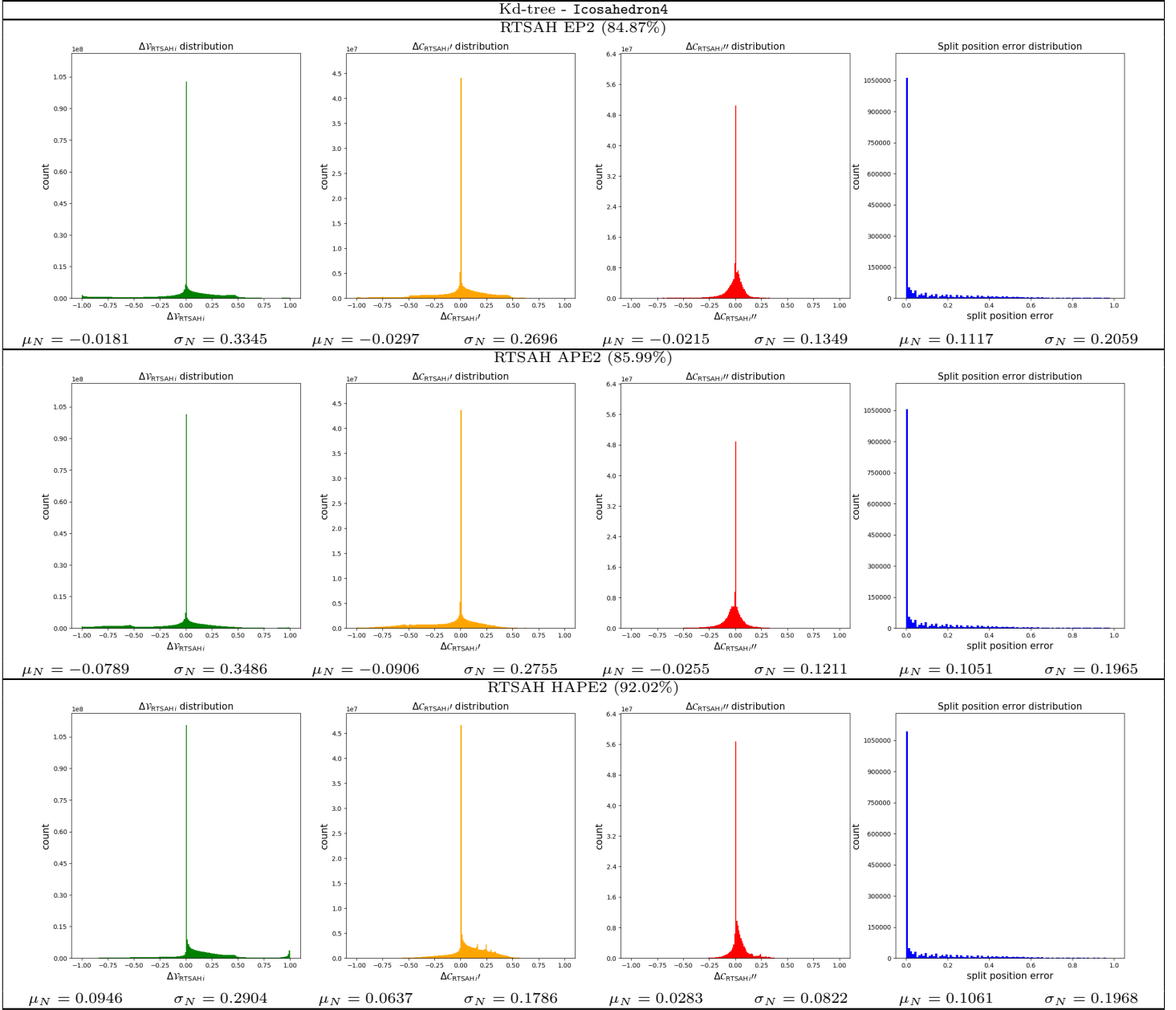


Table 68: The distributions (histogram, mean,  $\mu_N$ , standard deviation,  $\sigma_N$ ) of the visibility probability error,  $\Delta V_{\text{RTSAH}i}$ , the modified cost errors,  $\Delta C'_{\text{RTSAH}i}$  and  $\Delta C''_{\text{RTSAH}i}$ , and the split position error, and the optimal axis selection percentage for a **kd-tree** ADS, built with various build heuristics, for the **Icosahedron4** scene.

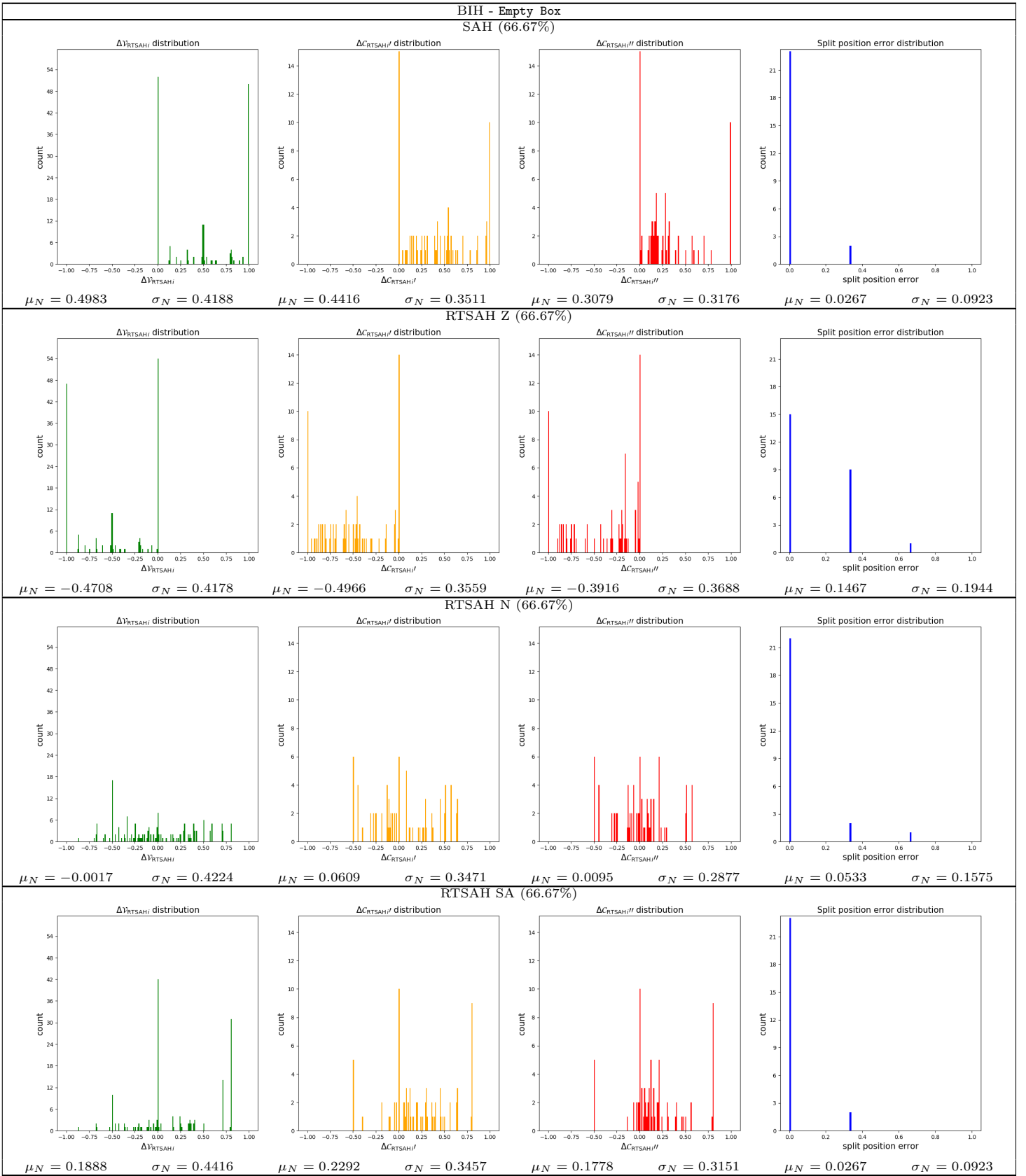


Table 69: The distributions (histogram, mean,  $\mu_N$ , standard deviation,  $\sigma_N$ ) of the visibility probability error,  $\Delta V_{\text{RTSAH}_i}$ , the modified cost errors,  $\Delta C'_{\text{RTSAH}_i}$  and  $\Delta C''_{\text{RTSAH}_i}$ , and the split position error, and the optimal axis selection percentage for a **BIH** ADS, built with various build heuristics, for the *Empty Box* scene.

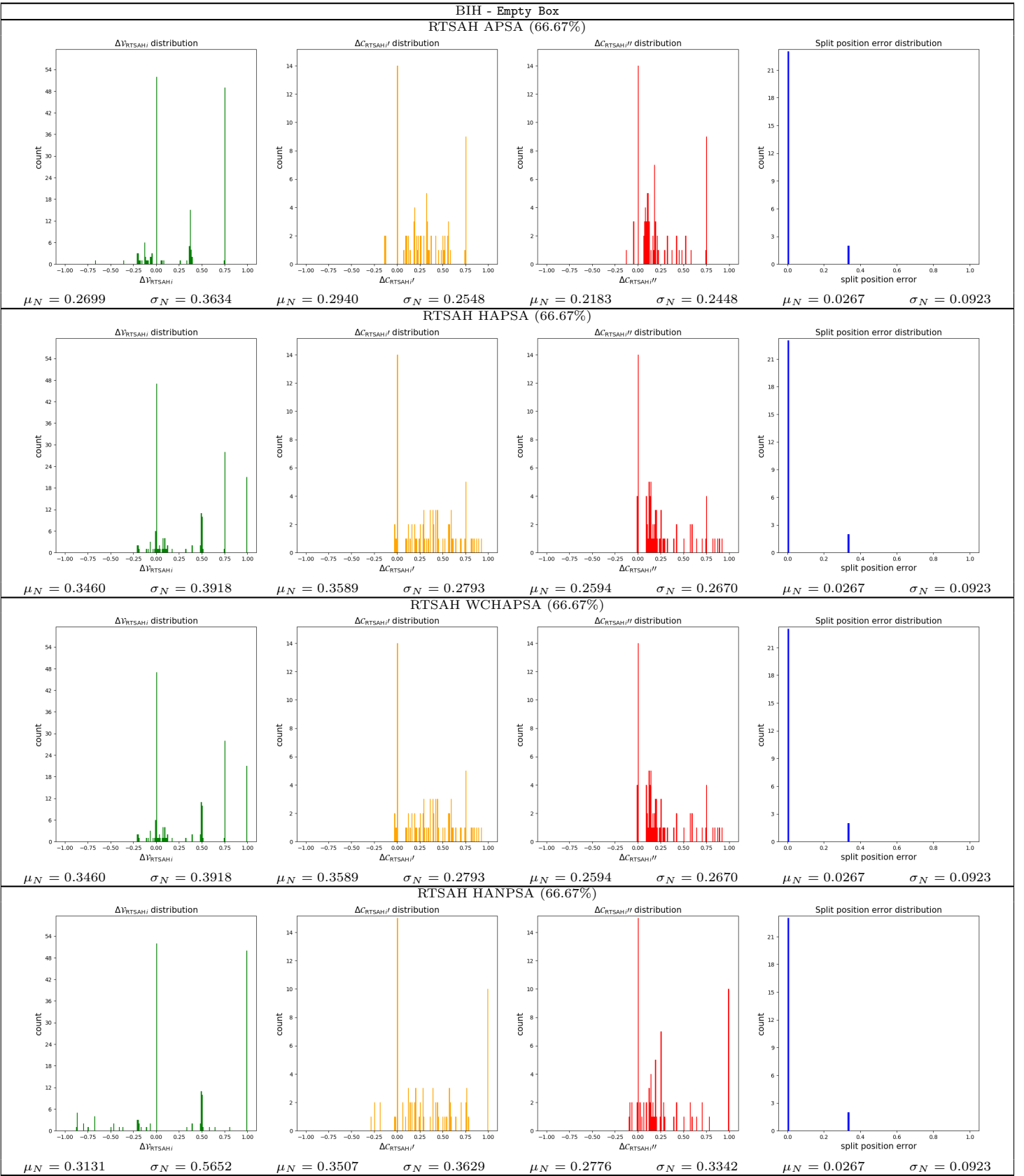


Table 70: The distributions (histogram, mean,  $\mu_N$ , standard deviation,  $\sigma_N$ ) of the visibility probability error,  $\Delta V_{RTSAH_i}$ , the modified cost errors,  $\Delta C'_{RTSAH_i}$  and  $\Delta C''_{RTSAH_i}$ , and the split position error, and the optimal axis selection percentage for a **BIH** ADS, built with various build heuristics, for the *Empty Box* scene.

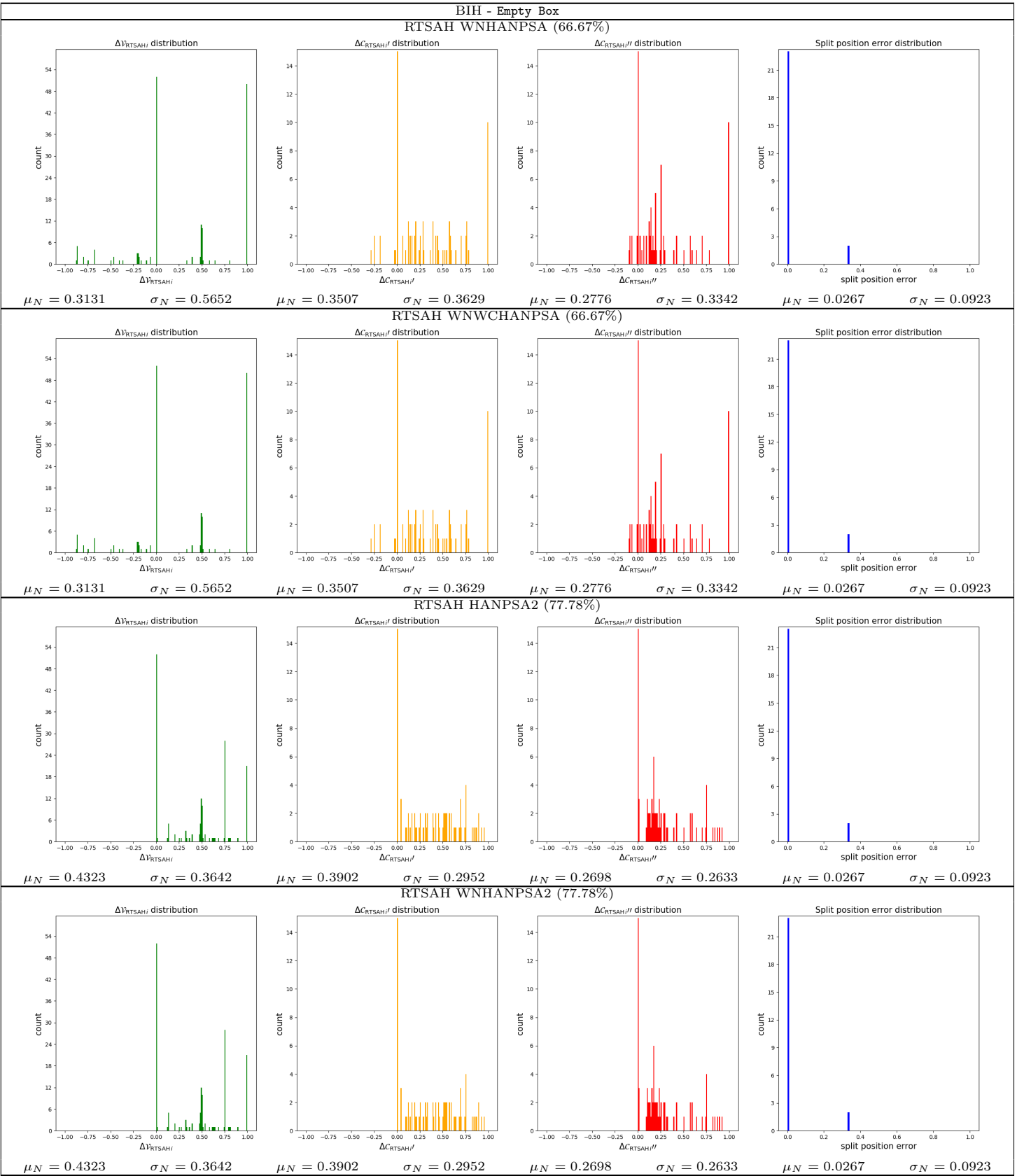


Table 71: The distributions (histogram, mean,  $\mu_N$ , standard deviation,  $\sigma_N$ ) of the visibility probability error,  $\Delta V_{RTSAH_i}$ , the modified cost errors,  $\Delta C'_{RTSAH_i}$  and  $\Delta C''_{RTSAH_i}$ , and the split position error, and the optimal axis selection percentage for a **BIH** ADS, built with various build heuristics, for the *Empty Box* scene.

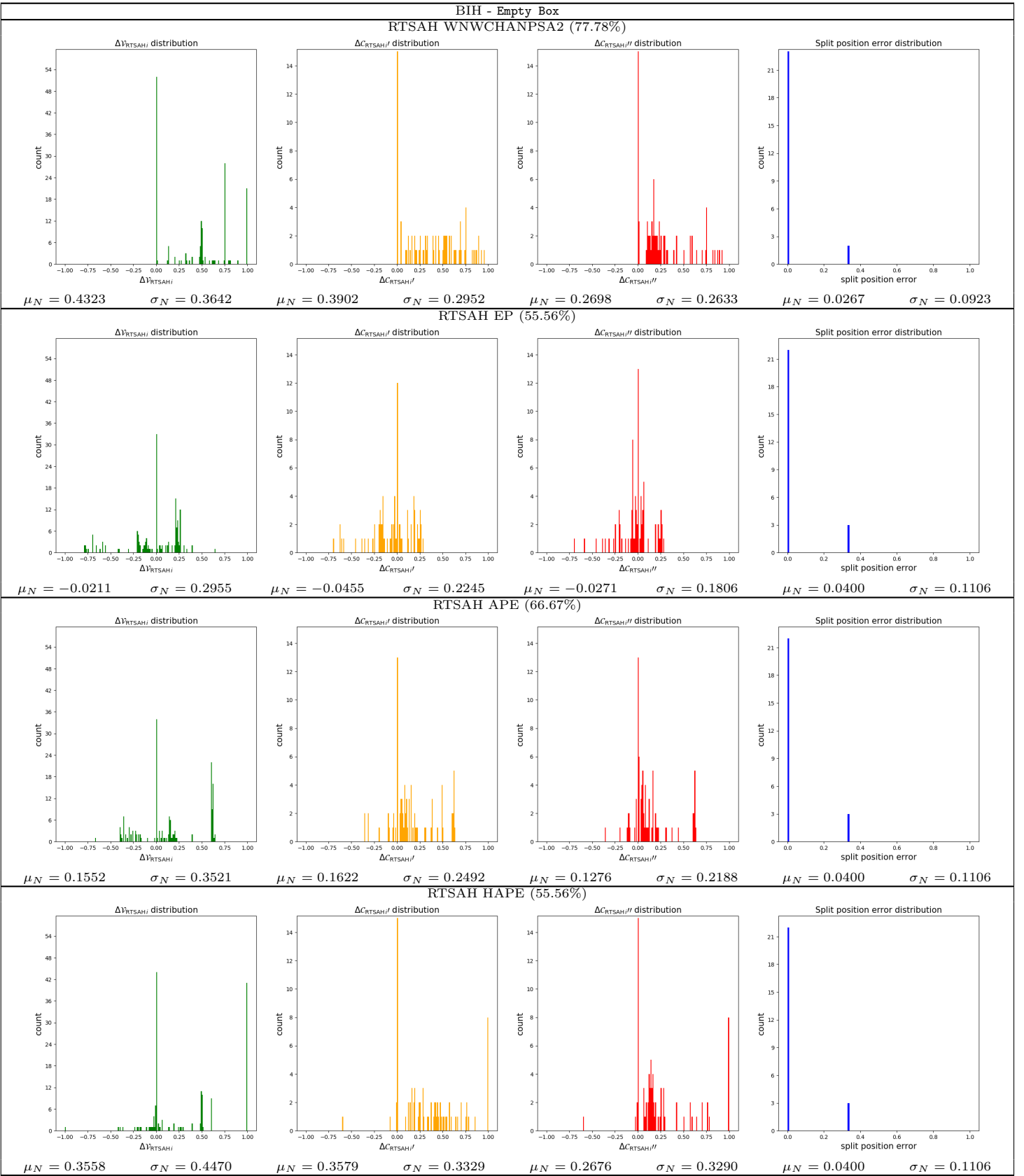


Table 72: The distributions (histogram, mean,  $\mu_N$ , standard deviation,  $\sigma_N$ ) of the visibility probability error,  $\Delta V_{\text{RTSAH}_i}$ , the modified cost errors,  $\Delta C'_{\text{RTSAH}_i}$  and  $\Delta C''_{\text{RTSAH}_i}$ , and the split position error, and the optimal axis selection percentage for a **BIH** ADS, built with various build heuristics, for the *Empty Box* scene.

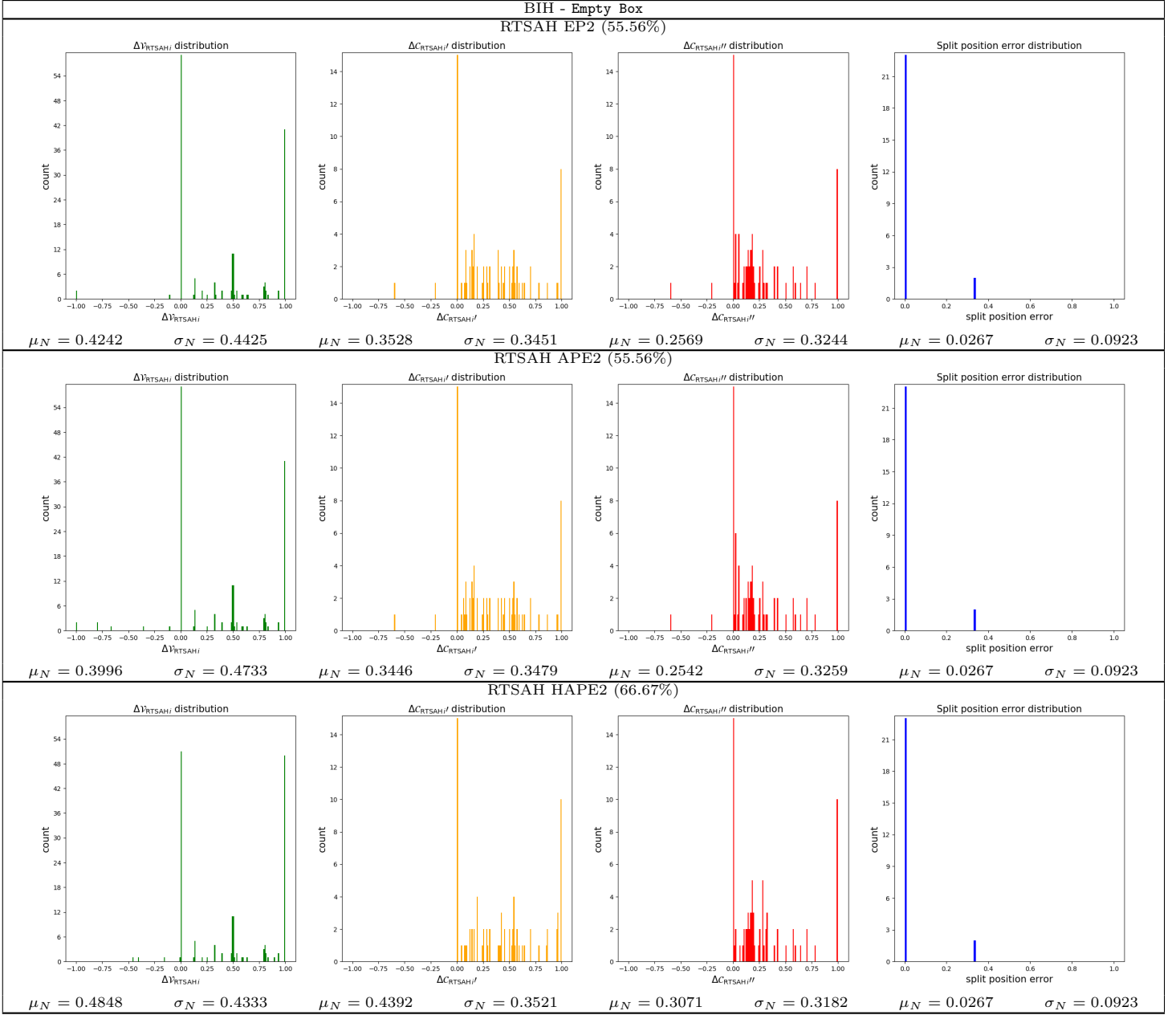


Table 73: The distributions (histogram, mean,  $\mu_N$ , standard deviation,  $\sigma_N$ ) of the visibility probability error,  $\Delta V_{RTSAH_i}$ , the modified cost errors,  $\Delta C'_{RTSAH_i}$  and  $\Delta C''_{RTSAH_i}$ , and the split position error, and the optimal axis selection percentage for a **BIH** ADS, built with various build heuristics, for the *Empty Box* scene.

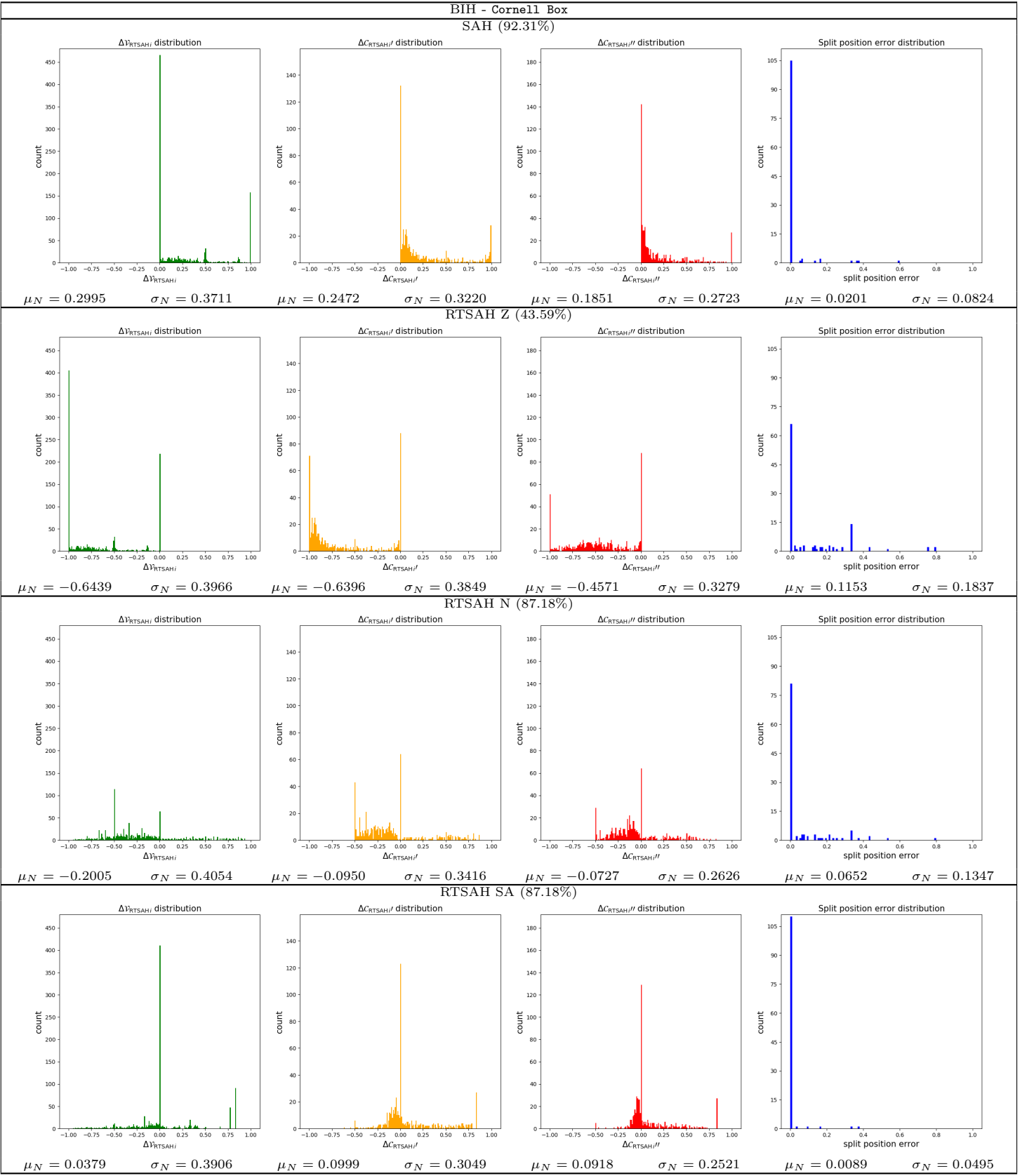


Table 74: The distributions (histogram, mean,  $\mu_N$ , standard deviation,  $\sigma_N$ ) of the visibility probability error,  $\Delta V_{RTSAH_i}$ , the modified cost errors,  $\Delta C'_{RTSAH_i}$  and  $\Delta C''_{RTSAH_i}$ , and the split position error, and the optimal axis selection percentage for a **BIH** ADS, built with various build heuristics, for the **Cornell Box** scene.

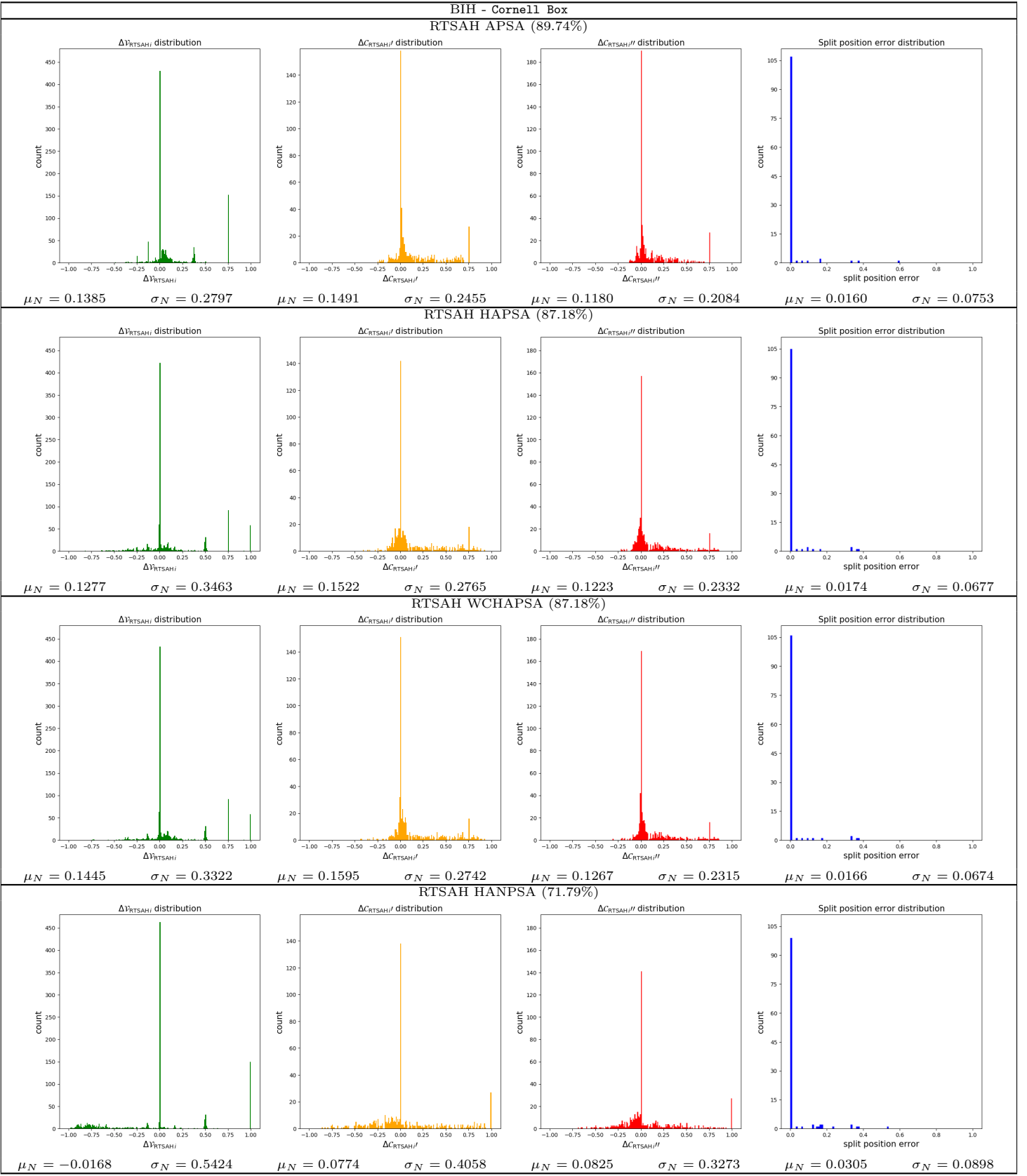


Table 75: The distributions (histogram, mean,  $\mu_N$ , standard deviation,  $\sigma_N$ ) of the visibility probability error,  $\Delta V_{\text{RTSAH}_i}$ , the modified cost errors,  $\Delta C'_{\text{RTSAH}_i}$  and  $\Delta C''_{\text{RTSAH}_i}$ , and the split position error, and the optimal axis selection percentage for a **BIH** ADS, built with various build heuristics, for the **Cornell Box** scene.

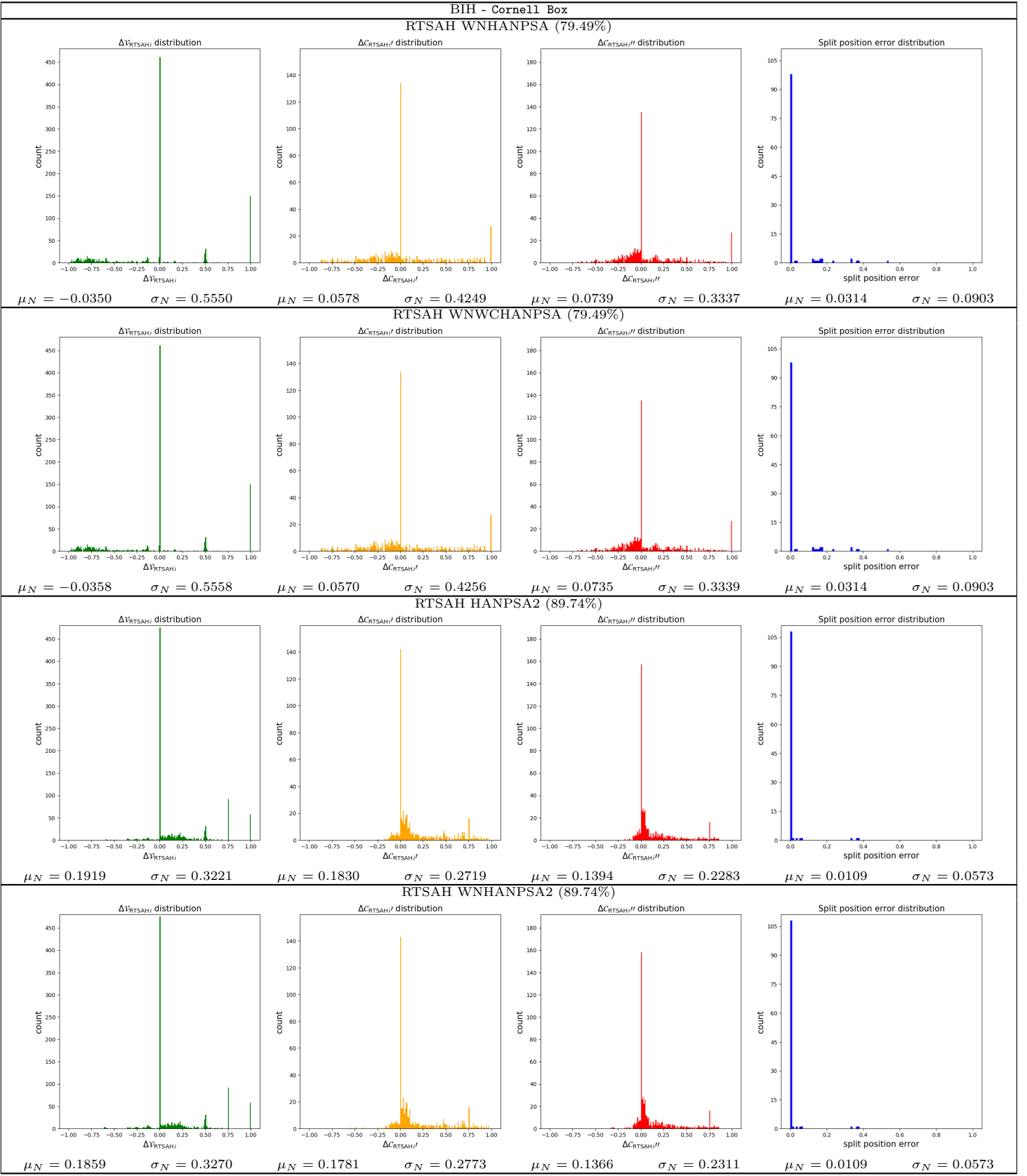


Table 76: The distributions (histogram, mean,  $\mu_N$ , standard deviation,  $\sigma_N$ ) of the visibility probability error,  $\Delta V_{\text{RTSAH}_i}$ , the modified cost errors,  $\Delta C'_{\text{RTSAH}_i}$  and  $\Delta C''_{\text{RTSAH}_i}$ , and the split position error, and the optimal axis selection percentage for a **BIH** ADS, built with various build heuristics, for the **Cornell Box** scene.

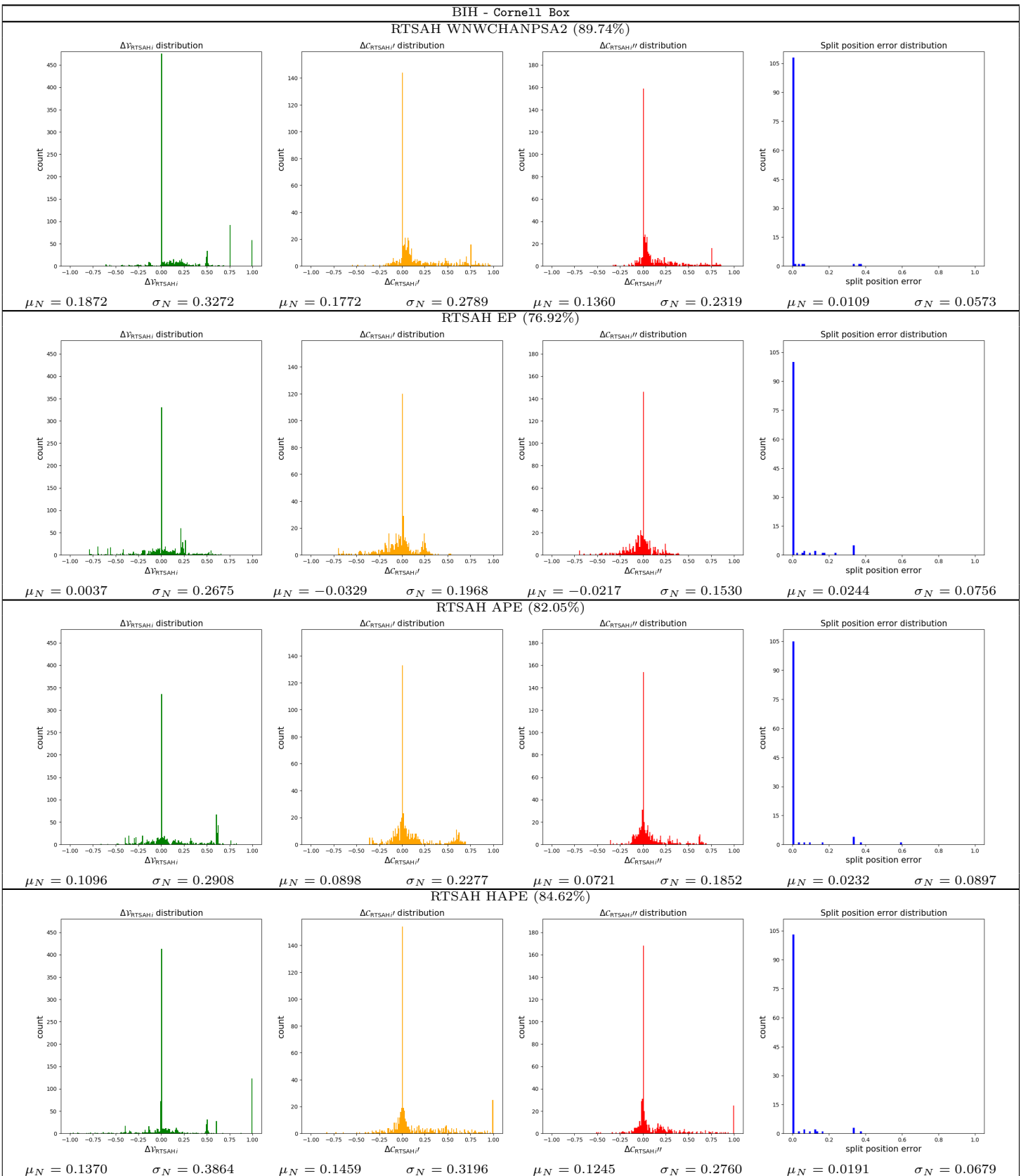


Table 77: The distributions (histogram, mean,  $\mu_N$ , standard deviation,  $\sigma_N$ ) of the visibility probability error,  $\Delta V_{\text{RTSAH}_i}$ , the modified cost errors,  $\Delta C'_{\text{RTSAH}_i}$  and  $\Delta C''_{\text{RTSAH}_i}$ , and the split position error, and the optimal axis selection percentage for a **BIH** ADS, built with various build heuristics, for the **Cornell Box** scene.

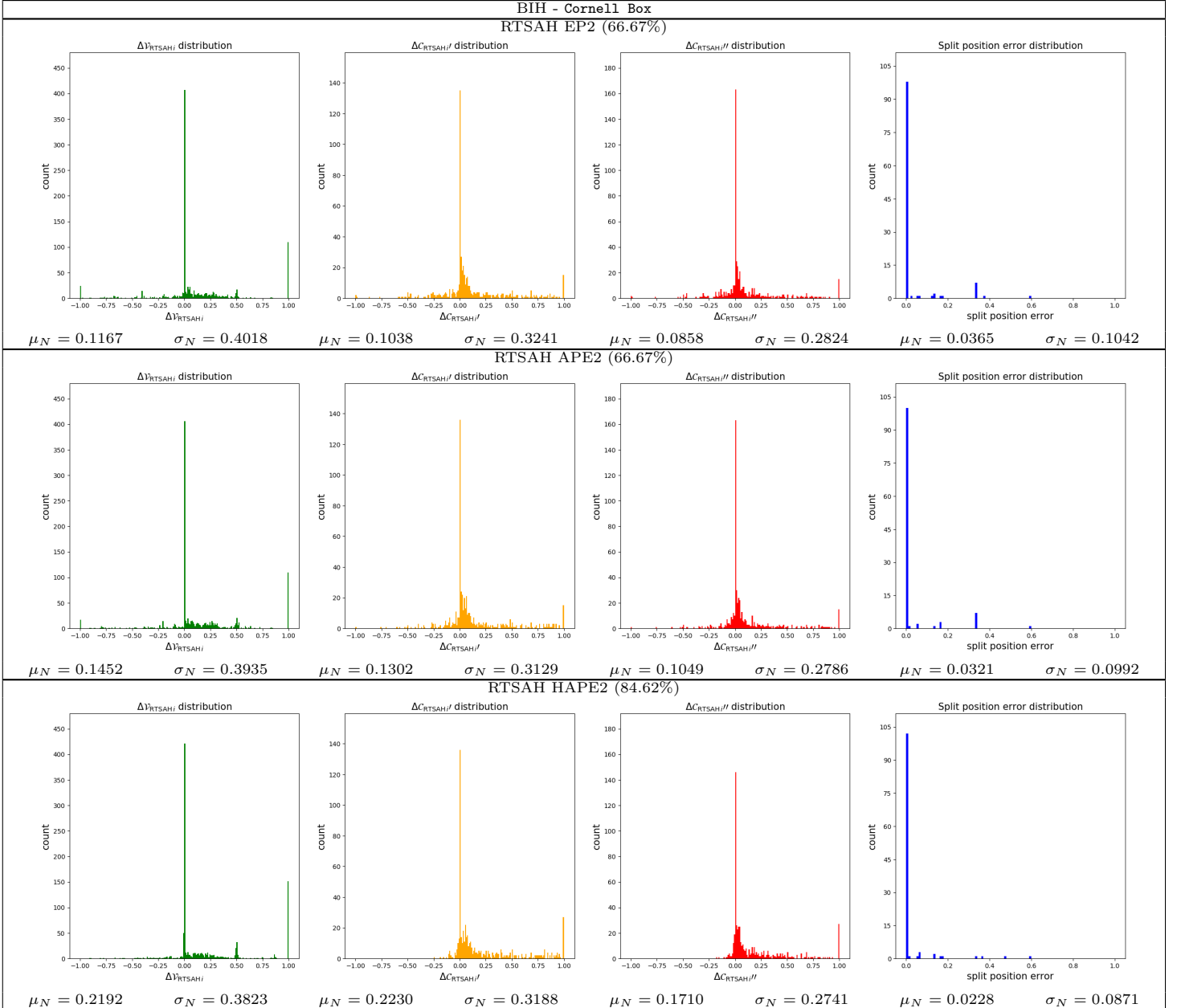


Table 78: The distributions (histogram, mean,  $\mu_N$ , standard deviation,  $\sigma_N$ ) of the visibility probability error,  $\Delta V_{\text{RTSAH}_i}$ , the modified cost errors,  $\Delta C'_{\text{RTSAH}_i}$  and  $\Delta C''_{\text{RTSAH}_i}$ , and the split position error, and the optimal axis selection percentage for a **BIH** ADS, built with various build heuristics, for the **Cornell Box** scene.

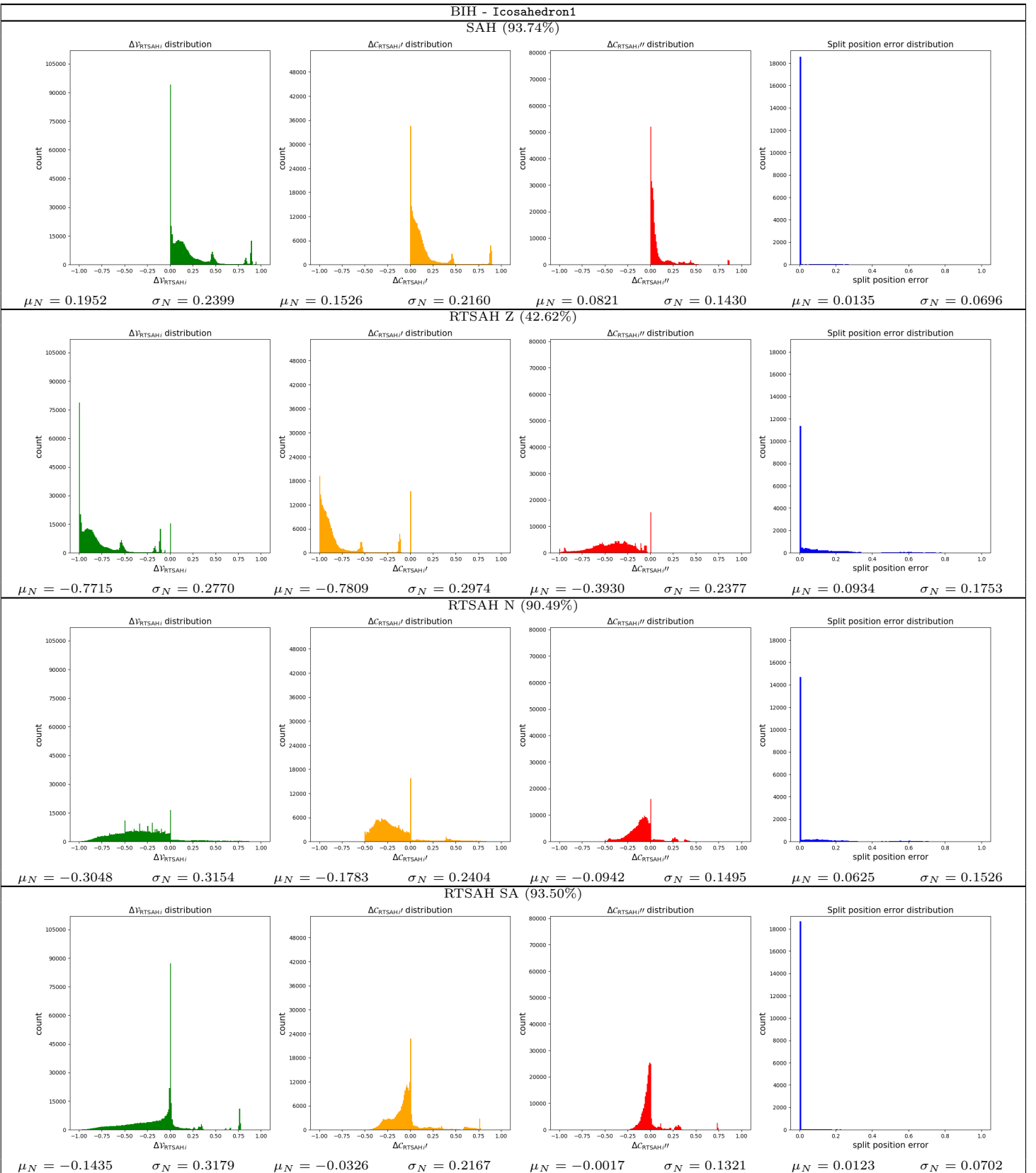


Table 79: The distributions (histogram, mean,  $\mu_N$ , standard deviation,  $\sigma_N$ ) of the visibility probability error,  $\Delta V_{\text{RTSAH}_i}$ , the modified cost errors,  $\Delta C'_{\text{RTSAH}_i}$  and  $\Delta C''_{\text{RTSAH}_i}$ , and the split position error, and the optimal axis selection percentage for a **BIH** ADS, built with various build heuristics, for the **Icosahedron1** scene.

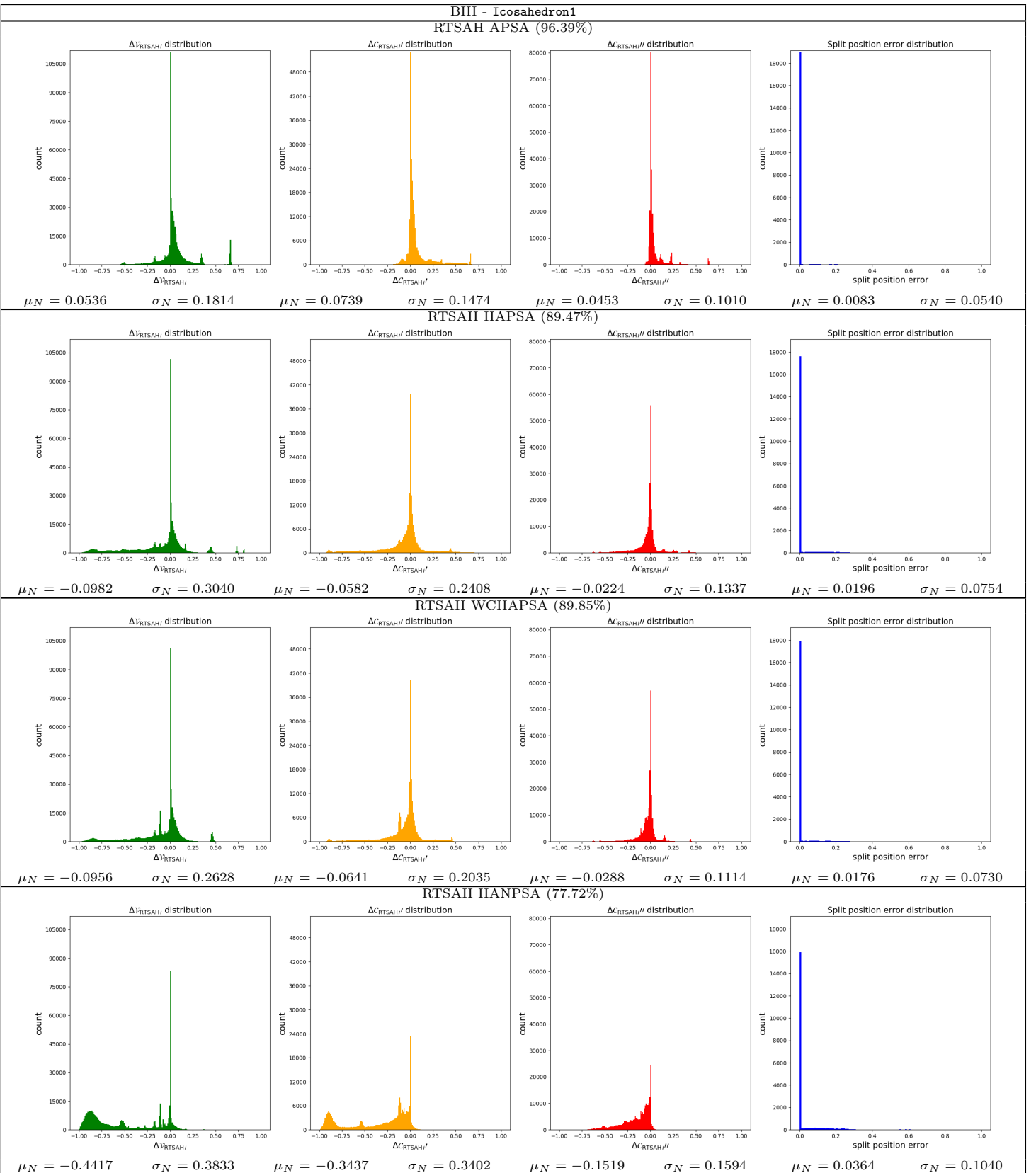


Table 80: The distributions (histogram, mean,  $\mu_N$ , standard deviation,  $\sigma_N$ ) of the visibility probability error,  $\Delta V_{RTSAH_i}$ , the modified cost errors,  $\Delta C'_{RTSAH_i}$  and  $\Delta C''_{RTSAH_i}$ , and the split position error, and the optimal axis selection percentage for a **BIH** ADS, built with various build heuristics, for the **Icosahedron1** scene.

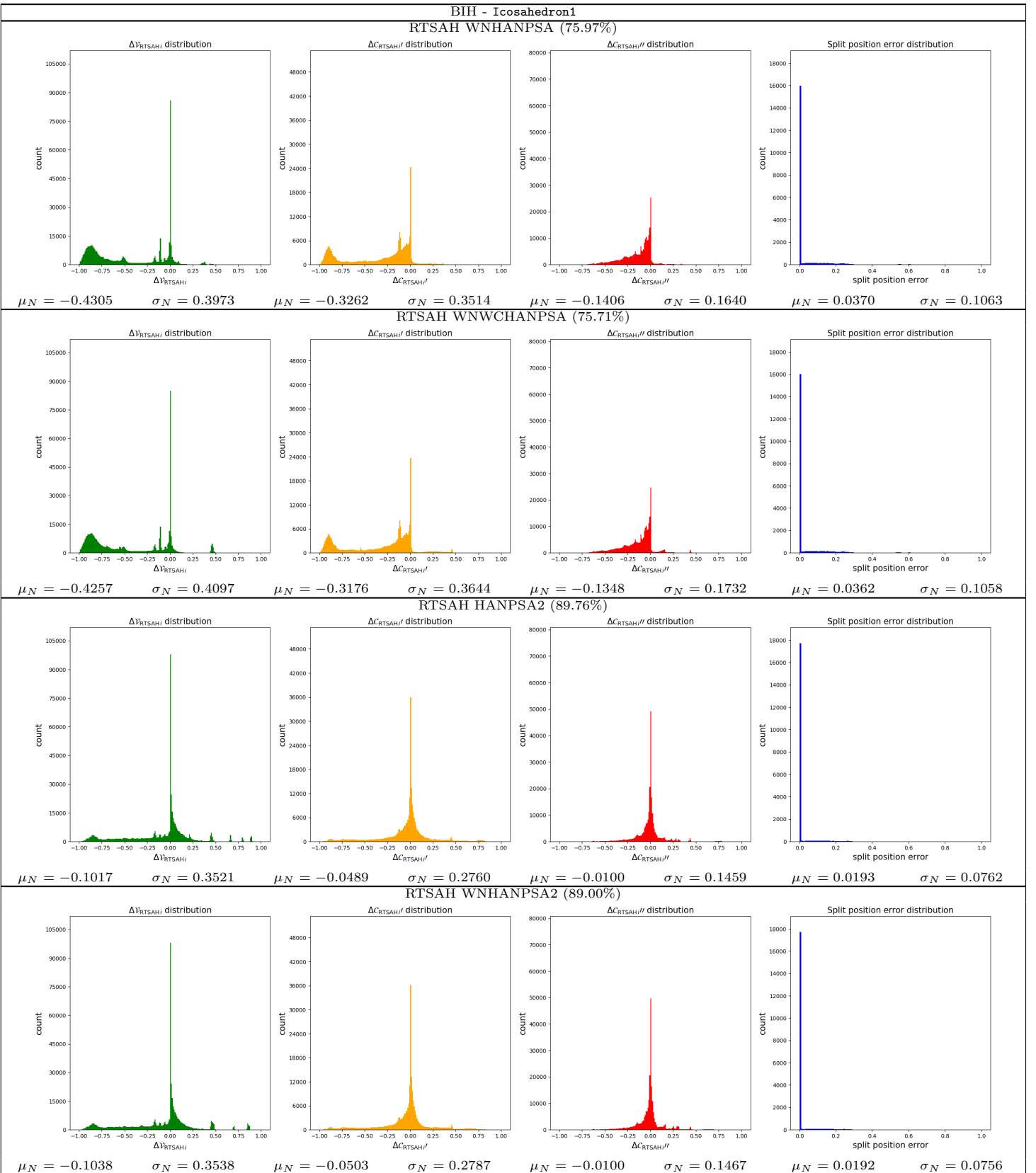


Table 81: The distributions (histogram, mean,  $\mu_N$ , standard deviation,  $\sigma_N$ ) of the visibility probability error,  $\Delta V_{RTSAH_i}$ , the modified cost errors,  $\Delta C'_{RTSAH_i}$  and  $\Delta C''_{RTSAH_i}$ , and the split position error, and the optimal axis selection percentage for a **BIH** ADS, built with various build heuristics, for the **Icosahedron1** scene.

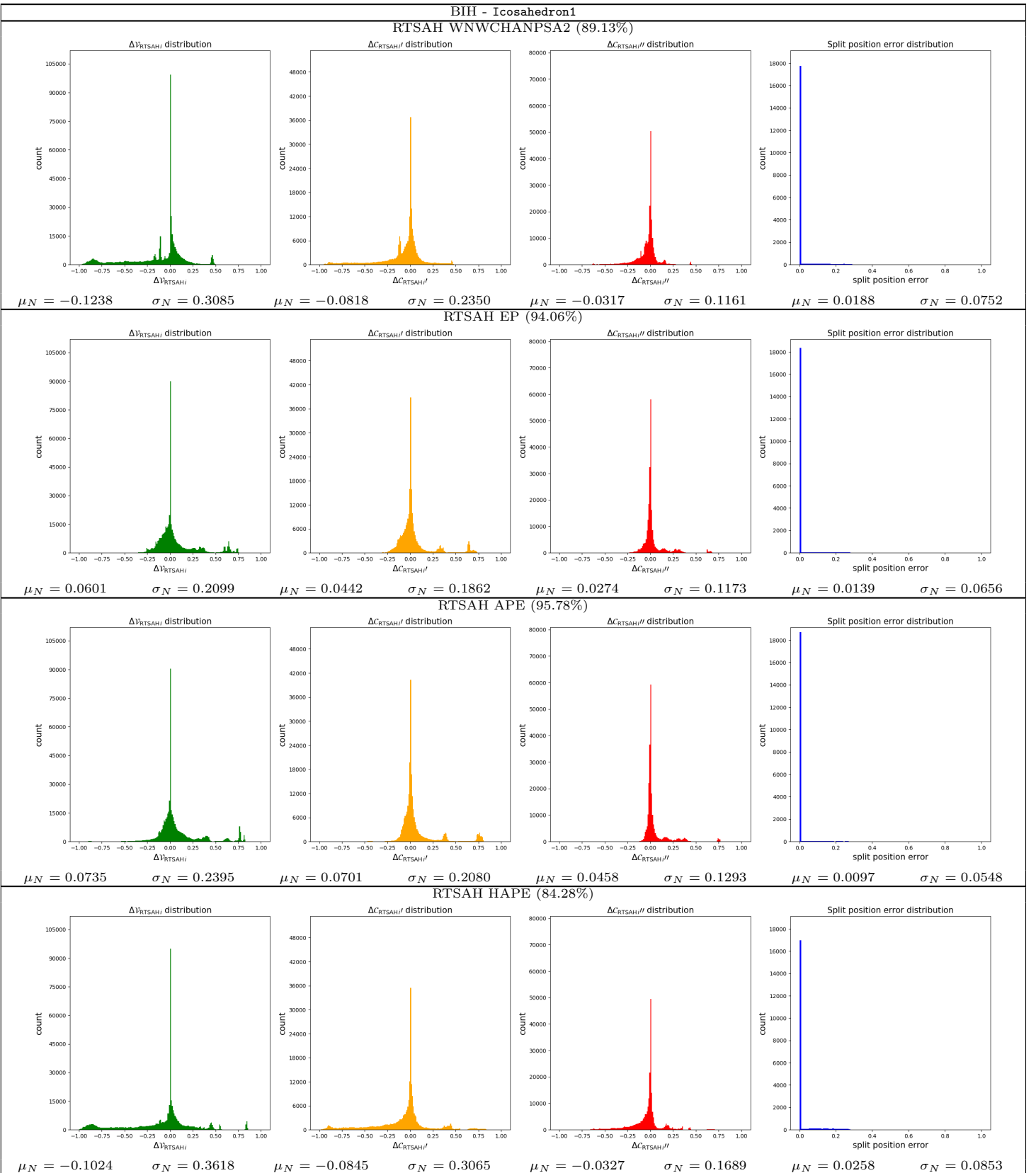


Table 82: The distributions (histogram, mean,  $\mu_N$ , standard deviation,  $\sigma_N$ ) of the visibility probability error,  $\Delta V_{\text{RTSAH}i}$ , the modified cost errors,  $\Delta C'_{\text{RTSAH}i}$  and  $\Delta C''_{\text{RTSAH}i}$ , and the split position error, and the optimal axis selection percentage for a **BIH** ADS, built with various build heuristics, for the **Icosahedron1** scene.

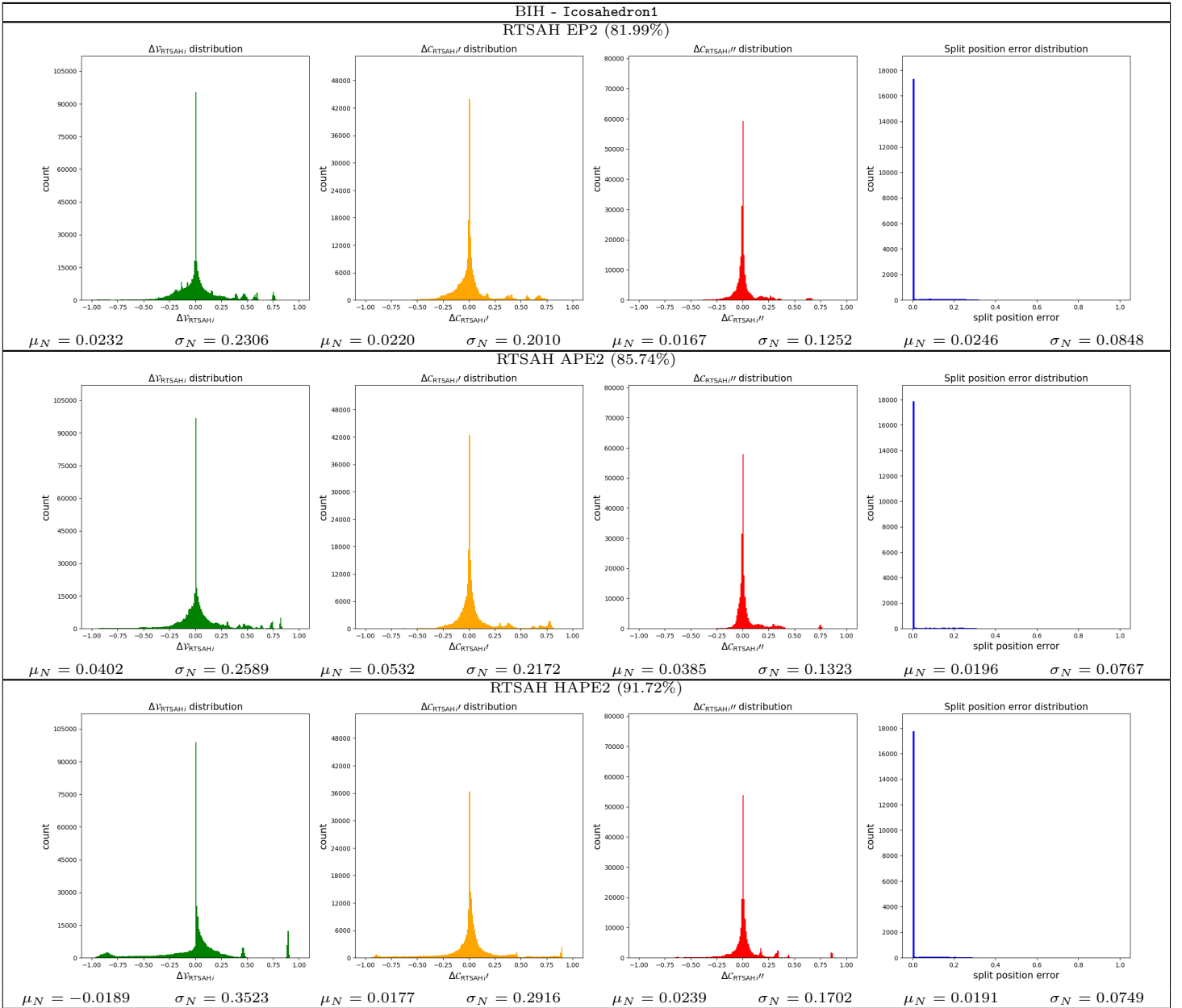


Table 83: The distributions (histogram, mean,  $\mu_N$ , standard deviation,  $\sigma_N$ ) of the visibility probability error,  $\Delta\mathcal{V}_{\text{RTSAH}i}$ , the modified cost errors,  $\Delta C'_{\text{RTSAH}i}$  and  $\Delta C''_{\text{RTSAH}i}$ , and the split position error, and the optimal axis selection percentage for a **BIH** ADS, built with various build heuristics, for the **Icosahedron1** scene.

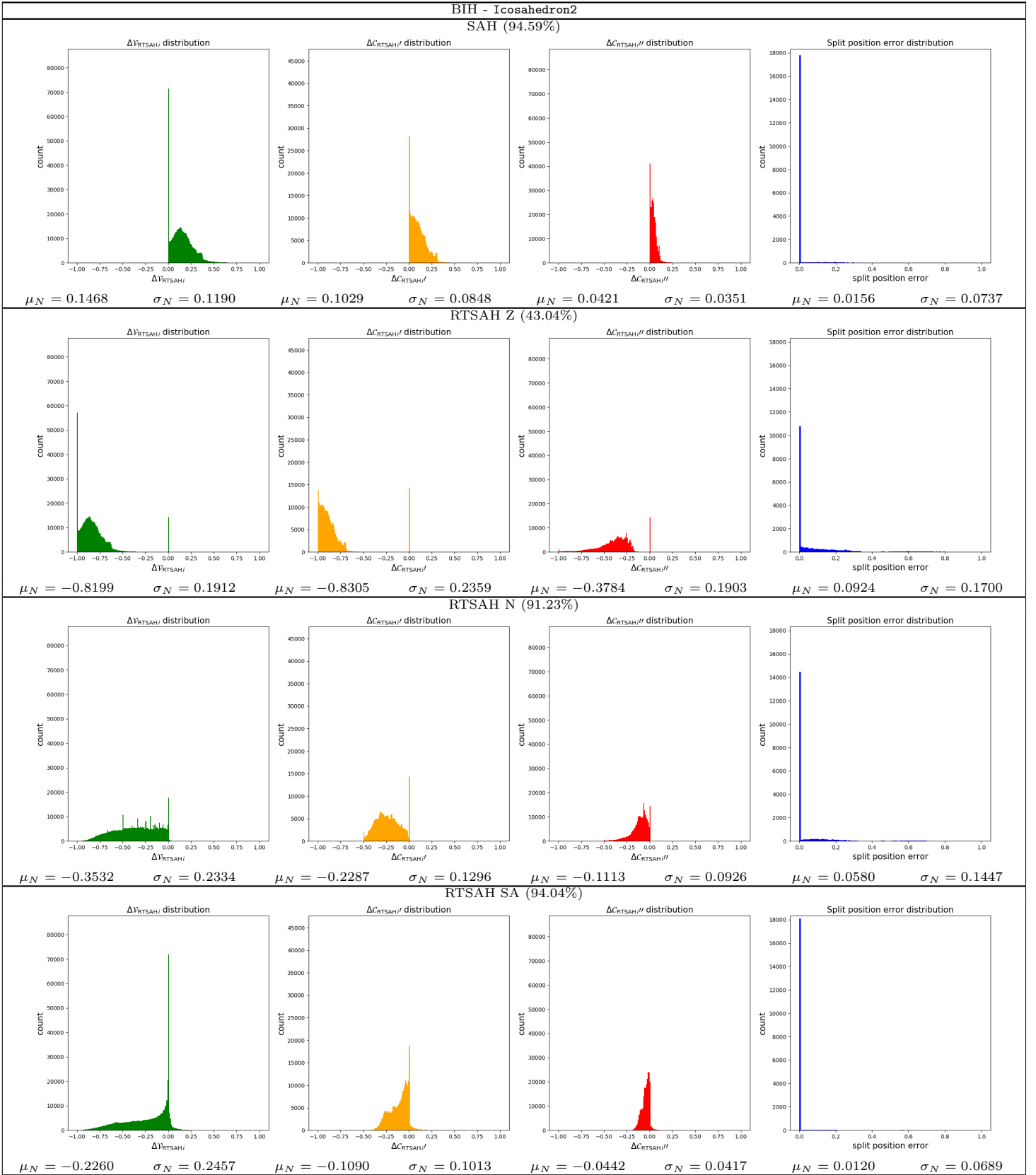


Table 84: The distributions (histogram, mean,  $\mu_N$ , standard deviation,  $\sigma_N$ ) of the visibility probability error,  $\Delta V_{\text{RTSAH}_i}$ , the modified cost errors,  $\Delta C'_{\text{RTSAH}_i}$  and  $\Delta C''_{\text{RTSAH}_i}$ , and the split position error, and the optimal axis selection percentage for a **BIH** ADS, built with various build heuristics, for the **Icosahedron2** scene.

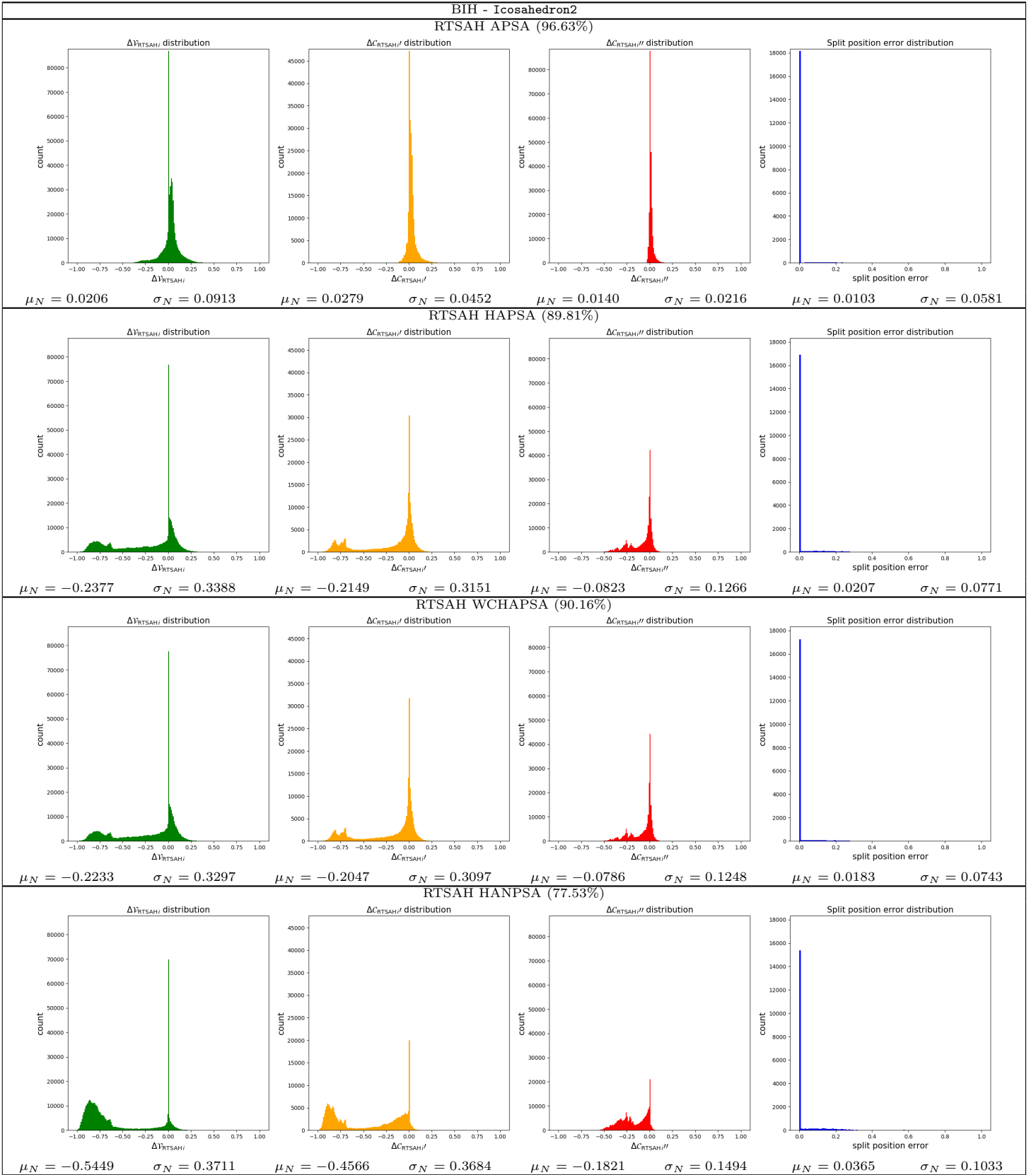


Table 85: The distributions (histogram, mean,  $\mu_N$ , standard deviation,  $\sigma_N$ ) of the visibility probability error,  $\Delta V_{\text{RTSAH}i}$ , the modified cost errors,  $\Delta C'_{\text{RTSAH}i}$  and  $\Delta C''_{\text{RTSAH}i}$ , and the split position error, and the optimal axis selection percentage for a **BIH** ADS, built with various build heuristics, for the **Icosahedron2** scene.

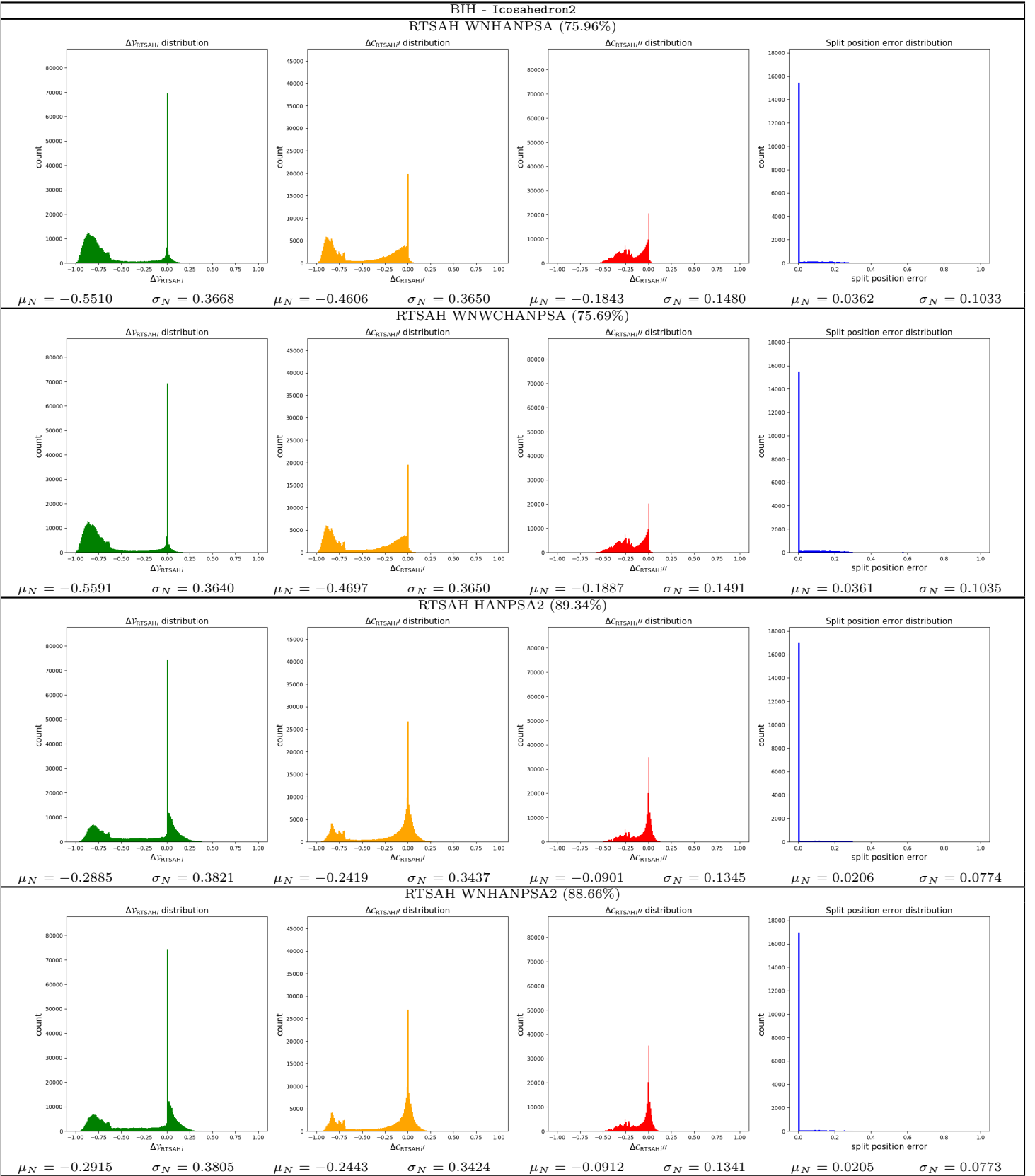


Table 86: The distributions (histogram, mean,  $\mu_N$ , standard deviation,  $\sigma_N$ ) of the visibility probability error,  $\Delta V_{RTSAH_i}$ , the modified cost errors,  $\Delta C'_{RTSAH_i}$  and  $\Delta C''_{RTSAH_i}$ , and the split position error, and the optimal axis selection percentage for a **BIH** ADS, built with various build heuristics, for the **Icosahedron2** scene.

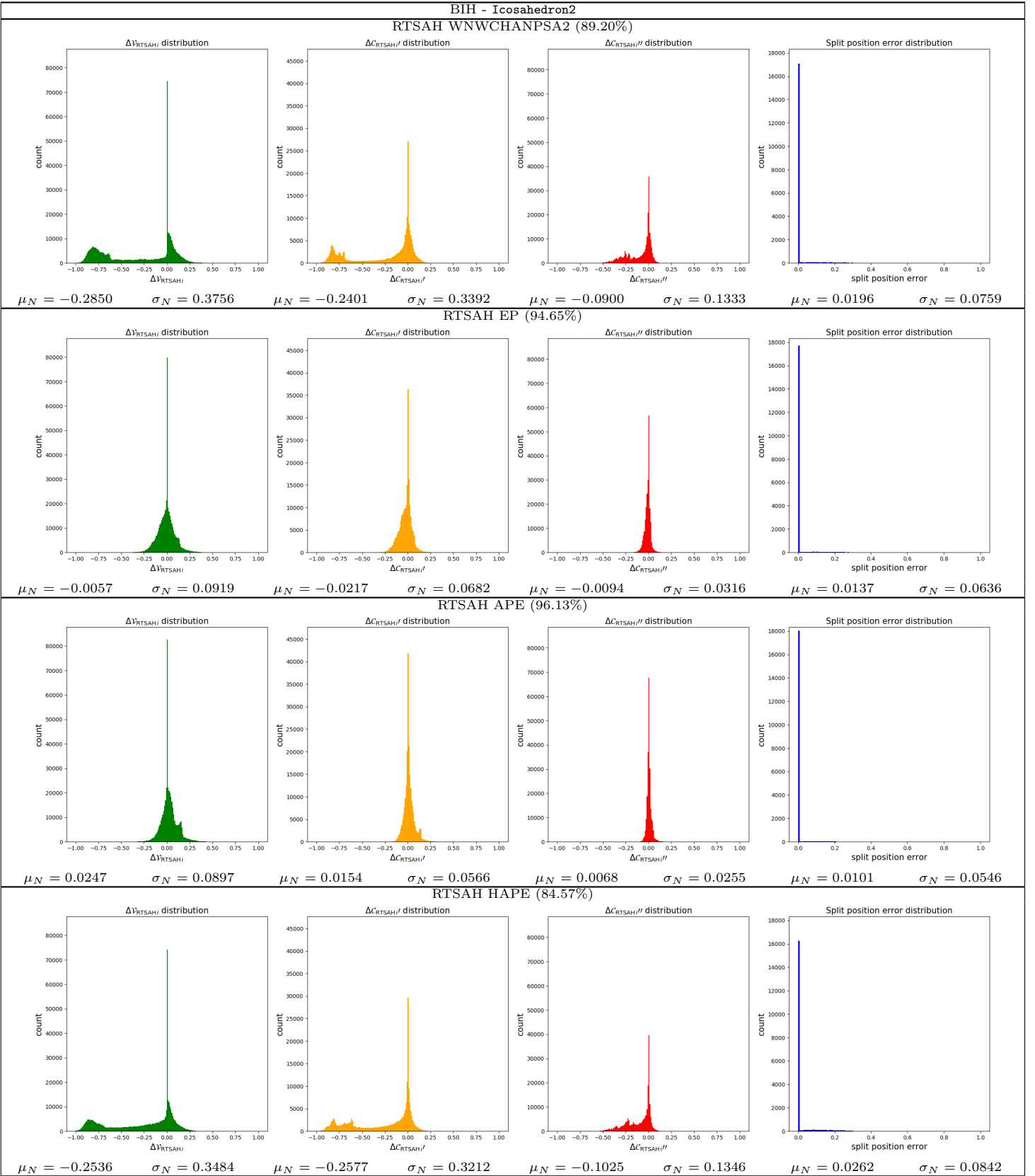


Table 87: The distributions (histogram, mean,  $\mu_N$ , standard deviation,  $\sigma_N$ ) of the visibility probability error,  $\Delta V_{\text{RTSAH}_i}$ , the modified cost errors,  $\Delta C'_{\text{RTSAH}_i}$  and  $\Delta C''_{\text{RTSAH}_i}$ , and the split position error, and the optimal axis selection percentage for a **BIH** ADS, built with various build heuristics, for the **Icosahedron2** scene.

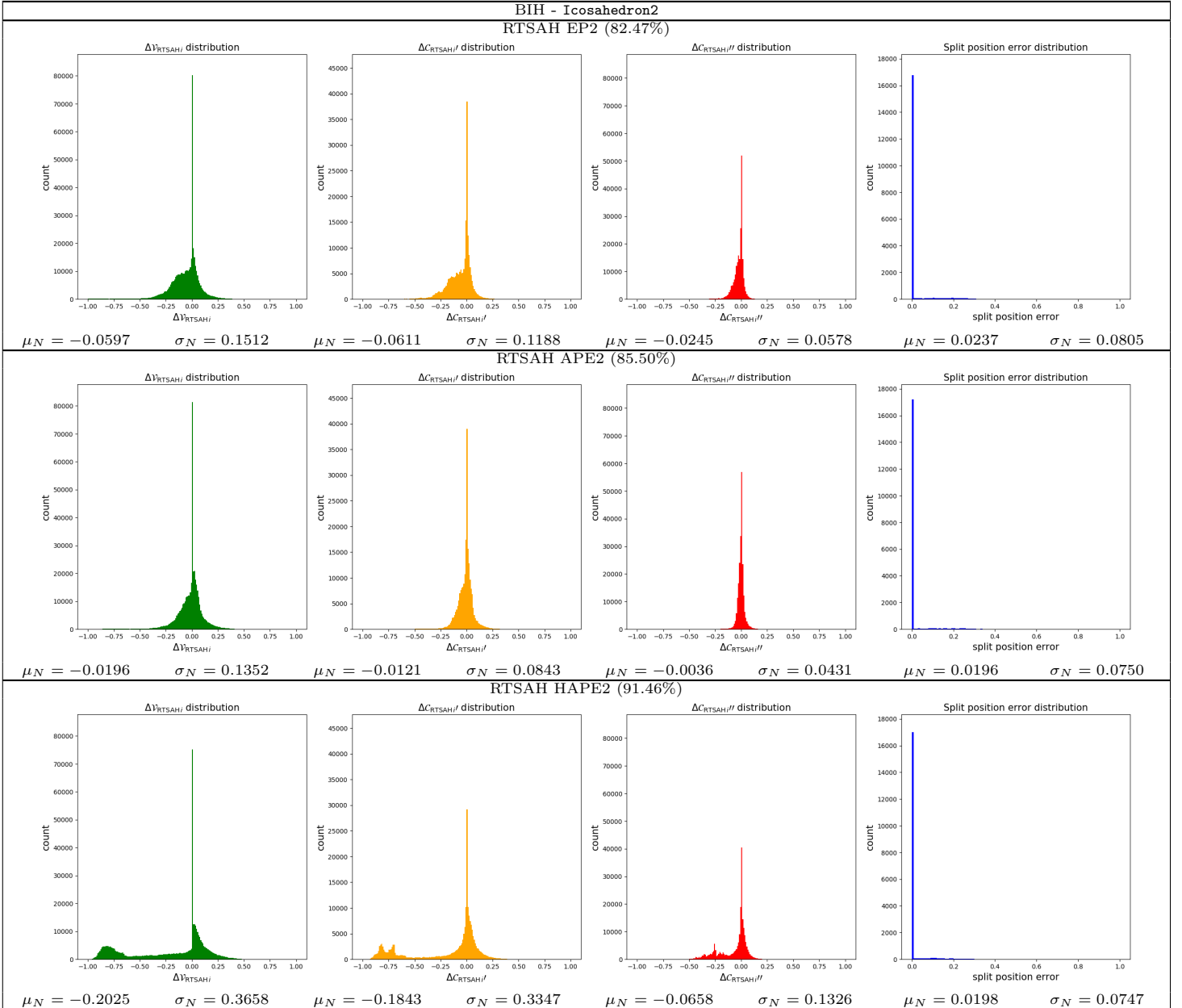


Table 88: The distributions (histogram, mean,  $\mu_N$ , standard deviation,  $\sigma_N$ ) of the visibility probability error,  $\Delta V_{\text{RTSAH}_i}$ , the modified cost errors,  $\Delta C'_{\text{RTSAH}_i}$  and  $\Delta C''_{\text{RTSAH}_i}$ , and the split position error, and the optimal axis selection percentage for a **BIH** ADS, built with various build heuristics, for the **Icosahedron2** scene.

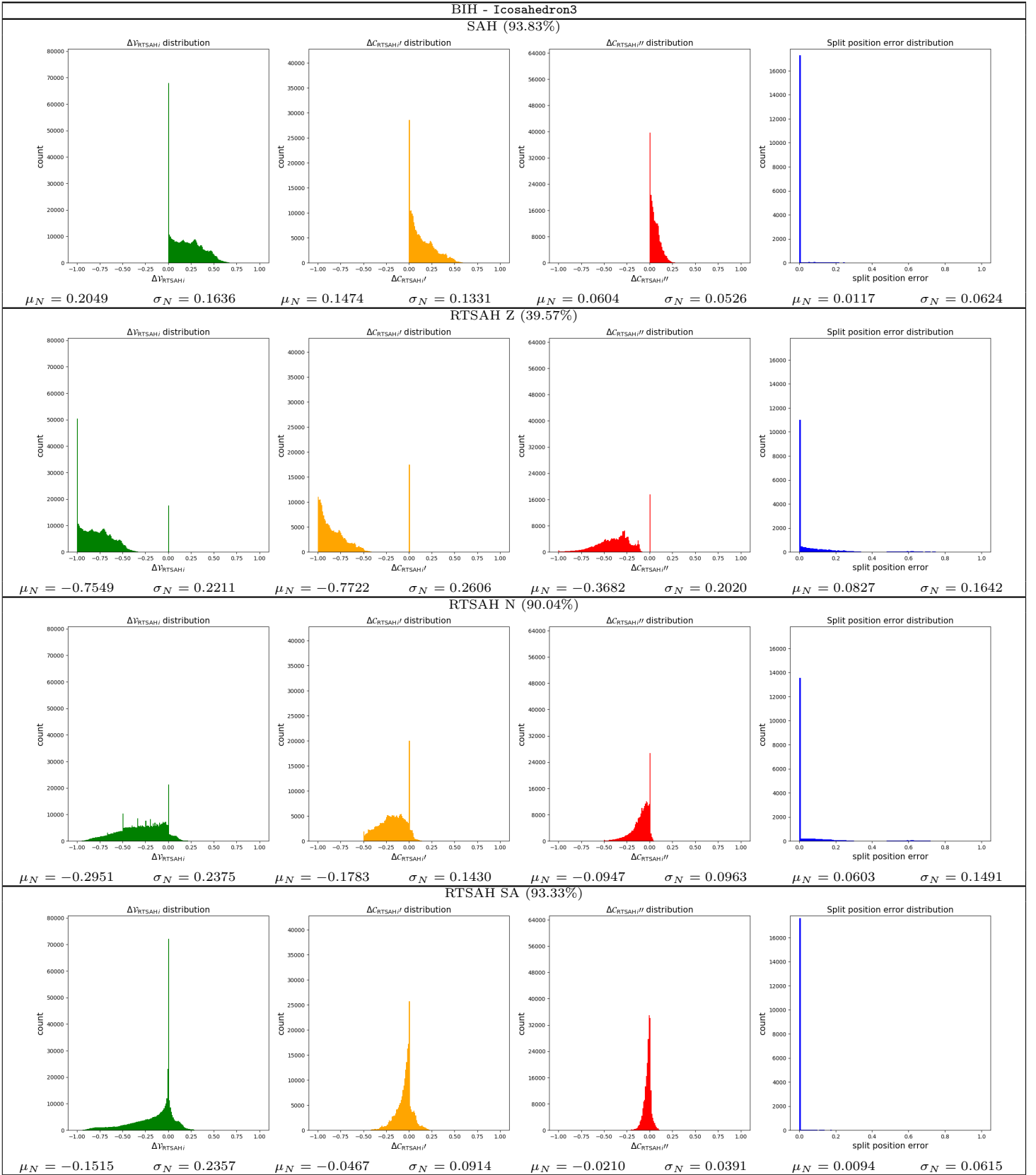


Table 89: The distributions (histogram, mean,  $\mu_N$ , standard deviation,  $\sigma_N$ ) of the visibility probability error,  $\Delta V_{\text{RTSAH}_i}$ , the modified cost errors,  $\Delta C'_{\text{RTSAH}_i}$  and  $\Delta C''_{\text{RTSAH}_i}$ , and the split position error, and the optimal axis selection percentage for a **BIH** ADS, built with various build heuristics, for the **Icosahedron3** scene.

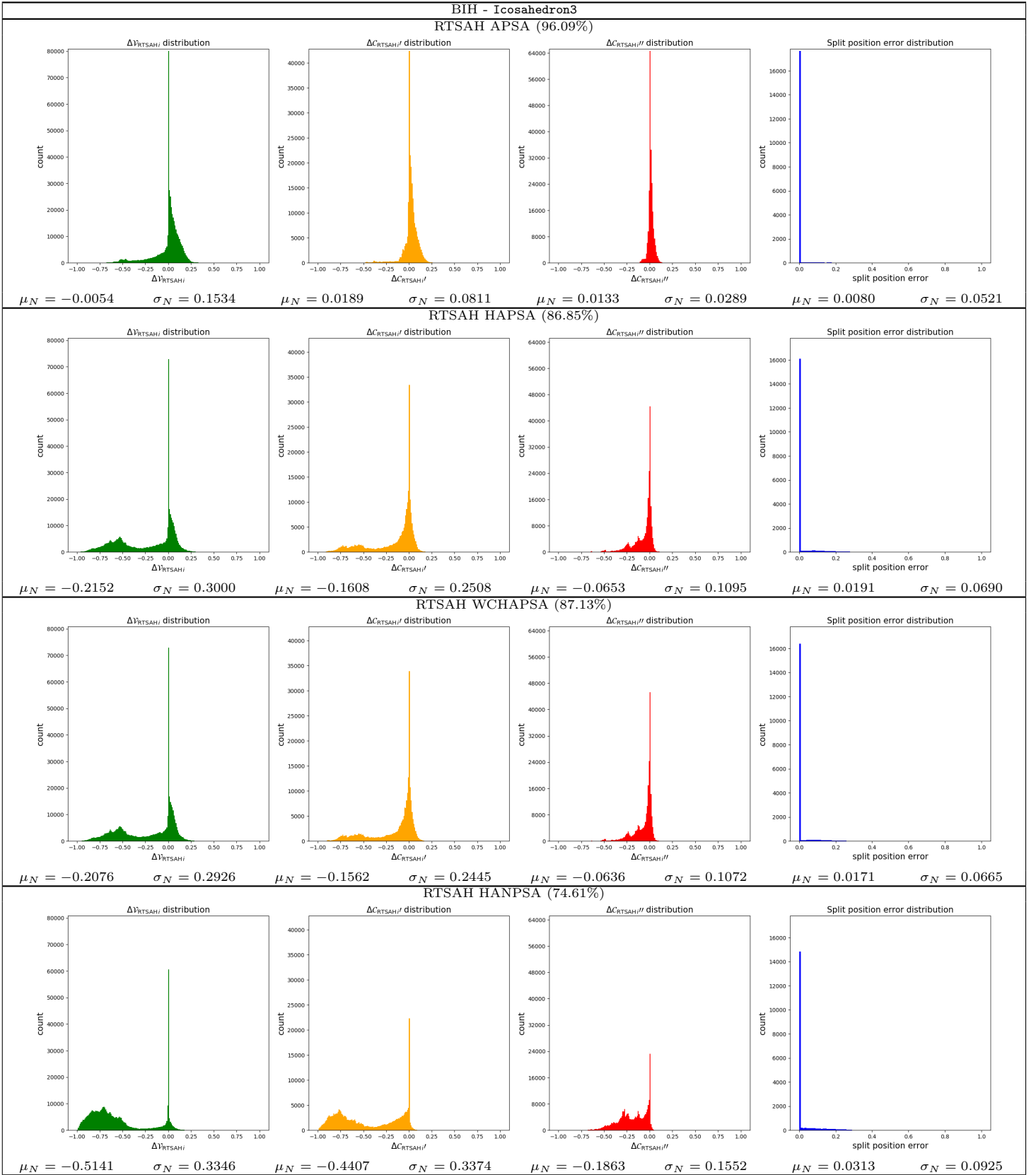


Table 90: The distributions (histogram, mean,  $\mu_N$ , standard deviation,  $\sigma_N$ ) of the visibility probability error,  $\Delta V_{RTSAH_i}$ , the modified cost errors,  $\Delta C'_{RTSAH_i}$  and  $\Delta C''_{RTSAH_i}$ , and the split position error, and the optimal axis selection percentage for a **BIH** ADS, built with various build heuristics, for the **Icosahedron3** scene.

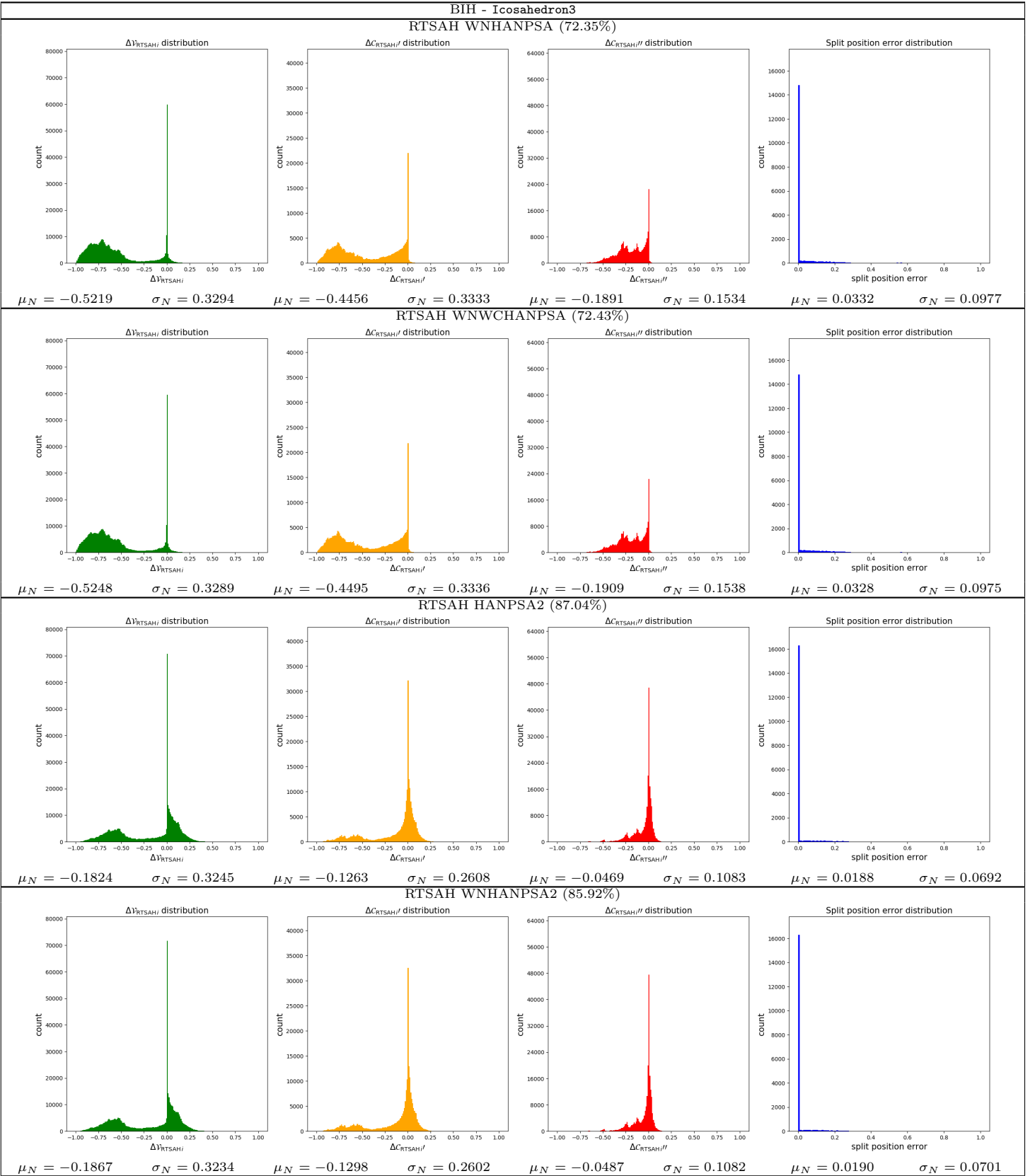


Table 91: The distributions (histogram, mean,  $\mu_N$ , standard deviation,  $\sigma_N$ ) of the visibility probability error,  $\Delta V_{\text{RTSAH}i}$ , the modified cost errors,  $\Delta C'_{\text{RTSAH}i}$  and  $\Delta C''_{\text{RTSAH}i}$ , and the split position error, and the optimal axis selection percentage for a **BIH** ADS, built with various build heuristics, for the **Icosahedron3** scene.

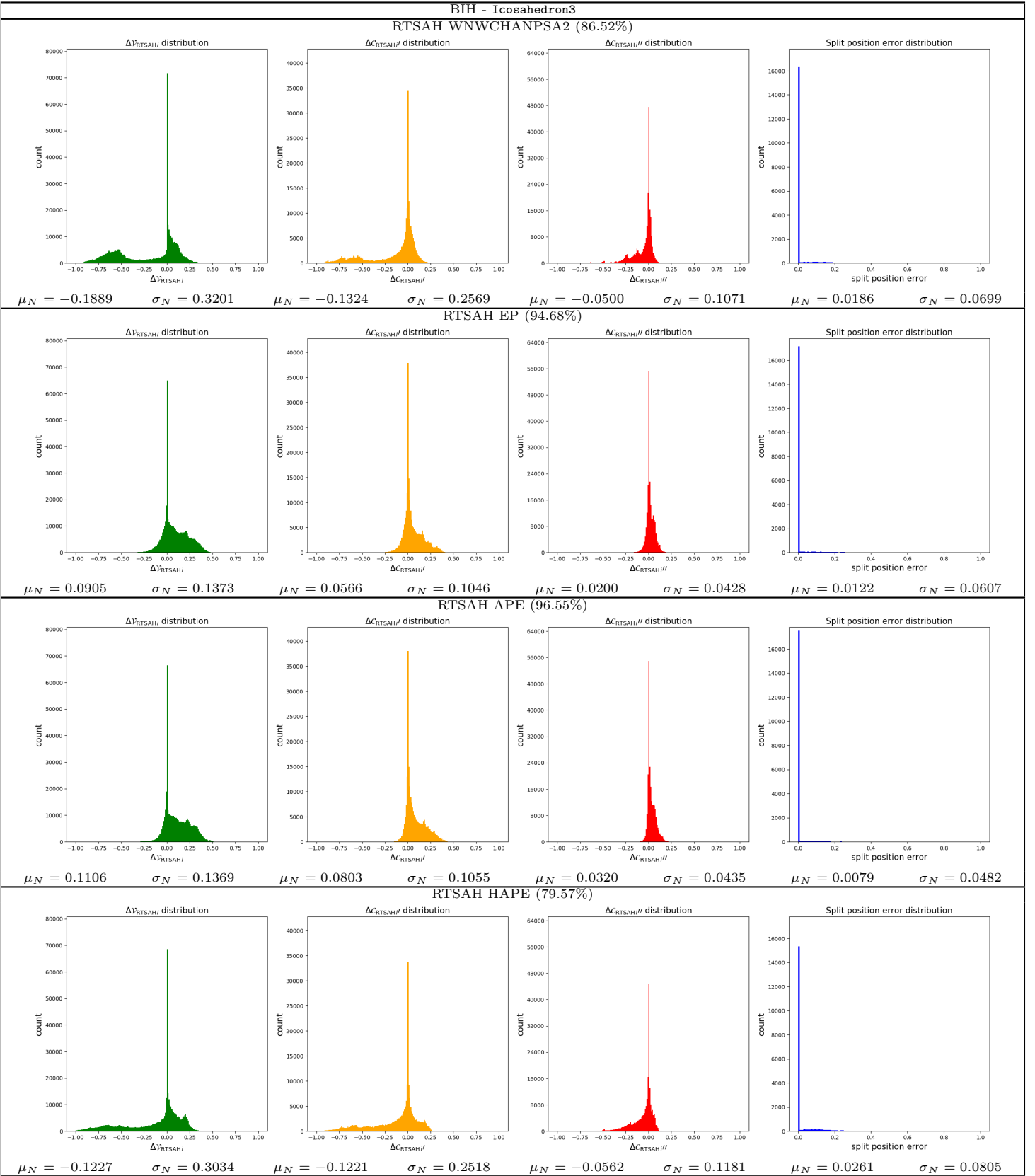


Table 92: The distributions (histogram, mean,  $\mu_N$ , standard deviation,  $\sigma_N$ ) of the visibility probability error,  $\Delta V_{\text{RTSAH}_i}$ , the modified cost errors,  $\Delta C'_{\text{RTSAH}_i}$  and  $\Delta C''_{\text{RTSAH}_i}$ , and the split position error, and the optimal axis selection percentage for a **BIH** ADS, built with various build heuristics, for the **Icosahedron3** scene.

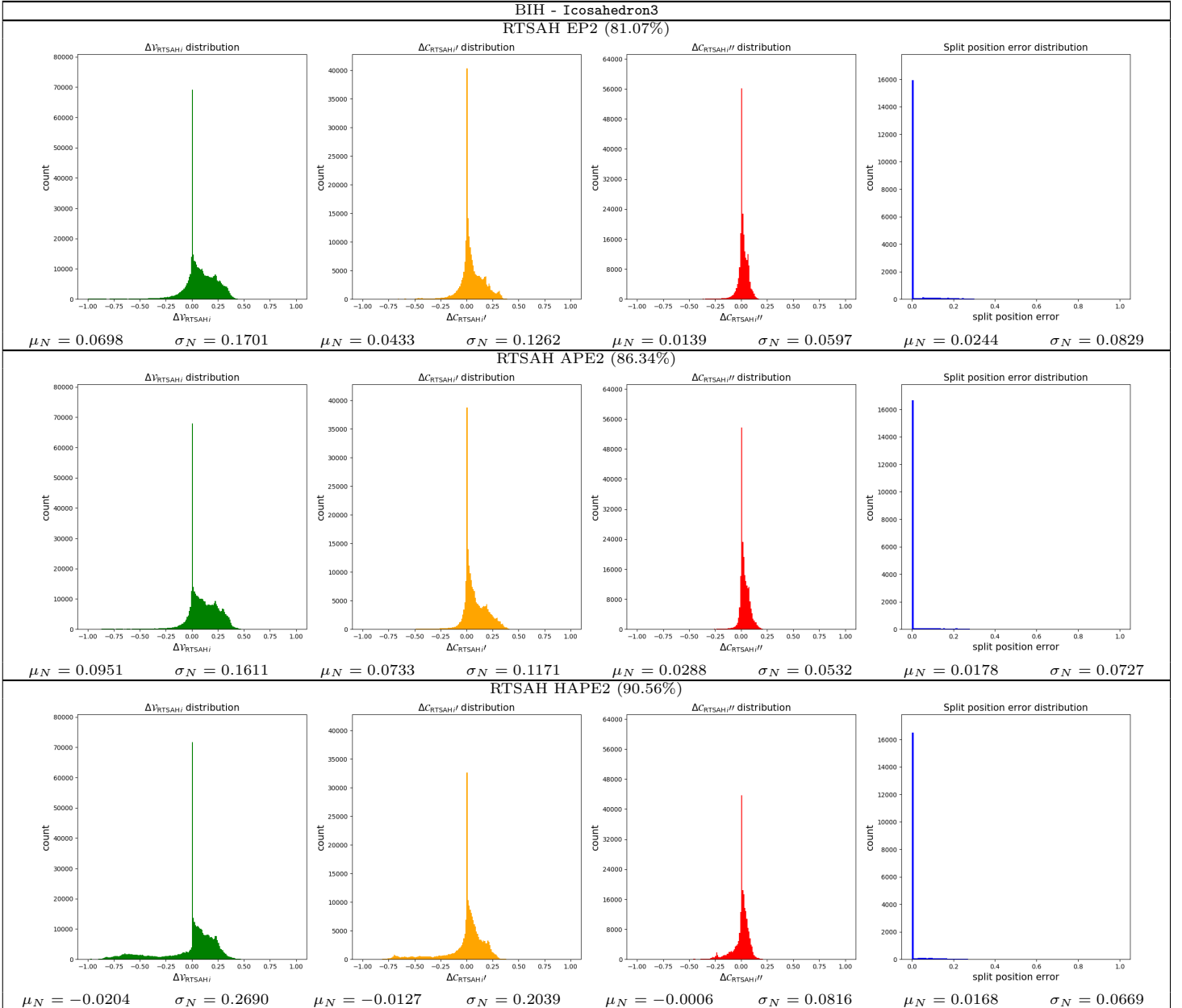


Table 93: The distributions (histogram, mean,  $\mu_N$ , standard deviation,  $\sigma_N$ ) of the visibility probability error,  $\Delta V_{RTSAH_i}$ , the modified cost errors,  $\Delta C'_{RTSAH_i}$  and  $\Delta C''_{RTSAH_i}$ , and the split position error, and the optimal axis selection percentage for a **BIH** ADS, built with various build heuristics, for the **Icosahedron3** scene.

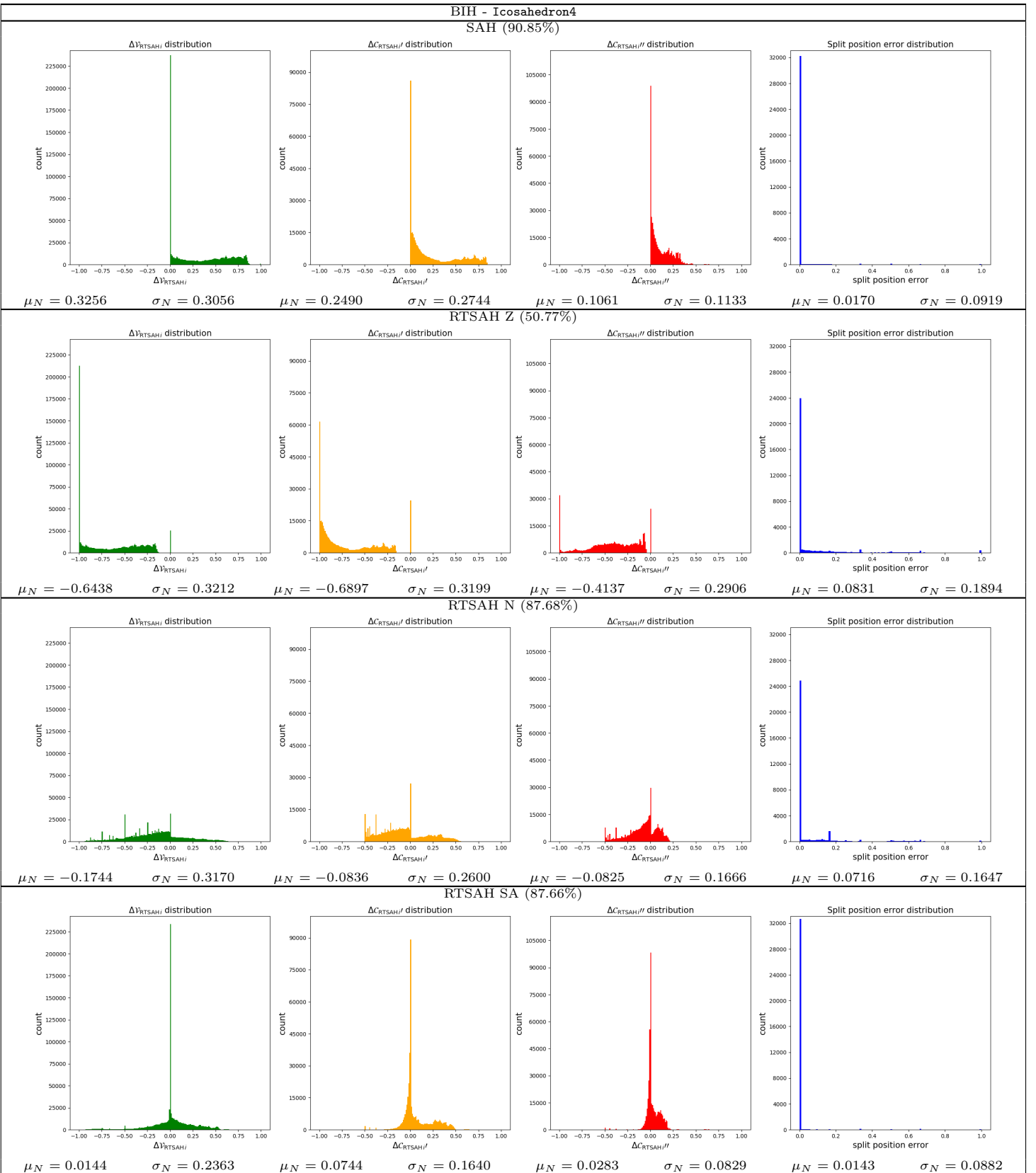


Table 94: The distributions (histogram, mean,  $\mu_N$ , standard deviation,  $\sigma_N$ ) of the visibility probability error,  $\Delta V_{\text{RTSAH}_i}$ , the modified cost errors,  $\Delta C'_{\text{RTSAH}_i}$  and  $\Delta C''_{\text{RTSAH}_i}$ , and the split position error, and the optimal axis selection percentage for a **BIH** ADS, built with various build heuristics, for the **Icosahedron4** scene.

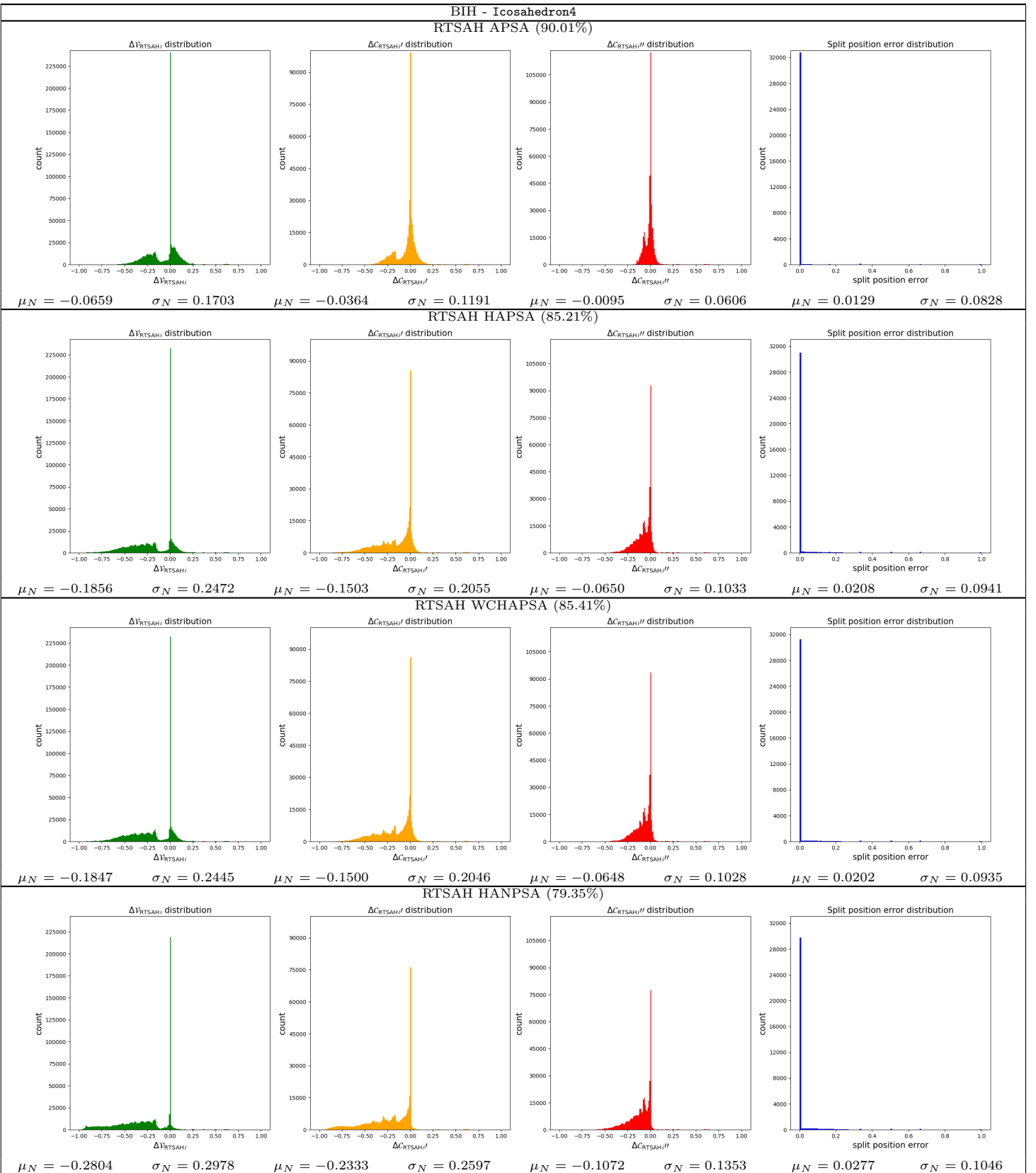


Table 95: The distributions (histogram, mean,  $\mu_N$ , standard deviation,  $\sigma_N$ ) of the visibility probability error,  $\Delta V_{\text{RTSAH}i}$ , the modified cost errors,  $\Delta C'_{\text{RTSAH}i}$  and  $\Delta C''_{\text{RTSAH}i}$ , and the split position error, and the optimal axis selection percentage for a **BIH** ADS, built with various build heuristics, for the **Icosahedron4** scene.

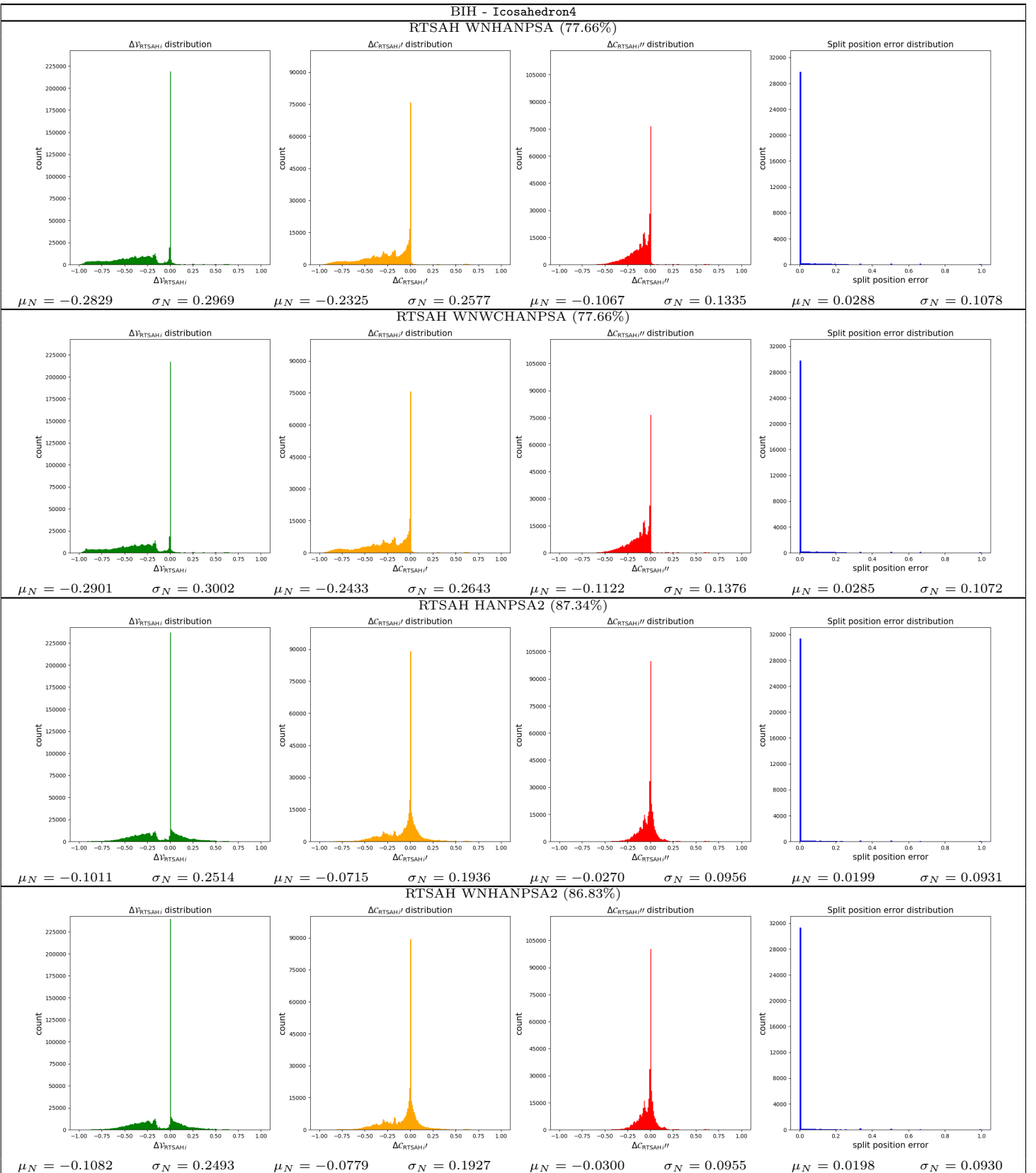


Table 96: The distributions (histogram, mean,  $\mu_N$ , standard deviation,  $\sigma_N$ ) of the visibility probability error,  $\Delta V_{\text{RTSAH}i}$ , the modified cost errors,  $\Delta C'_{\text{RTSAH}i}$  and  $\Delta C''_{\text{RTSAH}i}$ , and the split position error, and the optimal axis selection percentage for a **BIH** ADS, built with various build heuristics, for the **Icosahedron4** scene.

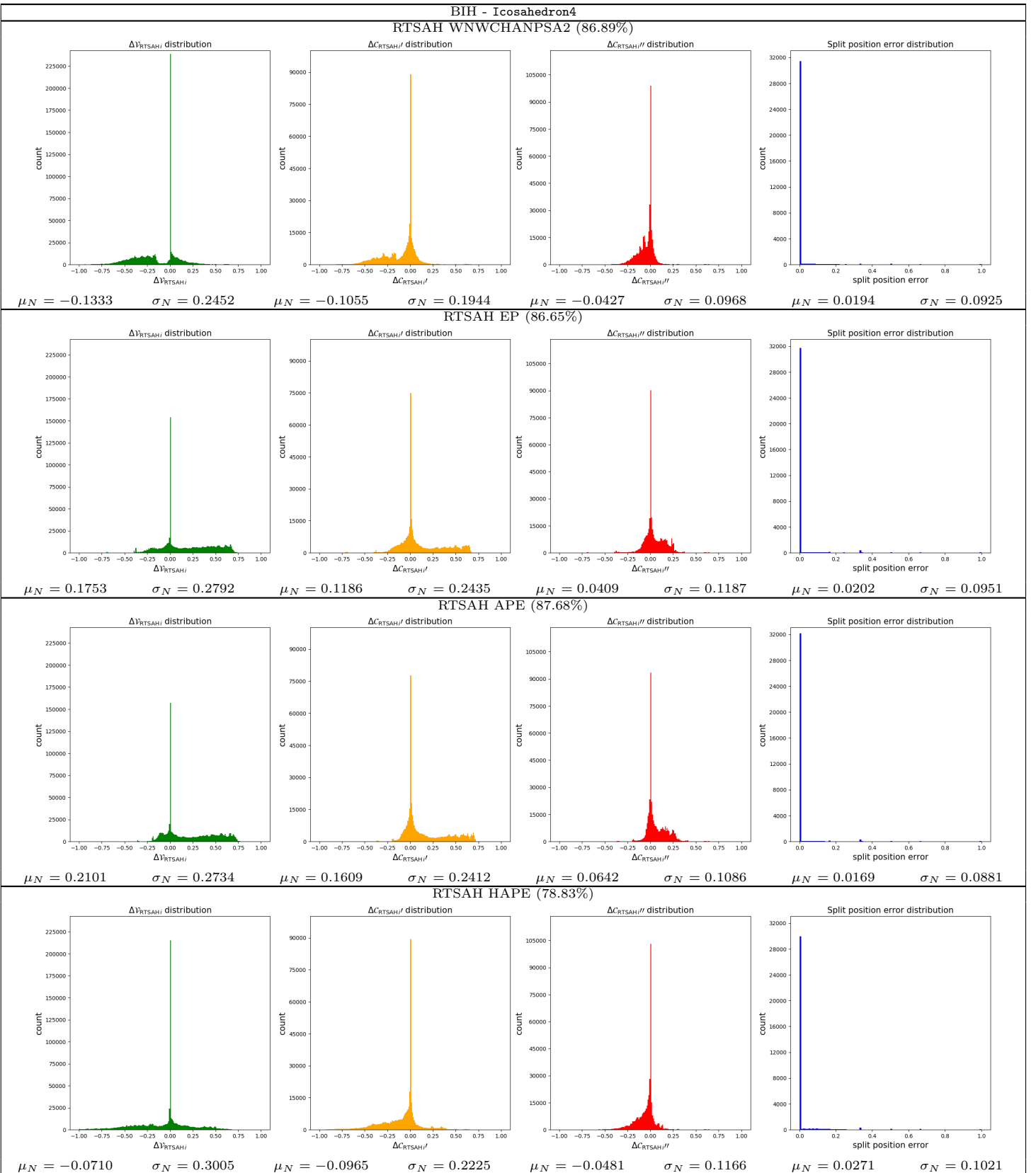


Table 97: The distributions (histogram, mean,  $\mu_N$ , standard deviation,  $\sigma_N$ ) of the visibility probability error,  $\Delta V_{RTSAH_i}$ , the modified cost errors,  $\Delta C'_{RTSAH_i}$  and  $\Delta C''_{RTSAH_i}$ , and the split position error, and the optimal axis selection percentage for a **BIH** ADS, built with various build heuristics, for the **Icosahedron4** scene.

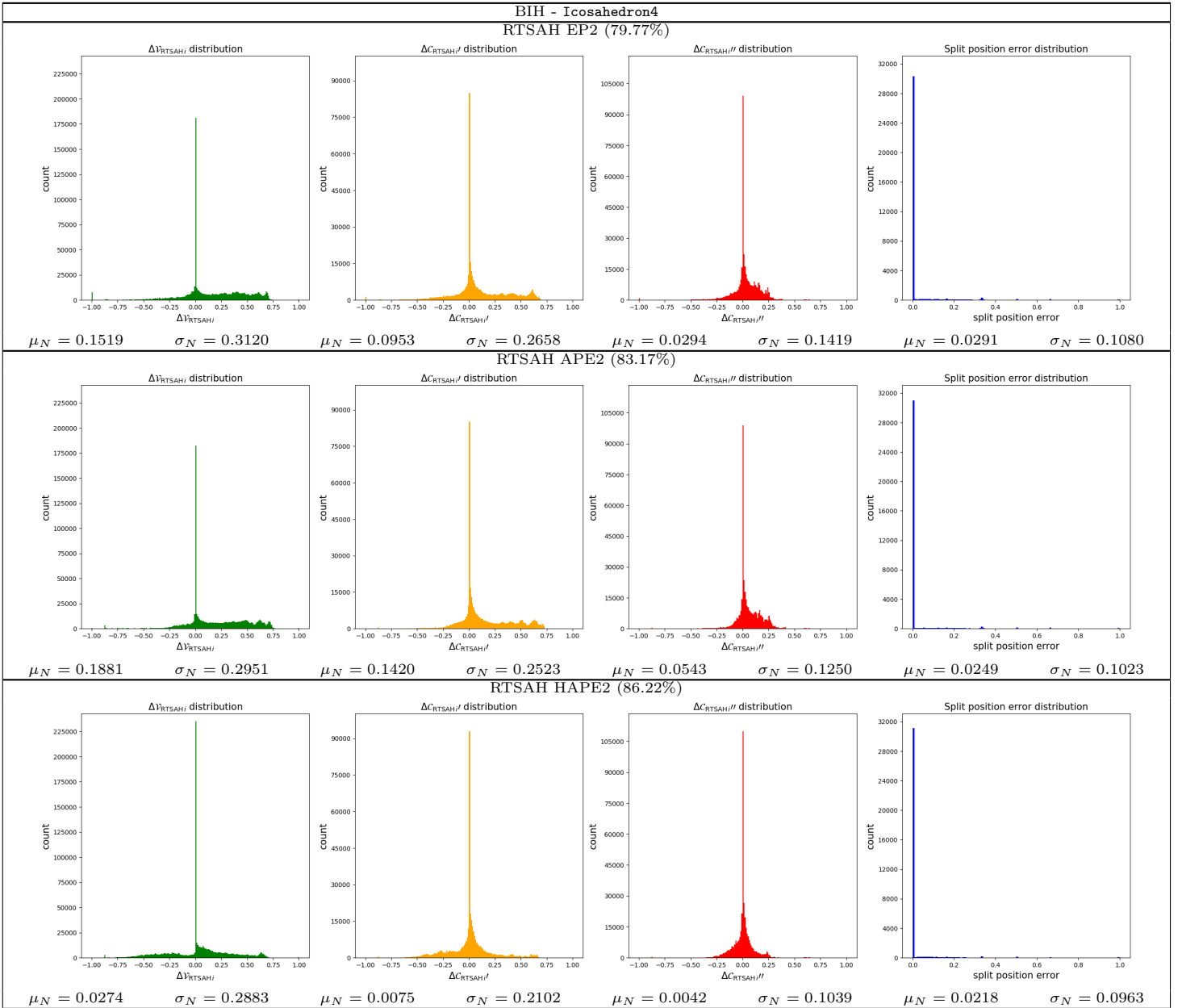


Table 98: The distributions (histogram, mean,  $\mu_N$ , standard deviation,  $\sigma_N$ ) of the visibility probability error,  $\Delta V_{RTSAH_i}$ , the modified cost errors,  $\Delta C'_{RTSAH_i}$  and  $\Delta C''_{RTSAH_i}$ , and the split position error, and the optimal axis selection percentage for a **BIH** ADS, built with various build heuristics, for the **Icosahedron4** scene.

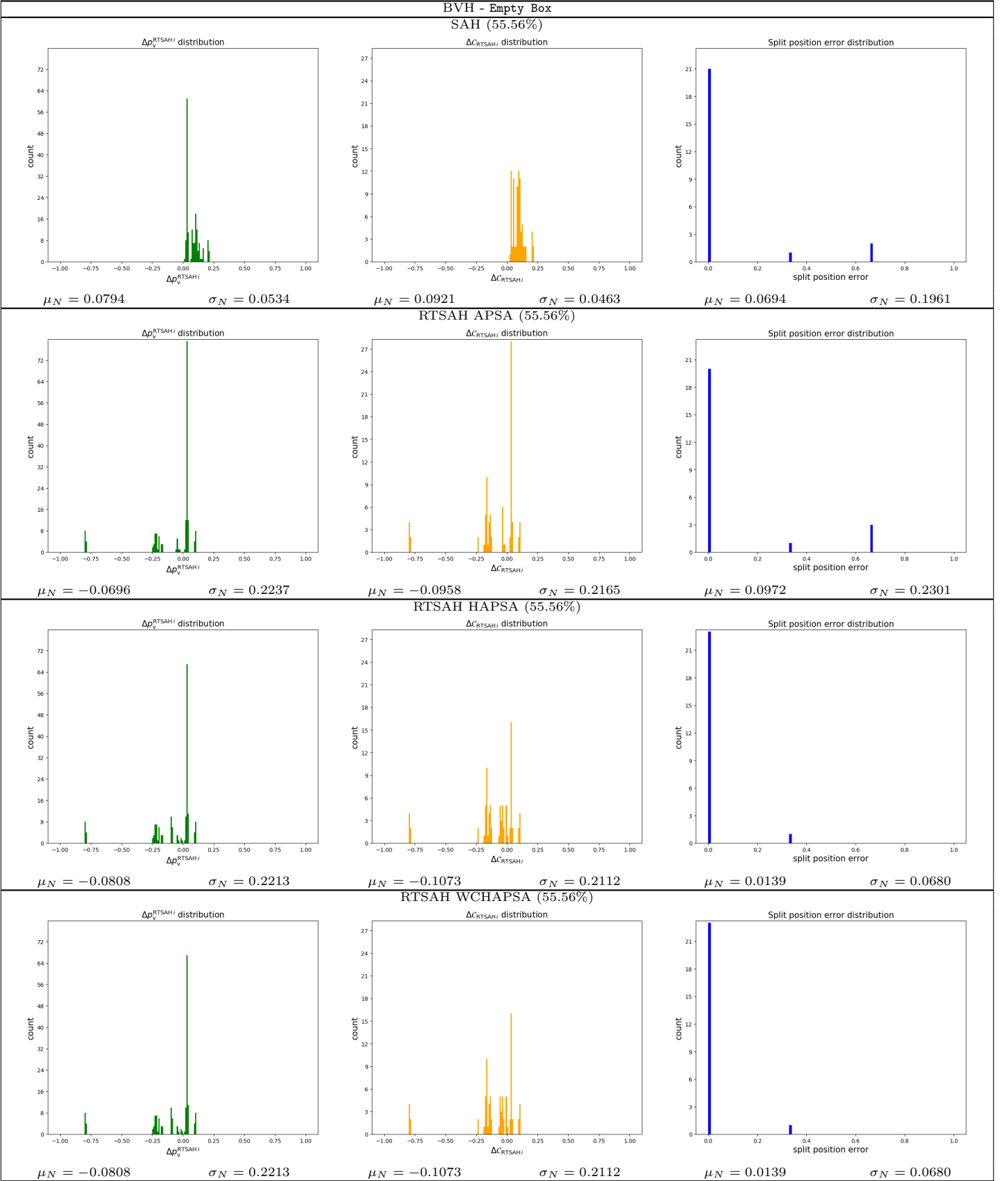


Table 99: The distributions (histogram, mean,  $\mu_N$ , standard deviation,  $\sigma_N$ ) of the combined piercing and visibility probability error,  $\Delta V_{\text{RTSAH}_i}$ , the cost error,  $\Delta C_{\text{RTSAH}_i}$ , and the split position error, and the optimal axis selection percentage for a **BVH** ADS, built with various build heuristics, for the **Empty Box** scene.

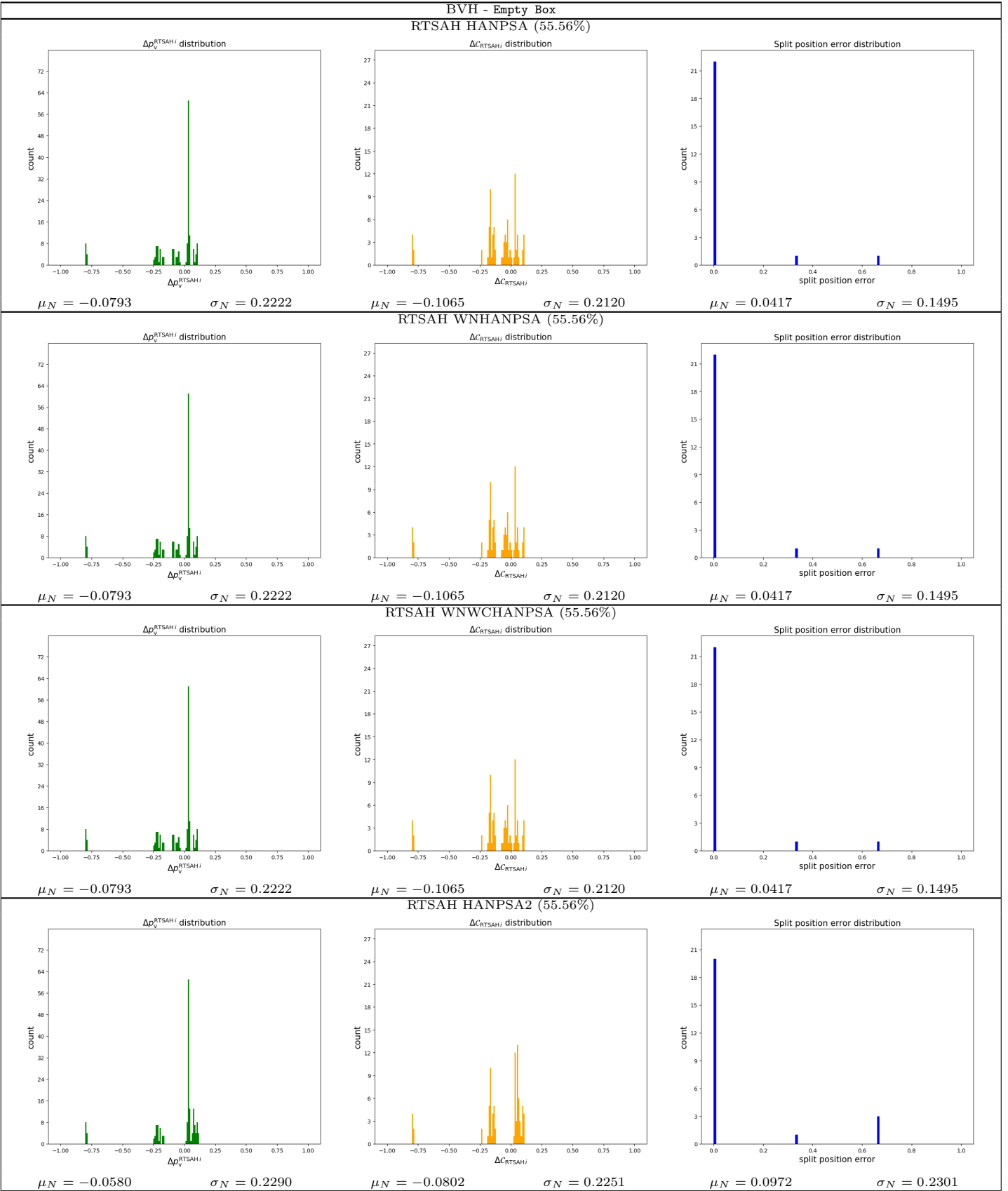


Table 100: The distributions (histogram, mean,  $\mu_N$ , standard deviation,  $\sigma_N$ ) of the combined piercing and visibility probability error,  $\Delta V_{\text{RTSAH}_i}$ , the cost error,  $\Delta C_{\text{RTSAH}_i}$ , and the split position error, and the optimal axis selection percentage for a **BVH** ADS, built with various build heuristics, for the **Empty Box** scene.

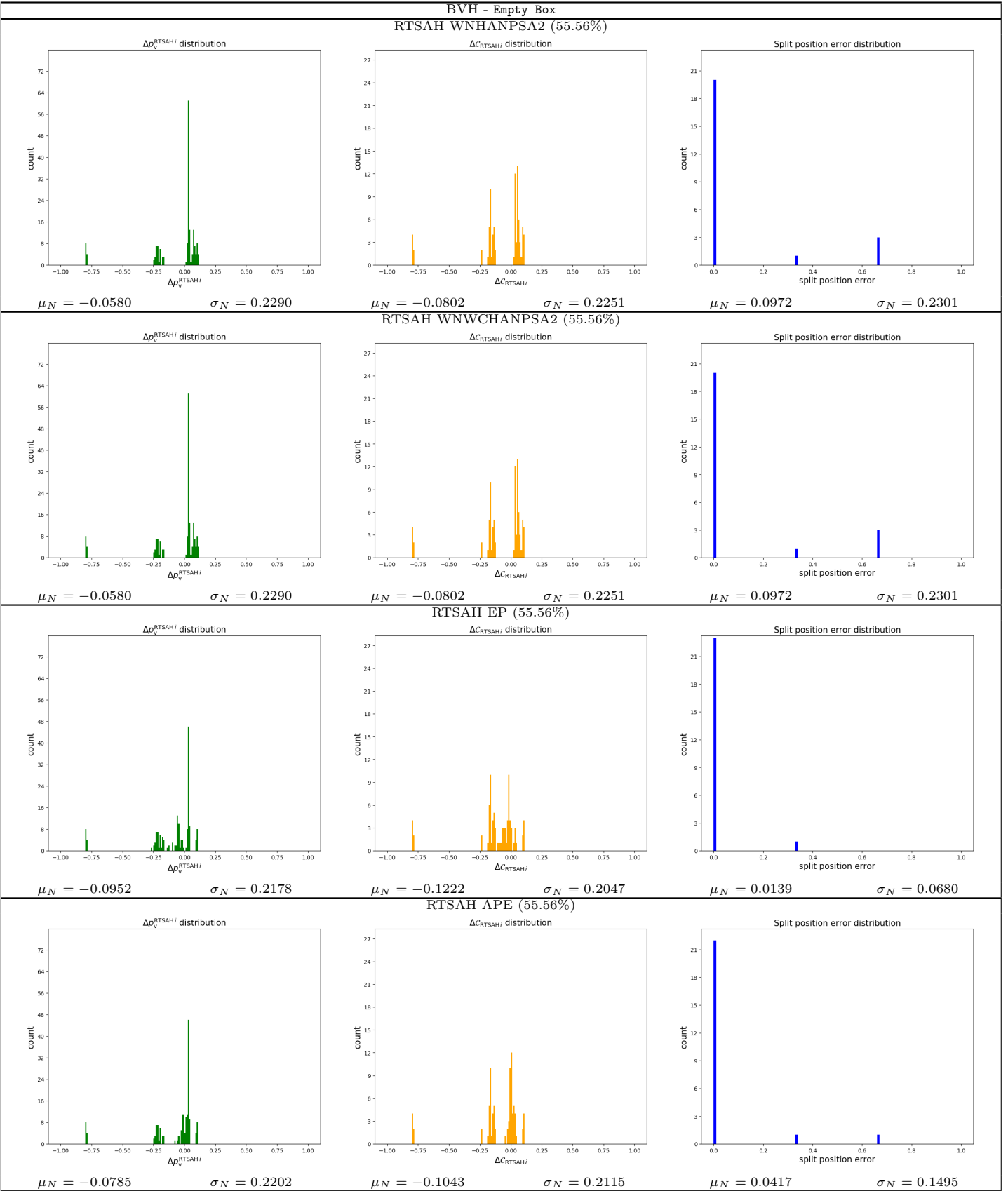


Table 101: The distributions (histogram, mean,  $\mu_N$ , standard deviation,  $\sigma_N$ ) of the combined piercing and visibility probability error,  $\Delta V_{\text{RTSAH}_i}$ , the cost error,  $\Delta C_{\text{RTSAH}_i}$ , and the split position error, and the optimal axis selection percentage for a **BVH** ADS, built with various build heuristics, for the **Empty Box** scene.

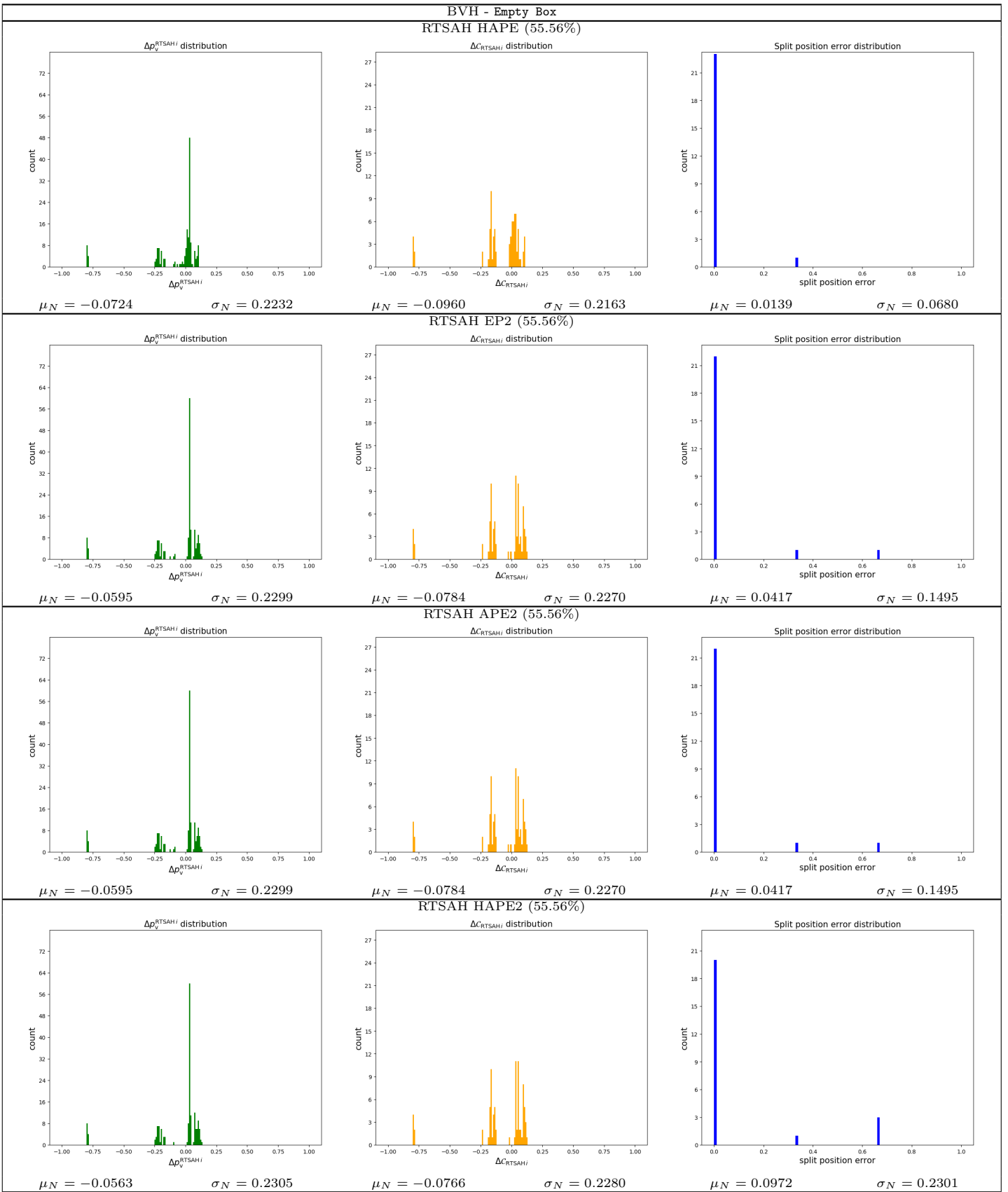


Table 102: The distributions (histogram, mean,  $\mu_N$ , standard deviation,  $\sigma_N$ ) of the combined piercing and visibility probability error,  $\Delta V_{\text{RTSAH}_i}$ , the cost error,  $\Delta C_{\text{RTSAH}_i}$ , and the split position error, and the optimal axis selection percentage for a **BVH** ADS, built with various build heuristics, for the **Empty Box** scene.

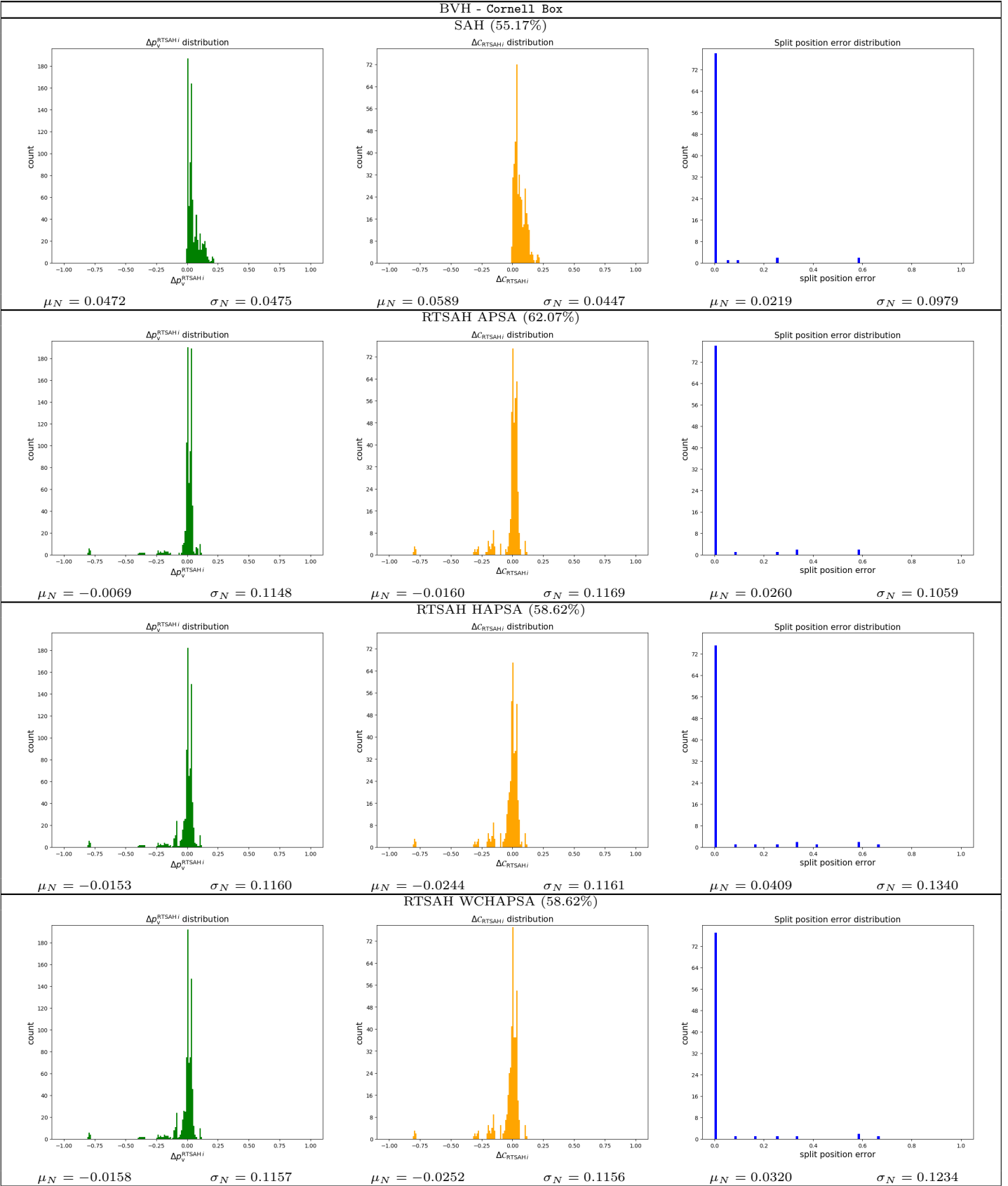


Table 103: The distributions (histogram, mean,  $\mu_N$ , standard deviation,  $\sigma_N$ ) of the combined piercing and visibility probability error,  $\Delta V_{\text{RTSAHi}}$ , the cost error,  $\Delta C_{\text{RTSAHi}}$ , and the split position error, and the optimal axis selection percentage for a **BVH** ADS, built with various build heuristics, for the **Cornell Box** scene.

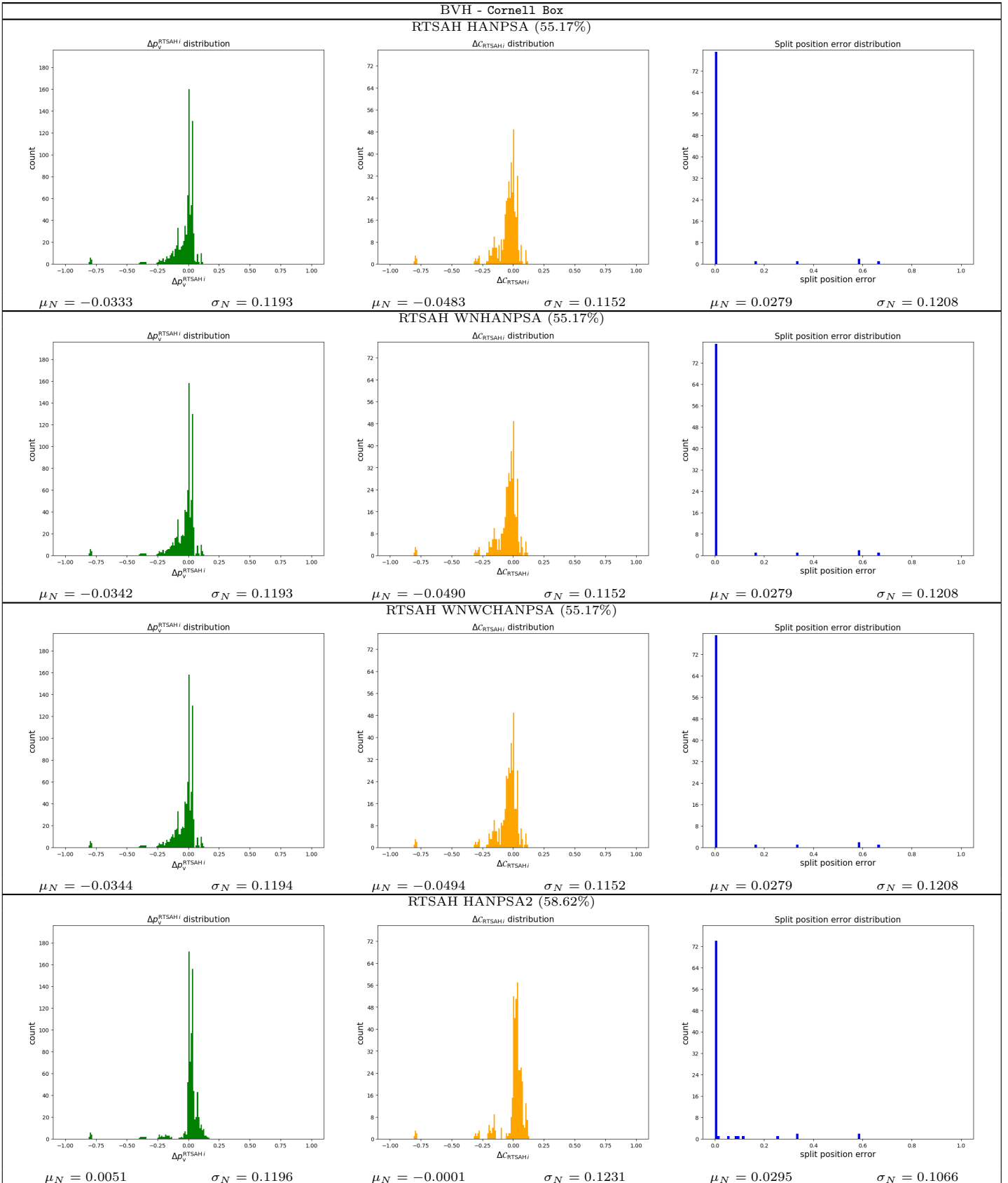


Table 104: The distributions (histogram, mean,  $\mu_N$ , standard deviation,  $\sigma_N$ ) of the combined piercing and visibility probability error,  $\Delta\mathcal{V}_{\text{RTSAH}i}$ , the cost error,  $\Delta C_{\text{RTSAH}i}$ , and the split position error, and the optimal axis selection percentage for a **BVH** ADS, built with various build heuristics, for the **Cornell Box** scene.

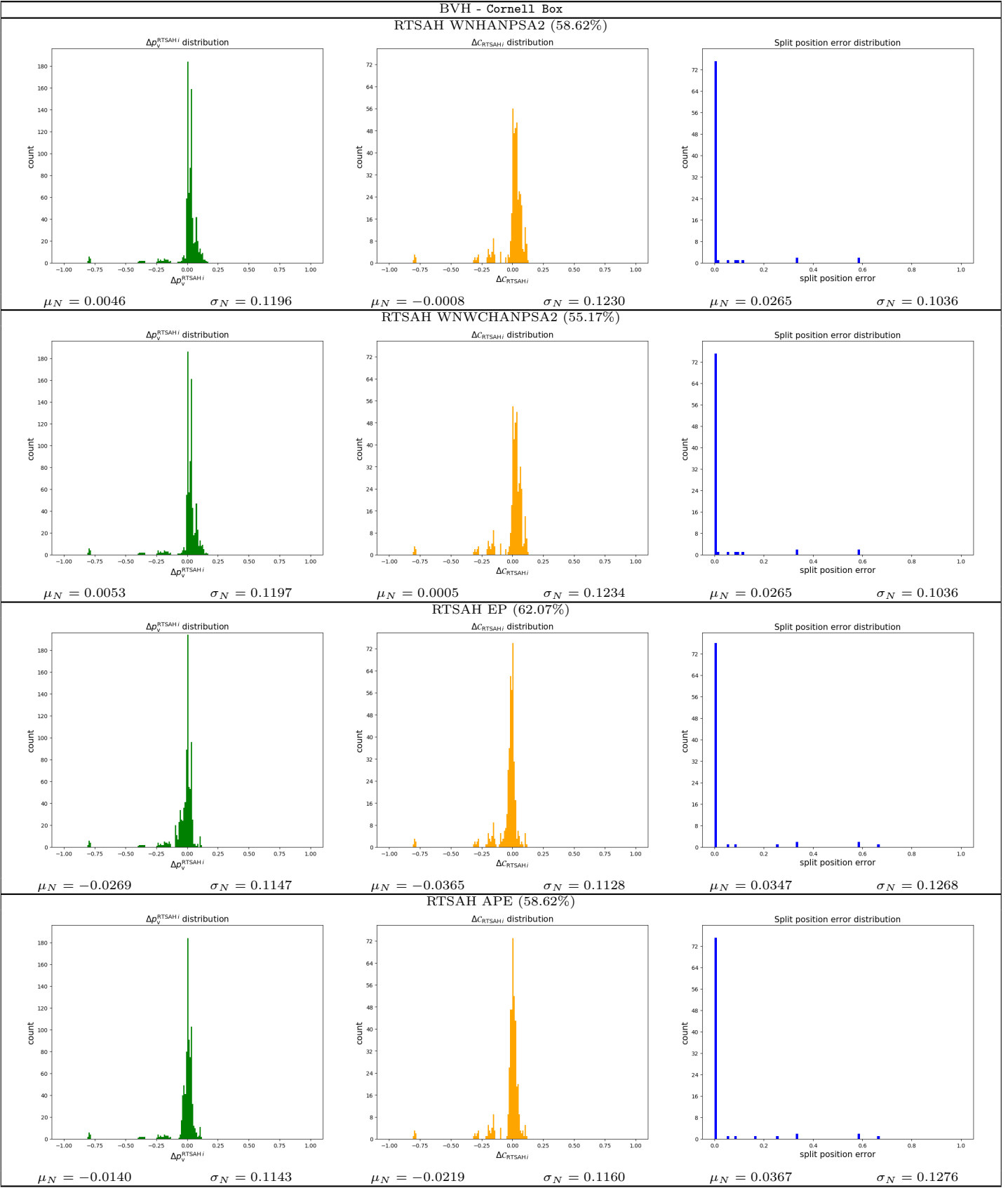


Table 105: The distributions (histogram, mean,  $\mu_N$ , standard deviation,  $\sigma_N$ ) of the combined piercing and visibility probability error,  $\Delta\mathcal{V}_{\text{RTSAH}i}$ , the cost error,  $\Delta C_{\text{RTSAH}i}$ , and the split position error, and the optimal axis selection percentage for a **BVH** ADS, built with various build heuristics, for the **Cornell Box** scene.

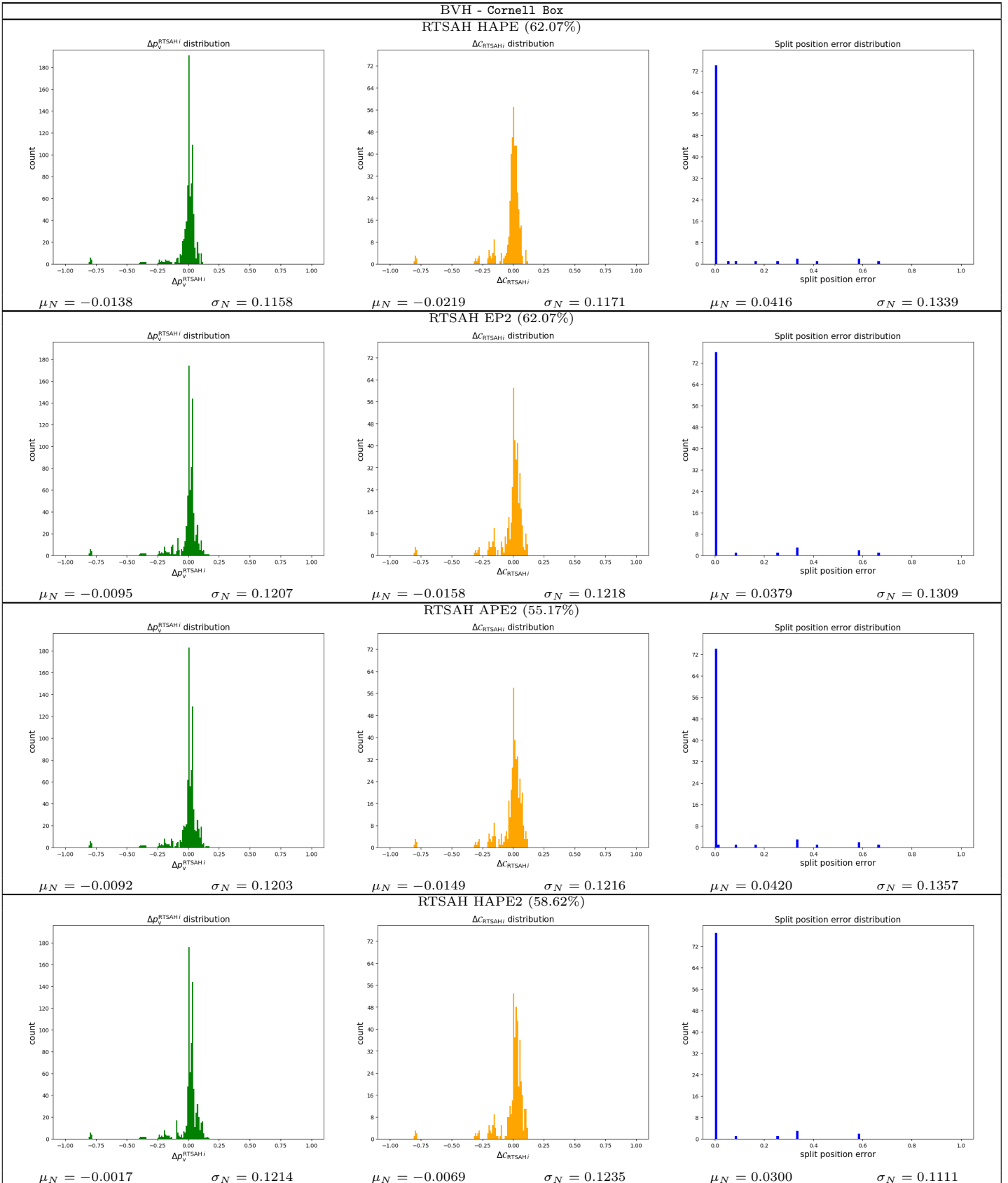


Table 106: The distributions (histogram, mean,  $\mu_N$ , standard deviation,  $\sigma_N$ ) of the combined piercing and visibility probability error,  $\Delta V_{\text{RTSAH}_i}$ , the cost error,  $\Delta c_{\text{RTSAH}_i}$ , and the split position error, and the optimal axis selection percentage for a **BVH** ADS, built with various build heuristics, for the **Cornell Box** scene.

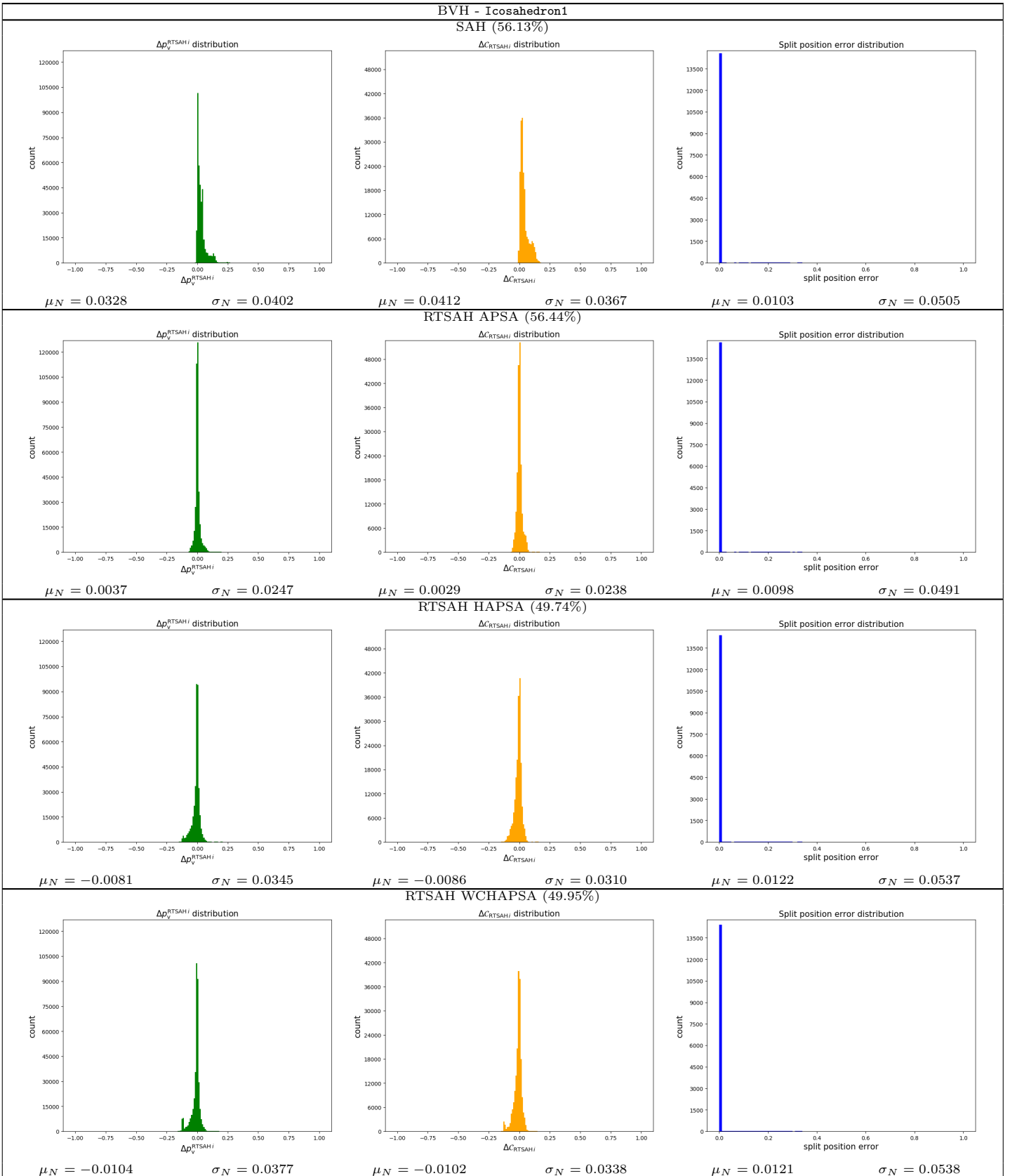


Table 107: The distributions (histogram, mean,  $\mu_N$ , standard deviation,  $\sigma_N$ ) of the combined piercing and visibility probability error,  $\Delta p_v^{\text{RTSAH}_i}$ , the cost error,  $\Delta C_{\text{RTSAH}_i}$ , and the split position error, and the optimal axis selection percentage for a **BVH** ADS, built with various build heuristics, for the **Icosahedron1** scene.

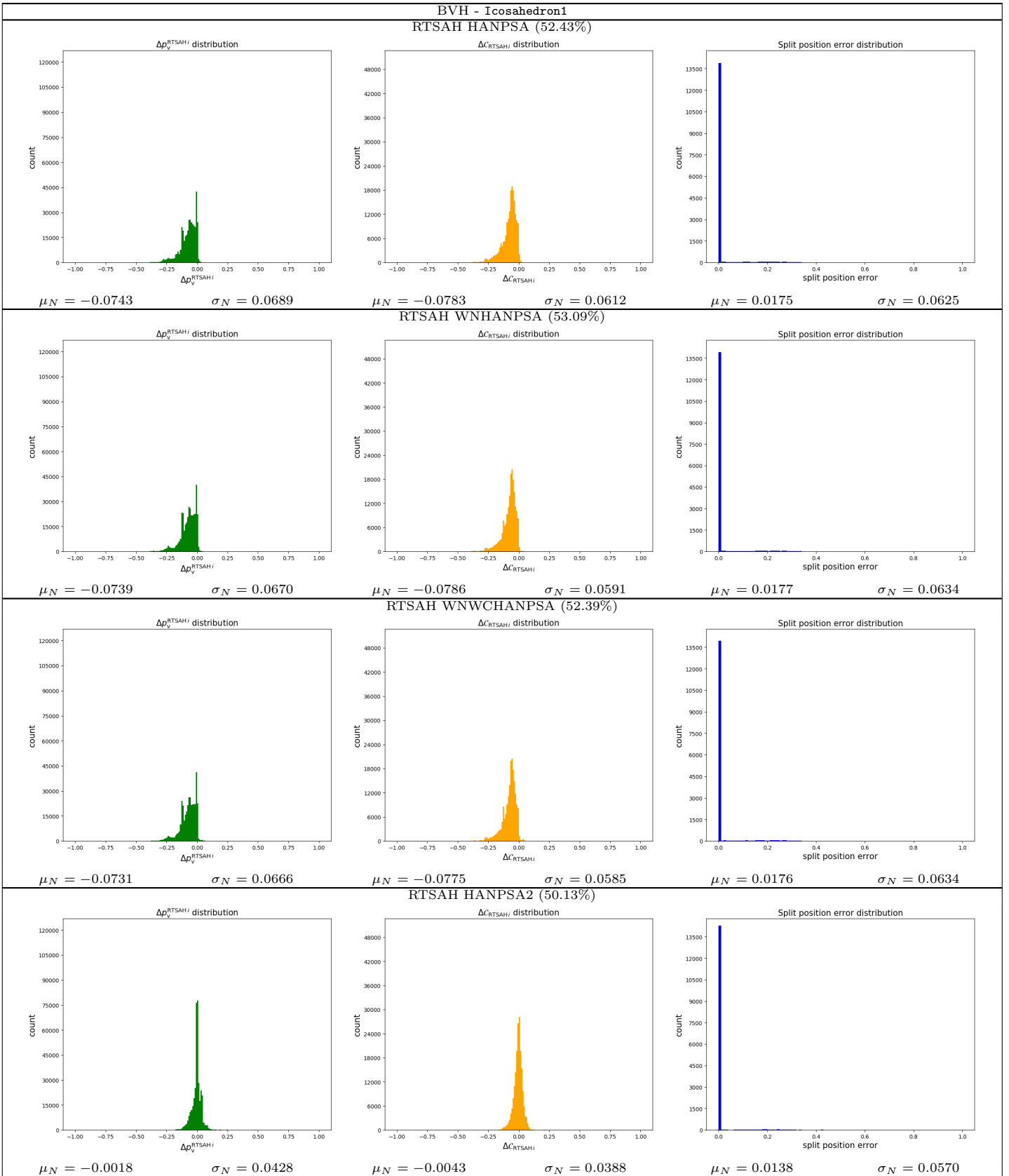


Table 108: The distributions (histogram, mean,  $\mu_N$ , standard deviation,  $\sigma_N$ ) of the combined piercing and visibility probability error,  $\Delta V_{\text{RTSAH}_i}$ , the cost error,  $\Delta C_{\text{RTSAH}_i}$ , and the split position error, and the optimal axis selection percentage for a **BVH** ADS, built with various build heuristics, for the **Icosahedron1** scene.

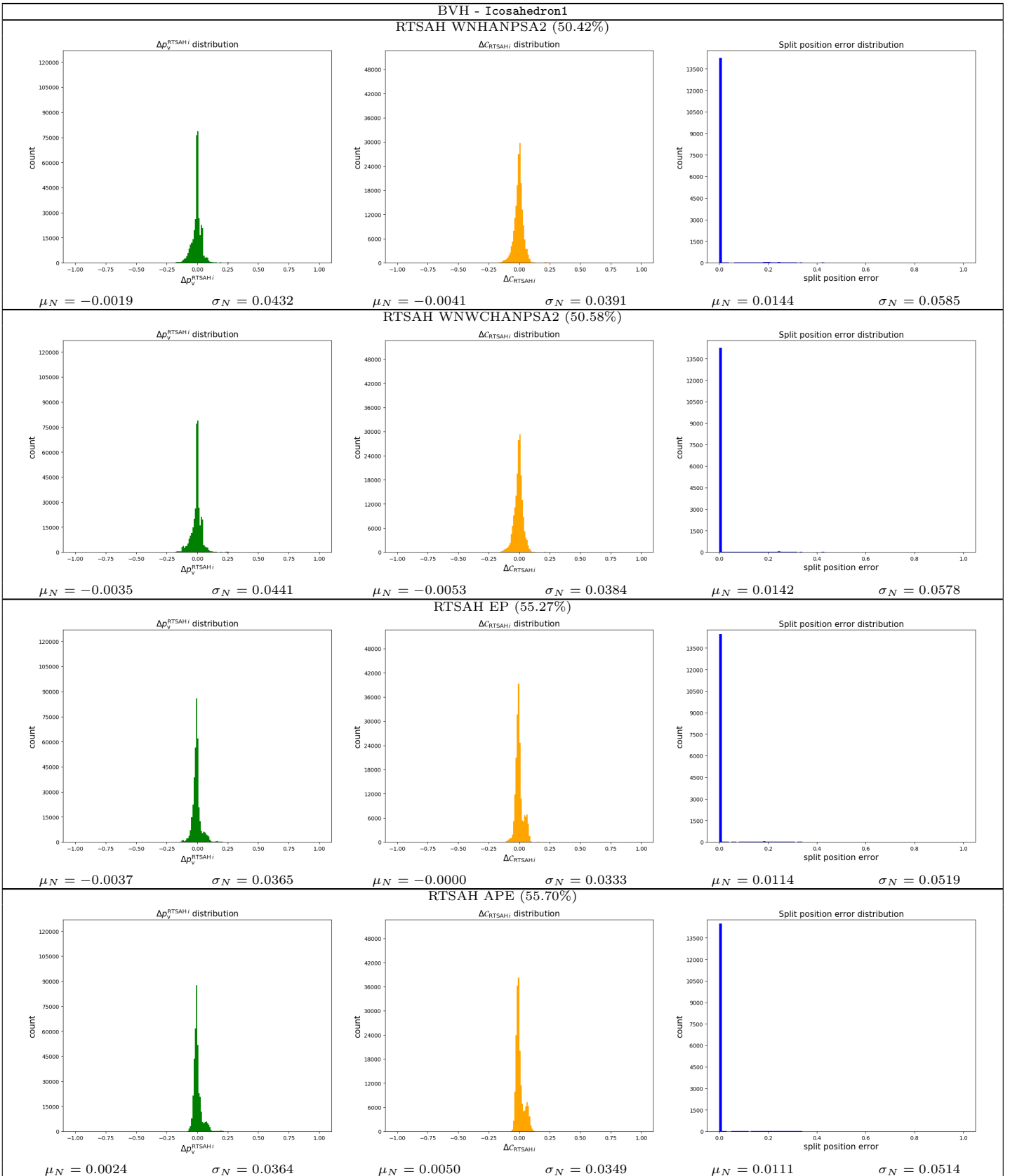


Table 109: The distributions (histogram, mean,  $\mu_N$ , standard deviation,  $\sigma_N$ ) of the combined piercing and visibility probability error,  $\Delta p_v^{\text{RTSAH}_i}$ , the cost error,  $\Delta C^{\text{RTSAH}_i}$ , and the split position error, and the optimal axis selection percentage for a **BVH** ADS, built with various build heuristics, for the **Icosahedron1** scene.

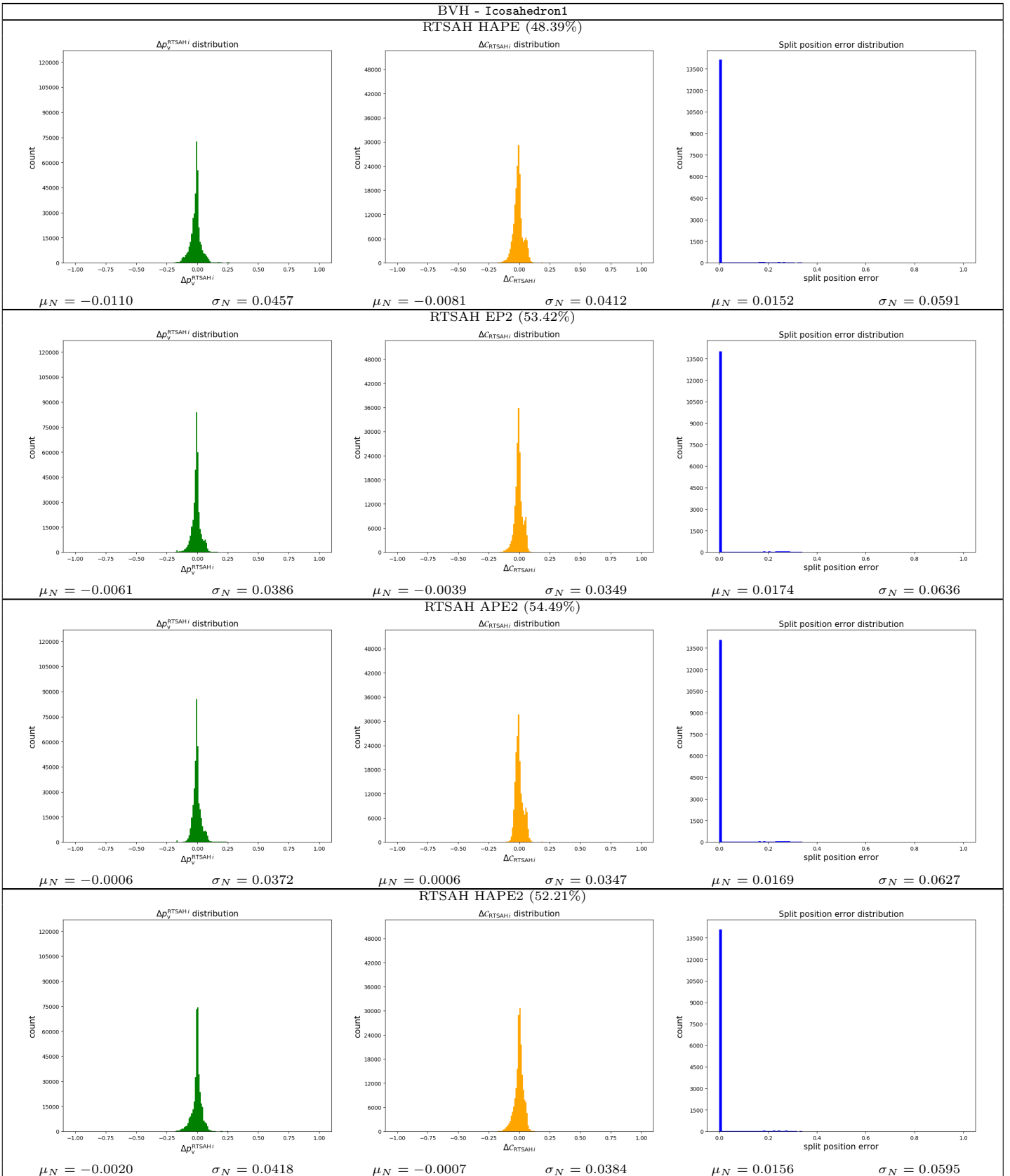


Table 110: The distributions (histogram, mean,  $\mu_N$ , standard deviation,  $\sigma_N$ ) of the combined piercing and visibility probability error,  $\Delta p_{\text{RTSAH}i}$ , the cost error,  $\Delta C_{\text{RTSAH}i}$ , and the split position error, and the optimal axis selection percentage for a **BVH** ADS, built with various build heuristics, for the **Icosahedron1** scene.

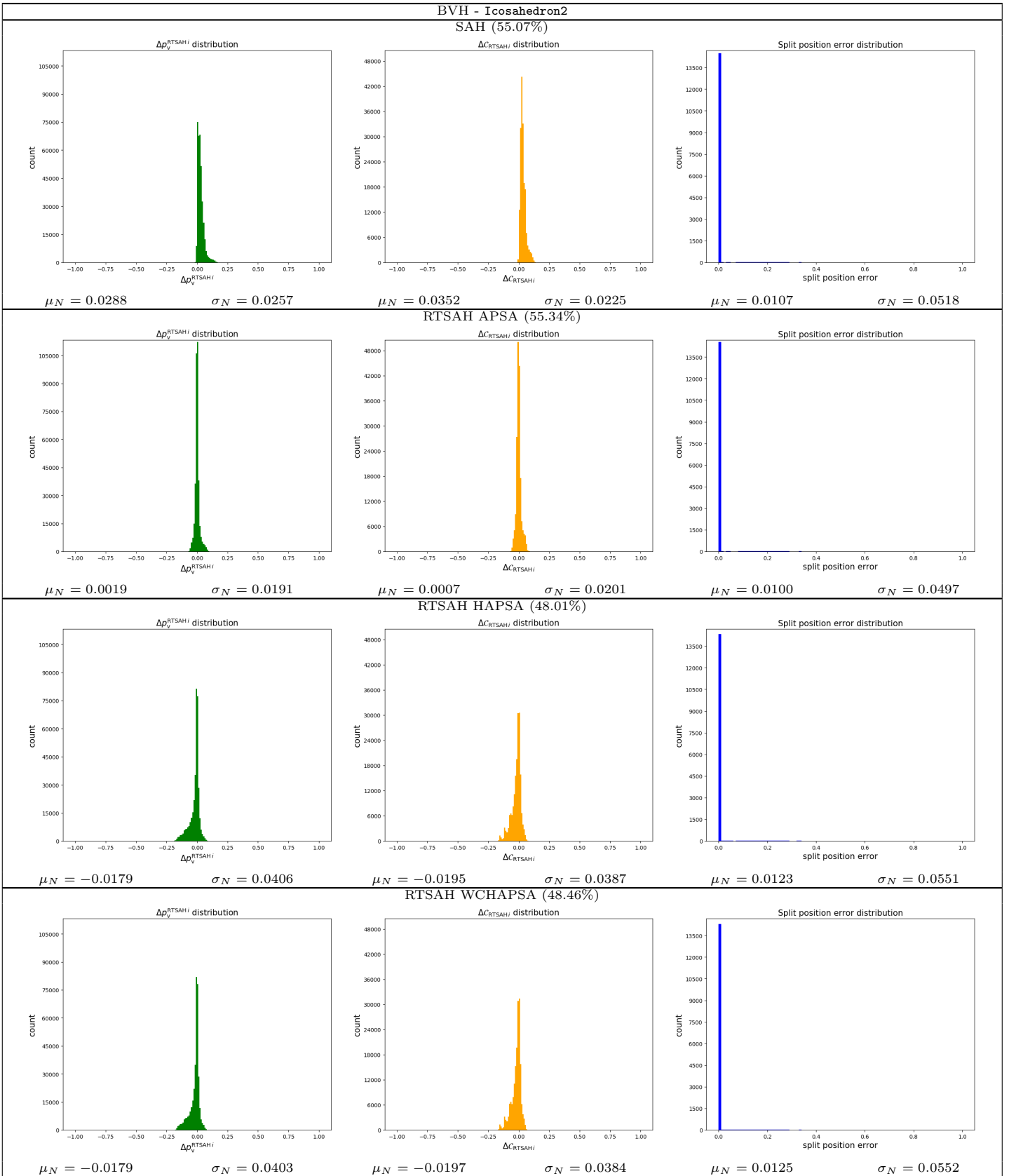


Table 111: The distributions (histogram, mean,  $\mu_N$ , standard deviation,  $\sigma_N$ ) of the combined piercing and visibility probability error,  $\Delta\mathcal{V}_{\text{RTSAH}i}$ , the cost error,  $\Delta C_{\text{RTSAH}i}$ , and the split position error, and the optimal axis selection percentage for a **BVH** ADS, built with various build heuristics, for the **Icosahedron2** scene.

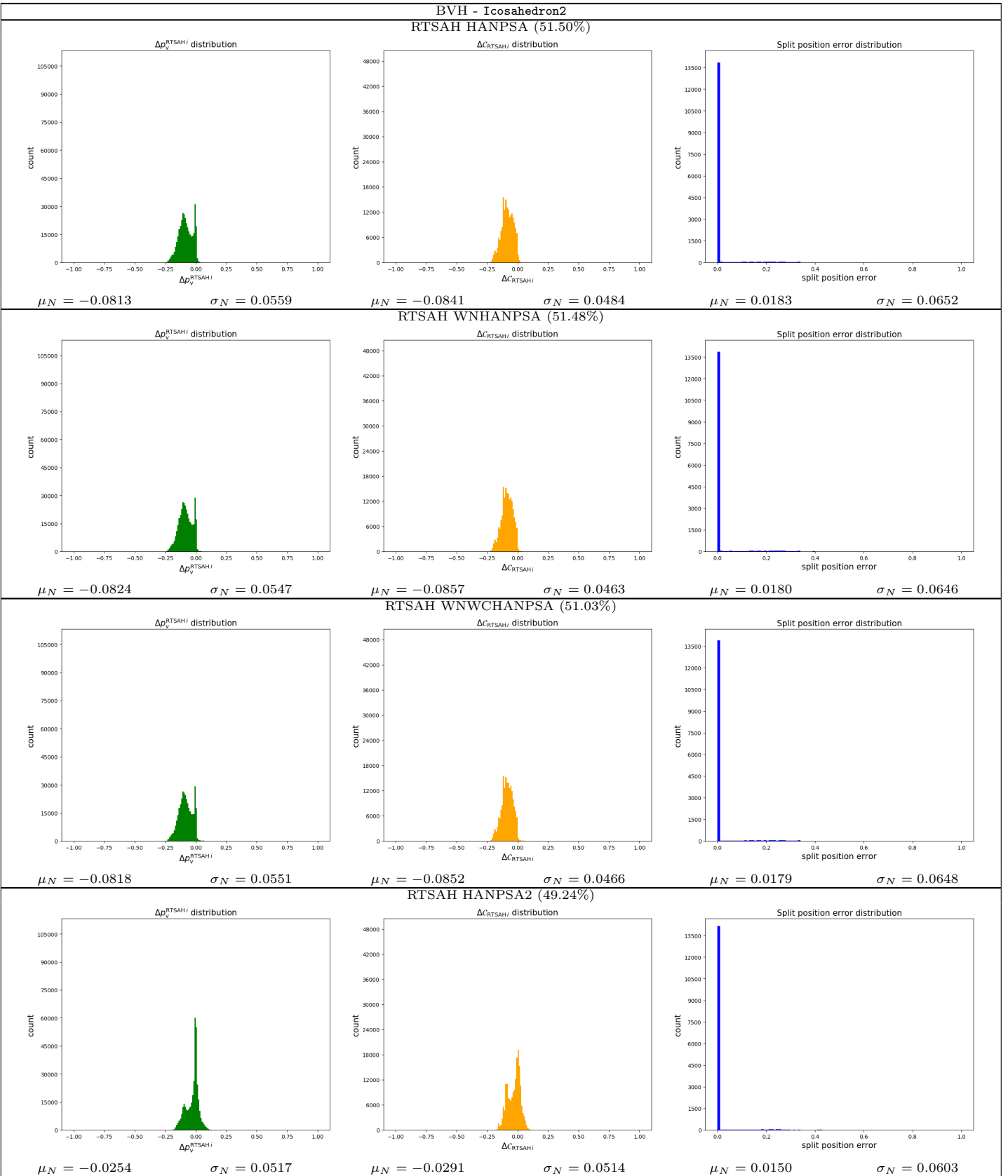


Table 112: The distributions (histogram, mean,  $\mu_N$ , standard deviation,  $\sigma_N$ ) of the combined piercing and visibility probability error,  $\Delta V_{\text{RTSAH}_i}$ , the cost error,  $\Delta C_{\text{RTSAH}_i}$ , and the split position error, and the optimal axis selection percentage for a **BVH** ADS, built with various build heuristics, for the **Icosahedron2** scene.

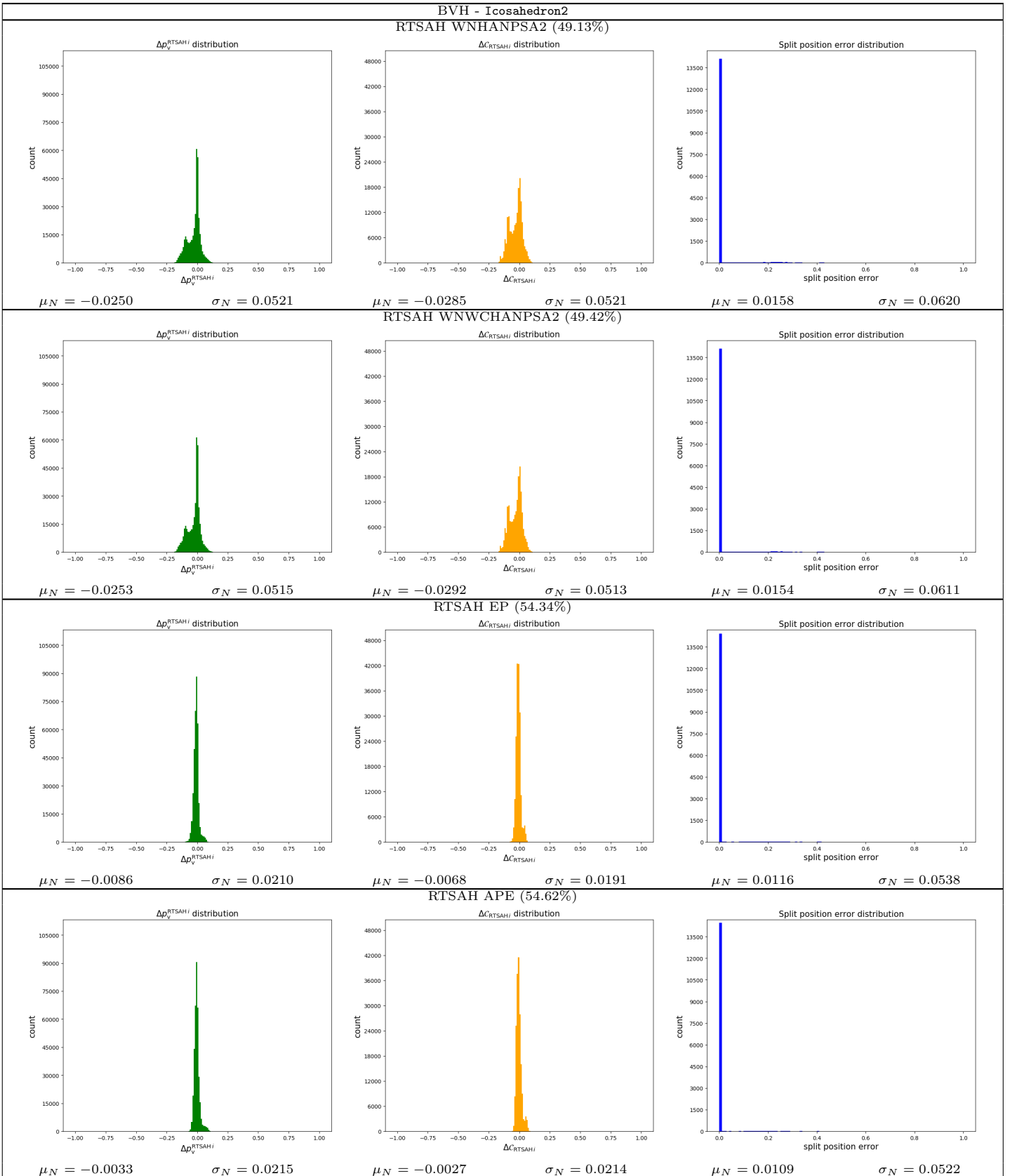


Table 113: The distributions (histogram, mean,  $\mu_N$ , standard deviation,  $\sigma_N$ ) of the combined piercing and visibility probability error,  $\Delta\mathcal{V}_{\text{RTSAH}i}$ , the cost error,  $\Delta C_{\text{RTSAH}i}$ , and the split position error, and the optimal axis selection percentage for a **BVH** ADS, built with various build heuristics, for the **Icosahedron2** scene.

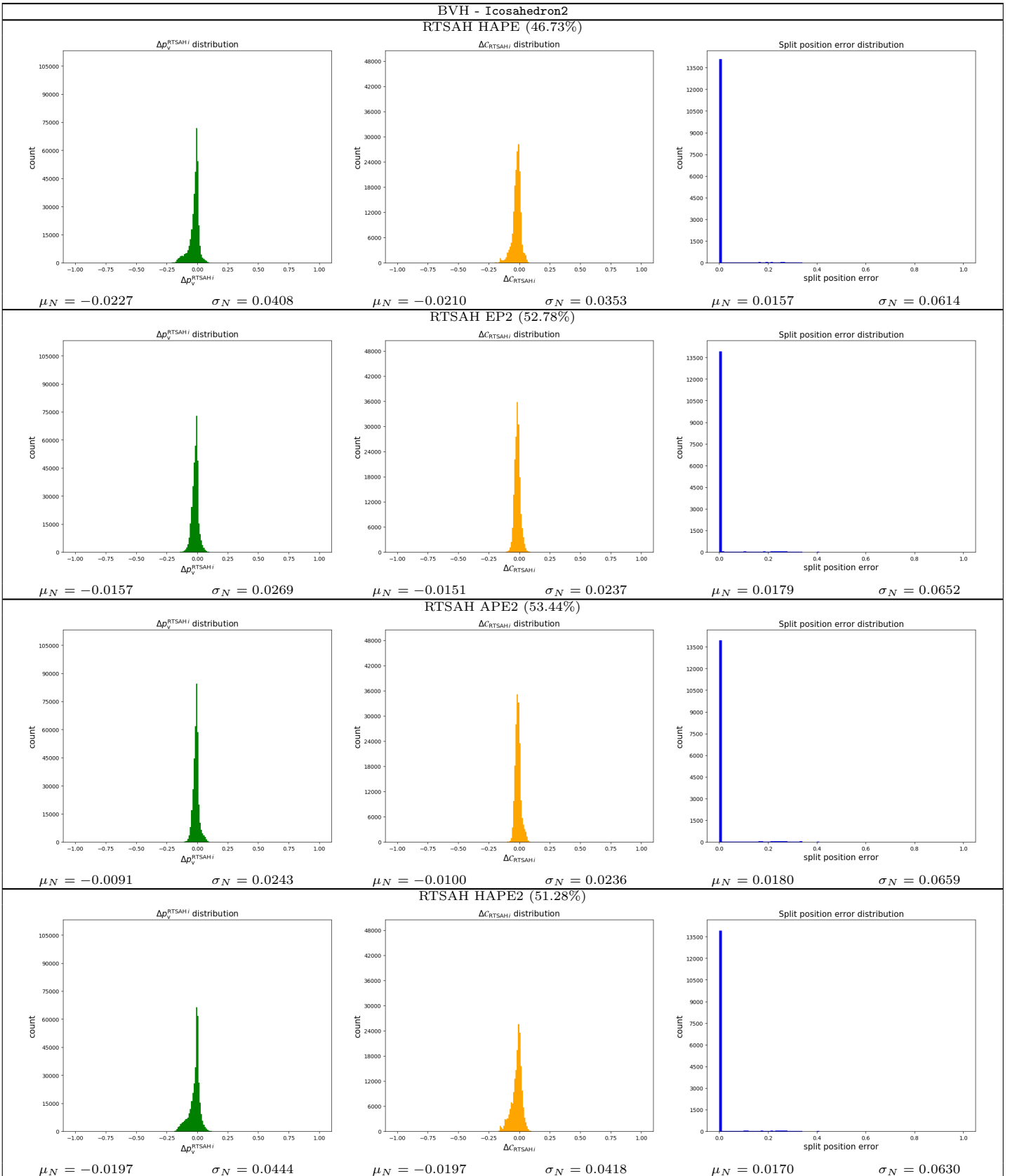


Table 114: The distributions (histogram, mean,  $\mu_N$ , standard deviation,  $\sigma_N$ ) of the combined piercing and visibility probability error,  $\Delta V_{\text{RTSAH}_i}$ , the cost error,  $\Delta C_{\text{RTSAH}_i}$ , and the split position error, and the optimal axis selection percentage for a **BVH** ADS, built with various build heuristics, for the **Icosahedron2** scene.

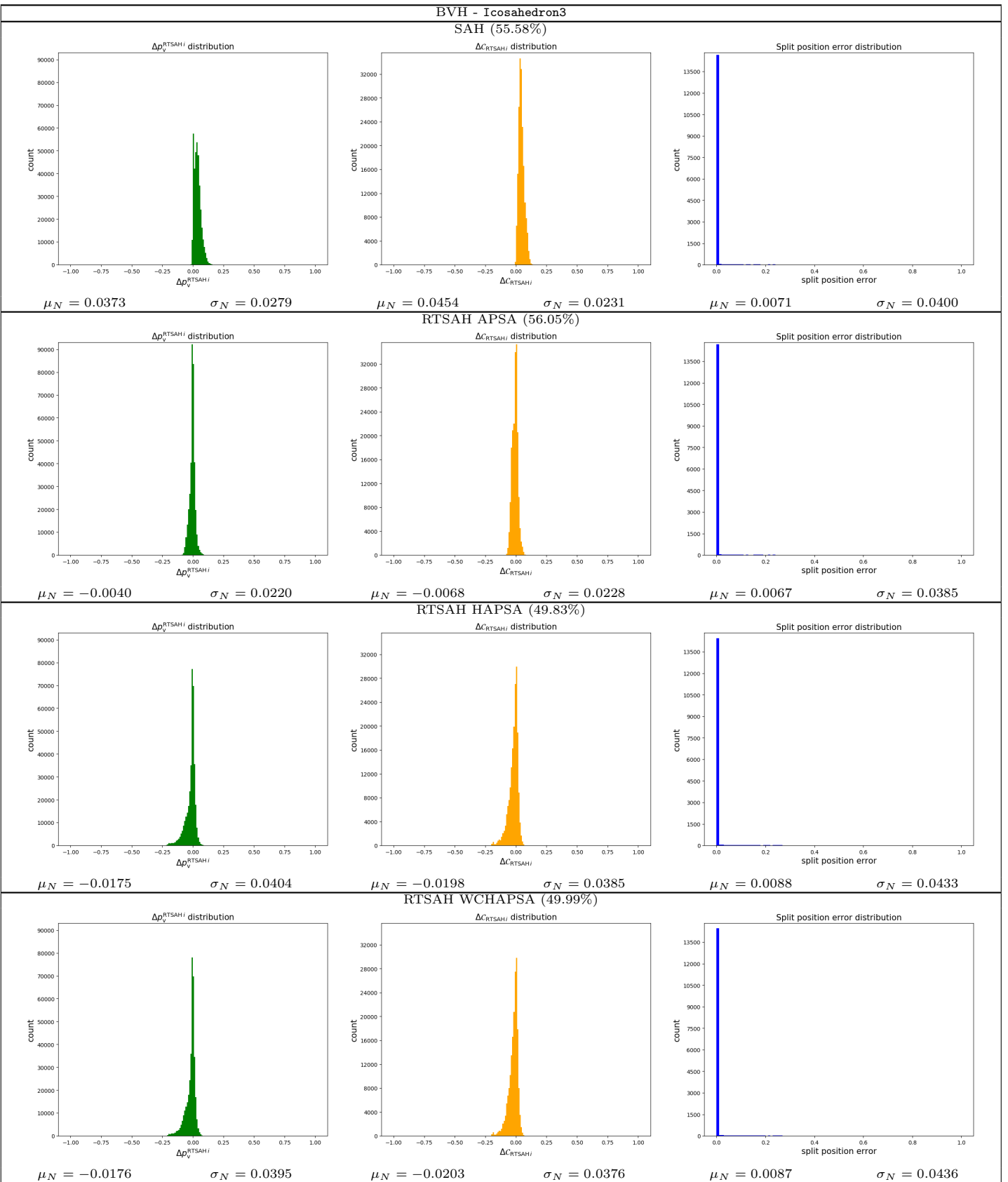


Table 115: The distributions (histogram, mean,  $\mu_N$ , standard deviation,  $\sigma_N$ ) of the combined piercing and visibility probability error,  $\Delta V_{\text{RTSAH}_i}$ , the cost error,  $\Delta C_{\text{RTSAH}_i}$ , and the split position error, and the optimal axis selection percentage for a **BVH** ADS, built with various build heuristics, for the **Icosahedron3** scene.

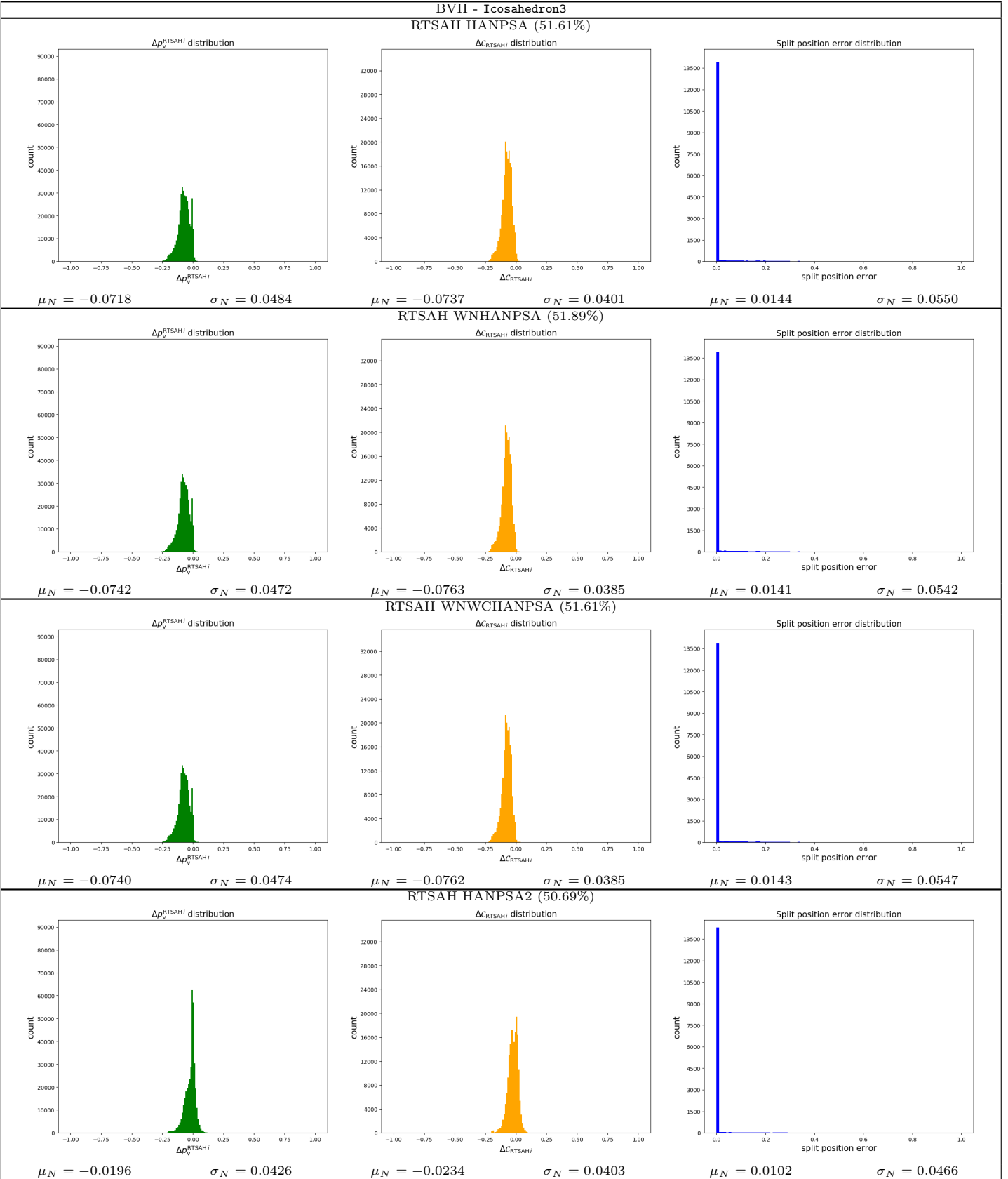


Table 116: The distributions (histogram, mean,  $\mu_N$ , standard deviation,  $\sigma_N$ ) of the combined piercing and visibility probability error,  $\Delta V_{\text{RTSAH}_i}$ , the cost error,  $\Delta C_{\text{RTSAH}_i}$ , and the split position error, and the optimal axis selection percentage for a **BVH** ADS, built with various build heuristics, for the **Icosahedron3** scene.

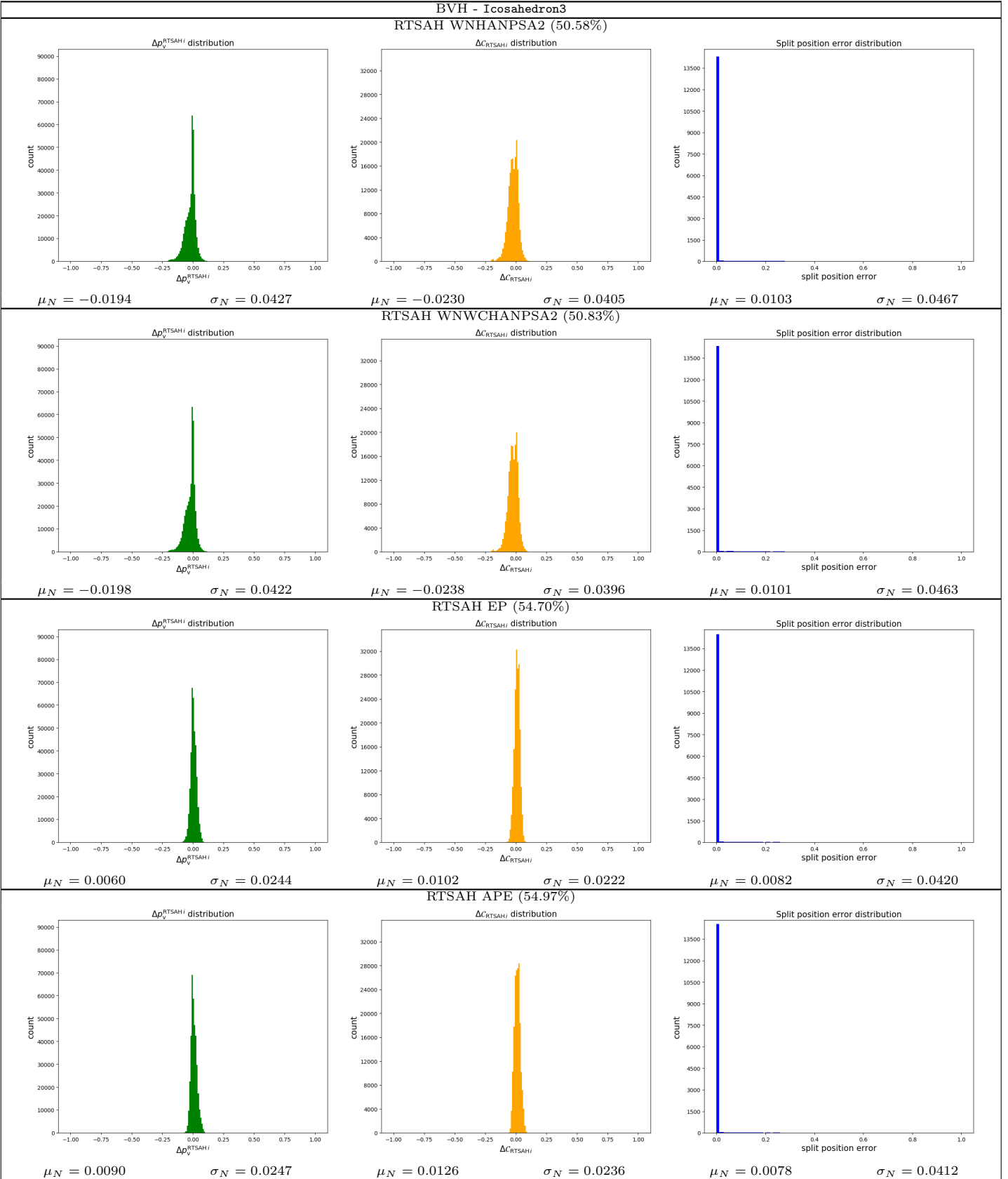


Table 117: The distributions (histogram, mean,  $\mu_N$ , standard deviation,  $\sigma_N$ ) of the combined piercing and visibility probability error,  $\Delta V_{\text{RTSAH}_i}$ , the cost error,  $\Delta C_{\text{RTSAH}_i}$ , and the split position error, and the optimal axis selection percentage for a **BVH** ADS, built with various build heuristics, for the **Icosahedron3** scene.

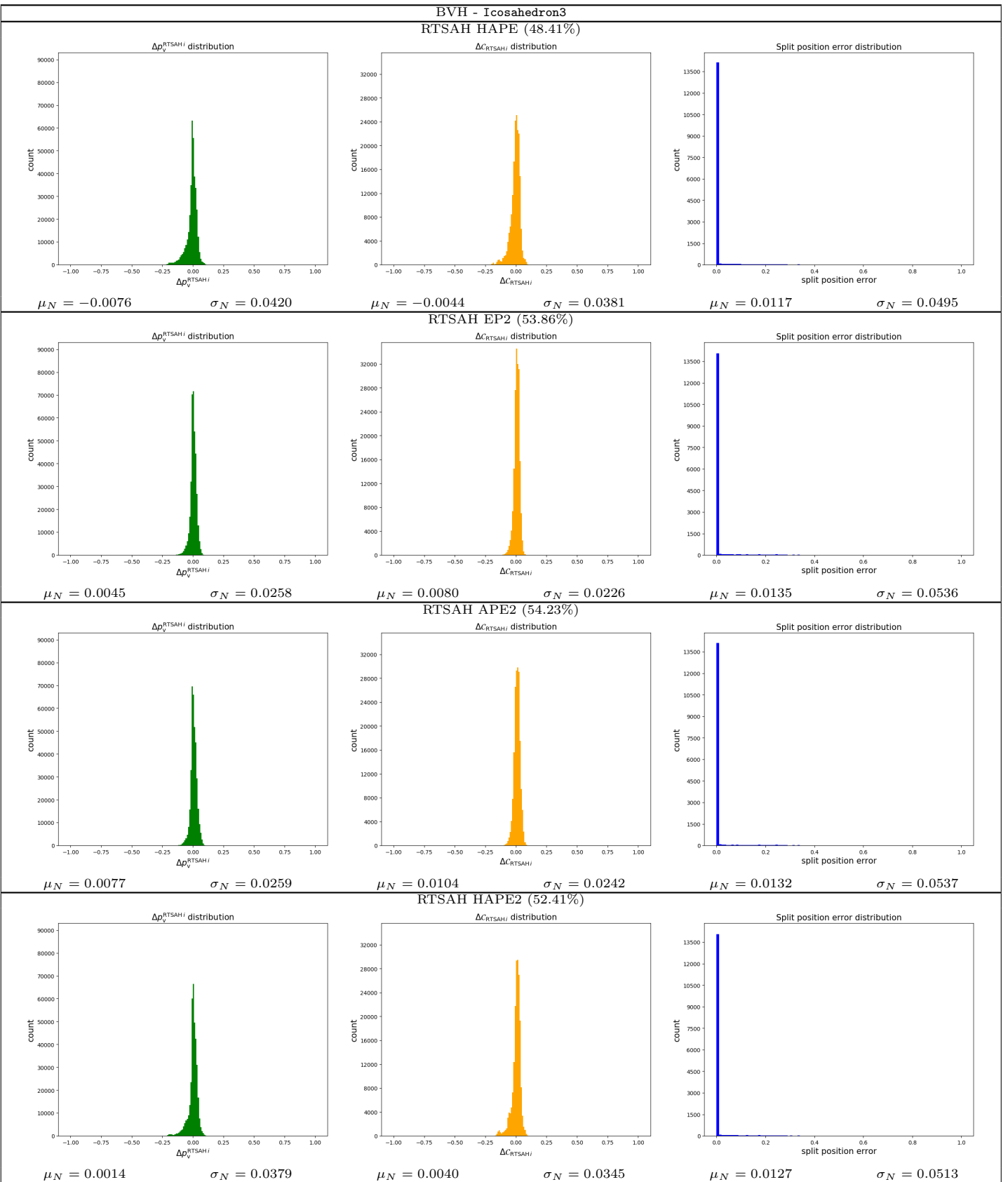


Table 118: The distributions (histogram, mean,  $\mu_N$ , standard deviation,  $\sigma_N$ ) of the combined piercing and visibility probability error,  $\Delta\mathcal{V}_{\text{RTSAH}_i}$ , the cost error,  $\Delta C_{\text{RTSAH}_i}$ , and the split position error, and the optimal axis selection percentage for a **BVH** ADS, built with various build heuristics, for the **Icosahedron3** scene.

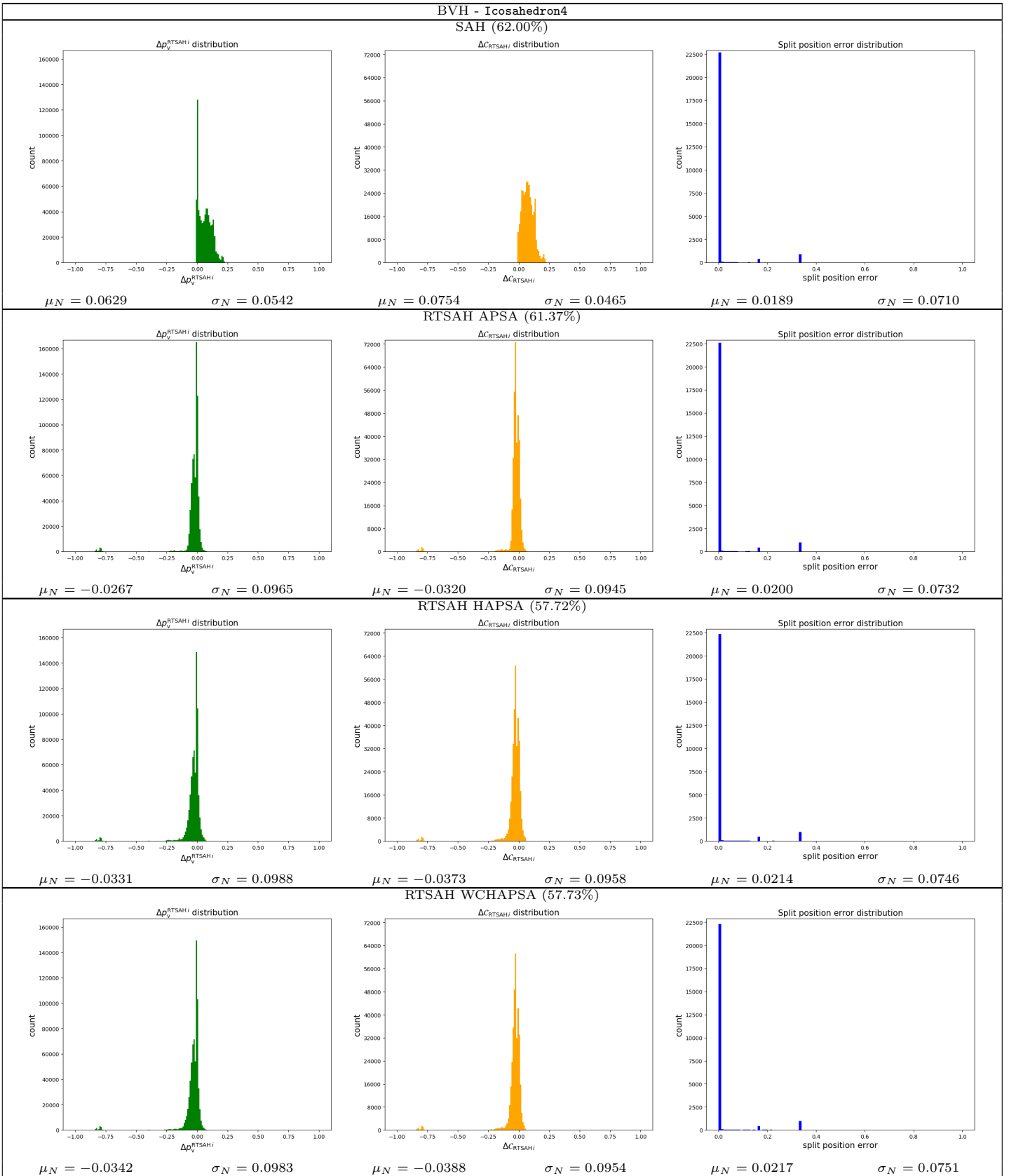


Table 119: The distributions (histogram, mean,  $\mu_N$ , standard deviation,  $\sigma_N$ ) of the combined piercing and visibility probability error,  $\Delta p_v^{\text{RTSAH}_i}$ , the cost error,  $\Delta C_{\text{RTSAH}_i}$ , and the split position error, and the optimal axis selection percentage for a **BVH** ADS, built with various build heuristics, for the **Icosahedron4** scene.

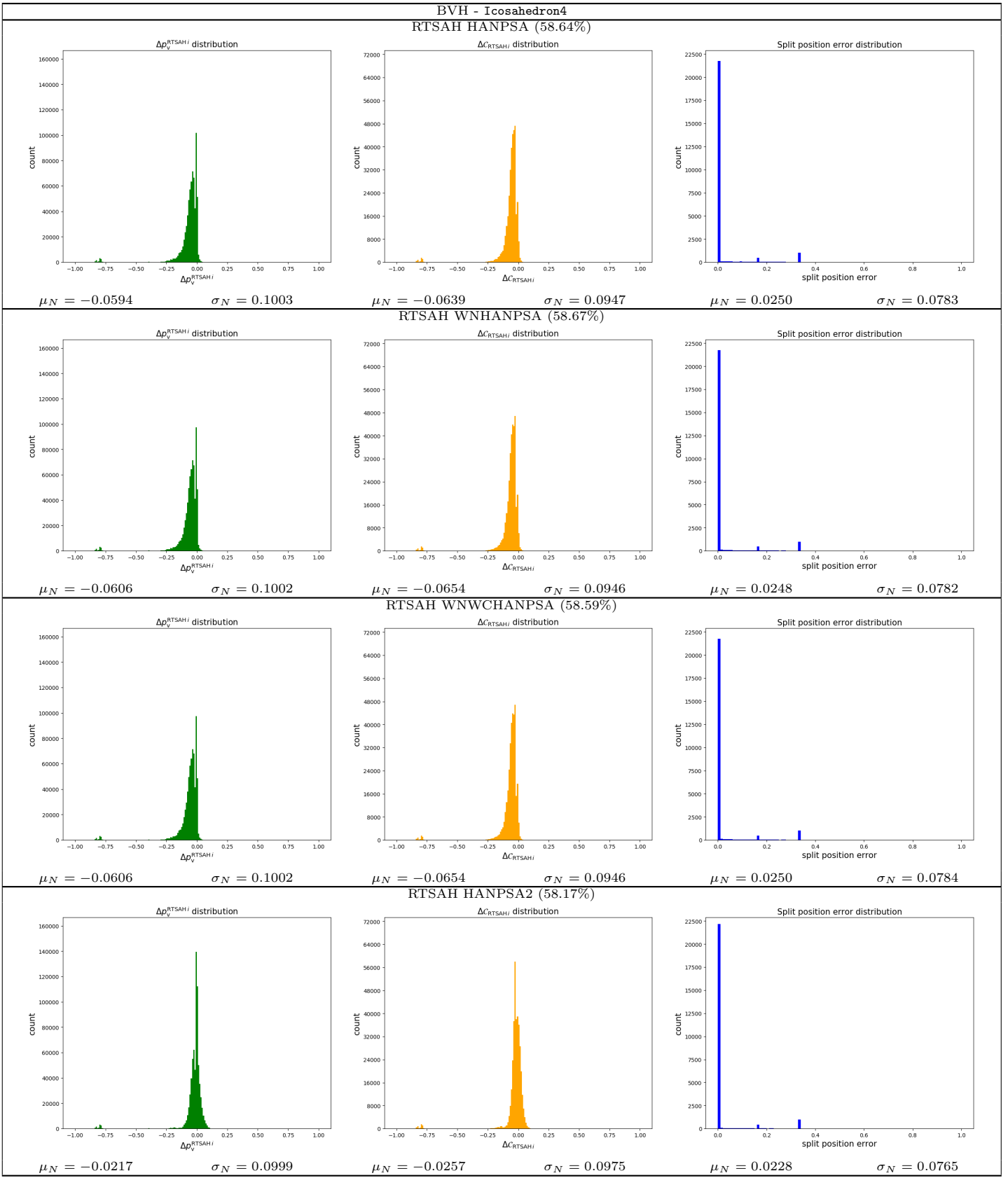


Table 120: The distributions (histogram, mean,  $\mu_N$ , standard deviation,  $\sigma_N$ ) of the combined piercing and visibility probability error,  $\Delta V_{\text{RTSAH}_i}$ , the cost error,  $\Delta C_{\text{RTSAH}_i}$ , and the split position error, and the optimal axis selection percentage for a **BVH** ADS, built with various build heuristics, for the **Icosahedron4** scene.

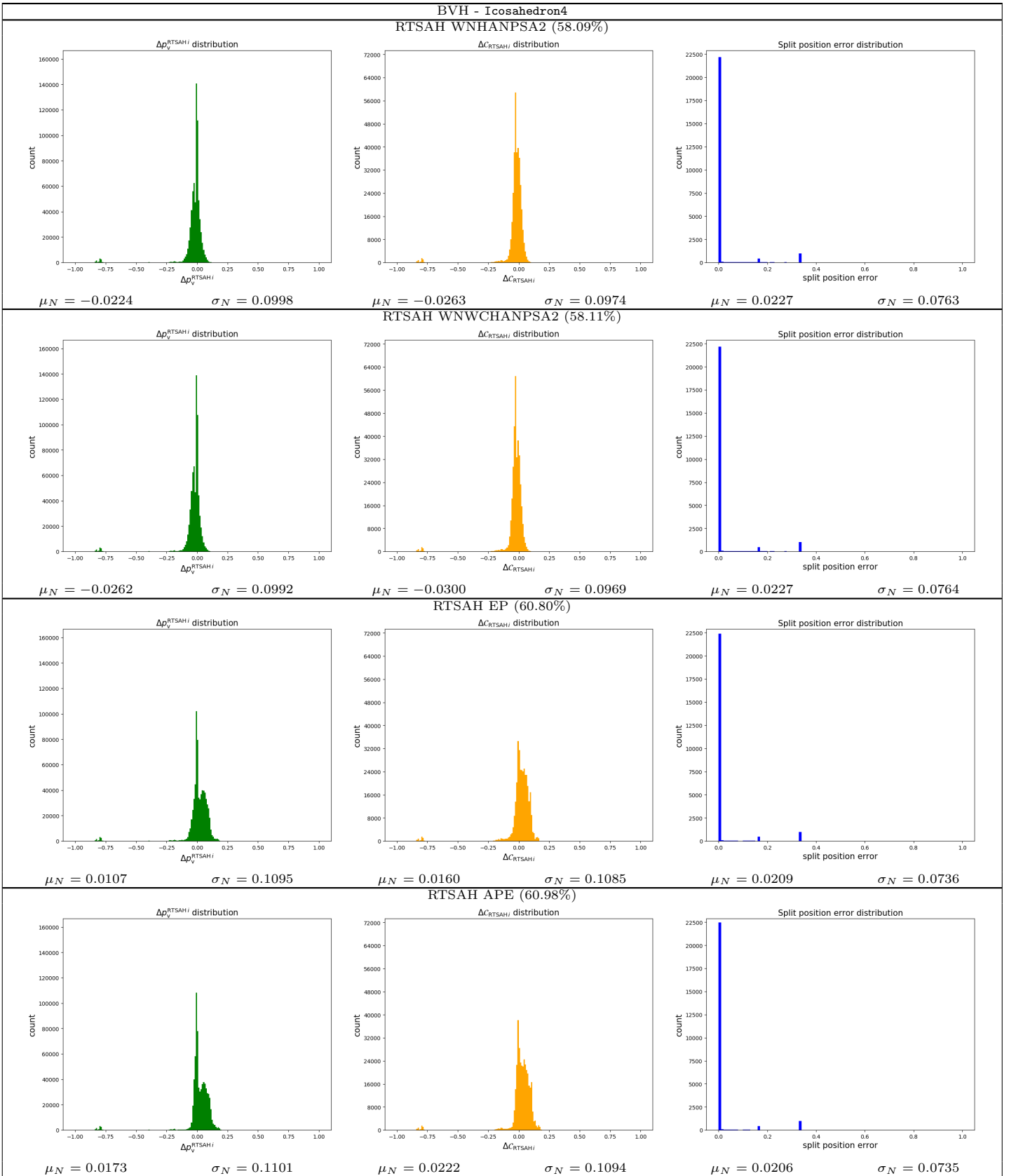


Table 121: The distributions (histogram, mean,  $\mu_N$ , standard deviation,  $\sigma_N$ ) of the combined piercing and visibility probability error,  $\Delta p_v^{\text{RTSAH}_i}$ , the cost error,  $\Delta C^{\text{RTSAH}_i}$ , and the split position error, and the optimal axis selection percentage for a **BVH** ADS, built with various build heuristics, for the **Icosahedron4** scene.

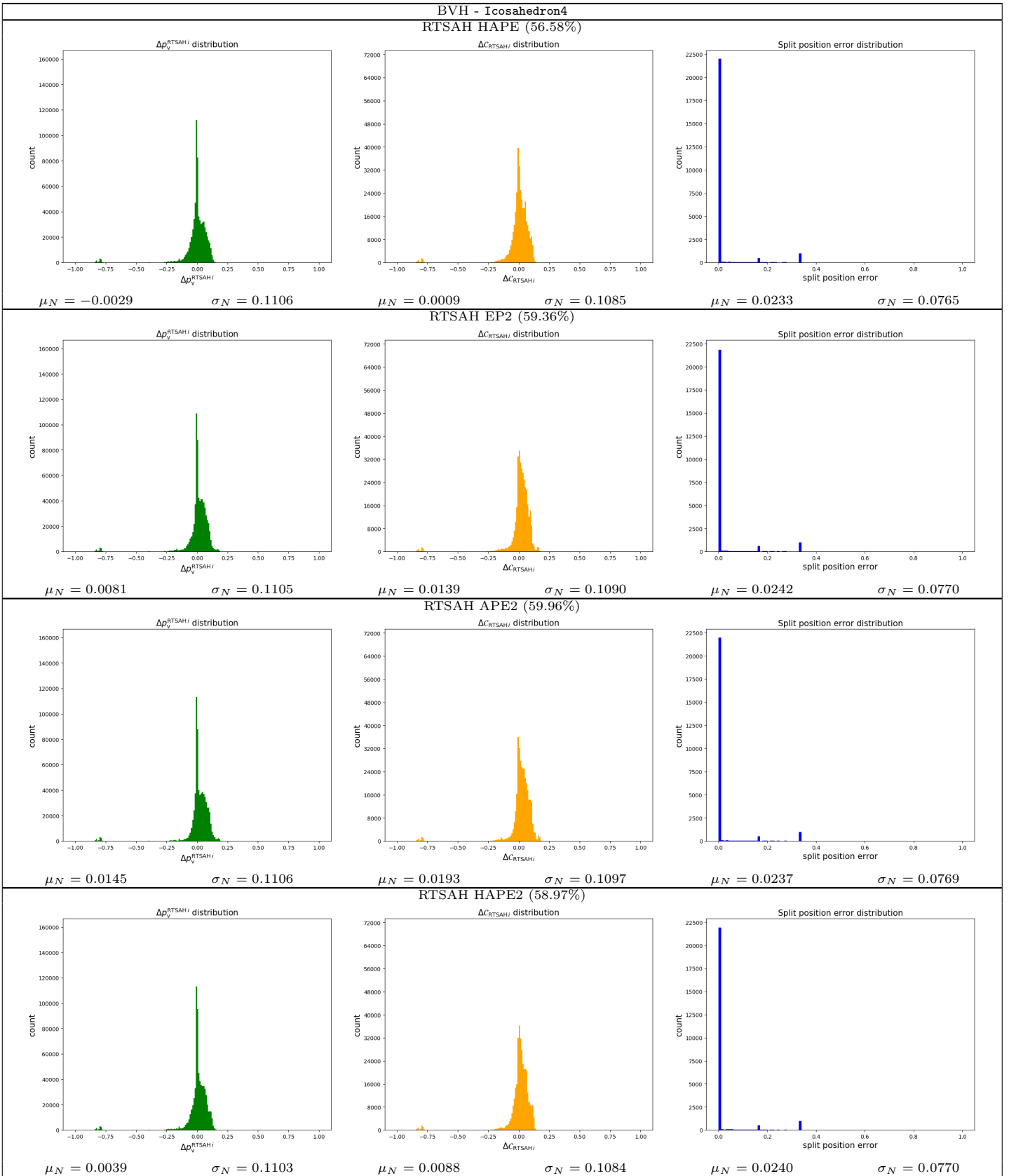


Table 122: The distributions (histogram, mean,  $\mu_N$ , standard deviation,  $\sigma_N$ ) of the combined piercing and visibility probability error,  $\Delta V_{\text{RTSAH}_i}$ , the cost error,  $\Delta C_{\text{RTSAH}_i}$ , and the split position error, and the optimal axis selection percentage for a **BVH** ADS, built with various build heuristics, for the **Icosahedron4** scene.

## References

- [BH06] BOULOS S., HAINES E.: Ray-Box Sorting. *Ray Tracing News* 19, 1 (Sep 2006).
- [BH09] BITTNER J., HAVRAN V.: RDH: Ray Distribution Heuristics for Construction of Spatial Data Structures. In *Proceedings of the 25th Spring Conference on Computer Graphics* (New York, NY, USA, 2009), SCCG '09, ACM, pp. 51–58.
- [CCI12] CHOI B., CHANG B., IHM I.: Construction of Efficient Kd-trees for Static Scenes Using Voxel-Visibility Heuristic. *Computers & Graphics* 36, 1 (2012), 38–48.
- [DK08] DAMMERTZ H., KELLER A.: The Edge Volume Heuristic - Robust Triangle Subdivision for Improved BVH Performance. In *IEEE Symposium on Interactive Ray Tracing 2008* (Aug 2008), pp. 155–158.
- [EG07] ERNST M., GREINER G.: Early Split Clipping for Bounding Volume Hierarchies. In *IEEE Symposium on Interactive Ray Tracing 2007* (Sept 2007), pp. 73–78.
- [Eri04] ERICSON C.: *Real-Time Collision Detection*. CRC Press, Inc., Boca Raton, FL, USA, 2004.
- [Fin09] FINCH T.: Incremental Calculation of Weighted Mean and Variance.
- [FLF12] FELTMAN N., LEE M., FATAHALIAN K.: SRDH: Specializing BVH Construction and Traversal Order Using Representative Shadow Ray Sets. In *Proceedings of the Fourth ACM SIGGRAPH / Eurographics Conference on High-Performance Graphics* (Aire-la-Ville, Switzerland, Switzerland, 2012), EGHH-HPG'12, Eurographics Association, pp. 49–55.
- [GD16] GANESTAM P., DOGGETT M.: SAH guided spatial split partitioning for fast BVH construction. *Computer Graphics Forum* 35, 2 (2016).
- [Hav00] HAVRAN V.: *Heuristic Ray Shooting Algorithms*. PhD thesis, Faculty of Electrical Engineering, Czech Technical University, Prague, Nov 2000.
- [HB02] HAVRAN V., BITTNER J.: On Improving Kd-Trees for Ray Shooting. In *Proceedings of Winter School of Computer Graphics 2002 Conference* (2002), pp. 209–217.
- [Hec82] HECKBERT P.: Color Image Quantization for Frame Buffer Display. *SIGGRAPH Comput. Graph.* 16, 3 (Jul 1982), 297–307.
- [HKRS02] HURLEY J. T., KAPUSTIN A., RESHETOV A., SOUPIKOV A.: Fast Ray Tracing for Modern General Purpose CPU. In *Proceedings of GraphiCon* (2002).
- [HMS06] HUNT W. A., MARK W. R., STOLL G.: Fast kd-tree Construction with an Adaptive Error-Bounded Heuristic. In *IEEE Symposium on Interactive Ray Tracing 2006* (Sept 2006), pp. 81–88.
- [IH11] IZE T., HANSEN C.: RTSAH Traversal Order for Occlusion Rays. *Computer Graphics Forum* 30, 2 (2011), 297–305.
- [Kap85] KAPLAN M. R.: The Use of Spatial Coherence in Ray Tracing. *ACM SIGGRAPH Course Notes* 11 (1985).
- [MBD15] MOULIN M., BILLÉN N., DUTRÉ P.: Efficient Visibility Heuristics for Kd-Trees Using the RTSAH. In *Eurographics Symposium on Rendering - Experimental Ideas & Implementations* (June 2015), Lehtinen J., Nowrouzezahrai D., (Eds.), The Eurographics Association, pp. 31–39.
- [NM14] NAH J.-H., MANOCHA D.: SATO: Surface Area Traversal Order for Shadow Ray Tracing. *Computer Graphics Forum* 33, 6 (2014), 167–177.
- [PGDS09] POPOV S., GEORGIEV I., DIMOV R., SLUSALLEK P.: Object Partitioning Considered Harmful: Space Subdivision for BVHs. In *Proceedings of the Conference on High Performance Graphics 2009*

(New York, NY, USA, 2009), HPG '09, ACM, pp. 15–22.

- [PGpSS06] POPOV S., GUNTHER J., P. SEIDEL H., SLUSALLEK P.: Experiences with Streaming Construction of SAH Kd-Trees. In *2006 IEEE Symposium on Interactive Ray Tracing* (Sept 2006), pp. 89–94.
- [PH10] PHARR M., HUMPHREYS G.: *Physically Based Rendering, Second Edition: From Theory To Implementation*, 2nd ed. Morgan Kaufmann Publishers Inc., San Francisco, CA, USA, 2010.
- [PWH16] PHARR M., WENZEL J., HUMPHREYS G.: *Physically Based Rendering, Third Edition: From Theory To Implementation*, 3th ed. Morgan Kaufmann Publishers Inc., San Francisco, CA, USA, 2016.
- [SFD09] STICH M., FRIEDRICH H., DIETRICH A.: Spatial Splits in Bounding Volume Hierarchies. In *Proceedings of the Conference on High Performance Graphics 2009* (New York, NY, USA, 2009), HPG '09, ACM, pp. 7–13.
- [SH74] SUTHERLAND I. E., HODGMAN G. W.: Reentrant Polygon Clipping. *Communications of the ACM* 17, 1 (jan 1974), 32–42.
- [SSK07] SHEVTSOV M., SOUPIKOV A., KAPUSTIN A.: Highly Parallel Fast KD-tree Construction for Interactive Ray Tracing of Dynamic Scenes. *Computer Graphics Forum* 26, 3 (2007), 395–404.
- [WH06] WALD I., HAVRAN V.: On Building Fast Kd-Trees for Ray Tracing, and on Doing That in  $O(N \log N)$ . In *IEEE Symposium on Interactive Ray Tracing 2006* (Sept 2006), pp. 61–69.
- [WK06] WÄCHTER C., KELLER A.: Instant Ray Tracing: The Bounding Interval Hierarchy. In *Proceedings of the 17th Eurographics Conference on Rendering Techniques* (Aire-la-Ville, Switzerland, Switzerland, 2006), EGSR '06, Eurographics Association, pp. 139–149.